

**ELECTROCHEMICAL DYNAMICS OF CYTOCHROME
P450-3A4 ISOENZYME BIOSENSOR FOR PROTEASE
INHIBITOR ANTIRETROVIRAL DRUG**

By

Hendricks Nicolette Rebecca

BSc (Hons), MSc



Submitted in partial fulfilment of the requirements for the degree of

DOCTOR OF PHILOSOPHY

WESTERN CAPE
in the

Department of Chemistry

Faculty of Science

University of the Western Cape

November, 2010

Supervisor: Prof. Emmanuel I. Iwuoha

Declaration

I, Nicolette Rebecca Hendricks declare that *Electrochemical Dynamics of Cytochrome P450-3A4 Isoenzyme Biosensor for Protease Inhibitor Antiretroviral Drug* is a dissertation generated from my own work, that has not been submitted for any degree or examination in any other university, and that all the sources I have used or quoted have been properly indicated and acknowledged by complete references

Nicolette Rebecca Hendricks



Signature.....

Date.....

Summary

The highly active antiretroviral therapy (HAART) drug agent, indinavir, and the endocrine disruptor compound, 2,4-dichlorophenol (2,4-DCP), are directly related to two of South Africa's, and in fact, two of the globe's most fundamentally important and comprehensively researched subjects areas, which includes, HIV/AIDS and water pollution. In fact these two compounds share multiple significant commonality factors. Firstly, they have a profound effect on the health aspects of humans, albeit from opposite sides of the 'equation'. Secondly, in the context of metabolism, they both share the same route of biotransformation, and as such, both have a profound effect on the main first pass metabolising hepatic enzyme, CYP450 3A4, as well as xenobiotics sharing the same metabolic pathway. Thirdly and perhaps more importantly, in direct relation to the human mortality, their levels preferentially require constant or regular monitoring, a process, at this stage, is still only officially possible with complex specialized analytically-based techniques. Moreover, these techniques are only based on centralized detection and quantification, which essentially means expensive procedures, and long waiting periods for results. This thesis firstly reports on the development and characterization of reagent-less and cobalt(III) sepulchrate $[\text{Co}(\text{Sep})^{3+}]$ mediated biosensor platforms (biosensor platform 1 and biosensor platform 2), with human recombinant heme thiolate, cytochrome P450 3A4 isoenzyme (CYP3A4), as biorecognition component. Secondly, each biosensor platform was evaluated by using an entirely different category of compound as model substrate, with the overall objective being the development of alternative analytical method for the detection and quantification of each of these substrates, by amperometric transduction method. In this regard biosensor platform 1 was evaluated for the detection of 2,4-dichlorophenol, whereas biosensor platform 2 was evaluated for the detection of protease inhibitor (PI) HAART drug, indinavir. Fourthly, this dissertation also reports on the use of genetic engineering as complimentary method during biosensor investigations, as source for continuous supply of catalytically active biological recognition component. With respect to the preparation of the biosensors in particular, biosensor platform 1 was

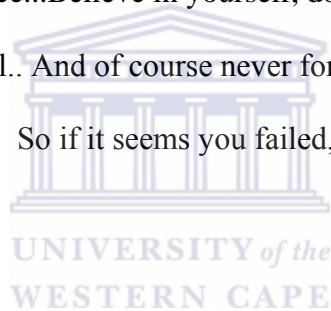
constructed by entrapping the commercially sourced full-length, wild type CYP3A4 on a pre-formed electroactive carrier matrix, consisting of $\text{Co}(\text{Sep})^{3+}$ -modified nafion membrane on a glassy carbon electrode. In this regard, the nafion- $\text{Co}(\text{Sep})^{3+}$ composite was prepared by integrating the $\text{Co}(\text{Sep})^{3+}$ species into a pre-formed nafion film through manual drop-coating and mixing methods. In addition to this, the so-formed biosensor was re-inforced by a thin nafion layer as outer-film. The complete biosensor may be denoted as $\text{GCE}||\text{naf}|\text{CME}-\text{Co}(\text{Sep})^{3+}|\text{f}|\text{CYP3A4}|\text{naf}$. Biosensor platform 2 on the other hand, was constructed by entrapment of the N-terminally modified human recombinant CYP3A4 (consisting only of the heme domain and the surrounding apoprotein), prepared locally through genetic engineering, as a histidine-tagged, catalytically active soluble construct, denoted nCYP3A4, in a biocompatible ionically crosslinked hydrogel-composite membrane. Enzyme immobilization in this case was also realized on a pre-formed nafion- $\text{Co}(\text{Sep})^{3+}$ carrier matrix film, however, in this case the electroactive carrier matrix was prepared by integrating the electroactive $\text{Co}(\text{Sep})^{3+}$ species deep within the nafion microstructure through potentiostatic electrodeposition method at a constant potential of +450 mV for 1200 sec. The so prepared biosensor, is denoted $\text{GCE}||\text{naf}|\text{E}|\text{Co}(\text{Sep})^{3+}|\text{nCYP3A4}|\text{Agrs-PEI-PVA}$. In this regard, biosensor for platform 2, different variables affecting the performance and stability of the biosensor were evaluated. Selected ex-situ characterization methods, including scanning electrochemical microscopy (SEM), Fourier Transform Infrared (FTIR) and UV-Vis spectroscopy was used as complimentary characterization methods. Morphological and structural characterization, revealed the formation of a highly stable electroactive composite film for the carrier matrix in biosensor platform 2, exhibiting a compact nature and a smooth consistency in which the electroactive $\text{Co}(\text{Sep})^{3+}$ mediating species was embedded deep within the microstructure of the pre-formed nafion film. Moreover, the method of preparation was highly reproducible, while voltammetric studies also corroborated the stability of the carrier matrix film. Overall, the design path used for this method was shown to be an improvement as compared to the design path used for biosensor platform 1, particularly with regard to the carrier matrix. Nevertheless, the proposed

substrates were successfully detected and quantified by the individual biosensor platforms. In this regard, the dynamic linear range of the GCE||naf|CME-Co(Sep)³⁺|f|CYP3A4|naf biosensor, for 2,4-DCP exhibited an upper limit of 45 μA , with the sensitivity determined as $0.038 \mu\text{A} \mu\text{M}^{-1}$. In addition to this, the LOD was calculated as $0.043 \mu\text{g L}^{-1}$, which was lesser than the USA Environmental Protection Agency's (EPA) drinking water equivalent level (DWEL) for 2,4-DCP. In the case of the GCE||naf|El-Co(Sep)³⁺|n|CYP3A4|Agrs-PEI-PVA biosensor, the linear concentration range for indinavir was shown to be between $2.183 \mu\text{M}$ — $3.552 \mu\text{M}$, while the sensitivity was determined as $0.035 \mu\text{A} \mu\text{M}^{-1}$. Moreover, the LOD value, determined as 59.72 mg L^{-1} was suggested to be of significance with regard to the maximum plasma concentration, C_{Max} , with respect to the ritonavir-boosted regimen, which is the proposed method of administering indinavir. This can also be of value for HIV/AIDS patients who are poor metabolizers, as they will have significantly elevated concentration of the drug, when administered with ritonavir as booster. Above and beyond these results, the overpotential for the reduction of dioxygen, which is a crucial step in the catalytic cycle of the CYP3A4 enzyme, was significantly reduced by the GCE||naf|El-Co(Sep)³⁺|n|CYP3A4|Agrs-PEI-PVA biosensor, as compared to the other biosensor.

Dedication

I dedicate this thesis to everybody suffering infirmity of any form, whether it may be a chronic illness, a slight disability or any other life issue seemingly keeping you back.

And also to people who have ever been labeled as potential failures...Look straight ahead at the price...Believe in yourself, do the best that you can and you will reach your end goal.. And of course never forget: “Success is failure turned inside out”. So if it seems you failed, try and try again.



Acknowledgements

Firstly, I wish to thank God Almighty, the Lord Jesus Christ and His wonderful Holy Spirit for always being my Refuge, my Hope, my Provider and my Joy. I am nothing without the Lord's supernatural All Knowing and All Powerful presence in my life. Secondly, I wish to give my most humble gratitude to my Supervisor, Professor Emmanuel Iwuoha, for his invaluable advice, guidance and support that enabled to complete this research. I especially thank him for believing in me, when I at times did not believe in myself. Also a big thanks to Dr. Nazeem Jahed and Prof. Priscilla Baker for their guidance and support during my time of research in the SensorLab. I wish to give a most sincere thanks to Natasha Beeton-Kempton and Anna Ignaszak for their contributions to this research work.

My sincerest thanks also to Professor Jonathan Blackburn who allowed me to freely use all of the equipment and materials at the Institute of Infectious Disease and Molecular Medicine (IIDMM) for the preparation of the enzyme. I wish to thank all of my friends Barbara Rodgers, Sarah Mauela, Vernon Somerset, Combs, and Tania Mabank for their friendship and supported especially at those times when I felt like giving up.

To all of my fellow SensorLab colleagues, both present and past, thanks much for all of your assistance and encouragement. A special thanks to our postdoc, Tesfaye, who always very patiently, was ready to answer any questions and engage in any long discussion about my work. I salute you! The final thanks goes to my most amazingly supportive family: Firstly, to my parents, who has sacrificed so much to see their children get somewhere in life and who has always been my greatest supporters, I can't begin to say how much You Both mean to me. To my brother Shaun and my sister Vanessa, thank you for always being there for me. Lastly, to my amazing husband, Shaun John Leukes who takes the meaning of "for better and for worse", "for richer and poorer", "in sickness and in health" to a

whole new level. I dont think there is a man on this earth that comes close to your loving, supportive and caring nature. You are my rock.



Table of Contents

DECLARATION	II
SUMMARY	III
DEDICATION	VI
ACKNOWLEDGEMENTS	VII
TABLE OF CONTENTS	IX
LIST OF FIGURES	XVI
LIST OF TABLES	XXV
ACRONYMS AND ABBREVIATIONS	XXVI
LIST OF PUBLICATIONS AND PRESENTATIONS	XXVII
CHAPTER 1	1
GENERAL INTRODUCTION	1
1.1 INTRODUCTION	1
1.2 BACKGROUND	1
1.2.1 Indinavir and HIV/AIDS: background overview and related aspects	1
1.2.2 Cytochrome P450 (3A4): Classification, structure and function	6
1.2.3 Endocrine disruptor compound: 2,4-Dichlorophenol (2,4-DCP)	10
1.2.4 Indinavir vs 2,4-DCP: The common factor shared by these two subjects	12
1.2.5 Molecular models and probes for xenobiotic metabolic profiling	14
1.2.5.1 Prospects of available biological probes for in vitro investigations with mammalian microsomal CYP 450s: advantages, drawbacks and new developments ----	14
1.2.6 Biosensors: The ultimate molecular probe	16
1.3 REFINEMENT OF RESEARCH AND RESEARCH QUESTIONS	20
1.4 SCOPE OF THE THESIS	24
1.3.1 Specific objectives to achieve the overall goal	26
1.6 LAYOUT OF THESIS	28
CHAPTER 2	31
BIOSENSORS: A REVIEW OF THE RELEVANT ASPECTS	31

CHAPTER PRELUDE	32
2.1 INTRODUCTION	33
2.2 BIOSENSORS	33
2.2.1 Biosensor structure and features	34
2.2.2 The Transducer	36
2.2.2.1 Amperometric Biosensors	38
2.2.3 Molecular Recognition	42
2.2.3.2 The enzyme electrode: Principles and classification from the microsomal cytochrome P450 viewpoint	46
2.2.3.1.2 Biomolecule solid-support tethering: Immobilization methods, biorecognition component coupling techniques, and other relevant aspects	50
2.2.4 Mediated Amperometric Biosensors	68
2.2.5 Nafion	75
2.3.6 Polymeric hydrogels	82
2.3.6.1 Agarose and related relevant subjects	84
CHAPTER 3	89
VARIABLES OF INVESTIGATION, PRACTICAL ASPECTS AND	89
GENERAL PROTOCOLS	89
CHAPTER PRELUDE	90
3A VARIABLES OF INVESTIGATION	91
3A.1 INTRODUCTION	91
3A.2 ELECTROANALYSIS (ELECTROANALYTICAL CHEMISTRY): THEORETICAL ASPECTS --	91
3A.2.1 Voltammetry	93
3A.2.1.1 Cyclic Voltammetry	97
3A.2.1.1.2 Aspects of chemical reactions coupled to electron transfer	108
3A.2.1.2 Pulsed Voltammetric Techniques	109
3A.2.1.2.1 Square-Wave Voltammetry (SWV)	110
3A.2.1.2.2 Differential Pulse Voltammetry (DPV)	113
3A.3 PRACTICAL CONSIDERATIONS	114
3A.3.1 Voltammetric investigations: Instrumentation and general practical requirements -	114
3A.3.1.1 The electrochemical cell	115
3A.3.1.2 Solvents and supporting electrolytes	117

3A.3.1.3	Conditions for requirement of oxygen removal-----	118
3A.3.1.4	Working electrodes -----	120
3A.3.1.4.1	Glassy carbon electrodes-----	120
3A.3.2	Human cytochrome P450 genetic engineering: Important theoretical preemptive and research design considerations -----	121
3A.3.2.1	Foreword-----	121
3A.3.2.2	The road to getting started: Important considerations-----	121
3A.3.2.3	Practical research design aspects and considerations for genetic engineering: cloning, purification and expression-----	123
3A.3.3	Enzyme kinetics-----	127
3A.3.3.1	Treatment of data-----	129
3A.3.3.2	Enzyme inhibition-----	130
3A.3.5	Biosensor performance aspects -----	130
3A.3.5.1	Sensor calibration: sensitivity, working and linear concentration range, detection determination limits [52, 57]-----	130
3A.3.5.2	Reproducibility, stability and lifetime-----	131
3B	GENERAL EXPERIMENTAL: PROTOCOLS AND METHODS OF INVESTIGATION -----	132
3B.1	INTRODUCTION -----	132
3B.2	MATERIALS AND REAGENTS -----	134
3B.2.2	Solutions -----	137
3B.2.2.1	Preparation of electrolyte buffer solutions-----	137
3B.2.2.2	Preparation of redox probes -----	137
3B.2.2.3	Preparation of working solutions for casting components for biosensor platform 1 and biosensor platform 2 -----	138
3B.2.2.3.1	Preparation of Nafion casting solution-----	138
3B.2.2.3.2	Preparation of electrolyte solution of cobalt(III) sepulchrates species for electrodeposition (for preparation of biosensor platform 2) -----	138
3B.2.2.3.3	Preparation of Eastman-AQ casting aqueous dispersion -----	139
3B.2.2.3.4	Preparation of 1% agarose (w/v)-----	139
3B.2.2.3.5	Preparation of aqueous poly(vinyl alcohol) solution-----	140
3B.2.2.3.6	Preparation of aqueous polyethyleneimine solution -----	140
3B.2.2.4.3	Preparation of Indinavir stock and working solutions -----	141

3B.3	VOLTAMETRIC INVESTIGATIONS -----	141
3B.3.1	Instrumentation, apparatus and general procedures -----	141
3B.3.1.1	Pre-treatment of the glassy-carbon working electrode -----	142
3B.5	COMPLIMENTARY EX-SITU CHARACTERISATION ANALYSIS-----	143
3B.5.1	Scanning Electrotron Microscopy (SEM)-----	143
3B.5.2	Fourier Transform Infrared Spectrocopy (FTIR) -----	144
3B.5.3	UV-Vis Absorption Spectroscopy -----	145
CHAPTER 4-----		146
RESULTS AND DISCUSSION: BIOSENSOR PLATFORM 1 -----		146
ABSTRACT-----		147
4.1	INTRODUCTION -----	148
4.2	MORPHOLOGICAL AND STRUCTURAL CHARACTERIZATION OF THE NAFION- CMECo(SEP) ³⁺ FILM (CARRIER MATRIX) FORMED ON THE GCE [GCE (GCE NAF CMECo(SEP) ³⁺)] -----	150
4.2.1	Morphological characterization: Scanning Electron Microscopy (SEM) -----	150
4.2.2	Structural characterization: Fourier Transform Infrared (FTIR) Spectroscopy-----	153
4.3	VOLTAMMETRIC CHARACTERIZATION OF THE MODIFIED ELECTRODE-----	156
4.3.1	Electrode Assembly -----	156
4.3.2	Electrochemical behaviour of the GC/naf/CMECo(Sep) ³⁺ /fICYP3A4/naf biosensor 163	
4.3.3	Electrocatalytic investigations of the fabricated biosensor (GCE//naf/CMECo(Sep) ³⁺ /fICYP3A4/naf)-----	165
4.3.3.1	(Electro)catalytic responses to co-substrate (oxygen) and substrate 2,4- dichlorophenol (2,4-DCP)-----	165
4.3.3.2	(Electro)catalytic response to native marker CYP450 3A4 substrate: Erythromycin -----	171
4.3.3.3	Electrocatalytic behaviour in the presence of inhibitor: ketoconazole-----	175
4.3.2.5	Critical assessment and additional observations of electrocatalytic behaviour of biosensor: A closer look at the bio-electrocatalytic response -----	176
4.3.4	Performance aspects: reproducibility and stability -----	179
4.4	CONCLUSIONS-----	180
4.5	EXPERIMENTAL PROTOCOLS-----	182
4.5.1	Reagents and Materials-----	182

4.5.2	Preparation of biosensor for voltammetric analysis -----	182
4.5.2.1	Pre-treatment of working electrode-----	182
4.5.2.2	Preparation of GCE naf CMECo(Sep) ³⁺ fICYP3A4 naf biosensor -----	183
4.5.3	Biosensor response experiments -----	183
4.5.3.1	Inhibition Experiments with Ketoconazole -----	184
CHAPTER 5 -----		185
RESULTS AND DISCUSSION: BIOSENSOR PLATFORM 2-----		185
CHAPTER PRELUDE -----		186
ABSTRACT -----		187
5A.1	INTRODUCTION -----	188
5A.2	ASSEMBLY: ELECTROCHEMICAL CHARACTERISATION OF THE GCE NAF EL-CO(SEP) ³⁺ 189	
5A.2.1	Long-term stability of the GC Naf El-Co(Sep) ³⁺ film-----	201
5A.2.2	Electrochemical behavior of GCE Naf Co(Sep) ³⁺ with Ruthenium(III) hexaamine redox probe -----	206
5A.3	MORPHOLOGICAL AND STRUCTURAL CHARACTERIZATION OF THE NAF-EL-CO(SEP) ³⁺ FILM -----	209
5A.3.1	Morphological characterization: Scanning Electron Microscopy (SEM) -----	210
5A.3.2	Structural characterization: Fourier Transform Infrared Spectroscopy (FTIR)-----	212
5A.4	CONCLUSIONS -----	217
CHAPTER 5B -----		218
N-TERMINALLY MODIFIED GENETICALLY ENGINEERED HUMAN RECOMBINANT P450-3A4 (NCYP3A4) BIOSENSOR FOR THE DETERMINATION OF PROTEASE INHIBITOR ARV DRUG, INDINAVIR: -----		218
5B.1	INTRODUCTION -----	220
5B.2	STRUCTURAL ASPECTS OF THE GENETICALLY ENGINEERED HIS ₆ -TAGGED N- TERMINALLY MODIFIED RECOMBINANT CYP3A4 (NCYP3A4) -----	223
5B.2.1	Fourier transform infrared spectroscopy (FTIR) characterization [151-152] -----	224
5B.2.2	Spectrophotometric characterization: UV-Vis Spectroscopy -----	226
5B.3	ASSEMBLY AND ELECTROCHEMICAL CHARACTERIZATION OF THE HYDROGEL-BASED ENZYME BIOSENSORS PREPARED ON GLASSY CARBON ELECTRODE -----	230

5B.3.1	Electrode Assembly: Optimisation of the variables concerning the indinavir amperometric biosensor assembly and behaviour -----	230
5B.3.1.1	The effect of carrier matrix assembly: Optimisation of constituents and method of preparation -----	230
5B.3.1.2	Outer layer optimisation: Effect of film constituents and/or ratio-----	239
5B.3.1.3	Optimisation of Enzyme (nCYP3A4) loading -----	243
5B.3.1.4	Optimisation of potentiostatic electro-deposition time for Co(Sep) ³⁺ -----	245
5B.3.2	Voltammetric characterization of the fabricated biosensor (prepared under optimized conditions): General electrochemical behaviour in anaerobic conditions -----	249
5.B.3.3	Bio-electrocatalytic activity of the GCE naf-El-Co(Sep) ³⁺ nCYP3A4 -PVA-PEI-Agrs biosensor	257
5B.3.3.1	Bio-electrocatalytic response to molecular oxygen and substrate (indinavir)	258
5B.5	MATERIALS AND METHODS OF INVESTIGATION-----	288
5B.5.1	Preparation of Recombinant N-terminally modified CYP3A4 (nCYP3A4) -----	288
5B.5.1.1	Reagents and materials -----	288
5B.5.1.2	Expression and purification of CYP3A4 construct -----	289
5B.5.1.2.1	Construct expression for CYP3A4/Preculture innoculation -----	289
5B.5.1.2.2	Preparation of the crude lysates-----	291
5B.5.1.2.3	Protein purification -----	291
5B.5.1.3	Total protein quantification-----	292
5B.5.1.3	Spectral analysis of and activity assays the prepared nCYP3A4 construct -	293
5B.5.1.3.1	FTIR spectral analysis-----	293
5B.5.1.3.2	UV-Vis spectra of resting state nCYP3A4 (nCYP3A4-Fe ³⁺) construct --	294
5B.5.1.3.3	Activity assay for the nCYP3A4 construct: Carbon monoxide complex-	294
5B.5.2	Methods and protocols for biosensor preparation, optimisation studies and voltammetric investigations -----	295
Table 5B.2	----- Materials and reagents used	295
5B.5.2.1	Preparation of Co(Sep) ³⁺ -mediated nCYP3A4-based biosensor (under optimized conditions) for voltammetric characterization and catalytic investigations --	296
5B.5.2.2	Preparation of un-mediated nCYP3A4-based biosensor for voltammetric characterization and catalytic investigations -----	297
5B.5.2.3	Preparation of the Co(Sep) ³⁺ based control sensor platform -----	298

5B.5.2.4	Preparation of the platforms for optimisation of the variables concerning the indinavir amperometric biosensor-----	298
5B.5.2.4.1	Preparation of Co(Sep) ³⁺ -mediated nCYP3A4-based biosensor platform with Eastman-AQ as base layer and crosslinked PVA as outer film-----	298
5B.5.2.4.2	Preparation of Co(Sep) ³⁺ -mediated nCYP3A4-based biosensor platform with nafion as base layer and crosslinked PVA as outer film-----	299
5B.5.2.4.2	Preparation of Co(Sep) ³⁺ -mediated nCYP3A4-based biosensor platform with nafion as base layer and crosslinked PVA as outer film-----	300
5B.5.2.4.3	Preparation of biosensor platforms for nCYP3A4 loading optimisation studies	300
5B.5.2.4.4	Preparation of biosensor platforms for Co(Sep) ³⁺ potentiostatic loading time optimisation studies-----	300
5B.5.2.4	Procedures for voltammetric characterization of the prepared platforms ---	301
5B.5.2.5	Procedures for catalytic response investigations-----	302
5B.5.2.6	Procedures for investigations of optimization of the variables -----	302
CHAPTER 6	-----	303
SUMMARY AND CONCLUSIONS	-----	303
6.1	INTRODUCTION -----	303
6.2	SUMMARY OF INDIVIDUAL RESULTS CHAPTERS-----	303
6.2.1	Chapter 4 -----	303
6.2.2	Chapter 5A -----	306
6.2.3	Chapter 5B -----	308
6.3	CRITICAL OVERVIEW OF THE STUDIES IN THIS DISSERTATION -----	310
6.4	RECOMMENDATIONS FOR FUTURE STUDY -----	311
6.5	OVERALL SIGNIFICANCE OF THE STUDY-----	312
REFERENCES	-----	314
APPENDIX	-----	327

List of Figures

	Title	Page
Figure 1.1	HIV/AIDS virus and mechanism of action of action of protease inhibitor ARV, Indinavir	32
Figure 1.2	(a) Ribbon drawing, showing the distal face view of cytochrome P450-3A4 (CYP3A4) secondary/tertiary structure a); (b) Prosthetic group of CYP3A4, (b-type heme): an iron-(III) protoporphyrin-IX linked with a proximal cystein ligand (fifth ligand of the heme iron)	38
Figure 1.3	Natural catalytic cycle of human hepatic microsomal CYP3A4	39
Figure 2.1	Schematic representation of biosensor components and operation	64
Figure 2.2	Contribution of major human hepatic cytochromes P450 isozymes ad non-P450 enzymes to phase I metabolism of all xenobiotics	72
Figure 2.3	Physiological catalytic reaction cycle of CYP3A4, showing enzyme-substrate interaction and natural electron transfer (ET) donor source, with general equation shown. Also shown, is the alternative sources of ET for CYP3A4 substrate catalytic function.	73
Figure 2.4	major immobilization methods for protiens, enzymes and other biological molecules onto solid (electrode) supports	81
Figure 2.5	Principle of operation of amperometric mediated biosensor	99
Figure 2.6	(a)The cage-type N-donor macrbicycle: Sepulchrates (b) Sepulchrates with incorporated Co(III) transition metal ion: Cobalt(III)sepulchrates	102
Figure 2.7	The structure of nafion®	105
Figure 2.8	Nafion structure showing schematic presentation of the different phases observable in a nafion membrane. The sulphonate groups are clustered in hydrophilic inclusions, referred to as phase A . Phase B referes to the teflon-like fluorocarbon backbone, and is essentially hydrophobic. Phase C is intermediate in	107

hydrophilicity.

Figure 2.9	The characteristic ionic sulfo cluster network in a Nafion membrane	108
Figure 2.10	Structure of Agarose	114
Figure 2.11	Structure of Poly(vinyl alcohol)	116
Figure 2.12	Structure of Polyethyleneimine (PEI)	117
Figure 3A.1	Potential-time excitation signal in cyclic voltammetric experiment	128
Figure 3A.2	Basic parameters for a cyclic voltammogram: E_{pa} refers to the potential of the anodic (forward) peak; E_{pc} represents the potential of the cathodic (reverse) peak; E_{λ} is the potential value at the inversion of the scan direction (switch potential); I_{pa} represents the current of the forward peak with respect to its baseline; i_{pc} is the cathodic (reverse) peak current with respect to its baseline; $(i_f)_0$ is the current at the inversion potential with respect to the zero current baseline	129
Figure3A.3	Cyclic voltammograms for irreversible (curve A) and quasi-reversible (curve B) redox processes.	133
Figure3A.4	Ideal cyclic voltammetric behaviour for reduction and oxidation of adsorbed/surface confined species. The surface coverage, Γ , can be obtained from the area under the peak	138
Figure3A.5	Time-potential waveform profile for square wave voltammetry. Showing initial potential, E_i ; pulse height (amplitude), E_p ; step height, E_{sh} ; pulse width, t_p (also known as square wave period), forward current- and reverse current sample	141
Figure3A.6	Typical square wave voltammogram exhibiting reversible electrochemistry	142
Figure3A.7	Potential wave form and time-dependence of applied potential in differential pulse voltammetry	144
Figure3A.8	A typical electrochemical cell used during a routine electrochemical investigation	146
Figure3A.9	Initial velocity v_i as a function of substrate concentration [S] for	157

enzyme-catalyzed reaction following Michaelis–Menten kinetics

Figure3A.10	Lineweaver-Burk double reciprocal plot of $1/v$ vs $1/[S]$ for the dependence of enzyme-catalyzed reaction velocity on substrate concentration	159
Figure 3B.1	Showing method of FTIR analysis with high-pressure anvil cell for dry samples	174
Figure 4.1	Top scanning electrochemical image of electrode (a) blank electrode (bl-E); (b) nafion modified electrode (Naf-E); (c) Naf-E with pre-concentrated $\text{Co}(\text{Sep})^{3+}$	181
Figure 4.2	Fourier Transform Infrared Spectroscopic (FTIR) spectra of (a) un-modified nafion membrane; (b) commercially obtained, pure cobalt (III) sepulchrates only; the nafion membrane modified with the chemically deposited $\text{Naf-Co}(\text{Sep})^{3+}$ -composite film $\text{naf CMeco}(\text{Sep})^{3+}$	184
Figure 4.3	Cyclic voltammogram of bare GCE in phosphate buffer saline (PBL, pH 7.4) containing 1 mM $\text{Co}(\text{Sep})^{3+}$. Inset shows the square wave (SW) voltammetric response of the GCE in 1 mM $\text{Co}(\text{Sep})^{3+}$, exhibited as the difference SW.	186
Figure 4.4	(a) Cyclic voltammetric response for the nafion-coated GCE (GCE naf), and the cobalt(III)sepulchrates modified- GCE naf (i.e., $\text{GC naf CMeco}(\text{Sep})^{3+} naf$) for experiments conducted in argon-degassed (Ar) 50 mM PBL at 10 mV s^{-1} . (b) Square wave voltammetric response of the $\text{GC naf CMeco}(\text{Sep})^{3+} naf$ also in ArPBL, presented as the difference spectrum. Experimental conditions: StepE = 4 mV; amplitude = 75 mV	189
Figure 4.5	(a) Cyclic voltammetric response for the flCYP3A4 based biosensor, i.e., $\text{naf flCYP3A4 Co}(\text{Sep})^{3+} naf \text{GC}$ electrode, for experiment conducted in argon-degassed (Ar) 50 mM PBL at 10 mV s^{-1} . (b) Square wave voltammetric response of the $\text{naf flCYP3A4 Co}(\text{Sep})^{3+} naf \text{GC}$ electrode in ArPBL, presented as the difference spectrum. (Plot shows the net current of the forward and reverse SWV response for a scan that was done cathodically). Experimental conditions are: square-wave amplitude 75 mV; potential step 4 mV. StepE = 4 mV; amplitude = 75 mV	191
Figure 4.6	Cyclic voltammograms of $\text{Naf CYP3A4 Co(III)Sep-Naf}$ -film in	194

phosphate buffer saline (pH 7.4) at scan rates 20 – 1500 mVs⁻¹.
 Inset: Plot of cathodic and anodic peak current vs $v^{1/2}$.

- Figure 4.7 Cyclic voltammograms of GCE||naf|CMECo(Sep)³⁺|naf 197
 (biosensor) in 50 mM PBS at 10 mV s⁻¹, showing: (a) biosensor
 in anaerobic PBS with 0 μM 2,4-DCP; (b) anaerobic PBL with
 11.04 μM 2,4-DCP; (c) air-saturated PBS containing 0 μM 2,4-
 DCP; (d) air-saturated PBL containing 11.04 μM 2,4-DCP
- Figure 4.8 Voltammetric response of the GCE||naf|CMECo(Sep)³⁺|naf 197
 biosensor, showing background capacitive current-subtracted
 CVs in: (a) the presence of
- Figure 4.9 Square wave voltammetric response of 199
 GCE||naf|CMECo(Sep)³⁺|f|CYP3A4|naf biosensor in 50 mM un-
 degassed PBL containing 0 → 264 μM 2,4-DC
- Figure 4.10 Dependence of catalytic peak current 200
 GCE||naf|CMECo(Sep)³⁺|f|CYP3A4|naf biosensor for 2,4-DCP
 for experiment performed in un-degassed 50 mM PBL
- Figure 4.11 Cyclic voltammograms of 202
 GCE||naf|CMECo(Sep)³⁺|f|CYP3A4|naf biosensor in 50 mM PBS
 at 10 mV s⁻¹, showing: (a) biosensor in anaerobic PBS with 0 mM
 erythromycin (ERM); (b) anaerobic PBS with 2.18 mM ERM; (c)
 air-saturated PBS containing 0 mM ERM; (d) air-saturated PBS
 containing 2.18 mM ERM
- Figure 4.12 Square wave voltammetric response of 203
 GCE||naf|CMECo(Sep)³⁺|f|CYP3A4|naf biosensor in 50 mM un-
 degassed PBS containing 0 → 164.4 μM erythromycin
- Figure 4.13 Full calibration plot for response of GCE||naf|CMECo(Sep)³⁺|naf 203
 biosensor to ERM for experiment performed in un-degassed 50
 mM PBS. Inset: Linear curve for 2,4-DCP
- Figure 4.14 Square wave voltammograms of GCE||naf|CMECo(Sep)³⁺|f|CYP3A4|naf 204
 biosensor in 50 mM air-saturated PBS: showing biosensor
 response to 2,4-DCP before (a) and after incubations with
 enzyme inhibitor, ketoconazole (b – d)
- Figure 4.15 Repeatability of measurements: Showing response of 209
 GCE||naf|CMECo(Sep)³⁺|f|CYP3A4|naf biosensor in oxygenated
 PBS to 24 μM for five consecutive measurements, with
 intermittent rinsing

Figure 5A.1	Cyclic voltammogram of GCE Naf at 10 mV s ⁻¹ in argon-degassed phosphate buffer (50 mM, pH 7.45)	220
Figure 5A.2	Voltammetric response of the nafion-cobalt(III) sepulchrate composite film, GC Naf El-Co(Sep) ³ in argon-degassed PB. Cyclic voltammogram taken at 3 mV s ⁻¹ , with cathodic and anodic waves indicated by negative and positive currents, respectively. Experimental conditions for square wave: StepE = 4 mV; S.W. amplitude = 25 mV; frequency = 1 Hz.	223
Figure 5A.3	Cyclic voltammograms of GC Naf El-Co(Sep) ³ showing voltammetric response in argon-degassed PB with increasing scan rate (4 – 50 mV s ⁻¹). Inset: Influence of scan rate on cathodic (I _{p,c}) and anodic (I _{p,c}) peak current	228
Figure5A.4	Plots of log I _p vs log v for cathodic and anodic peak currents, to show influence of scan rate on peak current for GC Naf El-Co(Sep) ³⁺ films	230
Figure5A.5	Cyclic voltammetric reponse showing variation in Faradaic current and peak parameters (I _{p,c} ; I _{p,a} ; E _{p,c} ; E _{p,a}) of the GC Naf El-Co(Sep) ³⁺ films with numbers on the curves denoting days elapsed after fabrication. The voltammograms were recorded in anaerobic PB (50 mM; pH 7.45)	232
Figure5A.6	Cyclic voltammograms (5 mV s ⁻¹) of the GC Naf El-Co(Sep) ³⁺ electrode in anaerobic PB containing 1 mM ruthenium(III) hexamine chloride [Ru(NH ₃) ₆ Cl ₃]. Voltammograms at 0-, 1-, 3-, and 6 hours are shown	237
Figure5A.7	Cyclic voltammograms showing the influence of scan rate on oxidation and reduction peak current for 1 mM ruthenium(III) hexamine chloride [Ru(NH ₃) ₆ Cl ₃], in 50 mM PB (pH 7.4) at the GC Naf El-Co(Sep) ³⁺ electrode. Scan rates in order of increasing peak height are 10, 20, 30, 40, 50, 60, 70, 80, 90, 100, 110, 120, 130, 140 and 150 mV s ⁻¹ . In set shows the linear relationship between peak current (I _{p,c} and I _{p,a}) and v ^{1/2} , with determined slopes	238
Figure5A.8	Top Scanning electrochemical microscopy images of electrode and films: (a) blank screen printed electrode (bSPE); (b) Naf modified SPE (nafSPE); (c) nafSPE with pre-concentrated Co(Sep) ³⁺ (SPE naf El-Co(Sep) ³⁺)	240
Figure 5A.9	Fourier Transform Infrared Spectroscopy (FTIR) spectra of (a) unmodified nafion membrane; (b) commercially obtained cobalt	244

- sepulchrates
- Figure 5B.1 Fourier transform infrared (FTIR) spectra of the pure synthesized N-terminally modified CYP3A4 construct (nCYP3A4). Inset shows full spectrum as obtained directly from FTIR analysis. Main spectrum shows the relevant spectral range for bands associated solely from nCYP3A4, restricted to the region of $1830\text{ cm}^{-1} - 1140\text{ cm}^{-1}$ 255
- Figure 5B.2 Electronic absorption spectra for the synthesized, N-terminally modified CYP450 3A4 (nCYP3A4). The UV-Vis absorption spectrum for pure nCYP3A4 (concentration μM) showing (a) nCYP3A4 in its resting low-spin Fe^{III} state; inset (b) nCYP3A4- Fe^{II} -carbon monoxide, prepared by reducing nCYP3A4 Fe^{III} with excess sodium dithionite and saturating with CO by bubbling for 2 min. Spectra in (b) were difference spectra taken against references of reduced nCYP3A4 before addition of CO. Working solution of nCYP3A4 was 20 mM potassium phosphate buffer, pH 7.40, 20% glycerol, EDTA, DTT 258
- Figure 5B.3(I-III) Voltammetric behaviour and electrocatalytic response of the nCYP3A4-based biosensor, fabricated from EastmanAQ(EAQ)-Co(Sep) $^{3+}$ carrier matrix (i.e. GCE||EAQ|Co(Sep) $^{3+}$ |nCYP3A4): plotI: CVs illustrating the biosensor in argon-degassed phosphate buffer solution (ArPBS) with increased equilibration time; plotII: cyclic voltammetric response of the biosensor in ArPBS (a), in the presence of dissolved oxygen (b), in the presence of $0.5\ \mu\text{M}$ indinavir in un-degassed PBS (c); plotIII: square wave voltammetric response to dissolved oxygen (b) and indinavir (c). Co(Sep) $^{3+}$ was pre-concentrated on pre-formed ionomer ionic polymer (nafion or EAQ film, respectively) by potentiostatic deposition at +450 mV. Arrows show the trend of the variation in peak current. 264
- Figure 5B.4 Cyclic voltammetric response of the GCE|naf|El-Co(Sep) $^{3+}$ |nCYP3A4|ClPVA biosensor in argon-degassed PBS, showing $E_{p,c}$ and $I_{p,a}$ variation with increased equilibration time, from 0 up to 60 min. Arrows show the trend of the variation in I_p . 266
- Figure 5B.5 (I): Voltammetric response of GC|naf|El-Co(Sep) $^{3+}$ |nCYP3A4|ClPVA electrode in (a) argon-degassed PBS; (b) un-degassed PBS; O $_2$ PBS containing $22.45\ \mu\text{M}$ indinavir. (II): Biosensor response to indinavir at concentrations ranging from $0.05\ \mu\text{M}$ up to $96.95\ \mu\text{M}$. Inset shows the linear calibration curve for the biosensor. 267
- Figure 5B.6 Voltammetric response of GC|naf|El-Co(Sep) $^{3+}$ |nCYP3A4|PVA-PEI-Ag electrode in: (a) argon-degassed PBS (ArPBS); (b) 270

response after 60min equilibration in aerobic conditions (OxPBS); and after ± 210 min in OxPBS (II). Note: The outerlayer of the biosensor is prepared with a ratio of PEI : PVA-Agrs of 0.25 : 1 (v/v). Experimental conditions: CVs taken in PB, pH 7.4 at 10 mV s^{-1} ; reductively scanned: $E_i = -100 \text{ mV}$, $E_f = -950 \text{ mV}$

- Figure5B.7 Voltammetric response of $\text{GC}|\text{naf}|\text{E}|\text{Co}(\text{Sep})^{3+}|\text{nCYP3A4}|\text{PVA-PEI-Agrs}$ electrode in: (a) argon-deaerated PBS (ArPBS); inset: response to dissolved molecular oxygen in aerobic conditions; Parameters: Ratio of biosensor outer-layer (PEI:PVA-Agrs) = 0.1 : 1 (v/v). Experimental conditions: CVs taken in PB, pH 7.4 at 10 mV s^{-1} ; reductively scanned: $E_i = -100 \text{ mV}$, $E_f = -950 \text{ mV}$. 272
- Figure5B.8 Effect of nCYP3A4 loading amount on the bio-electrocatalytic response of the nCYP3A4-based biosensor [$\text{GCE}|\text{naf}|\text{E}|\text{Co}(\text{Sep})^{3+}|\text{nCYP3A4}|\text{Agrs-PEI-PVA}$]. Slopes obtained from indinavir calibration plots in the $0.05 - 25.60 \mu\text{M}$ concentration range. Supporting electrolyte: 0.05 M aerobic PB (pH 7.4) 274
- Figure5B.9 Effect of $\text{Co}(\text{Sep})^{3+}$ electrostatic deposition loading time on bio-electrocatalytic response of the $\text{GCE}|\text{naf}|\text{E}|\text{Co}(\text{Sep})^{3+}|\text{nCYP3A4}|\text{Agrs-PEI-PVA}$ biosensor. Showing slopes of indinavir calibration plots in the $0.05 - 25.60 \mu\text{M}$ concentration range. Supporting electrolyte: 0.05 M aerobic PB (pH 7.4) 278
- Figure5B.10 Cyclic voltammetric response of (a) $\text{GC}|\text{naf}|\text{nCYP3A4}|\text{Agrs-PEI-PVA}$ electrode; (b) $\text{GCE}|\text{naf}|\text{Co}(\text{Sep})^{3+}|\text{nCYP3A4}|\text{Agrs-PEI-PVA}$ biosensor. Scans taken in substrate-free argon-degassed PB solution at $v = 3 \text{ mV s}^{-1}$. Scans done reductively, thus negative scan represent $I_{p,c}$ (cathodic) 281
- Figure5B.11 (a) Square wave (SW) voltammetry response of the $\text{GCE}|\text{naf}|\text{Co}(\text{Sep})^{3+}|\text{nCYP3A4}|\text{Agrs-PEI-PVA}$ biosensor (plot shows the difference SW current obtained for a cathodic scan). (b) Differential pulse waves, showing cathodic (red) and anodic scans for the $\text{GCE}|\text{naf}|\text{Co}(\text{Sep})^{3+}|\text{nCYP3A4}|\text{Agrs-PEI-PVA}$ biosensor. Experimental conditions: All scans were taken in substrate-free, argon-degassed PBS (pH 7.45). SWV: square wave amplitude 25 mV; potential step 4 mV. DPV: pulse amplitude 25 mV; sample width of 15 ms; pulse period of 200 ms 283
- Figure5B.12 Influence of scan rate on peak current. Inset: $I_{p,c}$ and $I_{p,a}$ as a function of $v^{1/2}$ for scan rates of $3 - 10 \text{ mV s}^{-1}$ 285

Figure5B.13	Influence of scan rate on cathodic peak potential for a GC naf El-Co(Sep) ³⁺ nCYP3A4 Agrs-PEI-PVA electrode	287
Figure5B.14	I: Cyclic voltammograms of the GC naf nCYP3A4 Agrs-PEI-PVA electrode in 50 mM PBS, showing biosensor response in (a) substrate-free argon-degassed PBS; (b) air-saturated PBS with 0 μ M indinavir; (c) air-saturated PBS with 14 μ M indinavir. II: square wave voltammograms of the GC naf nCYP3A4 Agrs-PEI-PVA electrode, showing response in (a) substrate-free argon-degassed PBS; (b) air-saturated PBS with 0 μ M indinavir; air-saturated PBS with (c) 1 μ M, (d) 2 μ M and (e) 14 μ M indinavir, respectively. Experimental conditions are: CVs scanned cathodically at 5 mVs-1. SWVs: square wave amplitude 25 mV; potential step 4 mV (showing difference SWs)	290
Figure5B.15	Cyclic voltammograms showing: (a) response of nCYP3A4-based biosensor, (GCE naf El-Co(Sep) ³⁺ nCYP3A4 Agrs-PEI-PVA) in argon-degassed PBS containing 0 μ M indinavir; (b) response of nCYP3A4-based biosensor in air-saturated PBS containing 0 μ M indinavir; (c) response of nCYP3A4-based biosensor in air-saturated PBS containing 5 μ M indinavir. (d – e): negative control, showing BSA-based control sensor in (d) air-saturated PBS containing 0 μ M indinavir; (e) air-saturated PBS containing 5 μ M indinavir	295
Figure5B.16	Square wave voltammograms showing: (a) response of nCYP3A4-based biosensor, (GCE naf El-Co(Sep) ³⁺ nCYP3A4 Agrs-PEI-PVA) in air-saturated PBS containing 0 μ M indinavir; (b) response of nCYP3A4-based biosensor in air-saturated PBS containing 5 μ M indinavir; (d) – (e) negative control showing: response of BSA-based control sensor (GCE naf El-Co(Sep) ³⁺ BSA Agrs-PEI-PVA) in air-saturated PBS containing 0 μ M indinavir [i.e. (a)] and response of BSA-based control sensor in air-saturated PBS containing 5 μ M indinavir	296
Figure5B.17	Square wave voltammograms showing response of GC naf El-Co(Sep) ³⁺ nCYP3A4 Agrs-PEI-PVA electrode to increasing indinavir concentrations, from 0 μ M up to a final concentration of 73 μ M	298
Figure 5B.18	Square wave voltammograms for the potential region of -490 \rightarrow -950 Mv for the GC naf El-Co(Sep) ³⁺ nCYP3A4 Agrs-PEI-PVA	298

electrode, for an experiment done with increasing indianvir concentrations (0 → 73 μM). Experimental conditions are: square wave amplitude 25 mV; potential step 4 mV. (Plots show the nett currents obtained from scans done cathodically)

- Figure 5B.19 Negative control: square wave voltammograms showing reactivity of BSA-based control sensor (GCE||naf|El-Co(Sep)³⁺|BSA|Agrs-PEI-PVA) with increasing indinavir concentrations from 0 → 16 μM in air-saturated PBS. Inset (i.e. II) shows the redox behaviour of the GC||naf|El-Co(Sep)³⁺|BSA|Agrs-PEI-PVA electrode in substrate-free argon-degassed PBS. Experimental conditions are: square wave amplitude 25 mV; potential step 4 mV. (Plots show the nett currents obtained from scans done cathodically) 300
- Figure 5B.20 Comparisons of effect of oxygen : Cyclic voltammograms showing: (a) (GC||naf|El-Co(Sep)³⁺|nCYP3A4|Agrs-PEI-PVA) electrode containing fresh nCYP3A4, (b) (GC||naf|El-Co(Sep)³⁺|nCYP3A4|Agrs-PEI-PVA) electrode containing nCYP3A4 which have been stored for □ six-eight months; (c) (GC||naf|El-Co(Sep)³⁺|BSA|Agrs-PEI-PVA) electrode (BSA-control) in substrate-free air-saturated PBS. 302
- Figure 5B.21 Calibration curves for GCE||naf|El-Co(Sep)³⁺|nCYP3A4|Agrs-PEI-PVA biosensor response to indinavir for the concentration range, 0.05 □ 147.5 □M. Inset shows the linear region. 305
- Figure 5B.22 Schematic representation of the reactions occurring at the modified glassy carbon working electrode during electrocatalysis experiments. 316
- Figure 5B.23 Suggested general scheme of the electrocatalytic reaction of nCYP3A4 (mediated by Co(Sep)^{3+/2+}) in the presence of oxygen. The presence of bound substrate is marked by (RH). All reaction pathways are included in a catalytic cycle for better indination/illustration of the possible processes. 316
- Figure 5B.24 Showing method of FTIR analysis with high-pressure anvil cell for wet nCYP3A4 samples 323

List of Tables

	Title	Page
Table 2.1	Biosensor transduction systems and measuring modes	66
Table 3.2	Summary of diagnostic criteria for electrochemical reversibility, irreversibility and quasi-reversibility of a redox couple, obtainable from cyclic voltammetric investigation	163
Table 3B.1	A complete comprehensive list of all materials used during the conduction of this PhD research investigation; listed also are sources and specific information	
Table 5B.1	Peak parameters as obtained from GCE naf El-Co(Sep) ³⁺ ; GCE naf El-Co(Sep) ³⁺ BSA Agrs-PEI-PVA (control sensor); GCE naf El-Co(Sep) ³⁺ nCYP3A4 Agrs-PEI-PVA	281
Table 5B.2	Materials and Reagents used	325



Acronyms and Abbreviations

AIDS	Acquired immune deficiency syndrome
ARV	Antiretroviral
CHAPS	3-[(3-chloramidopropyl)dimethylammonio]-1-propanesulphonate
CV	Cyclic Voltammetry
Co(Sep)	Cobalt(III) sepulchrate
CYP450	cytochrome P450
DET	Direct electron transfer
DDAB	Didodecyl dimethylammonium bromide
DPV	Differential pulse voltammetry
DWEL	Drinking water equivalent
E_m	Midpoint potential
$E^{0'}$	Formal potential
EAQ	Eastman AQ-55
EPA	USA Environmental Protection Agency
ET	Electron transfer
E_λ	Switch potential
E_p	Peak potential
$E_{p,c}$	Cathodic peak potential
$E_{p,a}$	Anodic peak potential
HIV	Human immunodeficiency virus
$I_{p,c}$	Cathodic peak current
$I_{p,a}$	Anodic peak current
KPBS	Potassium phosphate buffer solution
NADPH	
nCYP3A4	genetically engineered N-terminally modified cytochrome P450 3A4
NRTIs	Nucleoside reverse transcriptase inhibitors
NNRTIs	Nonnucleoside reverse transcriptase inhibitors
PBL	Sodium phosphate buffer saline
PBS	Sodium phosphate buffer solution
PDDA	Poly-(dimethyldiallylammonium chloride)
PI	Protease inhibitors
SWV	Square wave voltammetry
TDM	Therapeutic drug monitoring

List of Publications and Presentations

Papers

1. A. Ignaszak, N. Hendricks, T. Waryo, E. Songa, N. Jahed, R. Ngece, A. Al-Ahmed, B. Karebe, P. Baker, E.I. Iwuoha (2009). Novel therapeutic biosensor for indinavir – protease inhibitor antiretroviral drug. *Journal of Pharmaceutical and Biomedical Analysis*, 49: 498-501.
2. N.R. Hendricks, T. Waryo, O. Arotiba, N. Jahed, P.G.L. Baker, E.I Iwuoha (2009). Microsomal cytochrome P450-3A4 (CYP3A4) nanobiosensor for the determination of 2,4-dichlorophenol – An endocrine disruptor compound. *Electrochimica Acta* 54: 1925-1931.
3. N.R. Hendricks, P.G.L. Baker, E.I Iwuoha. Protein film electrochemistry of human recombinant CYP3A4 and electrocatalysis of Protease Inhibitor Antiretroviral Drug, Indinavir. *Submitted to European Journal of Pharmacology 2010*.
4. N.R. Hendricks, P.G.L. Baker, E.I Iwuoha. Amperometric CYP3A4 nanosensor system based on layer-by-layer assembly of polyaniline on carbon nanotube. *Submitted to Sensors 2010*.

Oral and Poster Presentations at Conferences

1. **2nd Southern Eastern Africa Network of Analytical Chemists (SEANIC)**,
Gaborone, Botswana, 16-19 July 2007
“*Nanobiosensor for protease inhibitor antiretroviral drugs*”
Iwuoha, E.; Hendricks, N.; Baker, P.; Al-Ahmed, A.; Ignaszak

2. **6th Spring Meeting of the International Society of Electrochemistry,**
Foz do Iguaçu, Brazil, 16 – 19 March 2008
“Microsomal CYP3A4 nanobiosensor for the determination of 2,4-dichlorophenol – An endocrine disruptor compound”.
Hendricks, N.R.; Waryo, T.; Baker, P.; Iwuoha, E.

3. **Electrochem South Africa (ECSA) International Symposium,**
Library Auditorium, University of the Western Cape, Cape Town, 9 – 11 July, 2008
Human recombinant cytochrome P450-3A4 (CYP3A4) biosensor for detection of protease inhibitor antiretroviral drug (Indinavir) and priority pollutant (2,4-Dichlorophenol).
Hendricks, N.R.; Jahed, N.; Baker, P.G.; Iwuoha, E.I.

4. **DST/Mintek Nanotechnology Innovation Centre (Sensors) Workshop,**
Gavin Relly Post Grad Village, Rhodes University, Grahamstown, 10 – 12 September 2008

UNIVERSITY of the WESTERN CAPE

5. **39th Convention of the South African Chemical Institute Conference,**
The conservator, University of Stellenbosch, Cape Town, 30th November – 5th December 2008.
Overoxidized polypyrrole-nanowire and gold nanoparticle composite for biosensor construction.
Hendricks, N.R.; West, N., Iwuoha, E.; Baker, P.; Blackburn, J.; Beeton-Kempton,



UNIVERSITY *of the*
WESTERN CAPE



UNIVERSITY *of the*
WESTERN CAPE

CHAPTER 1

General Introduction

1.1 Introduction

This thesis describes the electrochemical dynamics of cytochrome P450-3A4 isoenzyme biosensor for protease inhibitor (PI) antiretroviral drug. Chapter 1 gives a comprehensive overview of protease inhibitor antiretroviral (ARV) drugs and ARV agents in general. Special elaboration was dedicated to the PI, indinavir, since it is the model drug that was used during the experimental investigation for this study. In addition, other relevant subjects, including cytochrome P450 isozymes, therapeutic drug monitoring, biosensors and drug assay methods were also discussed. Since endocrine disruptor compound, 2,4-dichlorophenol was also used in a subsection of the research investigation, relevant aspects surrounding the chemical was also elaborated on. The latter division of this chapter included the research questions, problem statements, rational/motivation, objectives and sub-objectives, followed by a layout of the thesis.

1.2 Background

1.2.1 Indinavir and HIV/AIDS: background overview and related aspects

The HIV protease enzyme is a critical component of the replicative cycle of the virus. It processes polypeptides transcribed from the gag and pol genes late in

the viral replicative cycle – research has shown that this transcriptional process is essential for the assembly and maturation of infectious virions, and that inhibition of this enzyme leads to production of immature non-infectious viral progeny [1]. In this regard, indinavir (L-735,524; MK-0639; Crixivan), a protease inhibitor (PI) antiretroviral (ARV), with high oral bioavailability, is a mechanism-based designed drug, explicitly formulated to interrupt this specific biochemical pathway of the viral replication cycle. A schematic representation of the HIV/AIDS virus and the mechanism of action of PI ARV, indinavir, is shown in **Figure 1.1**.

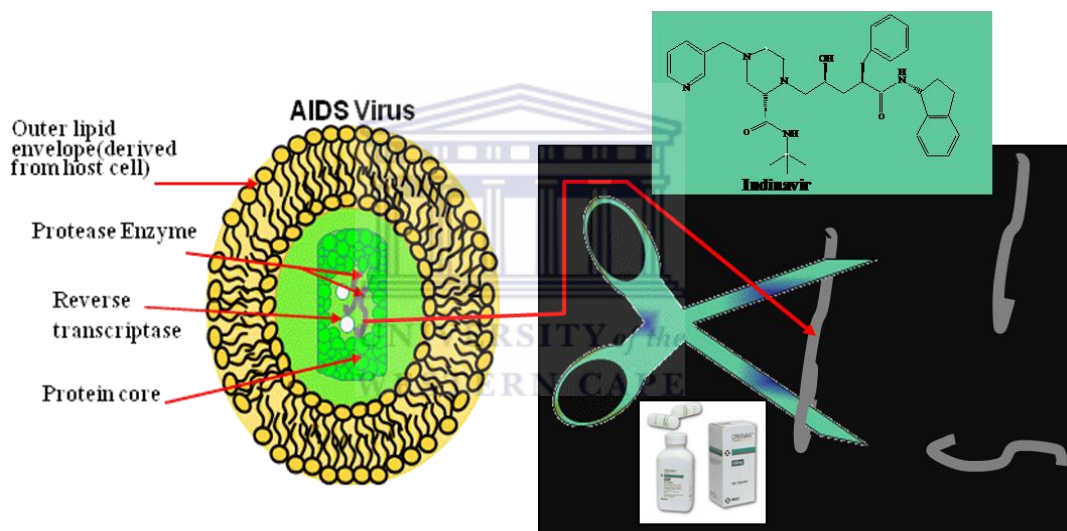
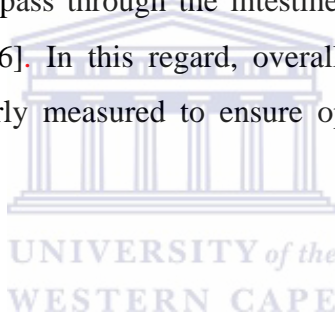


Figure 1.1: HIV/AIDS virus and mechanism of action of action of protease inhibitor ARV, Indinavir

As observed in **Figure 1**, indinavir functions by targeting the viral protease enzyme, inhibiting it and subsequently inactivating the enzyme, concomitantly leading to the production of immature non-infectious viral offspring [1-2], which in turn, keeps viral load at bay. Moreover, the qualitative attributes of indinavir is also exemplified in its ability to cross the blood-brain barrier (BBB) – this being a pivotal factor in treatment regimens, due to the highly probable risk factor of AIDS patients

developing behavioural disorders in the late stage of HIV infection, which results from the virus crossing the BBB and concomitantly affecting the individual's nervous system [1]. A noteworthy fact, however, is that successful HIV protease inhibition requires sustained, optimally high drug levels in the blood, particularly at the site of replication. These optimum drug concentrations are critical, not only to suppress viral replication, but also to reduce viral mutations. Moreover, this pivotal factor is a prerequisite for successful application of all clinically available ARVs, which includes the PIs, nonnucleoside reverse transcriptase inhibitors (NNRTIs) and the nucleoside analogues (NAs). These optimum drug concentrations is of course highly reliant on the oral bioavailability of the drug, which in turn depends on the rate of first pass metabolism, since the unique anatomical arrangement of our bodies is such that orally taken substances have to pass through the intestine and then liver, before reaching systematic circulation [3-6]. In this regard, overall, it is crucial that drug plasma concentrations are regularly measured to ensure optimum and sustained anti HIV effect [7].



Review of current literature have shown that of the three basic categories of ARVs, the PIs and NNRTIs undergo extensive hepatic first pass metabolism and as such share a similar metabolic pathway [2, 4, 8]. This essentially involves first pass oxidative metabolism by the cytochrome P450 (CYP450) enzymes present in the liver [2, 4], of which CYP450-3A4 (CYP3A4) is the most abundant isoform [3, 6, 9-10], and is as such primarily responsible for their metabolism [2, 4]. With respect to indinavir in particular, prior research investigations, based on in vitro and in vivo studies with regard to the pharmacokinetic fate of the drug, has shown it to have minimal extra-hepatic biotransformation – the drug actually determined to be exclusively metabolized by CYP3A4 [1, 11]. However, the variation in the magnitude and/or rate of first pass oxidative metabolism causes extensive inter-individual and ethnic variability [3, 7, 10, 12] – a finding that is not restricted to indinavir only, but pertains to the metabolism of all PI and NNRTI ARVs [2, 4]. This

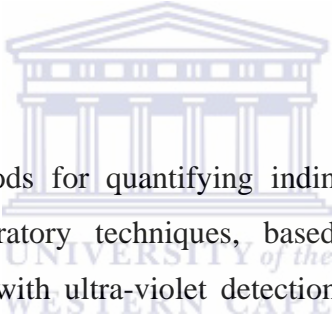
can result in significant unpredictability in the bioavailability and systematic clearance of these drugs, and in this regard, dosage must be tailored to allow for maximum efficacy and minimum toxicity, because as earlier stated, sub-optimal concentrations of these drugs will be ineffective. On the other hand, since HIV/AIDS is ubiquitously associated with a progressively deteriorating immune system, with patients inevitably suffering from a constellation of disorders – indinavir, like other PI drugs and ARVs in general, are always administered in combination regimens, as well as a plethora of other prescription drugs [2]. The combination therapy is referred to as Highly Active Antiretroviral Therapy (HAART) and since these drugs are administered at similar or overlapping time periods – the possibility of drug-drug interactions is highly probable. This is an especially crucial factor when the biotransformation of any two or more drugs share the same metabolic pathway, as they will thus compete for catalytic site binding on the same iso-enzyme [4, 10] - invariably leading to antagonistic, additive and/or other undesirable drug interactions, catalyzed mainly by enzyme inhibition or induction.

The recommended standard of care for HIV/AIDS patients requires the inclusion of at least one PI within a course of HAART regimen [2, 7, 13-14], but often the beneficial effects of a particular drug combination approach is not sustained, necessitating a change in the prescribed drug permutation. Consequently it may be necessary to expose patients to various combinations of PIs and/or PI/NNRTIs - which reiterates the inadvertent probability for unavoidably potentially dangerous pharmacokinetic interactions. On the other hand, these (synergistic, antagonistic and/or additive drug) interaction effects may beneficially be used to purposely alter in vivo drug concentrations of specific drugs, however, this is strictly only possible with absolute measurement of endogenous drug concentration [2, 7].

The cumulative effect of all the above factors complicates dosing of clinically diagnosed patients, and as such an urgent need for therapeutic drug monitoring (TDM) during HIV/AIDS treatment is highly emphasized and recommended. In view

of all the latter and preceding facts, the urgent need for TDM of indinavir and other ARV may be summarized as follows:

- To reduce drug toxicity by decreasing drug dose, while still maintaining adequate trough plasma concentration, particularly in the case of PIs and NNRTIs.
- To prevent adverse drug-drug interactions, by monitoring plasma concentration during multi-drug administration or prior to the addition of a new drug.
- It can be used as an objective measurement for non-adherence, thereby attenuate and possibly alleviating resistant viral mutations.
- To deliberately alter the concentration of a particular ARV during co administration.



Currently available methods for quantifying indinavir and other ARVs, is done through centralized laboratory techniques, based on high performance liquid chromatography (HPLC) with ultra-violet detection and/or liquid chromatography-mass spectrometry methods [7, 13, 15-16]. These techniques are very accurate indeed, but their preference is discouraged by their exceptionally expensive application and maintenance requirement, which includes amongst others, highly qualified personnel, rigorous sample preparation, expensive solvents and components, which concomitantly leads to long assay procedures and time consuming sensitive procedures [13, 15-16]. Overall, this causes long turn-around-periods [7, 17], and the delay in results may affect timely commencement of proper dosage/regimen modulation – a factor that can be detrimental to the HIV/AIDS patient. There is therefore undoubtedly a great demand for alternative drug assay measurement techniques, with the practical utility being to provide decentralised analysis, preferably at the doctor's office, emergency room or in the privacy of the patient's own house.

Since, first pass metabolism with cytochrome P450-3A4 evidently is a pivotal factor in the successful application of indinavir and most ARVs, it is only appropriate to discuss this enzyme in greater detail. In this regard, a brief, but succinct overview on CYP450 enzymes with particular reference to CYP3A4 follows:

1.2.2 Cytochrome P450 (3A4): Classification, structure and function

CYP3A4 falls under the sub-group, (mono)oxygenase-type enzymes, which in turn forms part of the superfamily of proteins, collectively referred to as cytochromes P450 (CYPs) [3, 6, 8-10, 18-20], which are present in all forms of life (plants, bacteria and mammals). Human CYPs are essentially membrane-associated (microsomal) proteins, located either in the inner membrane of the mitochondria or the endoplasmic reticulum (ER) of cells [6, 18, 21], of which, the ER association is confirmed by a characteristic stretch of residues, consisting of about 20-25 highly hydrophobic amino acids, known as the N-terminal region. In addition to this, these enzymes also contain a heme cofactor, situated at what is known as the C-terminus, and is flanked by a peripheral region of hydrophobic surrounding protein globule, functioning mainly to protect the heme from any unwanted reactions [22]. Thus, in essence, CYP450s can be considered as enzymes containing both an N-terminal domain, mainly functioning as a protein anchor, as well as a C-terminus, which contains the heme cofactor. Considering the hydrophobic residues contained within both of these regions, these enzymes are understandably considerably hydrophobic in nature. Also noteworthy, is that P450s are also known as heme-thiolate proteins, because in these proteins, the heme cofactor is covalently linked to the surrounding apoprotein through a cysteine group [21-24]. In this regard, they are similar proteins with the same porphyrin-heme complex as catalytic center, the so called "P450 signature", but with different amino acid sequences, altering the topography of the active site [21-22, 24-25] – hence the term "isozyme". In terms of function on the other hand, they are mixed function oxygenases (MFO), constituted by a multifarious

group of essential enzyme catalysts, which mainly function in the oxidative metabolism of various xeno- and endobiotic organic substances [22, 24, 26]. As such, collectively, these P450 isozymes play key roles in vital processes, such as steroid hormone biosynthesis, the activation and detoxification drugs and environmentally contaminating chemicals, the metabolism of polyunsaturated fatty acids, activation of vitamins A and D₃ to biologically active hormones, etc [3, 20, 24, 26]. With reference to the aforementioned processes, the reactions catalysed can be extremely diverse, such as, hydroxylations, N-, O- and S-dealkylations, sulphoxidations, ooxidations, deaminations, desulphurations, dehalogenations, peroxidations [21, 24]. Moreover, many of the individual P450s catalyze multiple reactions, and since almost every P450 isoform's selectivity is so broad – collectively, their presence provides a general defense system in the body against both synthetic and/or natural compounds, which are nearly unassailable to the attack by other enzymes and that would, upon exposure to them, otherwise accumulate and be harmful, if not metabolized to hydrophilic products [19, 24].

On the other hand, the liver is the major organ for the metabolism and detoxification of pharmaceutical drug-type xenobiotics [3, 6, 12, 24], an aspect that is crucial, since these drugs are normally lipophilic organic molecules, and as such has to undergo chemical modifications within the human body, either for drug activation and/or successful elimination. In this regard, the liver microsomal isozymes, are key players. With regard to CYP3A4 in particular, it is the major cytochrome P450 isoform and as such, the most influential. As all other human CYPs, it is a membrane-associated protein, residing primarily within the endoplasmic reticulum of the liver and contains a single iron protoporphyrin IX prosthetic group, (heme). **Figure 1.2(a)** shows the ribbon drawing of the secondary structure of human CYP3A4, whereas **Figure 1.2(b)** shows an enlarged detailed view of the heme cofactor.

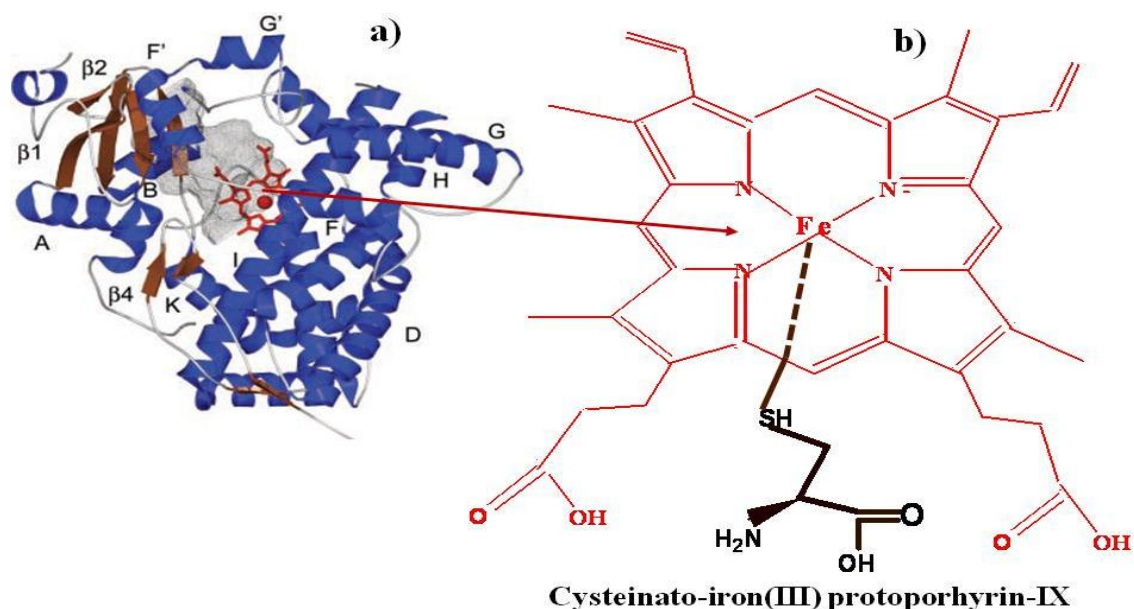


Figure 1.2:(a) Ribbon drawing, showing the distal face view of cytochrome P450-3A4 (CYP3A4) secondary/tertiary structure (a); (b) Prosthetic group of CYP3A4, (b-type heme): an iron-(III) protoporphyrin-IX linked with a proximal cystein ligand (fifth ligand of the heme iron)

From the ribbon drawing of the cytochrome P450 isozyme, CYP3A4, in **Figure 1.2(a)**, one can observe the secondary structure of the enzyme, which mainly consists of the heme (stick figures coloured in red) with its active site cavity (shown as a grey mesh) and the surrounding protein matrix (the apoprotein). On the other hand, Figure 1.2(b) shows the prosthetic group in greater detail – consisting of an iron (III) protoporphyrin-IX, which in terms of classification, is a b-type heme. The heme iron is ligated by a cystein group through its sulfur, and in this regard, overall, CYP3A4 prosthetic group may be referred to as a cysteinato-iron(III) protoporphyrin-IX. The prosthetic group is the active site of the enzyme, and as such, it is at this particular place that the enzyme interacts with the substrates to metabolise them. The substrate list of CYP3A4 is not limited to a small number of chemical classes, but rather is structurally diverse. A large number of these chemicals are human pharmaceuticals of various pharmacological actions. Overall, multiple metabolic pathways are catalyzed by CYP3A4, the major pathways being C- and N-dealkylation, C-hydroxylation.

Others include dehalogenation, N-demethylation, as well as allylic and benzylic hydroxylations in steroid molecules. Overall, the natural catalytic process of CYP3A4-substrate interaction, involves an insertion of one atom of elemental oxygen into the substrate compound (monooxygenation) – a process that occurs through a series of reaction steps and involves the obligatory presence of electron transfer donors and other molecules. A schematic representation of the catalytic reaction steps for the membrane-bound CYP3A4 is shown in **Figure 1.3**.

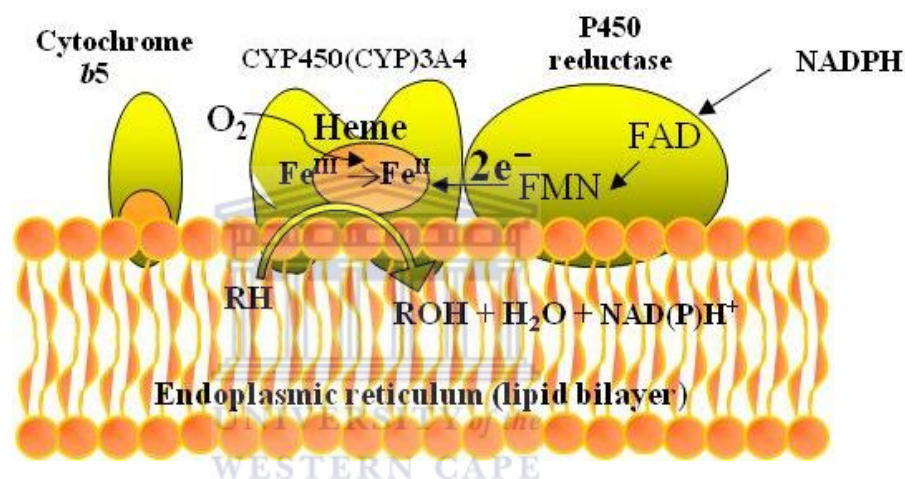
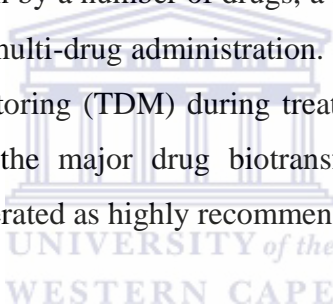


Figure 1.3: Natural catalytic cycle of human hepatic microsomal CYP3A4

As shown in **Figure 1.3**, CYP3A4 reacts with substrates (R—H) at the active site (heme). Overall, success of the catalytic process requires the transfer of two electrons and the presence of molecular oxygen. The electrons are supplied at separate intervals during the catalytic cycle, by the enzyme's natural electron donor, NADPH-P450 oxidoreductase, through its reducing equivalents, FMN and FAD. It is noteworthy to add that, depending on the substrate being metabolised, CYP3A4 sometimes also require the obligatory presence of cytochrome b5 during supply of the second electron. The series of steps following the first electron transfer is such that it eventually results in the formation of water and a high-valent iron-oxo species (iron-oxo(ferryl)-complex), known as Compound I, which is capable of oxygen atom transfer and as such, functions in the actual substrate monooxygenation. A much

more comprehensive description of the catalytic reaction cycle is given in **Chapter 2**. In terms of the electron transfer redox partner involved, CYP3A4 may be classified as a classII cytochrome P450, whereas with respect to the fact that the enzyme requires an external reductant, it may be categorised as an external monooxygenase.

Important considerations with regard to CYP3A4-substrate interaction include the fact that the enzyme is rather ‘promiscuous’ in its substrate selectivity and as such, known to metabolise a large variety of pharmaceutical compounds extensively varying in molecular weight, while also having a spacious active site, capable of accomodating a diverse range of compounds. Moreover, the expression of CYP3A4 varies between individuals, race and ethnic groups, while the enzyme is also subject to inhibition and/or induction by a number of drugs, a factor that can be life threatening during concurrent and/or multi-drug administration. Considering these facts, the need for therapeutic drug monitoring (TDM) during treatment of chronic illnesses where CYP3A4 metabolism is the major drug biotransformation pathway, such as in HIV/AIDS, should be reiterated as highly recommended.



1.2.3 Endocrine disruptor compound: 2,4-Dichlorophenol (2,4-DCP)

As stated earlier, CYP3A4 is the most ubandantly expressed CYP450 isozyme. In that context, it accounts for 60% of cytochrome enzymes in the liver and 70% of those in enterocytes in the gut wall, and appropriately, holds the dominant position in phase I metabolism [3, 9-10, 27-28] – naturally having the largest substrate listing and as such, plays a pivatol role in the in detoxification of exogenous bioactive compounds and lipophillic xenobiotics, including prescription medicines, drugs, environmental pollutants, pesticides, herbicides, herbal medicaments, food supplements, steroids, etc [9-10, 23, 27-31]. Amongst the latter

list, of particular importance are compounds with endocrine disrupting properties, because their effects are not only confounded to the individual exposed to them, but also their offspring, and as such cascades into transgenerational effects [32]. With regard to definitive context, endocrine disruption refers to a mechanism of toxicity that hinders the ability of cells, tissues and organs to communicate hormonally, resulting in a myriad of adverse health outcomes including reduced fertility and prolificity, spontaneous abortion, skewed sex ratios within the offspring of exposed communities, male and female reproductive tract abnormalities, polycystic ovarian syndrome, neuro-behavioural disorders, impaired immune functions and various cancers [32-36].

Amongst the studied potential endocrine disruptor (ED) chemicals, pesticides (i.e. herbicides, bacteriocides, fungicides, insecticides, and rodenticides) and associated mono- and polychlorophenols were shown to be ubiquitously associated with most related endocrine disrupting subject areas [32]. Of particular interest, is the pervasive environmental pollutant – the chlorinated phenol, 2,4-dichlorophenol (2,4-DCP), since it holds multiple industrial applications, including herbicide and pesticide production, feedstock for the manufacture of certain methyl compounds used in antiseptics and disinfectants, fungicides for use as wood preservatives, etc [37-38]. Moreover, it is a precursor for the synthesis of carcinogenic endocrine disruptor, 2,4-dichlorophenoxyacetic acid (2,4-D), which is the active ingredient of more than 1500 herbicides [39-40], while also being a major metabolite or degradation product of 2,4-D and many phenoxy-based herbicides [32, 40-41]. Furthermore, 2,4-DCP also commonly ends up in drinking water as a by-product of chlorination, as biocides, or as degradation product of the commonly used phenoxy herbicides [39, 42-43]. The toxicity linked to 2,4-DCP exposure has been shown to contribute in the promotion of the growth of breast, ovarian and prostate cancer tumor cells, while also shown as major causative agent in specific endocrine related cancers and chronic conditions such as chloracne and porphyria in humans [32, 41, 44]. Consequently, it has been classified as a priority pollutant, especially in terms of the aquatic environment [45], a

fact that is exacerbated by the knowledge that endocrine disrupting related chemicals are capable of exerting adverse effects on living organisms even in very small concentrations [32].

Overall, the maximum safe limit for 2,4-DCP and/or other chlorophenols in river water, pre-treatment potable water and drinking water has been ruled as 50 – 100 μgL^{-1} , 1 – 5 μgL^{-1} and 100 – 500 ngL^{-1} , respectively [WHO, EPA, EU]. Thus, the monitoring of the environment to make sure that this pollutant remains within safe limits of concentration requires very sensitive analytical methods. To this end, conventional analytical methods for determination of 2,4-DCP in water samples are based on gas chromatography (GC) and/or high performance liquid chromatography (HPLC), either applied directly in conjunction with mass spectrometry detection, or with solid-phase extraction (SPE)-electrospray ionization (ESI) assisted mass spectrometry detection [39, 43]. Other methods, based on advanced oxidation processes, such as O_3/UV , $\text{O}_3/\text{H}_2\text{O}_2$, $\text{UV}/\text{H}_2\text{O}_2$, Fenton and photo-Fenton, which functions by mineralizing the organic chemical, have also been applied [38]. Notwithstanding degree of accuracy and/or success of these methods, their popularity is restricted by numerous disadvantages, as well as the fact that they are not suitable for on-site application [38-39, 43], hence the compelling urgency for development of alternative assay methods.

1.2.4 Indinavir vs 2,4-DCP: The common factor shared by these two subjects

At this stage, the reader's curiosity may be kindled, as to the common aspect of

two such seemingly different subjects – PI ARV drug, indinavir vs priority pollutant/endocrine disruptor compound, 2,4-dichlorophenol. In this regard, the reader is requested ponder the following significant factors:

On a global scale, South Africa has one of the highest HIV infection and AIDS related mortality percentages. Geologically, on the other hand, South Africa suffers from several water related challenges, which overall, may be summarised as follows:

- There is an uneven spreading of ground- and other water resources across the country, due to its by-and-large arid/semi-arid nature – with a select few regions having the great fortune of receiving moderately regular rainfall patterns. Moreover, chlorophenols and/or other toxic pollutants are bound to eventually end up in our waterways, both directly and indirectly from industrial processes, especially the electricity supply sector which is highly reliant on the use of coal fired power stations – with the other major sector being the agricultural use of pesticides/herbicides for genetic modification of crops.

Considering the latter information, it should become obvious that indinavir and 2,4-dichlorophenol is directly related to two of our country's most eminent concerns, which is HIV/AIDS and the issue of water. Moreover, with reference to the preceding sections, these two chemicals have also been shown to share a common route of biotransformation, which involves monooxygenation by CYP3A4. On the other hand, knowing that CYP3A4 is such an influentially diverse enzyme catalyst, and the knowledge that this and other P450's are promising enzymes for the applications of biosensing probes, the much emphasized alternative assay technique for quantification of 2,4-dichlorophenol and indinavir, is realizable through the application of a small analytical instrument, known as the biosensor.

1.2.5 Molecular models and probes for xenobiotic metabolic profiling

1.2.5.1 Prospects of available biological probes for in vitro investigations with mammalian microsomal CYP 450s: advantages, drawbacks and new developments

Before tackling the aspects surrounding subjects of active in vitro models for studying CYP3A4 and other mammalian CYP450 enzymes, the reader is cautioned to consider the following factors:

Considering that drug metabolism is the major determinant of drug clearance, the importance of mammalian CYP 450s and in particular, the determinant role of predominant isoform, CYP3A4, in the therapeutic efficiency of most of the pharmaceutical drugs ingested by humans cannot be over estimated. Furthermore, it is the body's ultimate defense mechanism, rendering otherwise carcinogenic compounds to harmless metabolites, for example, the unprecedented role of CYP3A4's detoxification ability to metabolise the human hepatocarcinogen, aflatoxin B₁, to the harmless metabolite, the 3 α -alcohol. Also noteworthy, is the aspect of the extensive interindividual differences in pharmacokinetics existing between individuals and ethnic groups, largely attributable to polymorphism, genotype-phenotype relations within the isoenzymes, induction and overlapping drug selectivities of CYP3A4 and other mammalian CYP450 isoenzymes — of which these constricts can confer differences of up to 90% in drug uptake and clearance between individuals. (In this regard, polymorphism refers to the variation in gene expression for particular isoenzymes between individuals. In this regard, a small difference in DNA sequence, within a population can lead to very significant differences in drug metabolism. Genotype-phenotype differences, on the other hand, refers to the metabolising ability of individuals, in which some are poor-metabolisers, intermediate-metabolisers and ultrafast-metabolisers). A final consideration factor, which is inhibition of CYP450s, particularly, CYP3A4, caused

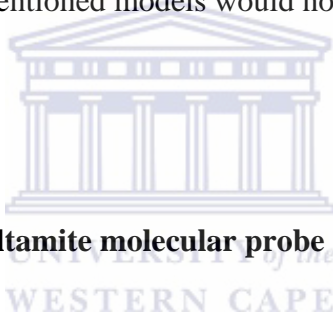
by competition between drugs taken concurrently and the enzyme's promiscuity confirmed by its ability to accommodate more than one substrate simultaneously can lead to severe adverse drug effects, particularly metabolic drug interactions, caused by altering the disposition of a drug by the presence of another compound.

The relevance of all the aforementioned constricts/factors, is based on the fact that they all have a direct consequence on the overall effect of pharmaceutical compounds, as well as other drug-type and/or carcinogenic xenobiotics entering the human metabolic system. In this regard, it is pivotal that *in vitro* models constituted by validated techniques are in place for the study and assessment of metabolic profiling of xenobiotics both pharmaceutical and otherwise, particularly in terms pharmacokinetics, therapeutic dose efficiency predictions, potential toxicity and potential enzyme-inducing or enzyme-inhibiting studies. In fact, with regard to pharmaceutical constituents, these studies play a significant role in preclinical drug development, particularly since the evaluation of potential drug-drug interactions has become mandatory for the registration of new drugs by most regulatory agencies.

For this purpose, various models/probes, based on various cytochrome P450 sources, in techniques which makes use of *in vitro*-based protocols, may be applied. These models include human hepatocytes, which are normally primary cultured (i.e. fully differentiated) and/or encapsulated hepatocytes; liver slices; microsomal fractions, prepared from human liver tissue; or microsomal fractions and/or hepatocytes from animal tissue, such as rats. Although these models have been in use for routine application, they are unfortunately all subject to various drawbacks. In this regard, with respect to hepatocytes in particular, primary cultured intact cells are used, which essentially means that these sources contain complete endoplasmic reticulum membrane, metabolic pathways, physiological cofactors, coenzymes and active gene expression. The particularly significant drawback of the aforementioned model, is that investigations with one particular isoenzyme is not really possible and for the requirement of such results, additional statistical analysis needs to accompany such

investigations, particularly since most CYP 450 isoenzymes exhibit distinct, but overlapping substrate selectivities

Although, these models are based on viable catalytically active CYP450 sources, their shortcomings make the need for alternative molecular models/probes an urgency. In this regard, biosensors can play a major role in replacing such systems. In the context of bioelectrochemical systems and biosensors in particular, it is essential that a constant supply of renewable sources of biological components are available. In this regard, genetically manipulated cells, expressing the specified single CYP gene, through permanent transfection with the cDNA of the particular enzyme is a highly suitable method to eloquently supply this constant demand, whereas any of the aforementioned models would not suffice.



1.2.6 Biosensors: The ultimate molecular probe

In the context of all the problem areas identified and elaborated in all the preceding sections within this chapter, one subject claims centre stage — the unprecedented urgency for alternative analytical devices for detection, quantification and monitoring of specific chemical species, with the overall aim being diverse areas of application. The only proposed analytical device able to meet these requirements, are biosensors, as they have been proven effective for continuous, real-time in vivo and/or non-invasive monitoring, as well as field-testing and commercialization, and as such may be used to complement and/or replace centralized laboratory techniques. From a panoramic perspective, the rationale behind biosensor design and application is based on the synergistic combination of molecular principles and bioelectrochemical dynamics, packaged as intelligent materials system in self contained integrated devices — capable of recognising stimuli, processing the information arising from the response to the stimuli and responding to it in an appropriate manner and time frame,

as such allowing virtually any complex to be screened with minimal assay development. Furthermore, research has shown promise in the potential of these devices to provide low-cost, rapid/real-time measurement and operationally-simple analytical tools for diverse applications, including environmental monitoring, chemical measures in agriculture, food and drug industries, as well as clinical diagnostics, disease- and therapeutic drug monitoring applications. Among the available biosensor types, electrochemical biosensors are the most preferred. In this regard, amperometric electrochemical biosensors are considered the superior choice, because they are known to be reliable, cheaper and highly sensitive for clinical, environmental and industrial purposes [46].

From a definitive perspective, overall, biosensors consist of two major parts — a molecular recognition component, which is of biological origin, and a transducer, whereas the major processes involved in any biosensor system are analyte recognition, signal transduction and readout. Since the clinical utility of such devices are highly dependent on the selectivity of the biorecognition component for the specific target analyte and to maintain this selectivity in the presence of other potentially interfering species, enzymes have received the major attention as recognition components. In this regard, enzymes are known to have high specificity and hold the ability to enable reactions that would otherwise not occur, thus making them nature's most preferred catalysts. Moreover, biotechnology have advanced to such an extent that any enzyme can be genetically engineered through the use of heterologous expression systems, such as mammalian-, yeast- (*Saccharomyces cerevisiae*), insect cells (*Spodoptera frugiperda*, i.e. Sf9 or Sf21) and/or bacterial systems (*Escherichia coli*), via a combination of cloning, expression and purification methods. This has been a particularly significant milestone for the application for mammalian CYPs, since this process allows for the preparation of only the terminal oxidase/heme domain of the particular isozyme, which can subsequently be used in an appropriate biosensor configuration, and as such alleviates the need for the external natural electron transfer-donors. Moreover, N-terminal modification, during the enzyme

expression/purification process circumvent the problem of low activity and aggregation normally experienced by full-length microsomal P450 isozymes, and as such enables the preparation of more soluble enzyme constructs, with good catalytic activity. A noteworthy fact to add, on the subject of enzymes, CYPs in particular, is that a key factor in the construction of such biosensors involve the development of suitable immobilization technologies for stable tethering of the enzyme to the transducer, the overall aim being, to provide durable and repetitive binding of the biological receptor to the transducer without impairing its catalytic activity and/or efficiency for the target analyte. This is of course only possible with well orchestrated transduction platforms, consisting of judiciously chosen carrier matrices and interfacial enhancer materials, since the activity of immobilized biological molecules are known to be dependent upon a combination of factors, including surface area, porosity, hydrophilic/hydrophobic character of immobilization matrix, reaction conditions, the chosen immobilization method etc. Moreover, the thick protein shell surrounding the enzyme active center introduces a kinetic barrier for electron transfer.

A popular method, that has proven effectual for enzyme immobilization, is a combination of entrapment and encapsulation. Effective entrapment materials which have shown immense success are polymer based. Polymers used for enzyme immobilization and development of modified electrode films for biosensor configurations may be divided into two major groups: ion exchange- (without electronic conductivity) and electron conducting polymers. The latter group also includes redox-active electron conducting polymers. Among the polymer matrices, the ion exchange polymer, nafion, has become a popular choice, and as such, much research investigations has been devoted to its use in a wide variety of electrochemical applications. This perfluorosulphonate ionomer is a tremendously versatile material, incurred by a range of inherently unique properties, which includes the following:

- i) It allows for simplistic membrane formation by either dip-, spin- or drop-coating;

- ii) It has high adhesion to electrode surface with low swelling in aqueous media;
- iii) Its fluorocarbon backbone allows formed polymer membranes to be highly thermal and chemically stable;
- iv) Nafion films feature internal segregation of hydrophilic and hydrophobic regions, as such improving physiological enzyme environment mimicking, a quality that can further stabilize the immobilized enzyme molecules.
- v) The polymer's incredible affinity for complex cations enables the pre-concentration of cationic redox-active species in the polymer;
- vi) The formed polymer confer perselectivity to the biosensor, particularly with regard to the exclusion of potentially interfering compounds, while simultaneously protecting the underlying electrode from fouling and also preventing non-specific binding of enzyme molecules to the electrode surface.

Nafion's ability to preconcentrate redox active species is an exceptionally pivotal factor, and as such, can be used for the preparation of mediator-based, reagentless biosensor configurations, which would allow simplified electron transfer between the enzyme active site and the transducer surface, through electron shuttling by the incorporated redox active mediator molecules. This is particularly beneficial in the case of cytochrome P450 enzymes whose active sites are deeply buried within the surrounding apoprotein and do not readily exchange electrons with the underlying electrode, while also alleviating the additional complication of the obligatory presence of NADPH electron transfer donors. The choice of encapsulation material, on the other hand, also plays a significant role in successful enzyme-film formation, since appropriate material will enable longer lifetime of the immobilized enzyme, particularly in the case of microsomal CYP450 enzymes, who are known to be labile and requires a suitable environment for to retain activity and function. On the subject of encapsulation, the natural biopolymer, agarose, well known for its bioaffinity and biocompatibility, non-toxic nature, water permeability, high mechanical strength and biomembrane like film formation, has been widely applied for enzyme-film formation, in which regard it has portrayed excellent enzyme

encapsulation with a superior degree of biological activity retention [47-48], particularly in the case of cytochrome P450 enzymes [49-50]. Moreover, agarose can be synergistically blended with other non-toxic, biocompatible, water-soluble polymers, such as poly(vinyl chloride) yielding hydrogel composites that provides a biocompatible aqueous microenvironment for the immobilized enzyme [51].

1.3 Refinement of Research and Research Questions

The preceding sections gave a succinct, but detailed review of the pertinent subjects pertaining to this dissertation. In this regard, the reader was familiarized with HAART drugs and endocrine disruptor/priority pollutant chemicals. With regard to the ARVs, special reference was given to the protease inhibitor ARVs, indinavir in particular, while other important issues, such as adverse drug reaction considerations, drug assay methods, therapeutic drug monitoring and biotransformation was emphasized. In terms of the other subject area on the other hand, much of the discussion was devoted to 2,4-dichlorophenol, particularly with respect to aspects surrounding its sources, applications, health impacts and assay methods. Moreover, in addition to the latter subject areas, detailed deliberations with regard to cytochromes P450 and biosensors were given. In reference to the major aspects outlined in those sections, a summary of research questions can be formulated which directs the focus to the relevant problem areas and as such provides more focused enlightenment on the motivation/rational for the current study.

- The PI ARV, indinavir is specifically designed to inhibit the HIV protease enzyme, leading to concomitant inactivation of virus particles.
- In general, primary antiretroviral drugs are based on three groups which includes the PIs, the NNRTIs and the NAs.

- Successful protease enzyme inhibition, and/or general anti HIV effect, require absolute optimum concentration of clinically available drugs at the site of replication.
- Drug plasma concentration needs to be regularly monitored to ensure optimum sustained anti HIV effect.
- The recommended standard of care for HIV/AIDS requires inclusion of at least one PI in a course of HAART regimen.
- The requirement of regular drug regimen modulation to prevent viral mutations etc., expose patients to various combinations of PIs and/or NNRTIs.
- PIs and NNRTIs share the same metabolic pathway, which primarily involves oxidative metabolism in the liver. The major enzyme involved is CYP3A4.
- Combination PI therapy can result in adverse additive and/or antagonistic drug interactions mediated by induction or inhibition of CYP3A4.
- Great subject variability in concentration of plasma PI levels, due to differences in each patient's cytochrome P450-CYP3A4, necessitates tailored dosage regimens to allow for maximum efficacy and minimum toxicity, because sub-optimal concentrations of PIs will be ineffective.
- Indinavir may be considered a model substrate for CYP3A4 since it is exclusively metabolized by this enzyme.
- Since drug clearance changes rapidly with age until adult stage is reached, TDM in pediatric patients, would tremendously aid the selection of correct dosing regimen.
- Constant TDM during antiretroviral treatment is necessary so as to ensure optimum trough plasma drug concentrations and thus preventing toxicity and non-adherence.
- HIV/AIDS patients are immuno-compromised and as such, in addition to ARVs, receive numerous other prescription drugs, and with CYP3A4 being the main isozyme responsible for metabolism of most ARVs and

pharmaceutical xenobiotics, potentially dangerous pharmacokinetic interactions are highly probable.

- Therapeutic drug monitoring during the treatment of HIV/AIDS is highly recommended, the main reasons being, to prevent adverse drug interactions, improvement of inter-individual therapeutic efficiency, preventing non adherence and to avoid drug associated toxicity.
- Current available assays for anti HIV drugs are based on centralized laboratory techniques whose advocacy in regard to TDM is discouraged by numerous disadvantages, which overall causes long turn-around-periods, leading to delay in results and affects timely commencement of proper dosage regimen adjustment. This is potentially dangerous for the patient.
- Smaller, faster and cheaper devices are highly desired for replacement of time-consuming laboratory-analysis.
- CYP3A4 being the highest expressed mammalian hepatic and small intestinal isoform, it also plays a major role in metabolism and detoxification of environmental pollutants, one of which is the pertinent endocrine disruptor chemical, 2,4-dichlorophenol.
- 2,4-DCP is a ubiquitous priority pollutant, ever-increasingly finding its way into our waterways, concomitantly putting increased strain on an already water-stressed country.
- Available detection and quantification methods for 2,4-DCP are laboratory-based GC and/or HPLC methods used in conjunction with complicated detection methods including SPE or ESI. Moreover, these techniques are not structured to enable on-the-spot field testing.
- As in the case of ARVs, alternative analytical devices for detection of 2,4-DCP is needed.
- Coupling of enzymes with deliberately modified electrodes, within a biosensor configuration, permits rapid, simple and direct determination of multifarious analytes, in complex biological fluids and/or environmental liquid samples. Such devices can be applied for single-use, intermittent-use or

continuous-monitoring applications. In this regard, cytochromes P450, particularly major isoform, CYP3A4, are promising recognition components, due to the extensive variety of substrate catalytic ability.

- Amperometric enzyme electrodes, having a wider linear range and the advantage of being able to produce continuous readings, holds a leading position among available biosensors systems presently available.
- Sensor is comprised of three essential components: the detector, which serves as recognition element; the transducer, which converts the stimulus to a useful invariable electronic, output; and the output system itself, which involves amplification, display, etc in an appropriate medium.
- The interface between the detector and transducer is an important consideration during biosensor construction and often constitutes the major hurdle in the development of an optimum operating device.
- Optimum biosensor performance is by-and-large depended with appropriate immobilization techniques.
- Requirements for effective immobilization serves to: retain biological activity of enzyme when attached to sensor surface, tightly associate biological film with transducer whilst retaining its structure and function, induce long term stability and durability of immobilized biological films, and of retaining a high degree of specificity of the biological material to particular biological components.
- Improvement of biocatalytic efficiency can be achieved through choosing carrier matrix materials with multifunctional features; tight immobilization of mediator molecules within the reagent layer; as well as creating biomembrane-like matrix to mimic physiological conditions.
- Among the known immobilization methods, research has found enzyme entrapment-encapsulation to be superior.

With regard to the latter research questions and preceding literature surveyed information, which highlighted specific problem areas as it pertains to this dissertation.-The main issues being HAART associated TDM and on-the-spot field assay methods for endocrine disruptor associated priority pollutants. The main focus in terms of the subject of TDM involves alternative analytical methods capable of decentralized analysis, and real-time measurements. The superior method for executing the task was shown to be enzyme-based amperometric biosensors, in which appropriate miniaturization of bio-recognition and transducer components (which includes carrier materials) is expected to allow for fast and accurate analysis. Considering these aspects, the motive for the current study was thus established.



1.4 Scope of the thesis

This dissertation presents and comprehensively discusses the obtained results for two separate biosensor platforms, biosensor platform 1 and biosensor platform 2, fabricated and applied for the detection of two distinctly different categories of substrates. With regard to the biosensor platforms in particular, they share four major commonality factors, the first of which is the category of bio-recognition component, which in both cases is the mammalian, microsomal heme-thiolate cytochrome P450 3A4 isoenzyme (CYP3A4). The second common factor is the mediating species, which is the electroactive metal-centred mediator, cobalt(III) sepulchrates $[\text{Co}(\text{Sep})^{3+}]$. The other aspect is that both platforms have been designed and fabricated to mediate the enzyme-based bio-electrocatalytic reaction in a reagentless manner. The fourth and final common factor, is with regard to one of the major objectives of the biosensors, which was focused on working towards providing decentralized analytically-based method for detection and quantification of the selected substrates.

The first part of the thesis involves the electrocatalytic detection and quantification of endocrine disruptor compound, 2,4-dichlorophenol. The biosensor was realized through sandwich-configuration, consisting of commercially obtained full-length microsomal CYP3A4 within cobalt(III)sepulchrates-derivatized nafion membrane. Entrapment of the cobalt(III)sepulchrates mediator within the nafion membrane, was done through a manual pre-concentration method, which involved a combination of drop-coating and mixing. Electrochemical dynamics for this biosensor is based on amperometric transduction. The results for this biosensor is presented and discussed in **Chapter 4**. This platform will be referred to as **biosensor platform 1** in the subsequent sections of this chapter.

The second part of this dissertation involves the electrocatalytic detection and quantification of PI ARV, indinavir. The recognition component for this particular biosensor is the heme-domain of N-terminally modified CYP3A4 (nCYP3A4), manufactured through genetic engineering, the process of which was done by the investigator and as such, was not commercially obtained. Enzyme immobilization in this particular biosensor is based on a combination of entrapment, behind the electroactive solid polymer electrolyte inner film, and encapsulation in biocompatible ionic hydrogel blended membrane. Incorporation of the cobalt(III)sepulchrates mediator within the inner-nafion membrane, was achieved through a novel electrochemically-based method. The results for this particular biosensor is presented and discussed in **Chapters 5 A and B**. This biosensor will be referred to as **biosensor platform 2**.

It should also be noted that the specific techniques applied in preparation of biosensor platform 2, was carefully planned to serve as improvement as compared to biosensor platform 1, particularly with reference to the preparation of the electroactive carrier matrix. Moreover, the improvement in the design path was also focused on working

toward lowering the operating potential of the reduction of oxygen, as compared to biosensor platform 1.

1.3.1 Specific objectives to achieve the overall goal

In this regard, specific key research questions for each biosensor platform was identified, which are subsequently elaborated.

1.3.1.1 Biosensor platform 1

- i) prepare a pre-formed nafion film on the glassy carbon electrode surface.
- ii) modify the formed nafion film with the electroactive mediating cobalt(III) sepulchrate species, to form an electroactive carrier matrix. The approach used here should be kept simple, by applying manual techniques.
- iii) characterize the prepared $\text{Co}(\text{Sep})^{3+}$ -modified nafion film with appropriate electrochemical and ex-situ morphological and structural techniques.
- iv) monomerize the commercially obtained full-length CYP3A4 (fCYP3A4) with a suitable detergent, for easy immobilization without aggregation of enzyme.
- v) immobilize the enzyme on the electroactive carrier matrix by simple drop-casting method.
- vi) re-inforce the reagent layer with a thin outer film, as to minimize leaching of any components.
- vii) Characterize the prepared biosensor with dc voltammetric techniques in appropriate buffer electrolyte medium.
- viii) Probe and investigate the electrochemical interactions of the enzyme-based biosensor with the selected model substrate.

1.3.1.2 Biosensor platform 2

- i) prepare the N-terminally modified human recombinant soluble CYP3A4 construct, to enable a constant locally available renewable source of biological component in a cheap simplified manner.
- ii) do the necessary structural characterization, of the prepared enzyme.
- iii) Prepare the pre-formed nafion film, however, the technique used here should be an improvement to method used in platform 1, as to create a more uniform film.
- iv) incorporate the electroactive cationic $\text{Co}(\text{Sep})^{3+}$ into the nafion film through the appropriate electrochemically based method.
- v) characterize the prepared carrier matrix to evaluate and highlight possible improvements in the formed film, as compared to the carrier matrix of biosensor platform 1.
- vi) create a suitable biocompatible hydrogel that can serve as replacement outer layer for nafion and function as stable encapsulator for the immobilized enzyme.
- vii) Immobilize the prepared enzyme on the electroactive carrier matrix and prepare the complete biosensor with hydrogel outer layer.
- viii) do comprehensive voltammetric characterization of the electrochemical characteristics of the biosensor

1.5 Other novel objectives

It is hoped that the work presented in this dissertation will provide an enhanced insight into the specific interactions between the biorecognition element and the selected substrates and such, provide an enhanced understanding/insight into the catalytic reaction cycle for the major human hepatic CYP3A4 enzyme, when the natural electron delivery system has been replaced by an electromotive force. This

would be a great milestone for these enzymes, since their application has been limited by the obligatory presence of specialized physiological electron transfer donors and other components which have proven to extensively complicate reconstitution systems and biosensor platforms for this isoenzyme category.

1.6 Layout of thesis

The thesis is divided into the following chapters:

Chapter 1 The chapter generally serves as an introduction with particular reference to the aspects that are of relevance to the entire scope of the dissertation, entitled “*Electrochemical dynamics of cytochrome P450-3A4 isoenzyme biosensor for protease inhibitor antiretroviral drug*”. Also discussed in this chapter is the main aims, objectives, as well as the layout of the dissertation.

Chapter 2 A comprehensive review of the literature of science of biosensors, with particular attention given to the aspects of relevance to the dissertation is given. In this regard, transducer aspects, molecular recognition, principles and classification of the enzyme electrode, solid polymer electrolyte, mediated amperometric biosensors, biocompatible polymeric hydrogels and biomolecule solid-support tethering are all discussed.

Chapter 3A This chapter comprehensively explains important theoretical aspects which are of relevance to the scope of the dissertation: The main aim here being to provide an enhanced understanding in the school of thought during data analysis of obtained results, and therefore provides enhanced understanding of the presented results. Discussed

here are the thermodynamic and kinetic parameters, performance factors, enzyme kinetics and genetic engineering aspects.

Chapter 3B General experimental protocols pertaining to the entire scope of the dissertation, tabulated listings of materials and reagents used, general preparative protocols of samples and reagents, relevant calculations and sample preparation and procedures for selected specialized ex-situ analysis.

Chapter 4 Here the results for **biosensor platform 1**, entitled, “*Microsomal cytochrome P450-3A4 biosensor for the determination of 2,4-dichlorophenol — an endocrine disruptor compound*” is presented and comprehensively” discussed. The nafion-CMECo(Sep)³⁺ carrier matrix was also subjected to morphological and structural characterization investigations for which the results are exhibited and discussed. The electrode assembly of the biosensor, the electrocatalytic response to dioxygen and substrate, as well as the biosensor response in the presence of selected inhibitor was evaluated with voltammetric investigations, for which the results are shown and discussed. In addition to this a critical assessment of the observed results are also discussed, providing enhanced insight into the observed results, as well as additional observations that was of significance.

Chapter 5A and B The results for the assembly, characterization and catalytic response for biosensor platform 2 is presented and discussed.

Chapter 5A The results for the assembly and characterization of composite film consisting of nafion and electrochemically deposited cobalt(III) sepulchrate [El-Co(Sep)³⁺] is presented and discussed.

Chapter 5B The results for the N-terminally modified genetically engineered human recombinant P450-3A4 (nCYP3A4) biosensor for the determination of protease inhibitor ARV drug, Indinavir is presented and discussed.

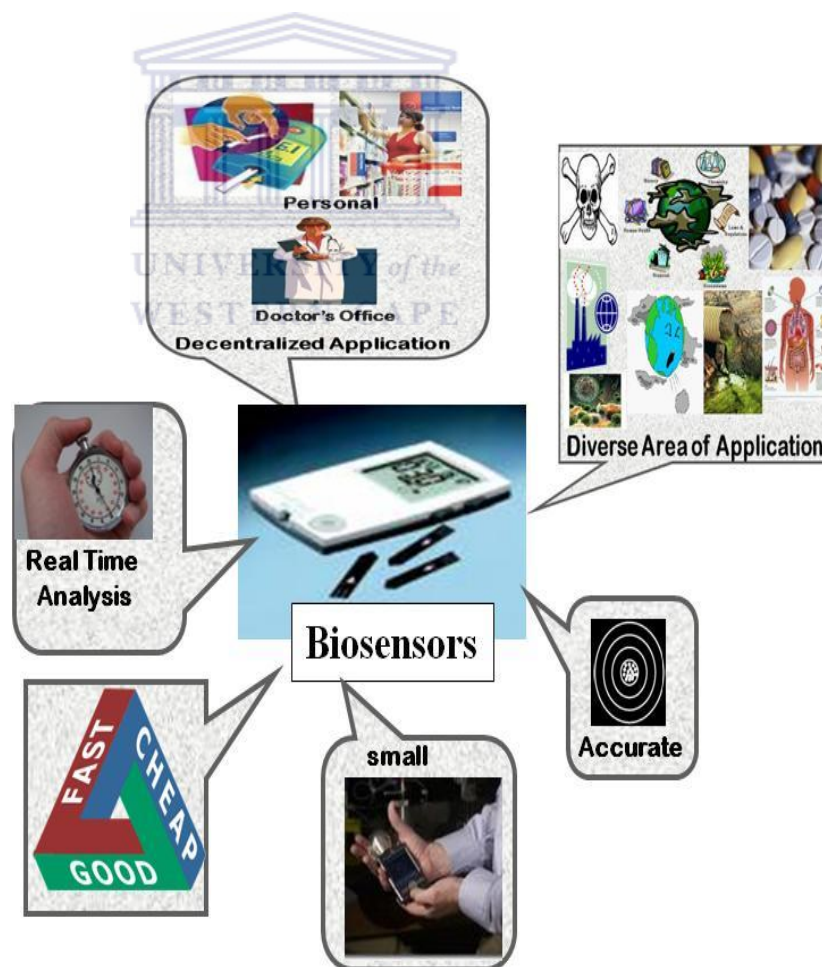
Chapter 6 This chapter summarizes all of the major findings as observed from the research investigation with respect to the results shown and discussed for biosensor platform 1 and biosensor platform 2. Important future recommendations are also given.

Chapter 7 References



CHAPTER 2

Biosensors: A Review of the relevant aspects



Chapter Prelude

The current chapter provides a comprehensive literature surveyd directory, of the relevant aspects and subjects on the area of sensors and biosensors as pertaining to the span of this dissertation. From a general perspective, a systematic description of a sensor and/or biosensor should include five features. These are (1) the detected, or measured parameter; (2) the working/operating principle of the transducer; (3) the physical and chemical/biochemical model (used to evaluate functional properties and quality of the sensor); (4) the area of application and (5) the technology and materials for sensor fabrication. These issues are discussed in great detail, with the key focus centering around approach, design and utility of biosensors from the cytochromes P450 viewpoint. Elaborated discussions of selected subject areas highlighted in chapter one, is also featured in this chapter.

2.1 Introduction

The human body is equipped with at least five sensors, including the nose, tongue, ears, eyes and fingers [1]. Each 'sensory-body-part' recognises a specific component, for example, the nose reconizes smells; the ear, sounds; the eyes colours and light, and the fingers reponds to physical touch – in effect, these recognition events may be referred to as a detection event. Concomitantly, the message from the detection event gets conveid to the brain, after which the body then, in turn, responds to the stimulus in an appropriate manner. In this context, a sensor may be defined as:

“a device that detects or measures a physical property, and records, indicates or otherwise responds to it” [52].

Sensors may be devided into three types, which includes physical sensors, chemical sensors and biosensors. Since physical sensors are not within the scope of this dissertation, they will not be elaborated on. A chemical sensor on the other hand, has definate relevance to biosensors and as such may be defined as follows:

“ A chemical sensor is a device which reponds to a particular analyte in a selective way through a chemical reaction and can be used for the qualitative or quantitative determination of the analyte” [52].

Biosensors, in turn, may be regarded as a sub-section of chemical sensors, but are usually treated as a subject in their own right, and thus may be discussed as a seperate topic.

2.2 Biosensors

Biosensors have a potentially large market, covering areas of clinical diagnostics, therapeutic drug monitoring, process control, food, military and environmental monitoring [53-55]. These analytical devices are unique in the sence that they may be described as self contained, all parts being packed together within

the same unit, the recognition element being in direct spacial contact with the transducer component [54, 56-57], and as such, the term ‘biosensor’ implies miniaturization and electronics. However, the latter description is not really definitive.

2.2.1 Biosensor structure and features

Biosensors are small devices which employ biochemical molecular recognition properties as basis for selective analysis, by making use of biological molecules as recognition element [54, 57-59]. The biological material is either intimately connected to, or intigrated within a transducer device which in turn converts the biochemical signal into a useful invariably electronic output . A schematic description of biosensor in terms of key components and operating principles are shown in

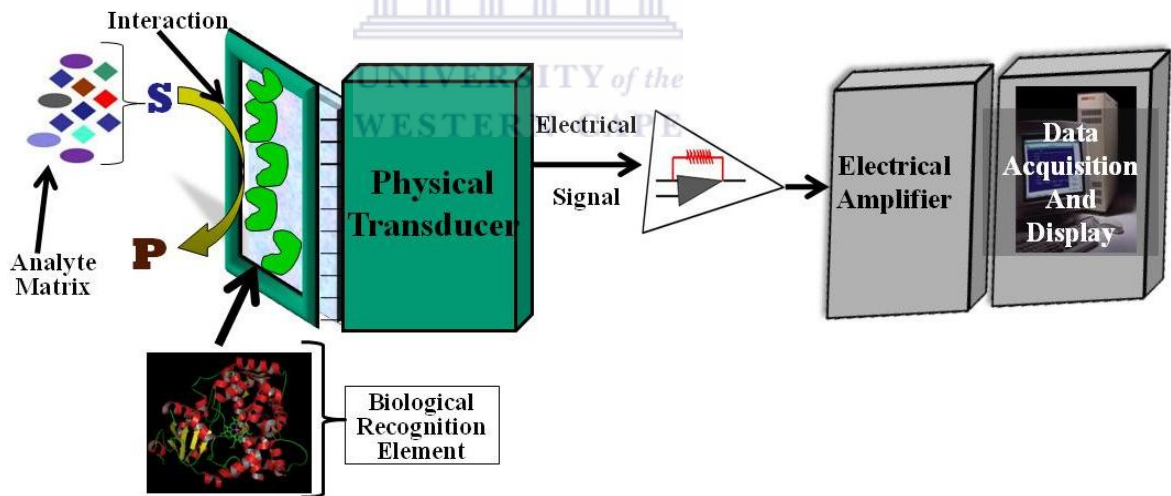


Figure 2.1 Schematic representation of biosensor components and operation

As shown in **Figure 2.1**, the essential components of a biosensor is, the biological component, the analyte matrix, the transducer, the amplification, processing and displaying systems [53-55, 59-60]. The biological component selectively recognises an analyte or class of analytes of interest (i.e. the physical stimulus), and as such

functions as the recognition element. The recognition component itself, may be divided into two distinct sub-groups, which is catalytic and non-catalytic. The catalytic group includes enzymes, micro-organisms, whole cells and tissues, whereas the non-catalytic group may include antibodies, receptors, nucleic acid, DNA etc [54]. *In the context of this thesis, enzymes are applied as recognition element.* On the subject of enzymes, an important fact to add, is that in terms research output and commercial application, they have enjoyed the major attention due to the fact that they are directly linked to the historical concept of the biosensor [17, 55-56], as well as their inherent qualities, the most eminent being their catalytic ability and substrate selective behaviour. The function of the transducer, on the other hand, is to convert the biological recognition event into a useful electrical signal/output [54, 58-59]. The conversion process confers bi-directional signal transfer to and from the biological recognition element (non-electrical to electrical and vice versa); also noteworthy is the fact that the transducer part of the biosensor is also a detector, or electrode [57]. The output from the transducer is amplified, processed and displayed by an output system, consisting of an electrical amplifier in conjunction with data acquisition and display instrumentation [54, 58-59]. Furthermore, on the subject of transducers, it is noteworthy to add that it also plays a pivotal role in enzyme stabilization, which is achieved through an interfacial region, consisting of specific carrier matrix materials which are normally intimately associated, or tightly bound to the transducer surface and as such, providing the matrix support for enzyme immobilization and electron transfer. With regard to the manifold functions of the transducer, it is irrefutable to admit that it plays a significant role in (bio)sensor functioning and application and in this regard may be discussed in greater detail.

2.2.2 The Transducer

An important aspect of biosensors are their classification, which amongst others, is highly dependant on the transduction process. In this regard, the specific operation principle of the transducer is a key factor, since it tells us how the biological recognition process being monitored is converted and transduced to obtain a detectable signal. In view of the latter, the transducer makes use of a physical change accompanying the recognition reaction, which, depending on the type of biosensor, differs accordingly. These may be [59]:

- The heat output (or absorbed) by the biochemical reaction: *calorimetric biosensors*;
- changes in the distribution of charges causing the production of a electrical potential: *potentiometric biosensors*;
- movement of electrons produced in a redox reaction: *amperometric biosensors*;
- light output during the reaction or a light absorbance difference between the reactants and products: *optical biosensors*; or
- Effects due to the mass of the reactants or products: *piezo-electric biosensors*.

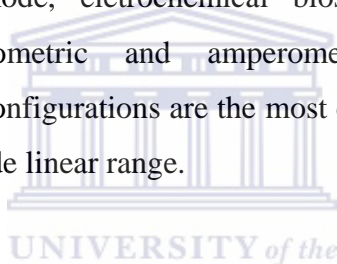
A compilation of biosensors classified in terms of their transduction method and application, respectively, is shown in **Table 2.1**.

Table 2.1: Biosensor transduction systems and measurement modes

Transducer Type	Detection or measurement mode	Transducer Type	Detection or measurement mode
Electrochemical	Amperometric	Optical	Fluorescence
	Potentiometric		Luminescence
	conductometric		Reflection
			Absorption
			Surface plasmon
			Resonance scattering
Thermal	Calorimetry	Piezoelectric	QCM

Enzyme thermistor (heat of reaction or absorption)	SAW SH/APM Lam wave
--	---------------------------

Among the list tabulated in **Table 2.1**, biosensors with electrochemical transduction systems have been found to overcome most of the disadvantages which inhibit the use of other types of biosensors, and as such have incurred the most attention, and appropriately, much research has been dedicated to this type of biosensor development. These devices can operate in complex (turbid) media, have comparable instrumental sensitivity and are more amenable to miniaturization. In terms of the specific measurement mode, electrochemical biosensors may be divided into conductometric, potentiometric and amperometric types. Amongst these, amperometric biosensor configurations are the most common, the main reasons being its high sensitivity and wide linear range.



With regard to the practical aspects of investigation purposes, the transducer refers to an electrode, which is in intimate contact or integrated with the biological recognition component — otherwise known as the working electrode (WE). Research has shown that the rate of electron transfer across an electrode-solution interface is directly dependent on the physical and chemical properties of the working electrode material. In this regard, the selection of WE is very important. Electrochemistry and electron transfer of proteins and/or enzymes has been investigated on various types of electrodes, including Au, Pt, metal oxide electrodes (such as In_2O_3), glassy carbon electrodes, pyrolytic graphite electrodes, etc. Amongst the latter list, glassy (or vitreous) carbon has shown tremendous promise because of its excellent mechanical properties, wide potential window, chemical inertness (highly solvent resistant), increased reversibility for several redox complexes and reactions involving subsequent proton transfer, as well as its relatively reproducible performance. Appropriately, glassy carbon electrode (GCE) was used as WE in the research

investigation outlined in the current dissertation. In particular, a GCE, deliberately modified with appropriate material including permselective membrane, electrochemically and/or manually pre-concentrated mediator species and hybrid composite biocompatible biopolymer hydrogels — in short chemically modified glassy carbon working electrode was used. Material types and specific techniques are discussed in greater detail in subsequent sections within this chapter and following chapters.

Since the biosensor configurations in this thesis is based on amperometric measurement, this subject area will be discussed in greater detail, and all relevant subsections will be discussed in terms of this specific operating principle.



2.2.2.1 Amperometric Biosensors

The origin of the novel field of analytical biotechnology as whole, is directly linked to amperometric devices, and as such, this class of biosensors are the most prevalent, the most extensively researched — having the widest available configurations, while also being the most successfully commercialized devices of biomolecular electronics [17, 56]. The pioneering work in the history of amperometric biosensors was done by Clark and Lyons [55, 61-62], who placed the enzyme, glucose oxidase, at the surface of the oxygen “Clark electrode” covered with a semi-permeable dialysis membrane, so creating an enzyme-based electrochemical-amperometric biosensor configuration. In this regard, it can be unequivocally stated that they invented the concept of the “enzyme electrode” [17, 56]. Their work was further researched and developed by Urdake and Hicks [17, 56, 63], and, overall, the combined efforts set the stage for the eventual realization of the first successful commercial biosensor, the eminent glucose sensor [17] – an indisputably valuable asset for sufferers of the chronic condition known as diabetes. Being small, portable

and with high specificity it enables the patient to do rapid routine blood and/or urine glucose level measurements, which in turn allows for manual adjustment of insulin dosage, and as such its development has revolutionized the health care and pharmaceutical industries. Since then, the scientific arena has witnessed a huge proliferation of amperometric biosensor configurations, in diverse areas of application, including drug and metabolite measurement, clinical diagnostics, environmental monitoring, chemical measurements in agriculture and food, etc [58].

In a definitive context, the principle of the amperometric technique is based on the measurement/monitoring of the current associated with the electrochemical oxidation or reduction of an electroactive species involved in the recognition process [55, 57-58]. The process of amperometry is usually performed by maintaining a constant potential at a Pt, Au, or carbon based working electrode or on array of electrodes. The fact that a sufficient voltage across the working electrode is essential to allow a specific (oxidation/reduction) to take place requires a reference electrode with known, fixed and stable electrode potential to be included in the cell design, examples being silver-silver chloride- or calomel electrode. With regard to enzyme-based amperometric biosensors, the electrochemically reduced or oxidized enzyme catalytically converts electrochemically non-active analytes (substrates) into products at the working electrode at a specific potential with respect to the particular reference electrode. The resulting current is directly correlated to the bulk concentration of the analyte or its consumption rate within the area adjacent to the biocatalytic layer or to the product, since the product is proportional to the non-electroactive enzyme substrate.

Due to the nature of their operational principle, amperometric sensors, including biocatalytic amperometric sensors, alter the concentration of the analyte in their vicinity; these sensors may reach a steady state but they never reach equilibrium. With regard to specific steps involved in the recognition process, multiple steps are known to occur during the biocatalytic reaction which includes the following [52]:

- The electron transfer reaction, which encompasses the transfer of electrons between the electrode surface and molecules in the analyte solution adjacent to the electrode surface. This process is heterogeneous.
- The other process involves the transport of molecules from the bulk solution to the electrode surface, which normally involves the movement of material from a high-concentration region of the solution to a low concentration region (the electrode surface) and may thus also be referred to as diffusion.
- Chemical reactions coupled to the electron transfer reaction.

The rate of the overall reaction is generally determined by the rate of the slowest step, known as the rate limiting step, and as such, the actual response may thus reflect mass-transport or kinetic limitations.

Overall, amperometric biosensors can be classified into three generations [52, 58, 64-65]: In the earliest or *first generation biosensors* (FGB), the normal product of the molecular recognition reaction diffuses to the transducer and causes electrical response (current induction). The original glucose electrode, which relied on molecular oxygen as the oxidizing agent belongs to this group of biosensors. The decrease in oxygen, or the formation of hydrogen peroxide is measured with a Clark oxygen electrode. This generation of biosensors, however, have some inherent drawbacks:

- a) The applied potential required is too high, resulting substantial interference from other species in complex matrices;
- b) The concentration of the dissolved oxygen is fluctuant, which leads to systematic convolution;
- c) The tenuity of the dissolved oxygen extensively decreases electrical currents, which in turn influences the detection limit.

To circumvent the inherited drawbacks of first generation biosensors, the idea of electroactive, artificial compounds was proposed, giving rise to *second generation biosensors* (SGB). The operating principle of second generation biosensors involve soluble low molecular weight redox compounds, known as mediators, which shuttles

electrons between protein (enzyme) and transducer in order to generate an improved response. Common mediators are ferrocene complexes, whose structures consist of a sandwich of the cation between two cyclopentadienyl (Cp) anions. The result of using these artificial electron acceptors, is that measurements become insensitive to oxygen fluctuation and can be performed at lower potentials that do may preclude reactions with interfering species. For this biosensor class, the mediator is normally contained within the test-solution, adjacent to the biocatalytic layer. Such devices have been commercialized, mostly as single-use testing format. The other group, *third-generation biosensors* (TGB), are signified by the progression from the use of freely diffusing mediator (O₂ or artificial), to a system where the protein (enzyme) and mediator are co-immobilized at an electrode surface, making the biorecognition component an integral part of the electrode transducer. Co-immobilization of the protein (enzyme) can be accomplished by different methods, such as redox mediator labeling of the enzyme followed by enzyme immobilization, enzyme immobilization in a redox active polymer, or enzyme and mediator immobilization in a conducting polymer. Overall, third-generation biosensors offer all the benefits of second-generation sensors, with the inclusion of some modifications and new additions. These biosensors are self-contained in the sense that there is no need for adding additional mediators or enzyme. Therefore, this design facilitates repeated measurements. Also noteworthy, in the context of third-generation biosensors, is that due to enzymes' renowned superior selectivity and high affinity toward substrates, direct electrical contact of enzyme to electrode has also been attempted and reported. This would obviously be the superior choice, since it would enable a lower operating potential and thus less susceptibility to interfering reactions, however due to their physiological make-up (which will be discussed later, specifically in terms of microsomal CYP450 enzyme), most enzymes cannot exhibit direct electron transfer (DET) at normal electrode surfaces. Hence, achieving DET within the development of TGB has been a "bottleneck", with success only achieved with a select few proteins (enzymes). One such protein, is cytochrome c.

The concept and principles of mediators and mediated-biosensors will be more comprehensively discussed within the context of amperometric configurations for microsomal P450 enzymes in subsequent sections.

2.2.3 Molecular Recognition

As highlighted in previous sections, an important aspect/feature of amperometric biosensors, is the molecular recognition event, which depending on the nature of the specific biological element (i.e. catalytic or non-catalytic), in turn determines the type of analyte or substrate to be measured/detected. *In the case of the current dissertation, the recognition element is enzyme based, and as such catalytic in nature. In particular, the enzyme used is cytochrome P450 isozyme, CYP3A4.* As discussed in **Chapter 1**, it is the major human hepatic cytochrome P450 isozyme, and as such, is the most important enzyme in the metabolism and detoxification of xenobiotics within the human body. A schematic representation of the contributions of CYP450 isozymes and non-CYP450 enzymes is illustrated in **Figure 2.2**.

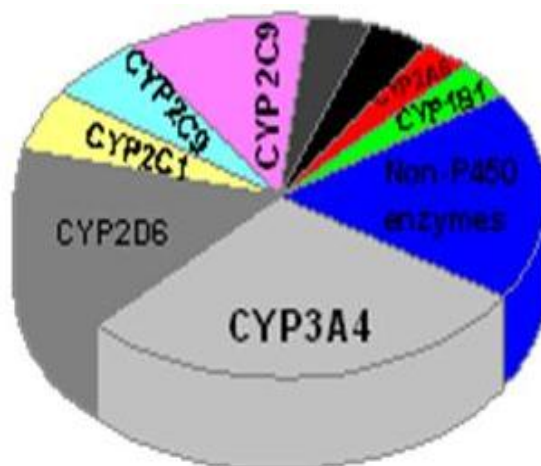


Figure 2.2 Contribution of major human hepatic cytochromes P450 isozymes and non-P450 enzymes to phase I metabolism of all xenobiotics

As shown in the above figure, the major contribution to phase I metabolism is assigned to CYP3A4. The structure of CYP3A4 has already been comprehensively discussed in **Chapter 1**, and as such will not be elaborated on at this stage, but in short: CYP3A4 is a class II, microsomal heme thiolate enzyme, whose main function is the monooxygenative metabolism of lipophilic xenobiotics. A schematic representation, showing a comprehensive overview of the stepwise catalytic reaction cycle, of the monooxygenation process is illustrated in **Figure 2.3**.

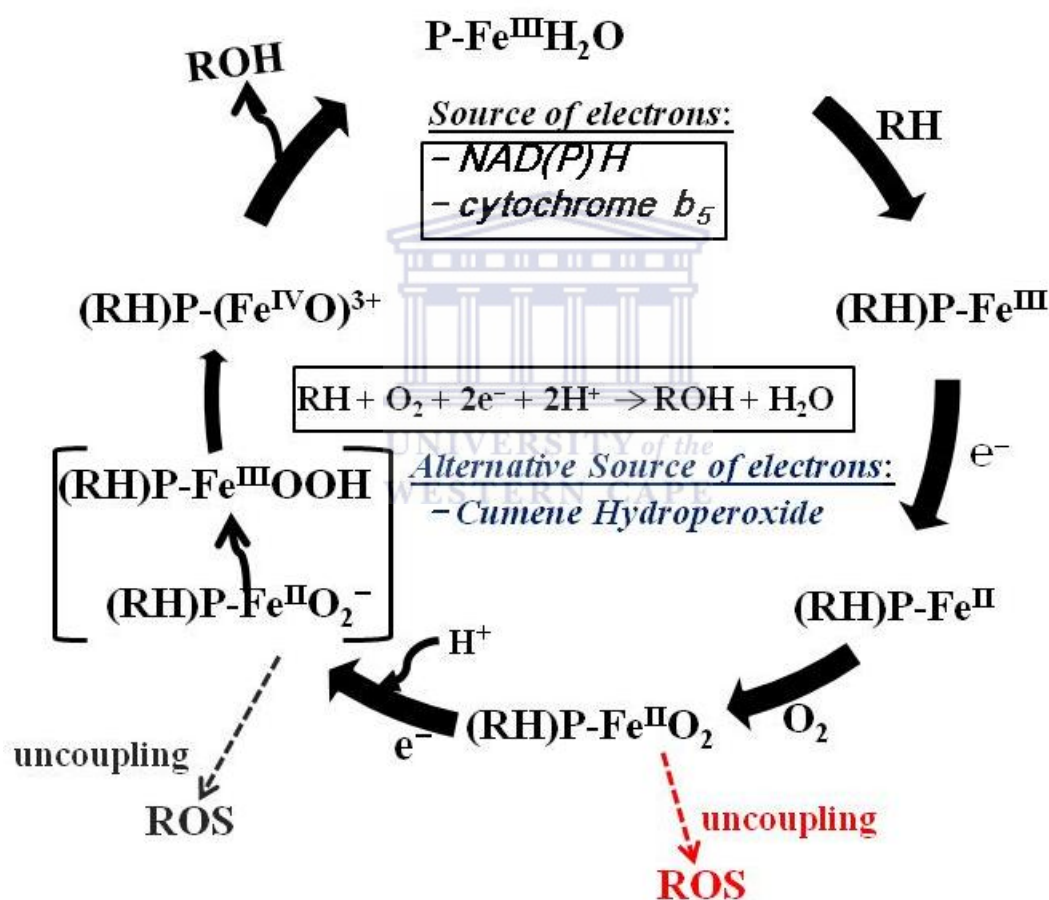
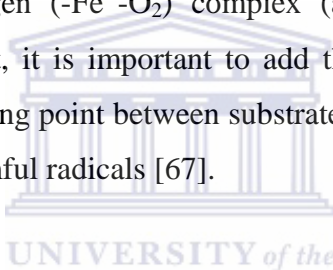
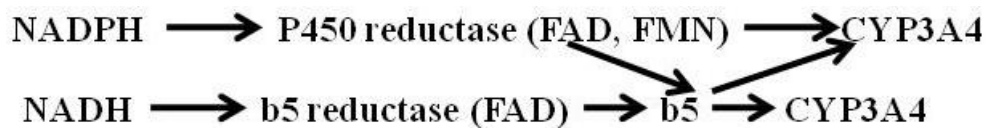


Figure 2.3 Physiological catalytic reaction cycle of CYP3A4, showing enzyme-substrate interaction and natural electron transfer (ET) donor source, with general equation shown. Also shown, is the alternative sources of ET for CYP3A4 substrate catalytic function

As observed from **Figure 2.3**: In the absence of a substrate, at the beginning of the cycle, CYP3A4 heme iron is in the hexacoordinated low spin Ferric (Fe^{3+}) state with water being the sixth ligand. Substrate binding to the hexa-coordinated low-spin ferric enzyme displaces water ligand from the active site, resulting in a change to the 5-coordinate high-spin state, which is accompanied by a marked positive shift in redox potential ($\pm 130\text{mV}$) [66], signifying the thermodynamic favourability of the first electron transfer step. It is noteworthy to add though, that in some instances, substrates may induce only partial spin shift thus resulting in a much smaller or even no redox potential shift. The transfer of the first electron from native electron transfer donor, NADPH-P450 reductase (via FMN and FAD) follows, thus reducing the ferric iron to ferrous ($\text{Fe}^{\text{III}} + e^- \rightarrow \text{Fe}^{\text{II}}$) state of heme. This can now bind molecular oxygen, forming a ferrous-dioxygen ($-\text{Fe}^{\text{II}}-\text{O}_2$) complex (also known as the oxy-ferrous complex). On this subject, it is important to add that the oxy-ferrous intermediate represents the first branching point between substrate turnover and the abortive decay with the formation of harmful radicals [67].



After the formation of the oxy-ferrous intermediate, the second electron is transferred to produce a ferric peroxy anion, which is concurrently followed by protonation of the ferric peroxy anion, yielding an iron-hydroperoxo($\text{Fe}^{\text{III}}-\text{OOH}$) (intermediate) complex, which undergoes subsequent heterolytic (O—O) cleavage, to release a water molecule and a highly active iron-oxo ferryl species, formally equivalent to a $\text{Fe}(\text{V})=\text{O}$ species named, *Compound I* [23]. This compound (or a similar reactive, electrophilic iron-oxo intermediate) then ‘attacks’ the substrate, so placing one molecule of molecular oxygen into the substrate and as such yielding the hydroxylated product which dissociates to let the cycle start again. An important factor to bare in mind, during the second electron transfer step, is that, in addition to NADPH-reductase, depending on the substrate, additional redox pathways involving cytochrome b5 may also be necessary. These can occur through the following scheme:



Although CYP450 enzymes' catalytic cycle is always described in terms of substrate binding being the initial step, electron transfer may of course also proceed without the presence of substrate, but the **likelihood** of reactive oxygen species, is more probable in such case.

With regard to the overall catalytic reaction cycle for CYP3A4 and all microsomal CYP450 enzymes in general, there are two possible major abortive reactions (shown in red and grey, respectively in **Figure 2.3**): (i) autooxidation of the oxy-ferrous enzyme intermediate with concomitant production of harmful radicals (a self inactivation process) and (ii) oxidase uncoupling with oxidation of the ferryl-oxo intermediate. Both of these reactions, known as uncoupling/decoupling reactions, produce highly active oxygen species (ROS) by autooxidation in vitro and in vivo, particularly without the presence of substrate and as such, extensively complicates the reaction cycle of this enzyme. With the regard to these uncoupling reactions, the first one has been documented as the most significant, because it was shown to be the first branching point in the catalytic cycle of microsomal cytochromes P450 enzymes, in which the efficiency of the substrate metabolism may be curtailed by the side reaction of autooxidation. In a definitive context, this particular uncoupling reaction is characterized by the release of superoxide within the enzyme, followed by its disproportionation and generation of hydrogen peroxide, a source of harmful hydroxyl radicals. In humans, such abortive decay reactions can induce apoptosis, a process which may result in cell death and cancerous growths. In this regard, this oxyferryl intermediated has been documented as being the most important natural determinant of CYP3A4 activity and/or human xenobiotic metabolism.

2.2.3.2 The enzyme electrode: Principles and classification from the microsomal cytochrome P450 viewpoint

In light of preceding literature reviewed sections on the structure and function of CYP3A4, both in the current and previous chapter, one point is infallibly clear: Electron transfer (ET) is the key juncture to generating the necessary catalytically active species within the enzyme heme pocket for successful function and/or substrate metabolism — an aspect that pertains to all P450s, whether microsomal, mitochondrial, or bacterial. As shown, *in vivo*, these pivotal ET steps are achieved through structured schemes with native freely dissociated NAD(P)H ET donors. However, the whole process is complicated and compromised by the possibility of uncoupling reactions, which may abort substrate monooxygenation. In this regard, being such a versatile and pivotal mammalian enzyme, with multipurpose *in vitro* studies being highly opportune, these complications needs to be taken into account and innovative techniques would have to be applied to prevent such occurrences, since such studies is normally done with the obligatory presence of the ET donors, either in the form of fusion protein constructs (containing heme domain of P450 enzyme linked to flavoprotein domain of NADPH-P450), or seperately added within the enzyme reconstitution sample. Moreover, mammalian microsomal CYP450 enzymes are known to be labile, especially in reconstitution solutions, requiering several reagents, such as glycerol, dithiothreitol, phospholipids and protease inhibitors for some degree of stabilization, which means that such aforementioned complications would compromise the function of an already unstable enzyme. Furthermore, NAD(P)H is expensive, decomposis over time, gets exhausted after the first electron donation step and needs to be regenerated, but is difficult to recover once oxidized.

One the other hand, the heme iron, may be regarded as a sink for receiving electrons, and in this regard, alternative sources of ET to the enzyme may be an option.

Interestingly, the so-called “shunt” reaction, which involves the application of peroxides, such as hydrogen peroxide, cumene hydroperoxide or tert-butyl hydroperoxide as alternative electron source has been documented [23, 68]. The reaction works on the principle of cytochrome P450-dependent catalytic substrate metabolism without the necessity of stepwise activation of molecular oxygen or interaction with native electron donating systems. Indeed, success in substrate turnover has been attained, however, this is at the expense of shortened enzyme activity [68-69], with enzyme denaturation observed within as short as one hour. Needless to say, for modern day requirements in healthcare, pharmaceutical, industrial and even (bio)catalytic chemistry-related research activities, this would be impracticable, and as such, alternative methods of electron sources has become a highly envisaged quest. One of the alternative methods of P450s reduction is electrochemical methods with an electrode as electron source. Enzyme electrodes based on P450s are promising for the application of biosensors and bioreactors. Moreover, enzyme-based biosensors function on the premise of an immobilized enzyme, an aspect in itself that, if done judiciously with carefully orchestrated interfacial enhancer matrix material, would significantly stabilize the biological molecule, since the latter are generally known to have very short lifetime in solution. As earlier stated, electrochemical biosensors with amperometric transduction is the most preferred biosensor configuration.

The design path and development of such an enzyme-based biosensor platform is not just a frivolous, extemporized putting together of components, but requires an absolute meticulous approach, particularly since the aim is the fabrication of a reagentless configuration in which the enzyme is integrated within the (electrode) transducer. In this regard, there are fundamental aspects that needs to be taken into consideration, as well as specific criteria that needs to be satisfied for the biosensor to be of practical use. These include the following:

- The iron(III) protoporphyrin-IX prosthetic group of the enzyme is deeply buried within the active site and surrounded by a thick protein shell. This is a natural

phenomenon, particularly in P450 enzymes, designed by nature to protect the redox state of the integrated cofactor, thus avoiding any unwanted processes with free-diffusing redox species. However, the thick protein shell introduces a kinetic barrier to electron transfer. The significance of this intrinsic property, is that direct transfer, involving a simplistic electron tunneling mechanism between the electrode and enzyme active site is not really feasible and as such, specialized ET mechanisms need to be used.

- Proteins and enzymes tend to undergo rapid, non-specific and irreversible adsorption onto (metal) electrodes, coupled with conformational changes and the consequent loss of activity (denaturation), the result of which is the formation of an insulating protein layer which hinders/prevents electron exchange with electrodes. Thus, appropriately, preventative measures need to be in place, to avoid such unwanted interactions. Such methods will be discussed in greater detail in subsequent sections.
- During the course of the reactions sequence in amperometric biosensor operation, the redox state of the enzyme is altered and as such, has to be re-generated at the electrode surface which is poised at a suitable potential. This can only occur if the enzyme is immobilized in a favourable, “productive” (anisotropic) orientation that will enable effective electron transfer to and from the enzyme’s prosthetic group.
- According to the Marcus theory for biological electron transfer [], one of the major factors affecting electron transfer, is the distance between the redox species, which in enzyme-based biosensors, is highly dependent on the accessibility of the enzyme’s redox site, as well as the specific orientation of the immobilized enzyme. In this regard, the deeply buried-electrically insulating nature of CYP3A4 prosthetic group in itself lengthens the electron transfer distance between the enzyme and electrode. Moreover, the added effect of possible unfavourable enzyme orientation will further drastically impede ET. This essentially means that innovative techniques is required to enable electrochemical communication between the enzyme prosthetic group,

while also allowing anisotropic orientation of the integrated enzyme atop the electrode surface. This can only be achieved through the inclusion of suitable electrode modifiers and ET enhancers, collectively known as interfacial enhancing material.

- The other major factors which, according to Marcus' theory directly affects the kinetics of electron transfer between two redox species, is the driving force (i.e. the potential difference) and the reorganizational energy. Of the aforementioned factors, the reorganizational energy qualitatively reflects the structural rigidity of the redox species and in terms of an immobilized enzyme, is decidedly determined by the immobilization method. Enzyme immobilization needs to be flexible enough to retain the structural and catalytic integrity of the enzyme, while also facilitating electron transfer to and from the electrode surface and allowing access to the active site for the specific substrate without requiring large reorganizational energy during electron transfer and/or electrocatalytic functioning.
- Proteins and enzymes and most other biomolecules is vulnerable to extreme conditions such as temperature, pH and ionic strength and in this regard, the enzyme film needs to provide the necessary protective environment to maintain intrinsic properties of the immobilized biomolecule.
- The immobilised biological film needs to have long term stability and durability.
- Reagentless biosensor configurations require tight fixation of all sensor components on the electrode surface, coupled with an ET pathway either by direct electron tunneling, or securely immobilised redox relays. Appropriately, sensor architecture have to be designed with this purpose in mind.

In consideration of the preceding factors and to fulfill the criteria of designing an optimised enzyme(CYP3A4)- based amperometric biosensor, it is apparent that the main aim should be to increase the electronic coupling by using electrode architectures with predefined ET pathways interconnecting the redox site within the

enzyme and the electrode surface and facilitating communication between the latter two species, while making the ET distance as short as possible. This is in turn critically dependent on the immobilization method and as such needs to be discussed in greater detail.

2.2.3.1.2 Biomolecule solid-support tethering: Immobilization methods, biorecognition component coupling techniques, and other relevant aspects

As discussed in the forgoing sections, an essential step in biosensor development is binding of the biological component to the transducer element. This immobilization feature will dictate the ultimate reliability and performance of the biosensor. Several methods can be used to tether biological molecules to solid electrode support, of which the main methods include adsorption, crosslinking, entrapment and covalent binding. A schematic representation of these methods are shown in **Figure 2.4**. These methods may be used in combination with each other or in conjunction with other techniques – a thorough discussion of the various techniques follows subsequently. In this regard, subsequent discussion is based on a combination of documented literature [17, 53-54, 58, 64-65, 70]

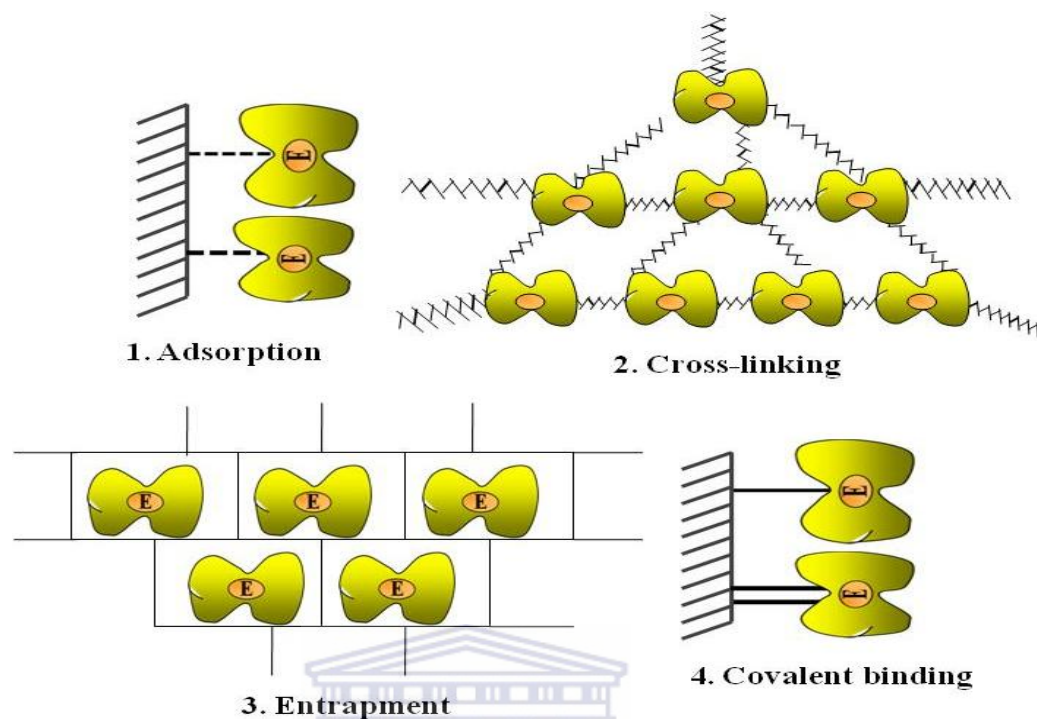


Figure 2.4: Major immobilization methods for proteins, enzymes and other biological molecules onto solid (electrode) supports

Amongst the above methods, the most simplistic and oldest involves adsorption. Adsorption of biomolecules from solution onto solid surfaces can proceed by means of either physical or chemical interactions. Physical adsorption involves van der Waals forces, ionic binding or hydrophobic forces, whereas in chemisorption on the other hand, there is a sharing or transfer of electrons to form a chemical bond. Adsorption has been successfully applied to couple proteins and/or enzymes to various solid supports, including derivatized glass, plastics, silicone rubber and most recently, conductive electrodes for biosensor application. The binding of such biological components through physical adsorption can be directly measured via a piezoelectric quartz crystal microbalance (QCM) or surface acoustic wave device which functions by detecting frequency changes, which are related to the amount of protein/enzyme bound onto the solid surface. In addition to the aforementioned methods, optical techniques of surface plasmon resonance (SPR) and ellipsometry

have also been employed to detect refractive index changes at the surface of a thin metal film as a result of biomolecule adsorption. Overall, the main advantage associated with adsorption, is that it is a simple method which can be performed under mild conditions. However, on the other hand, biomolecules tethered through adsorption were found to exhibit a certain degree of reversibility and furthermore, the forces involved in the binding are not very strong. In this regard, with respect to long term stability, durability and tight association of the enzyme film, on its own, this particular method is not entirely conducive.

One alternative approach to attachment of biomolecules to electrode surfaces is through covalent binding, which involves attachment onto the solid surface through the formation of defined linkages. This technique has been documented to result in minimal loss of biomolecule activity, and in addition, have been shown to overcome problems associated with instability, diffusion and aggregation, or inactivation of proteins commonly experienced when biomolecules are trapped on sensor surfaces by other methods. Bifunctional reagents and spacer molecules, such as glutaraldehyde, carbodiimide, succinimide esters, maleimides and periodate are commonly used for this method. The principle of covalent binding is based on the premise that biomolecules such as proteins and enzymes have many functional groups present for covalent linkage onto surfaces; these include amino-acid side chains (e.g. lysine amino acid groups), carboxyl groups (e.g. aspartate and glutamate), sulfhydryl groups (e.g. cysteine), phenolic, thiol and imidazole groups. The actual coupling procedure between the enzyme or the protein and the solid support is best achieved through functional groups on the biomolecule which are not required for its biological activity. On the other hand, the solid support is usually chemically modified, with specific reagents in order to introduce a functionality (also known as surface activation) which may then be coupled with the protein/enzyme. Covalent binding generally have the advantage that the biomolecule is usually strongly immobilized on the surface and therefore unlikely to detach from the surface during use. However, absolute care has to be taken that the reagents used in achieving immobilization of the

biomolecules on the surfaces do not result in a loss of activity due to reactions involving the functional groups. Moreover, although covalent coupling procedures have yielded a substantial degree of success for a number of biosensor systems, the drawbacks of this method and associated techniques have been documented as the production of randomly oriented, non-uniform structures of inactivated enzymes or protein molecules on the electrode (solid support or sensor) surface. This in turn highlights the need for immobilization methods which are capable of producing uniform, active layers of immobilized protein/enzyme.

The next method which proved to compensate for short-comings observed in the aforementioned methods, involves a procedure based on entrapment of the biomolecule. In this regard entrapment matrices include (semi)permeable membranes, polymers (including non conductive-, conductive and redox polymers), surfactants, sol-gels, biopolymer hydrogels and/or redox hydrogels with redox centres such as $[\text{Os}(\text{bpy})_2\text{Cl}]^{+2+}$. In a definitive context, entrapment simply involves the confinement of the specific biological molecule (e.g. a solution of enzyme, a suspension of cells, or a slice of tissue) as a thin film covering/integrated onto the transducer (electrode). With regard to membrane and/or non conductive-based polymer confinement, the negatively charged perfluorinated sulphonate polymer, Nafion™, has proven to be quite popular, particularly, due to its inherent property of reducing interference reactions through charge repulsion and as such, enabling it to also be utilized as semipermeable membrane. Overall, Nafion™ has been utilized in numerous biosensor configurations for enzyme/protein integration onto electrode surfaces. *Since the specific protocols applied in this dissertation includes Nafion membrane confinement, the specific structure and function of Nafion is discussed in subsequent sections.* A number of other polymers have been used for inclusion of proteins, enzymes, cells and organells. These include poly(vinyl-alcohol), polyvinyl chloride, cellulose acetate, polycarbonate and polyacrylamide. With regard to conductive polymer confinement on the other hand, the method of electropolymerization has widely been used to immobilize proteins in electrochemically formed polymer films

at electrode surfaces. This allows for electron transfer through molecular wiring of the protein/enzyme to the electrode and as such, has been of immense interest in electrochemical biosensors. Various polymer films, have been created on electrodes using this approach, the most eminent being polypyrrole and polyaniline-based. Immobilization of the protein/enzyme in a polymer film at an electrode by polymerization can be performed in two ways: (i) electropolymerization from a solution containing protein or enzyme, mediator and monomer (one-step method); or electropolymerization from the monomer- (and mediator) containing solution, followed by drop-coating or electrochemical adsorption of the protein or enzyme (two-step method). Entrapment of protein (enzymes) in thin bilayer lipid membrane films has become popular, since it is thought to provide a biomembrane-like environment, characterised by a liquid-crystal milieu. Such membranes can be fabricated by drop-coating or langmuir blotting (LB) deposition. Entrapment within self assembled monolayer films are also common. Overall, entrapment-based methods do, however, suffer from the weakness of leakage of biological species during use, resulting in some loss of activity. In this regard, additional re-inforcement through cross-linking usually alleviates the problem of biomolecule leakage.

Cross-linking of biological molecules by means of multifunctional reagents affords improved stability of biological molecules, confined both as adsorbed, entrapped or covalently bound species. Glutaraldehyde, which couples with lysine amino groups of proteins (enzymes), is undoubtedly the most common cross-linking agent in biosensor applications. In addition to glutaraldehyde, other examples of cross-linking agents include hexamethylene di-isocyanate, 1,5-difluoro 2,4-dinitrobenzene and diazobenzidine-2,2'-disulphonic acid, etc. Indeed, as with any technique, there are of course a number of disadvantages associated with this method: (i) complete control of the reaction is difficult and tricky; (ii) the protein/enzyme layer formed is frequently gelatinous and not rigid; most often, large amounts of biological material are required; (iv) cross-linking can result in the formation of multilayers of protein/enzyme, which may result in low activity of the immobilized layers; (v) large

diffusional barriers to the transport of species may result, leading to retarded interactions.

The other alternative method for the immobilization of biological molecules is encapsulation, which can be done in ceramics, glasses and other inorganic materials using sol-gel encapsulation technique. With respect to the sol-gel procedure, biological molecules are entrapped in an aqueous microenvironment in a porous matrix, an example being the polymeric oxo-bridged SiO₂ network. In this regard, the matrices are porous wet gels formed by the hydrolysis and condensation-polymerization of metal and semi-metal alkoxides, mostly SiO₂ materials. Such matrices are optically transparent, so enabling the chemical interactions of the entrapped biological molecules to be optically monitored. The advantages of this particular technique is that it can be carried out at ambient temperature and that the conditions of the sol-gel process are relatively mild and thus do not normally denature the immobilized biomolecules. The drawbacks on the other hand are as follows: Although biomolecules immobilized with this procedure retain their activity to a large extent and are chemically, thermally and structurally stable, sol-gels with reproducible pore sizes are required, and problems due to diffusional limitations inside the porous network, brittleness of the glassy matrix, reproducibility and variations in the preparation procedures confer some degree of limitation and as such must be taken into consideration.

Finally, other immobilization may also be achieved through bulk modification of entire electrode material, e.g. enzyme modified carbon paste or graphite epoxy resin.

It is noteworthy to add, that in most aforementioned methods: (i) The biological material may also be immobilized together with carrier proteins, such as bovine serum albumin, which also functions to minimise non-specific binding of the biomolecule. (ii) A low molecular weight, redox inactive compound, known as a

promoter, which may or may not be further activated and/or modified, is in many cases initially adsorbed onto the solid surface, followed by enzyme linkage.

Also worth mentioning, is that besides the reacting layer or membrane, many biosensors, especially those designed for biological or clinical applications, incorporate one or several inner and outer layers. Such membranes serves specific important functions [57]:

- *Protective barrier.* The outer membrane prevents large molecules, such as proteins of the biological samples from interfering with the reaction layer. It also reduces leakage of the reacting layer components into the sample solution. Moreover, a properly selected membrane exhibits permselective properties which may be additionally beneficial to the biosensor function. It may decrease the influence of possible interfering species detected by the transducer.
- *Diffusional outer barrier for the substrate.* As most enzymes follow some form of Michaelis-Menten kinetics, enzyme reaction rates are largely non-linear with concentration. Nevertheless, linear dynamic ranges may be large if sensor response is controlled by the substrate diffusion through the membrane, rather than by enzyme kinetics. This control is achieved by placing a thin outer membrane over highly active layer. The thinner, the membrane, the shorter is the biosensor response time.

Another interesting aspect to add, still on the subject of biomolecule-electrode coupling, is, that in some cases the structure of carrier matrix materials have been further manipulated, usually done by a reduction in particle size and/or the inclusion of selected (conductive) nanoparticles within the matrix in order to try and improve biocatalytic efficiency of the immobilized biomolecule. The premise here is that in the case of surface attachment, smaller particles can provide a larger available surface area for attachment of proteins or enzymes, while providing enhanced conductivity, for example, in the case of gold nanoparticles.

A final noteworthy factor to add at this stage, with the emphasis on reiteration of the absolute need for maintaining the catalytic activity of the immobilized biomolecule, is that, bioelectrocatalytic and/or biosensor coupling efficiency assesment investigations may be complimented with in-situ and/or ex-situ spectroscopic studies, in order to provide a more in-depth examination of the integrity of the protein/enzyme conformational state and substrate binding ability. This is an especially pivotal aspect in the case of cytochromes P450 in particular, who have to maintain their active conformational state, guaranteed by the presence of a specific thiolate bond between the heme iron and the highly conserved cystein residue (see **Figure 1.2(b)**) [71-72]. In this regard, such an active state can be spectroscopically interrogated and identified as a reduced carbon monoxide complex with an absorbance maxima at 450 nm [24, 71-72]. Weakening, or distortion of the heme-thiolate bond usually gives rise to the formation of an inactive species called P420 that is characterized by an absorbance maxima at 420 nm of its reduced CO complex ($\text{Fe}^{\text{II}}\text{-CO}$), rather than the expected signature P450. In this context, such assesment studies, is a preferred accompaniment to electrochemical investigations, in order to distinguish the electrochemical behaviours of the active form from that of the inactive one when developing devices based on cytochromes P450. In terms of electrochemical studies in particular, on the other hand, CO $\text{Fe}^{\text{III}}/\text{Fe}^{\text{II}}$ complex formation is usually portrayed by cyclic voltammetric peak potential shift and current signal changes, based on the premise that CO is known to rapidly bind as a sixth ligand to the reduced heme iron [73]. However in the presence of artificial mediating electron shuttlers, the exhibition/portrayal of CO- Fe^{II} complex formation is complicated by the fact that electron transfer occurs via the mediator to the enzyme prosthetic group. In this regard and to further elucidate enzyme catalytic activity, additional electrocatalytic studies with native model substrates, specifically known to be metabolized by a particular isoenzyme, accompanied by metabolite analysis and/or with inclusion of added electrochemical techniques, such as chronoamperometry and/or rotading disk electrochemistry can also be done. The aforementioned electrochemical methods is known to provide essential information regarding the number of electrons utilized

during the required oxygen reduction, a prerequisite for successful substrate metabolism, and as such, also enables the investigator to conclusively identify any uncoupling reactions. Specific complimentary spectroscopic methods to investigate CO-binding in particular, include UV-spectrophotometric studies, UV-Vis spectroscopic studies or cyclic voltabsorptometry (CVS) techniques. More on the subject of CO-binding, as well as complimentary spectroscopic and electrochemical methods, with emphasis on definitive aspects and method of operation is discussed in more detail in **Chapter 3A and B**.

In the quest to perfect the art of biomolecule tethering to electrodes in biosensor configurations, numerous peer-reviewed reports with various methods of biomolecule linkage, based on latter and aforementioned techniques either individually or in combination protocols, has been published, some of which have been summarized in the discussion below:

In a study conducted by Iwhuoa et al., an amperometric biosensor with genetically engineered cytochrome P450_{cam} as recognition component for the detection of camphor, adamantanone and fenchone, was constructed by entrapping the enzyme in the presence of BSA within vesicle dispersions of water-insoluble surfactant, didodecyldimethylammonium bromide (DDAB) on a glassy carbon electrode surface. The immobilization was reinforced by gluteraldehyde cross-linking, while cobalt (III) sepulchrates were used as diffusional electron transfer mediator for electrocatalytic experiments with substrate interactions [74]. In a different study, biosensor configurations were constructed with heme-proteins including myoglobin (Mb), hemoglobin (Hg) and horseradish peroxidase (HRP). In this regard, biomolecule immobilization was achieved by entrapment within N,N-dimethylformamide-agarose hydrogel composite, on an edge-plane pyrolytic graphite (EPG) electrode. The entrapped proteins portrayed direct and reversible electron transfer, corresponding to $\text{Fe}^{\text{III}} + \text{e}^- \rightarrow \text{Fe}^{\text{II}}$ [48]. In yet another study, a reagentless, mediated biosensor was

prepared with HRP as recognition component for the detection of hydrogen peroxide. The biosensor was constructed by galvanostatically electrodepositing polypyrrole in the presence of HRP on the surface of a carbon composite electrode which was derivatized with a ferrocenecarboxylic acid/sol-gel composite prior to the polymer/enzyme deposition [75]. The enzyme-based biosensor had good stability showing reversible electrochemistry and a formal potential of 275 mV. Other studies involving cytochrome P450 in particular, which includes bacterial, microsomal and mitochondrial, various methods, by different researchers were used. In this regard a comprehensive summary is given below:

- In a study, conducted by Paternolli et al. [76], three genetically engineered cytochrome P450 isoforms, CYP450-2B4, P450SCC (CYP11A1) and P4501A2, prepared as fusion enzyme construct (glutathione S-transferase-fused), N-terminally modified construct and low purity grade full-length isozyme construct, respectively, was used for biosensor construction. Two methods were evaluated for immobilization of the biological recognition elements, which included the langmuir blodged technique and entrapment within a biocompatible agarose hydrogel matrix. The enzyme-based biosensor configurations were then tested with regard to electrocatalytic response to respective substrates, of which the findings showed that both methods proved to be successful. However, in terms of robustness, agarose hydrogel proved superior, and in this regard even portrayed effective for stabilization of low purity enzyme constructs, a task which is normally problematic due to hindrance of ET by molecular impurities within such prepared enzymes.
- In four different studies conducted by Shumyantseva et al. [77-80], different cytochrome P450 isoforms, were used as recognition elements for construction of various enzyme-based amperometric configurations: In the first study, semisynthetic flavocytochromes RfP450-1A2, RfP450-2B4 and RfP450-11A1, each consisting of the microsomal-purified holoenzyme and a riboflavin (a synthetic flavin molecule containing FMN and FAD), conjugated to each other

by covalent binding, was immobilized onto screen printed rhodium-graphite electrodes (SPRGE) through glutaraldehyde cross-linking within vesicular dispersions of phospholipid surfactant films. Immobilization was done in the presence of BSA carrier protein molecules, while the riboflavin molecules, functioned as electron transfer mediator during electrochemical investigations, and as such, served as electron-tunneling relay between the enzyme prosthetic group and the electrode. In the other study, purified CYP11A1 holoenzyme was immobilized onto a SPRGE either through glutaraldehyde cross-linking on a diloroylphosphatidylcholine (DLPC) derivatized electrode in the presence of BSA, or through agarose-hydrogel entrapment with concurrent vesicular DLPC dispersion. In both of the latter methods, the enzyme was tethered to the electrode together with the electrochemical mediator, which in both cases was riboflavin. The third study involved microsomally purified CYP2B4, which was immobilized in a colloidal montmorillonite clay film in the presence of nonionic detergent, Tween80, which functioned to monomerise the hydrophobic enzyme for better immobilization and catalytic reactivity. The aim here was to produce an amperometric enzyme-based configuration for the detection and metabolic profiling of selected phenobarbital drugs. The drugs tested included aminopyrine and benzphetamine, and concomitant metabolite analysis corroborated electrochemical results. In the fourth investigation on the other hand, purified CYP2B4, CYP1A2 and CYP51b1 was immobilized on screen printed graphite electrodes through entrapment within a nano-structured liquid crystal film consisting of DDAB surfactant stabilized colloidal gold nanoparticle vesicular milieu. Substrates studied during electrocatalytic studies in this investigation include benzphetamine and lanosterol.

- In a study conducted by a different group [81], with regard to CYP3A4 in particular, genetically engineered, N-terminally modified CYP3A4 isoenzyme construct, either as fusion enzyme or heme domain only, was used for preparation of modified enzyme-based electrodes. The fusion constructs consisted of two parts, which were fused at genetic level during the engineering

process, and they include the heme domain of CYP3A4 isoenzyme and the soluble NADPH-dependent oxidoreductase domain from bacterial enzymes. Two methods were evaluated for enzyme linkage to the electrode, the first of which, involved electrostatic adsorption onto a PDDA polyelectrolyte-modified glassy carbon electrode. The other method was based on covalent coupling through reagents including 3-(Maleimido)propionic acid and N-hydroxysuccinimide ester onto a cysteamine-modified gold electrode. Midpoint potentials (E_m) obtained with regard to the Fe^{III}/Fe^{II} redox transitions for the CYP3A4-modified electrodes determined by cyclic voltammetry, were -297 and -357 mV vs Ag/AgCl on the GC and Au electrodes, respectively. E_m for the fusion construct on the other hand, were determined as -345 and -341 mV on GC and Au electrodes, respectively. Electrocatalytic investigations for determining catalytic activity of the immobilized enzymes was investigated with native CYP3A4 substrate, the macrolide antibiotic, erythromycin. These results showed that both the immobilized heme domain and fusion enzyme were catalytically active, and as such, both yielding metabolism products, with higher coupling efficiency observed for the fusion enzyme-modified electrode configurations.

- In a few other studies, the focus has been on the bacterial cytochrome P450, P450_{BM3} (CYP102A1) [71-73, 82], which in many aspects, resembles membrane-bound mammalian P450s [] and as such could be used as model recognition component for bioelectrochemical studies in various biosensor configurations. Various methods, by different research groups have been used to tether the enzyme to electrode surfaces for electrochemical studies: In one study, both the complete wild type holoenzyme, as well as the heme domain was each immobilized on edge-plain pyrolytic graphite (EPG) electrodes by entrapment within DDAB vesicle dispersions. $Fe^{III} \rightarrow Fe^{II}$ redox transitions could be observed of which the E_m for the heme domain was determined as -500 mV (vs Ag/AgCl). Electrocatalytic studies in the presence of atmospheric oxygen showed markedly increased reduction currents. In a different study,

conducted by Udit et.al, the integrity and bonding properties of the immobilized P450BM3 heme was studied in more detail within DDAB liquid crystal films, with the aid of in situ spectrophotometric and FTIR spectroscopic measurements. The results showed that the a combination of a hydrophobic effect and enhanced H-bonding stabilizes the ferrous (Fe^{II}) state of heme and cumulatively increases the redox potential, while also favoring a P420-state of heme. Furthermore, cyclic voltammograms did not show any significant increase in heme redox potential in the presence of CO. Overall, the findings in the latter study were that, on the one hand, the significant stabilization of the ferrous state coupled with a heme-carbonyl interaction produces a system where the added benefits of heme- π -back-bonding to CO are greatly diminished, while on the other hand, the P420-like state of heme reduces overall success in achieving substrate turnover. Their conclusions were that similar perturbations of the heme environment within such surfactant films may be particularly exhibited by mammalian cytochrome P450s. In another study, also conducted by Udit et al., the heme domain of wild-type cytochrome P450 BM3 was immobilized within a carrier matrix consisting of a liquid crystal-polyelectrolyte film, which is a combination of surfactant vesicle dispersions, DDAB and anionic polyelectrolyte, polystyrenesulphonate (PSS). The surfactant-polyanion film, DDAPSS, proved to be a stable environment for the immobilized enzyme and E_m for $\text{Fe}^{\text{III}}/\text{Fe}^{\text{II}}$ transitions was determined as ± -200 mV vs Ag/AgCl. Moreover, results were consistent with surface confined species, whereas CO studies showed a marked positive increase in redox potential. Furthermore, electrocatalytic studies in oxygen atmosphere, resulted in the signature increase in reduction current, whereas additional rotating disk electrochemical studies, on the other hand, revealed the formation of H_2O_2 , which may have also contributed to the increased reduction current and also reveals the accompaniment of uncoupling reactions during electrocatalytic interactions of the immobilized enzyme. In yet another study, the main purpose here centred on the in depth characterization of the active/inactive state of heme

environment and conformational integrity of the immobilized P450_{BM3} — cyclic voltammetry was combined with cyclic voltabsorptometry to elucidate the aforementioned aspects. In this investigation, the heme domain (BMP) of P450 BM3, prepared through genetic engineering, was immobilized within a polyelectrolyte film of either PDDA or PEI through electrostatic adsorption on a nanocrystalline SnO₂-modified solid support. In these results, reduction potentials for the active P450 form immobilized on the PDDA-SnO₂ and PEI-SnO₂ electrodes were determined as -390 mV and -580 mV vs Ag/AgCl, respectively. Furthermore, voltabsorptometric experiments revealed that, depending on the environment of the carrier matrix, both the inactive P420, as well as the active P450 species may be present, and in such cases may both contribute to the observable background current in cyclic voltammograms. In particular, it was proposed that the local environment plays a direct role in inducing the P450-P420 transition either by dehydrating the substrate binding cavity or by interfering with the H-bonding network responsible for stabilization of the thiolate bond.

- For the past few decades, Rusling and co-workers has done a significant amount of bioelectrocatalytic investigations with various heme proteins (enzymes), including hemoglobin, myoglobin and selected cytochromes P450, using different immobilization matrices, of which the findings have been documented in various peer reviewed publications, some of which is subsequently discussed [83-86], the emphasis of course being P450-modified electrodes in particular. In one study, cytochrome P450cam was entrapped within a liquid crystal film, consisting of vesicle dispersions of either DDAB or dimyristoyl-L- α -phosphatidylcholine (DMPC) on pyrolytic graphite (PG) electrodes. The electrochemical behaviour of of both P450cam-modified PG electrodes exhibited reversible electrochemistry with E_m determined as -213 mV for the DMPC-film and -220 mV for the DDAB-film (vs Ag/AgCl), while the CO Fe^{II} interaction was accompanied by a anodic potential shift, as well as the signature P450 absorption spectra shown by accompanying UV-

spectrophotometric studies. In electrocatalytic studies, interaction with oxygen and/or substrate, trichloroacetic acid (TCA) was investigated. In this regard, results showed that the electrochemically generated $P450Fe^{II}$ reacted rapidly with dioxygen, which was signified by significant increase in reduction current. Furthermore, substrate interaction induced an additional increase in reduction current, a phenomenon that was also observable in anaerobic atmosphere, whereas overall, the results did not suggest any autooxydation or uncoupling reactions, thus signifying the coupling efficiency of the enzyme-based film. In a second study, cytochrome P450cam was immobilized through onto polyion films, by making use of either positively charge polyelectrolytes or negatively charged polyelectrolytes. In the case of the cationic polyion film matrix, a combination of PDDA and PEI was used, whereas in the case of the anionic matrix, poly(styrenesulphonate) (PSS) was used. Depending on the charge of the polyelectrolyte, the enzyme was either immobilized through electrostatic adsorption, or with the aid of DNA as bonding material, while, on the other hand, enzyme immobilization within the polyelectrolyte film was done on a mercapto-1-propanesulphonic acid self assembled monolayer-modified gold electrode. Overall, the results showed that in multilayer assemblies, only the first layer of polyelectrolyte/CYP450cam was electroactive, while the MPS|PEI-PSS|P450cam exhibited the best results in terms of electron transfer and electrocatalytic efficiency with substrate, styrene. Metabolite analysis for electrolysis experiments, further confirmed enzyme activity, while on the other hand, results also showed that a small percentage of H_2O_2 was formed which also contributed to the formation of one of the metabolites, i.e. benzaldehyde. This essentially means that the reduction of oxygen in the catalytic cycle of the immobilized enzyme, gave rise to the formation of reactive species, in this case, H_2O_2 , which in itself, as discussed earlier can induce substrate metabolism on the one hand, but on the other hand, shortens the lifespan of the enzyme. In yet another study, also conducted by Rusling and coworkers, the heme domain of genetically engineered cytochrome P450-1A2 was used as recognition

component. In the platform used in these studies, the enzyme was immobilized through electrostatic adsorption in a PSS polyelectrolyte film on a carbon cloth electrode. The average E_m for the enzyme-modified electrode was determined as -70 mV (vs NHE). $Fe^{II}-O_2$ interaction was signified by a characteristic increased reduction current, which in the presence of the substrate, styrene, exhibited an anticipated further increase. Although control experiments without CYP1A2 showed no detectable formation of the enzyme-catalyzed metabolite, styrene oxide, the addition of H_2O_2 scavenger, catalase, in the presence of immobilized enzyme, also resulted in no styrene oxide formation. This essentially means that electrochemically produced H_2O_2 significantly contributed to the substrate turnover in bioelectrocatalytic experiments. In the next research investigation, microsomes, constituted by fusion proteins, consisting of selected genetically engineered cytochrome P450 isozyme heme domain, and cytochrome P450 reductase protein (with flavins, FAD and FMN), were the subjects of investigation in these bioelectrochemical studies. The P450 isozymes studies were cytochromes P450 1A2 and 3A4, for which the prepared microsomes were denoted CYP1A2ms and CYP3A4ms. Once again, polyions were used as immobilization matrix for the enzyme-modified electrodes, while the flavin cofactors of reductase, functioned as mediator. In this regard, clean gold electrode solid supports were initial modified with a 'base layer' consisting of PEI|PSS|PEI, followed by alternate adsorption of the particular microsome and PEI, thus preparing six bilayers in a layer-by-layer fashion. In both cases, enzyme configurations exhibited quasi-reversible thin film electrochemistry, with peak current proportional to scan rate (v) for up to 1000 $mV s^{-1}$. Moreover, E_m for both enzyme-modified electrodes was determined as -530 mV (vs Ag/AgCl). As earlier stated: upon reduction in the presence of CO, heme proteins form $Fe^{II}-CO$ complexes that is normally signified by a shift in E_m via the influence of complexation following ET., however, cytochrome P450 reductases have flavin cofactors and are not influenced by CO. In this regard, upon addition of CO no observable change in peak potential or current

could be detected. Overall, the results revealed that electron transfer to the enzyme heme occurs via the reductase, and as such follow the natural ET pathway observed in native physiological systems. Moreover, electrocatalysis with substrates with or without the presence of H_2O_2 scavengers showed the formation of similar amount of metabolites, while only very small amounts of H_2O_2 could be detected in the microsomal-modified films. In this regard, it was concluded that oxygen reduction competed poorly with reduction of reductase, which essentially prevented the formation of reactive H_2O_2 species and as such showed adequate coupling efficiency.

Finally, in light of all the preceding and aforementioned discussions, clearly a plethora of methods and techniques, each with its own attributes and shortcomings, are available to tailor biomolecule immobilization and electron transfer pathways for bioelectrochemical (sensor) configurations. Furthermore, secure immobilization may incur multifaceted privileges, such as securing long term sensor stability, avoiding loss of biological recognition element to the bulk of the analyte solution, as well as predefining the overall sensor architecture and proposed signal transduction process. On the other hand, however, the type of immobilization and coupling method directly affects the operational stability of the enzyme-based sensor, as well the efficiency of ET from electrode (the coupling efficiency). Furthermore, the immobilization procedure is absolutely dictated by and adapted to the specific features of the biological recognition element, such as intrinsic stability, presence of available non-essential functional groups for covalent binding, possible inhibition due to active site modification by reagent molecules, impact of binding mode on substrate diffusion to the enzyme active site (defining the linear range of the calibration graph), the local concentration of the biorecognition element (defining the maximum signal), as well as the location of the biorecognition element with respect to the transducer surface. In the case of CYP3A4 in particular, recalling all of its structure, reconstitution and reaction cycle complexities, very few research investigations endeavor utilizing it as

recognition component in sensor and/or bioelectrochemical studies. In this regard, of all the peer reviewed articles cited and and discussed in the preceding section, only three focussed on CYP3A4.

As recap, being of microsomal origin and essentially membrane bound; highly hydrophobic; requiring the obligatory presence of specific external electron transfer donors and other specialized compounds in reconstitution systems; being labile and quite vulnerable to extremities; its prosthetic group hidden within a highly insulating protein shell. Moreover, the high probability of uncoupling reactions, mostly caused by autoxidation of oxyferrous $\text{Fe}^{\text{II}}\text{-O}_2$ complex (see **Section 2.2.3**), giving rise to reactive oxygen species, a phenomenon that is common amongst membrane-bound microsomal and mitochondrial mammalian cytochrome P450 enzymes, adds further constrictions. In this regard, clearly, electrode linkage and electron-transfer pathways in biosensor configurations for this enzyme is obviously quite a challenging task, as such requiering considerable ingenuity with regard to platform design. In the same breath, however, according to documented literature findings, it has been suggested that biosensors based on such enzymes fall under the category of disposable ones [64, 87]. On the other hand, for practice application, the prosthetic group would have to be recycled during such P450-enzyme sensor operation – a task that some people have tried to overcome by co-immobilization of native NAD(P)H cofactor. However, NADPH has known inherent complications, some of which was discussed in Section **3.2.1.1**. In this regard, it is expensive, is known have a high likelihood of inhibiting the enzyme without the presence of substrate, direct regeneration of NADPH requires substantially high overpotentials. Furthermore, regeneration occurs through via a two step intermediate radicals that tend to dimerize under the formation of insoluble products, which in many cases leads to electrode fouling [88], as well as its expensive nature, its application would be impracticable. Moreover, it would defeat the main purpose of biosensors, which of course is providing alternative, cheaper methods to compliment and/or compete with existing analytical techniques. While electrochemical, chemical, enzymatic and whole cell systems for regenerating

NAD(P)H are available, these approaches are frequently inefficient or difficult to implement on a practice scale [89].

In view of the latter and preceding issues and based on peer reviewed documented research, it is suggested that harnessing membrane bound P450s and heme thiolate proteins in general, is best approached with electrochemical systems by utilizing soluble or co-immobilized surrogate, artificial mediators. *Appropriately, the approach in research design in this dissertation is based on mediated enzyme-based biosensor configuration.*

2.2.4 Mediated Amperometric Biosensors

Mediators are artificial electron transferring agents that can readily participate in the redox reaction with the biological component, and a such, assist in the rapid electron transfer. In this regard, in a more definitive context, it is a low molecular weight redox couple, which shuttles electrons from the surface of the electrode to the redox center of the enzyme. During the catalytic reaction, the electrochemically reduced/oxidized mediator reacts with the enzyme, to reduce/oxidize it and then diffuses back to the electrode surface to undergo rapid electron transfer again. An outline of the this process is illustrated in **Figure 2.5**.

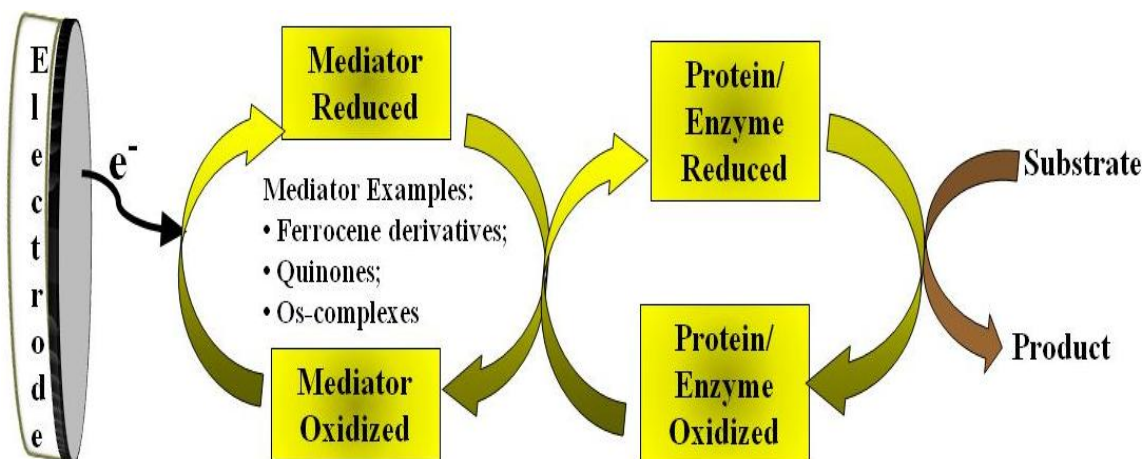


Figure 2.5: Principle of operation of amperometric mediated biosensor

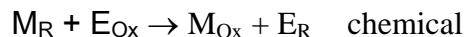
As shown in **Figure 2.5**, during the mediator facilitated electron transfer of the enzyme (protein/biological molecule), the mediator is cycled between its reduced and oxidized forms. Overall, the process is thermodynamically, but not kinetically favourable. The following equations show a more detailed sequential flow of the overall sequence of events with and without mediated electron transfer to get an idea of the main benefit of the presence of the mediator,



2.1(a)



2.1(b)



2.1(c)

where M_{Ox} and E_{Ox} are the oxidized forms and M_R and E_R are the reduced forms of the mediator and enzyme, respectively. In a bioelectrochemical setup, the overall electrochemical reaction occurs at the characteristic potential of the mediator. The M_{Ox} is thus regenerated close to the electrode surface and does not have to diffuse

very far to again undergo rapid electron transfer. In this regard, thus, a significant enhancement of the current may be observed for only a small amount of E_{Ox} present, provided the chemical reaction with the mediator is rapid. The observed current may be related to the concentration of E_{Ox} present, and therefore the mediator approach has been widely applied for the fabrication of biosensors with various biological compounds as recognition component. Since reaction of the electrogenerated M_R is not very specific however, care must be thus taken to exclude other potential oxidants that can compete with E_{Ox} , so that mediator can successfully and efficiently divert the flow of electrons between the electrode and enzyme active site. On the subject of effectiveness and efficiency, to confirm successful mediation, a mediator species should preferentially fulfill certain criteria, including the following:

- A mediator should be stable under required working conditions and should not participate in the side reactions during electron transfer.
- The mediator should preferentially have a lower redox potential than the other electrochemically active interferences in the sample.
- The redox potential of the mediator should provide a suitable potential gradient for electron transfer between the enzyme's active site and electrode.
- The redox potential of the mediator (compared to the redox potential of the enzyme prosthetic group (active site)) should be more negative for reductive biocatalysis or more positive for oxidative biocatalysis.
- A suitable mediator has to be able to regenerate the active site of the enzyme with fast kinetics, to diffuse back to the electrode to be converted there to its initial stage.
- The redox mediator has to be stable in both oxidation states and should not have a toxic nature.
- The mediator has to diffuse with high diffusion coefficient between the enzyme and electrode.
- The overpotential for the regeneration of the mediator should be pH independent.

Overall one other aspect surrounding the characteristics of an ideal mediator, is that in its reduced form, it should preferentially not react with oxygen, however, since many mediators exhibit some degree of oxygen interaction, if indeed it does, the reaction should be slow enough to not compete with the electron transfer kinetics of mediator-enzyme interaction, since it may otherwise lead to false signals. There are many available mediating species which may be used in electrochemical systems, the most common being ferrocene and its derivatives, quinones, tetrafulvalene, Os-complexes and conducting salts [46, 56, 90]. With regard to cytochromes P450 enzymes in particular, research conducted by Estabrook and co-workers has identified the compound, cobalt(III) sepulchrane as an effective electron shuttle for these enzymes. In this regard cobalt(III)(sepulchrane-mediated (electro)catalysis with a variety of P450s, including mammalian (membrane bound) and bacterial, with rates approaching that of native NAD(P)H-driven systems have been realized.

Generally, cobalt(III) sepulchrane $[\text{Co}(\text{sep})^{3+}]$ is a cage compound. The term cage compound refers to the class of transition metal complexes enclosed by encapsulating ligands ('cages'). Generally, these encapsulating cages are macro-multicyclic ligands, which consist of a non-planar arrangement of three arms enclosing a 3D space, into which donor atoms have been incorporated, which in turn allows encapsulation of metal ions within these cages. Examples of cage-type macrocycles, are 'clathrochelates', 'cryptans' and 'bis-tren derivatives', where the latter two contains mixed N-O donor atoms, while the former one contains unsaturated N-donors within the 3D space. Sepulchrane, on the other hand, is a class of saturated amine-donor macrobicycles (1,3,6,8,10,13,16,19-octaazabicyclo[6.6.6]eicosane), called 'cage amines', of which a graphical illustration is shown in **Figure 2.5(a)**. Incorporation of the metal ion (Co^{3+}) into the sepulchrane cage results in a thermodynamically and kinetically inert complex $[\text{Co}(\text{sep})^{3+}]$, in which the metal ion is not easily released. A graphical illustration of $\text{Co}(\text{Sep})^{3+}$ is shown in **Figure 2.5(b)**

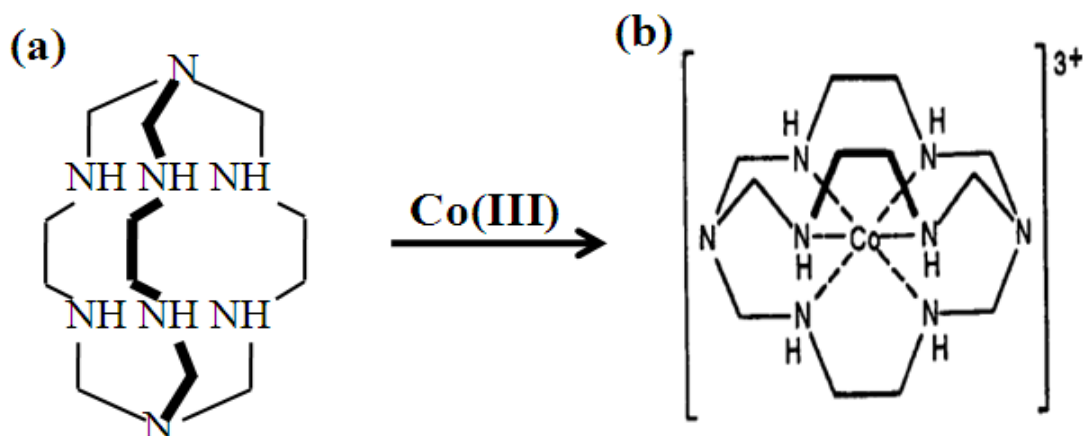


Figure 2.6 (a)The cage-type N-donor macrobicyclic: Sepulchrates
 (b)Sepulchrates with incorporated Co(III) transition metal ion:
 Cobalt(III)sepulchrates

The distinctiveness about these cage complexes, is the excellent reversible metal-based electrochemistry in aqueous and other solvents, which is particularly interesting for applications as electron relays in electrocatalysis. With regard to $\text{Co}(\text{Sep})^{3+}$ in particular, which according to research findings was shown to have a formal potential (E°) of between ± -550 to -700 mV (vs Ag/AgCl) which of course is a sufficiently negative potential to be able in turn reduce the ferric ion of the cytochromes P450 enzyme heme group, hence the popularity of applying this particular compound as surrogate mediator for these enzymes, to couple them to an electrode.

In a general context, mediation may be homogeneous or heterogeneous. Since homogeneous reactions refers to both the mediator and enzyme freely diffusing in solution, it will not be further discussed, as it falls out of the scope of this thesis. With regard to heterogeneous mediation on the other hand, particularly in terms of amperometric biosensor configurations – depending on the level of integration of the mediating species within the transducer surface, the biosensor may be secondary or

reagentless and/or tertiary configuration. In secondary biosensor configurations, as mentioned in **Section 2.2.2.1**, the mediator is added to the bulk of the solution. Reagentless configurations on the other hand, requires mediator confinement as close as possible to the electrode, along all other necessary components. Moreover, tight fixation of the mediating species is important, while architecture should to be such that leakage is prevented, which is crucial, since mediator leakage will obviously directly affect the obtained signal. Moreover, such leakage will concomitantly affect the long-term biosensor stability, while inadvertently, can also lead to contamination of the adjacent sample. On the other hand, movement of the mediator is an absolute prerequisite for productive and successful electron transfer in amperometric biosensor configurations. In addition to this, most mediators are small molecules, with molecular weights close to that of the enzymes' substrates, which makes retaining them at the electrode surface more difficult, as long-term leaking is highly probable. Taking into consideration the latter and aforementioned constricts, options for conferring effective retainment of mediators at electrode surface, while concurrently allowing mass diffusional movement of mediator, as well as rapid electrochemical communication are fairly limited. In this regard, techniques based on different mechanisms have indeed been formulated. (i) A relatively easy approach is based on simply mixing the mediator into a carbon paste, followed by enzyme immobilization on top of the carbon paste surface. Further modification with additives, such as stabilizers or polyelectrolytes may also be added. (ii) Another approach involves modification of the enzyme (protein) itself with covalently bound redox mediators, as such forming 'electroenzymes'. The premise here is that the covalently bound redox relays are supposed to shorten the electron transfer distance between the deeply buried active site and the enzyme surface by allowing an "electron hopping" via the enzyme-bound artificial mediators. A third approach combines flexibility with binding of the redox mediator by covalent attachment of the redox mediator molecules via long spacer chains, either to the electrode surface (seaweed mechanism), a suitable matrix, or the outer surface of the enzyme itself (whip mechanism). Alternatively, covalent binding of redox species to the backbone the

immobilized matrix, such as a conductive polymer, can be done, thus creating a redox polymer which is then used to wire the enzyme to the electrode. “Redox hydrogels” consisting of a poly(vinyl imidazole), a poly(vinyl pyridine), a poly(acrylic acid) or poly(allylamine) backbone with covalently bound osmium-complexes or poly(siloxane) backbones with covalently bound ferrocene units have also been applied to provide an increased local concentration of redox mediator.

Although theretically, these techniques are promising, in practise, as with any subject area, they are each associated with some constricts or drawbacks, for instance, techniques are only successful when the enzyme is in solution, while most suffer from mediator leakage from the reagent layer. Moreover many of these methods involves modification of the enzyme/protein itself, which can only be successful for highly stable enzymes, a demand which is essentially unrealistic, while some techniques also require extremely technically complex and expensive approaches. Furthermore, covalent mediator attachment, theoretically identified as the most attractive method – in practise have not been able to ensure coupling of redox groups close enough to the enzyme’s redox center to ensure fast enough electron transfer in order to effectively compete with molecular oxygen. Nonetheless, in spite of such complications and drawbacks, with regard to the aforementioned techniques, some degree of success was indeed attained. Although at this stage, choosing an appropriate mediator confinement technique may seem like an exercise in futility; a good approach is still realizable, by choosing a multifaceted matrix that not only allows fairly simplistic mediator uptake/coupling, but also contributes to sensor performance by promoting permselectivity. In this regard, in terms of versatility, permselectivity, as well as numerous other inherently novel attributes, the superior choice would be the eminent polymer electrolyte, nafion[®].

chemically and thermally very stable, mostly due to an absence of sites for attack by reactive oxygen radicals, since C–F bonds generally cannot react with hydroxyl (OH) and other radicals even at elevated temperatures. Moreover, the unique anatomical combination and arrangement of the PTFE, the fluorocarbons and the ionized sulphonic acid groups, confers a unique heterogeneity to nafion, complimented by numerous inherent peculiar features such as ion exchange selectivity, good wetting properties, self-organization in hydrophobic/hydrophilic domains, chemical and biological inertness, thus enabling the polymer to have numerous and diversified applications that is unparalleled by most other polymers, whether electron conductive, non-conductive and/or electropolymerized. To fully understand and appreciate these features, the microscopic structure of nafion is further elucidated. The first eminent structural unique quality of nafion, is the fact that nafion films feature internal segregation of hydrophobic and hydrophilic domains: On a microscopic level, this ion containing polymer is known to separate into different phases, including ionic, organic and interfacial regions – resulting from a unique cluster type structure containing “water-filled pockets” and aqueous ions embedded in a continuous hydrophobic fluorocarbon surrounding. The first phase constitutes the hydrophilic ionic cluster phase which contains the sulfo ion groups, the dissociable counter ions and hydrated water, of which the latter in its properties do not differ from water that occurs in the bulk of the solution. The second phase is the teflon-like fluorocarbon framework (backbone) surrounding these clusters and is essentially hydrophobic. The third phase on the other hand, refers to the minor subsidiary area between the hydrophobic backbone and the hydrophilic ionic clusters which mainly consists of a flexible amorphous part of the perfluorocarbon backbone and in general constituted by an intermediate hydrophilic phase. A schematic representation of the phase segregation in a nafion membrane is shown in **Figure 2.6.2**.

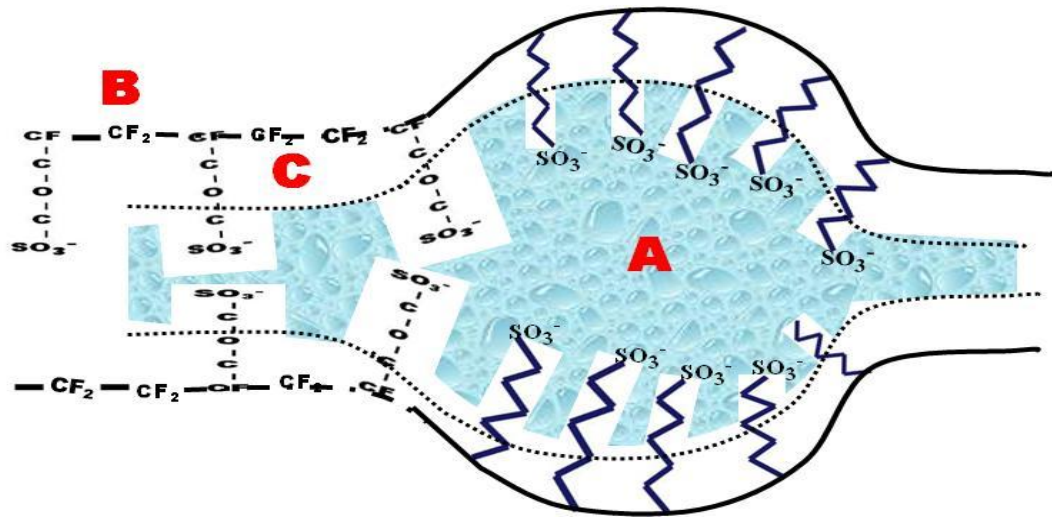


Figure 2.8: Nafion structure showing schematic presentation of the different phases observable in a nafion membrane. The sulfo groups are clustered in hydrophilic inclusions, referred to as phase A. Phase B refers to the teflon-like fluorocarbon backbone, and is essentially hydrophobic. Phase C is intermediate in hydrophilicity.

With regard to the physical characteristics of the ionic clusters, different models by various researchers has been proposed, but generally — they are roughly spherical in nature with a diameter of $\pm 40\text{-}50 \text{ \AA}$ (4-5 nm), which varies with water content, as well as the equivalent weight of the particular nafion membrane and the type of cation (counter ion) contained within the clusters. Generally, these clusters are randomly distributed throughout the backbone tetrafluoroethylene (TFE) polymer and they are inter-connected by small channels of approximately 10 \AA (1 nm) in diameter. It has also been proposed that the average cluster contains about 70 exchange sites and approximately 1000 water molecules. A graphical illustration of the cluster network, highlighting the physical characteristics of the sulfo ionic clusters is shown in **Figure 2.6.3**.

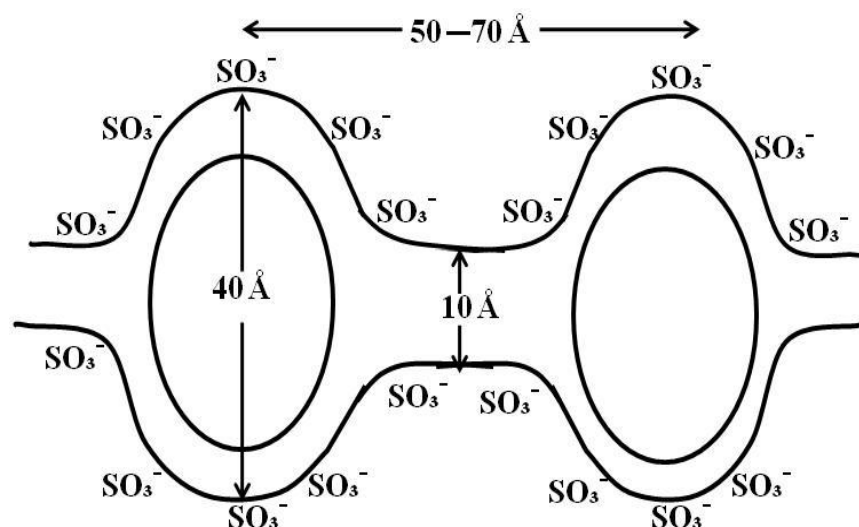


Figure 2.9: The characteristic ionic sulfo cluster network in a Nafion membrane

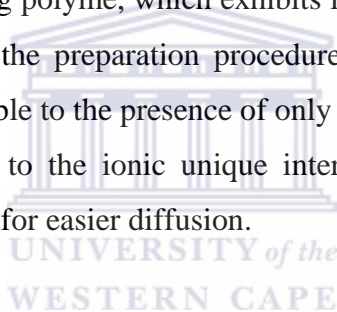
The channels connecting the ionic clusters are generally thermodynamically stable and they function mainly in determining the transport properties of the ions (counter-ions) and water, while the water content/degree of hydration is of great importance since it by-and-large dictates the properties of Nafion polymer membrane/film. The water content is in turn determined by the type of counter-ion contained within the ionic cluster phase. On the subject of the water content and the type of counter-ion — in these nafion ionomer films, the water increases the free volume of and decreases the PTFE polymer chain concentration in the ionic cluster, and as such, in this context, the water of hydration acts as a plasticizer for the ionic cluster region in nafion and ionic polymers in general. On the other hand, though, the water content of the ionic clusters decreases as the size of the counter-ions increases, and since Nafion is known to have a high preference for large organic cations relative to smaller organic and inorganic cations, this is not an uncommon phenomenon. In this regard, thus, as the water content of the cluster decreases, the polymer chain material must unequivocally play an increasingly significant role in determining the chemical environment of the cluster region. Since the TFE backbone in nafion is highly hydrophobic and has an extremely low dielectric constant, this essentially means,

that, in the case when a large organic cation is the counter-ion and as its concentration increases, the ionic cluster resembles a lipophilic phase; conversely, when a small cation is the counter ion, the water decrease is considerably less, and as such, in such cases, the ionic clusters in nafion remain essentially hydrophilic. An important aspect to add in the context of counter ions, is that nafion's high affinity for (large) hydrophobic cationic counter ion species is contrary to the characteristics exhibited by conventional ion-exchange material. Moreover, research has conclusively shown that nafion's method of retention/pre-concentration of cationic species within the polymer is dictated by hydrophobic interactions, which differs considerably from conventional ion-exchange resins and/or electrostatic binding polymers, in which electrostatic forces dominate the retention interactions. These fundamental differences in exchange characteristics between nafion and other ion-exchange materials/polymers is best explained by highlighting the eminent structural differences between the them: Firstly, conventional ion-exchange resins are covalently crosslinked while nafion is not. In this regard, the Gibbs-Donnan equation, which is the fundamental thermodynamics equation for exchange reactions, accounts for the effect of crosslinking through inclusion of the so called PV term, which is a term that functions to discriminate against ions of large size. Since nafion is not cross-linked, there is no PV-based discriminating against large ions, and thus, such ionic species may be partitioned into nafion without the thermodynamic penalty inherent in the Gibbs-Donnan equation. The second significant structural difference, is that in nafion only about one in eight monomer units is sulphonated, conventional ion-exchange resins are close to 100% sulphonated. This essentially means that the large segments of uncharged chain material allow for hydrophobic interactions which drive ion-exchange reactions for cations in nafion. Other inherent dissimilarities between nafion and electrostatically binding polymers which are of significance in this subject area is the difference in dielectric constant of the chain material and the charge density divergence: nafion has a very low dielectric constant, as well as a fairly low charge density, whereas the converse is exhibited by the other electrostatically binding polymers.

One other area of significance, is the subject of transport properties within nafion polymer films, which is a pertinent aspect, especially since the ionomer is known to take up electroactive counter ions, a feature that is of particular relevance in the application of electrochemical studies and biosensors. In this context, unlike in other membranes where transport, in accordance with the Donnan equilibrium, is a one-dimensional process; in Nafion, transport does not comply with the Donnan effect and actually occurs through a three dimensional process, largely controlled by an effect known as percolation. The actual mechanism of charge transport in nafion polymer films (in the absence of chemical kinetic complications), consist of mass transport (diffusion) of the electroactive species, electron hopping and migration of counter ions. However, research has conclusively determined the electron hopping process to be equivalent to diffusion, and as such, the overall mechanism of charge transfer within nafion polymer films, in the absence of chemical kinetic complications, is by-and-large dictated by diffusion and as such, the overall rate can be described by an apparent diffusion coefficient (D_{app}). On the other hand, depending on the thickness of the formed nafion film, regions of monolayer (thin-layer) behaviour may or may not be observed, for example, in a study conducted by Bard and coworkers, a nafion film with thickness $\approx 0.1\mu\text{m}$ with incorporated $\text{Ru}(\text{bpy})_3^{2+}$ on a glassy carbon electrode exhibited thin-layer behaviour below 30 mVs^{-1} , accompanied by a small separation between anodic and cathodic peak potential (ΔE_p), which was independent of scan rate (v) and a linear behaviour of peak current (I_p) vs v ; whereas nafion film thicker than $2\mu\text{m}$ with incorporated $\text{Ru}(\text{bpy})_3^{2+}$ exhibited no region of monolayer behaviour.

The aforementioned segments provided important insight into nafion's peculiar structural characteristics and subsequent distinctiveness in behaviour and function relative to other ionic-, ion-exchange- and electrostatically-binding polymers and/or materials. As gathered by these discussions, considerable differences are eminent,

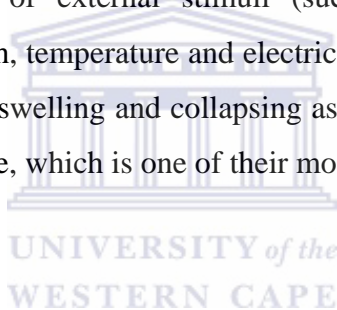
which of course would profoundly affect anticipated results at chemically modified electrodes based on nafion as apposed to other ionic polymer and coordinating polymer electrodes, some of which was highlighted and discussed. In this regard, a last few relevant variations are highlighted, which provides more insightful incentive for the polymer's popularity of application. Firstly, research has shown that nafion-based films has a greater lifetime than other electrodes of this type. Moreover, the the retention of the electroactive molecule is more stable, while the counter ion species is retained and film stays on for longer. Such etxtended lifetime is of course highly beneficial in possible applications. Secondly, nafion polymer films shows no difference in observed electrochemical properties irrespective of preparation method, i.e. wether one-step- or multiple-step coating procedure, which is unlike what can be observed for a coordinating polyme, which exhibits large variation in electrochemical properties, depending on the preparation procedure. It has been proposed that the difference can be attributable to the presence of only comparatively weak electrostatic interaction in nafion and to the ionic unique interchannel-connected ionic cluster morphology which allows for easier diffusion.



In a final note, based nafion's diverse areas of application, its peculiar structural features, coupled with its simplistic film formation, which simply involves traditional dip-, spin-coating or casting procedures from the ionomer solution, known biocompatibility and its unparallelled discrimination ability bewteen positively and negativele charged species, creates an easy comprehension of its popularity in polymer film/membrane application. Moreover, the fact that electroactive mediating species can be stably incorporated into its matrix allows for close proximation to subsequently immobilized enzymes in bioanalytical applications, which in itself is invaluable for electrochemical communication purposes.

At this stage, to recapitulate — latter and previous sections provided comprehensive insight into important aspects of tayloring electrode architecture for

stable CYP450-3A4 tethering, with special reference to enzyme structural and functional features and requirement constricts, immobilization methods, mediator aspects etc. In view of the extensive elaboration on these aspects, there is not much left to discuss, however, one final important aspiration for biosensor to be of practical use, is that that once formed, the biological film must be adaptable to different environments. In particular, the immobilized films need to be resistant to a wide range of physiological pHs, maintaining their stability and activity with changes in temperature, ionic strength and chemical composition [59]. In this regard, polymeric hydrogels, in particular has proven to be tremendously beneficial, especially in the case of membrane-bound CYP450 isoenzymes. In this regard, they exhibit various physical and chemical phenomena, such as bending and volume change in the presence of external stimuli (such as changes in pH, solvent composition, ionic strength, temperature and electric field [60]. Moreover, these gels can undergo considerable swelling and collapsing as a function of their environment, up to 1000 times in volume, which is one of their most eminent qualities.



2.3.6 Polymeric hydrogels

The inherent biocompatibility of polymeric hydrogels together with their ability to simulate natural tissues makes them potentially important electrode-coating materials, and as such, they are excellent carriers of biomolecules, which can be immobilized within the hydrogel matrices.

Hydrogels are three-dimensional, hydrophilic, polymeric networks capable of absorbing large amounts of water or biological fluids. The networks are composed of homopolymers or copolymers and are insoluble in water, through the presence of chemical cross-links, otherwise known as tie-points or junctions; physical crosslinks,

such as permanent entanglements; and/or ionic interactions. These hydrogels exhibit a thermodynamic compatibility with water which enables them to not dissolve in water at physiological pH, but allows them to swell considerably in aqueous media. Moreover, gel volume transitions can be induced by temperature, pH, or ionic strength among other stimuli, and collectively these phenomena has inspired research investigations for applications of these gels as potential actuators, artificial muscles, in sensors, controllable separation membranes and drug delivery vehicles. With regard to sensor application in particular, hydrogels can either be used in the interior of sensors, as a gel matrix to imbed bio-recognition proteins, such as enzymes; or they may be applied to the exterior of the sensor. As exterior coatings, the polar, (un)charged, water swellable, flexible materials mask the underlying surfaces by producing a hydrophilic interface between the solid surface and aqueous bulk.

With respect to known labile isoenzymes, membrane-bound CYP450s in particular, it was documented that a soft hydrogel is the most suitable environment to retain the enzyme's activity and integrity. In this regard, the greatest promise was shown with water soluble agarose. Moreover, agarose can be blended with other water soluble non-toxic polymers, such as poly(vinyl alcohol) (PVA), to create biopolymeric gel that ensures stable enzyme encapsulation and catalytic retention. Both agarose and PVA are promising outer membrane coatings for sensors, because water-soluble analytes can readily diffuse through the water-swollen polymer gel layer. The degree of analyte diffusion is readily modulated by controlling crosslink density of the gel, which in turn controls the gel water content and openness of the polymer network.

2.3.6.1 Agarose and related relevant subjects

Agarose is a highly prominent natural biopolymer, which has a long-standing application in the separation and/or purification of various biological molecules, including enzymes, polysaccharides, nucleic acids and proteins, usually done through gel permeation- and/or affinity chromatography methods. This polymer is a naturally occurring polysaccharide, and in a definitive context, it is a neutral component of polygalatoside agar; in particular, it is one of the two major components of agar, with the other major component being agarpectine. The structure of agarose is based on a linear polymer consisting of repeating units of **alternating** 1,4-linked 3,6-anhydro- α -L-galactopyranose and 1,3 linked β -D-galactopyranose. A schematic illustration of the structure of agarose is exhibited in **Figure 2.7.1**.

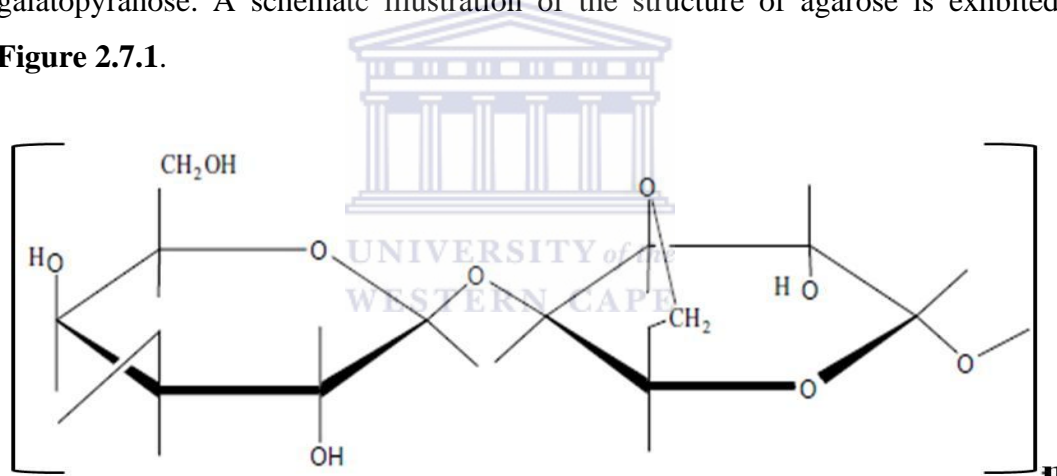


Figure 2.10: Structure of Agarose

When dissolved in water, agarose forms thermoreversible gels, the characteristics of which essentially involves a temperature controlled liquid-to-gel forming process. In this regard, in a hot solution, agarose chains exist in stiff and disordered configuration, whereas upon cooling below ± 40 °C, the coils form orderly helices which subsequently aggregates into thick bundles through forming inter- and intramolecular hydrogen bonds. These bundles contain large pores of water, and are characterized by a soft porous gel consistency, of which the pore size can be

controlled by the concentration of the agarose. In general, agarose gel matrices exhibit considerable elasticity and high turbidity, complimented by an aqueous microenvironment and significant bioaffinity, and the cumulative effects of these features makes it an ideal biopolymer for the immobilization of biological molecules on solid substrates, including electrodes. In fact, agarose has proven to be the superior polymer gel for preserving enzyme activity in bioreactor-based electrochemical studies with microsomal CYP450, compared with other tested gels, such as polyacrylamide, calcium alginate and prepolymerized polyacrylamide hydrazide — which, overall is highly significant study, since suitable immobilization methods for mammalian microsomal P450 enzymes are not well established, because these enzymes are labile. Moreover, it was documented that gel-entrapment is the preferred immobilization method if the purpose is the construction of reusable bioreactor and/or biosensor.

The beneficial aspects of agarose can be further exploited by combining it with other biocompatible polymers, in the form of blends, copolymers and/or interpenetrating polymer networks or gels. Moreover, polymer blending is one of the most effective methods for providing highly specialized composite materials that combine the physicochemical qualities of both components and overcome their individual shortcomings. In this regard, the hydrophilic polymer, poly(vinyl alcohol) (PVA), which is non-toxic, is frequently used in biomedical applications and protein immobilization, has numerous industrial applications and is equally well-known for its good membrane forming ability has proved highly compatible in combination with other polymeric materials. In fact, agarose and PVA are often used to form bi-composite matrix for enzyme immobilization.

Generally, in a definitive context, PVA is an uncharged, water soluble polymer which is commercially prepared by the hydrolysis of poly(vinyl acetate). A schematic illustration of PVA is shown in **Figure 2.7.2**.

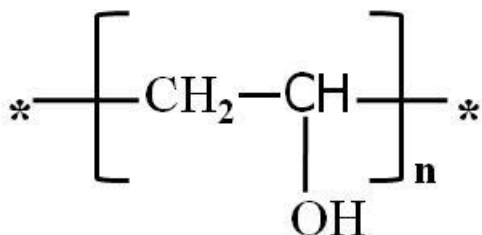


Figure 2.11 Structure of Poly(vinyl alcohol)

In a general context, different ‘grades’ of PVA are commercially available with varying degrees of hydrolysis and a range of molecular weights; however, irrespective of grade and/or molecular weight, their hydrophilicity and chemical inertness remains an essential part of the polymer’s structural integrity, which are two aspects that play an eminent role in their biocompatibility. In fact, a thin thin surface coating of PVA is frequently applied in biosensors to ensure the prevention of non-specific binding of protein molecules, which in itself, is a fundamental prerequisite for success of performance criteria in such devices. Above and beyond, the aforementioned attributes, PVA hydrogels can easily be formed by polymer-grafting, or simple ionic complexation and/or crosslinking with suitable reagents, such as poly(acrylic acid), citric acid, glutaraldehyde and acid catalysts, or polyelectrolytes. Moreover, the aforementioned interactions concurrently confers insolubilization of PVA during hydrogel formation and as such, alleviates its poor instability in aqueous medium, (which is a known weakness of ‘pure’ PVA), while simultaneously enhancing the structural porosity, mechanical stability and robustness of PVA. A particular popular choice among these blending-crosslinking agents, is amine-containing polyelectrolyte, polyethyleneimine (PEI), which induces hydrogel formation in PVA through ionic interactions.

Generally PEI is a charge modifier which has found widespread application as membrane surface modifier, by blending it with the interfacial enhancing matrix material. Its contribution to the improvement of biosensor performance is a

particularly interesting area of application, and in this regard, it confers multivalent bonding interactions between reagent-layer components, while concurrently improving hydrophilicity on electrode surfaces, and its presence also contributes to providing unique microenvironment for the immobilized enzyme. In a definitive context, PEI is a branched chain cationic hydrophilic polymer with an abundance of amine groups, which at physiological pH, are highly protonated, thus conferring multiple interactive functional sites to ionically interact with other polymer species with anionic groups. A schematic representation of the structure of PEI is shown in **Figure 2.7.3**.

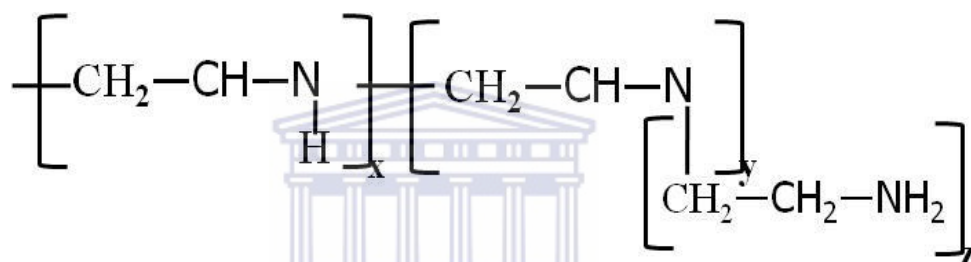


Figure 2.12 Structure of Polyethyleneimine (PEI)

With reference to the interaction between PVA and PEI in particular — the interaction during the blending of the two homopolymers is highly ionic in nature, resulting from ion complexation between the anion (CO²⁻) group of the PVA and the cationic (NH₃⁺C) of the PEI, of which the overall result is an ionically crosslinked composite, which is insoluble. The so produced blend, is highly hydrophilic and preferentially absorbs water, due to the extensive interaction arising from intra and inter molecular hydrogen bonding and dipole-dipole interactions between water and the functional groups of PVA/PEI such as amine, acetal and hydroxyl, as well as some unreacted amine moieties.

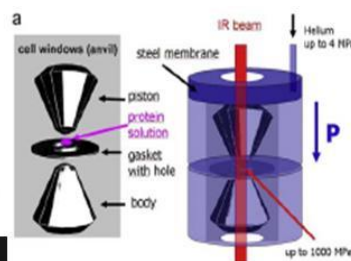
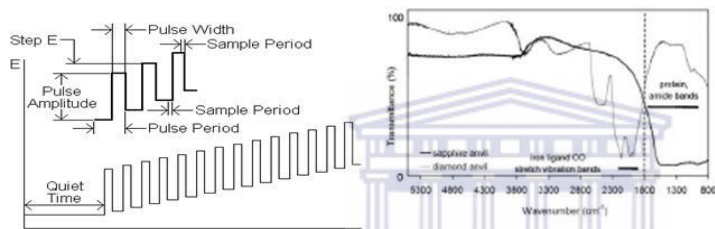
In all analytical techniques, as is the case in any (bio)sensor, based on molecular recognition, standard protocols for evaluation of performance criteria, in accordance with standard IUPAC definitions needs to be examined. Amongst these criteria are:

- (i) Calibration characteristics which; are based on sensitivity, working and linear concentration range, detection and quantitative determination limits;
- (ii) precision, accuracy and repeatability;.
- (iii) Selectivity and reliability; and finally,
- (iv) time factors, which includes response times, recovery times and lifetime of the biosensor.

It has already been established that the optimisation of biosensors is by and large dependant on the immobilization technique used, however, as biosensors are self-contained, all parts being packed together in the same unit, elegant research on new sensing concepts, coupled with numerous technological innovations, has opened the door to achieving higher sensitivity, specificity, simplicity and inherent miniaturization of modern electrical bioassays permitting them to rival the most advanced protocols

CHAPTER 3

Variables of Investigation, Practical Aspects and General Protocols



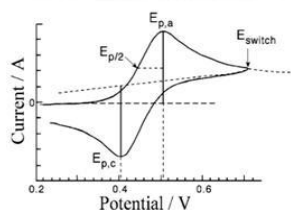
Michael Faraday



William H. Nernst



Scanning Electron Microscopy



A.M. Ampère

Chapter Prelude

This chapter consists of two parts. Part A takes a much closer look at the specific variables which needs to be considered during the application of cytochrome P450-3A4 biosensors as applied in the scope of current dissertation. In this regard, the aspects covered in this chapter is aimed at forming the basis of the experimental methods of investigation, particularly in terms of biosensor configurations including thermodynamic parameters, kinetic parameters, as well as performance factors which include range, linear range, detection limits, time factors, precision, accuracy and repeatability. Furthermore, the significance of this review is that it aims at providing the reader an enhanced understanding of obtained results, since it comprehesively explains and defines important aspects, as it applies to the enzyme-based electrochemical and/or bioelectrocatalytic factors in this study. The second part, gives a succinct overview of general experimental protocols as pertaining to the dissertation as a whole. Also included are all the materials and reagents used throughout the conduction of the PhD research, including general preparative protocols of samples and reagents. In addition to this, the school of thought with regard to relevant calculations of specific parameters are also provided.

3A Variables of Investigation

3A.1 Introduction

A biosensor in the context of this thesis may be described as a (bio)analytical device which exhibits the chemistry of the immobilized biological component, with respect to its electron transfer processes, its reduction and oxidation, adsorption phenomena, kinetics of electron transfer and reaction mechanisms and catalytic interactions – by through electrochemical methods ~~and~~ by making use of analytical tools. To effectively determine the aforementioned phenomena, the type of transduction method is a key juncture, which according to the scope of the current dissertation is electrochemically based. Generally, electrochemical transduction operates on the fact that during a bio-interaction process, electrochemical species such as electrons are consumed or generated, and as such, producing a measurable electrochemical signal. In this regard, it is evident that evaluation of all of the relevant aspects and parameters pertaining to the operation, and performance of the prepared biosensors are by-and-large based on analytical electrochemistry methods, which are collectively referred to as Electroanalysis. Appropriately, this subject, together with all relevant related topics are subsequently defined and discussed.

3A.2 Electroanalysis (Electroanalytical Chemistry): Theoretical Aspects

On a broad scale, electroanalysis may be described as the science of carrying out analytical chemistry by making use of electrochemistry. At the core of this subject area, are two prominent electroanalytical observables, which includes potential (E) (also called voltage) and the current (I) (or its integral, i.e. charge (Q)). During electroanalytical analysis experiments, the interplay between these observables (E , I) and chemical parameters are observed, assessed and subsequently

exhibited in appropriate configuration. It is noteworthy to also add that since current is expressed per unit time (current (i) = amperes (A); i.e. coulombs/second) – time also plays a significant role in electroanalytical techniques. Generally within the context of electroanalysis, potential measured is referred to as potentiometry, while current measurement done in association with amperometry and its main co-topic, voltammetry. In a more descriptive context, potentiometric detection requires two electrodes, which includes the working electrode and the reference electrode and measurements is made at thermodynamic equilibrium conditions, which essentially involves conditions with no current flow. The potential difference, measured between the two electrodes is then related to the quantity of the electroactive species/analyte. In current measurement detection techniques on the other hand, the focus is on the current passing through a polarizable electrode, which is generally measured as a function of careful potential manipulation (controlled potential methods). The magnitude of the current is directly proportional to the concentration of the electroanalyte species in the electrolyte solution. Compared to potentiometry, amperometric techniques has high precision and accuracy, and is much more versatile. Moreover, a complete study of an electrode process requires measurements of kinetics, as well as thermodynamics, for which potentiometry is inadequate, while amperometric based techniques on the other hand can be applied to determine all parameters categorized under kinetics and thermodynamics.

Generally, the chemical questions that can be answered by such use of electrical measurements in amperometric techniques include (1) the standard potentials (E°) of the compound's oxidation-reduction reactions, (2) evaluation of thermodynamics of the compound, (3) determination of the electron stoichiometry, (4) evaluation of the heterogeneous electron-transfer kinetics and mechanisms of the compound, (5) study of pre- and postchemical reactions, heterogeneous (thermodynamics and kinetics) that are associated with the electron transfer of a reaction, (6) study of effects of the solvent, supporting electrolyte and solution acidity on oxidation-reduction reactions and (7) study of reaction and product formation in relation to heterogeneous catalysis.

It is not possible to measure current during a homogeneous reaction, since an electrode and an electrolyte solution is required, which each represents a different phase. Moreover, amperometric type electroanalytical measurements takes place across an electrode-solution interface, and as such these methods are based on heterogeneous electron-transfer reactions. Also noteworthy, is that since amperometric analysis does not occur at equilibrium, these techniques are dynamic in nature, and as such is accompanied by compositional changes in the electrochemical cell material. The most common techniques directly associated with amperometry is polarography (when a mercury electrode is used) and voltammetry.

3A.2.1 Voltammetry



Voltammetry has its roots from the discovery of polarography in 1922 by the Czech chemist, Jaroslav Heyrovsky, for which he was subsequently honored by the 1959 Nobel Prize in chemistry. In this regard, voltammetry is based on exactly the same principles that pertains to polarography. In a more definitive context, generally, the common feature shared by all voltammetric techniques is the application of potential (E) to the working electrode and the monitoring of the resulting current (I) flowing through the electrochemical cell. Depending on the particular type of voltammetric technique, the potential may either be scanned between selected potentials (E_1 and E_2), or the potential of the working electrode may be changed instantaneously, whereas the resulting current may monitored as a function of potential or time (depending on the type of voltammetric technique). Thus, overall, one can conclusively say that all voltammetric techniques can be described in terms of some function of E , I and time. With reference to the applied potential in particular, depending on the desired effect, it can be used to derive an overall reduction or oxidative process. In effect, here, the potential is used to force the

electroactive species to either gain or lose an electron, which essentially happens in a potential region that makes electron transfer thermodynamically and kinetically favorable. Thus at the core of voltammetry, is also the transfer of electrons:



where Ox and R refers to the oxidized and reduced forms of the redox couple, respectively. Such oxidation/reduction reactions, derived by electron transfer, is governed by Faraday's law (i.e., the amount of chemical reaction caused by the flow of I is proportional to the amount of electricity passed). In this regard, the resultant observable voltammetric response, exhibited as the Faradaic current, is directly proportional to the concentration of the electroactive (analyte) species ($C_{\text{Ox}}^0, C_{\text{R}}^0$). Moreover, the surface concentrations of the analyte species involved in the Faradaic processes are related to the electrode potential by the thermodynamic Nernst equation:

$$E = E^{\circ} + \frac{2.3 RT}{nF} \log \frac{C_{\text{Ox}}^0}{C_{\text{R}}^0} \quad \text{3A.2}$$

Where (E°) is the standard potential for the redox reaction, R is the universal gas constant ($8.314 \text{ J K}^{-1} \text{ mol}^{-1}$), T is the Kelvin temperature and F is the Faraday constant ($96,487$). As the electrode is polarized and Faradaic current is passed, the potential is in effect moved away from the equilibrium and a concurrent change in the concentration of $C_{\text{Ox}}^0, C_{\text{R}}^0$ is enforced, however, for a system that is controlled by the laws of thermodynamics (Nernstian conditions), equilibrium needs to be continuously re-established as changes are made, and as such, the potential and the surface concentrations are always kept at equilibrium with each other by fast charge-transfer process. In effect, the potential forces the respective concentrations of Ox and R at the surface of the electrode to a ratio that is in compliance with the Nernst equation, which essentially means that, changing the applied potential will concurrently induce a change in the ratio of $\frac{C_{\text{Ox}}^0}{C_{\text{R}}^0}$, so as to satisfy **Equation 3A2**. On the other hand, due to the fact that the applied potential enforces a gaining or losing of electrons, it may be viewed as “electron pressure”, and as such, the faradic current

also reflects the rate at which electrons move across the electrode-solution interface. In this regard, the rate of reaction can be described by the Butler-volmer equation, which is one of the prominent laws that describe voltammetry:

$$\frac{I}{nFA} = k^{\circ} \{ C_{Ox}^0 \exp[-\alpha\theta] - C_R^0 \exp[(1-\alpha)\theta] \} \quad \mathbf{3A.3}$$

where $\theta = nF(E-E^{\circ})/RT$, k° is the heterogeneous rate constant, α is the transfer coefficient, and A is the area of the electrode. As can be observed from **Equation 3A.4**, the Butler-volmer equation links the variables for current, potential and concentration, which is a very useful relationship for the benefit of many voltammetric techniques. Moreover, it allows one to determine the values of the two analytically important parameters, I and k° . Another noteworthy fact is, that charge transfer (current flow) is always accompanied by diffusional-mass transfer. This essentially happens, since no equilibrium exist between the surface- and the bulk-solution concentrations, because, as the reagent is consumed or the product is formed during the redox reaction of Ox and R., concentration gradients between the locality of the interface and the bulk solution arise, which in effect, induces diffusion, and as such, reactants or products are continuously transported to, or away from the electrode surface (or to/from the bulk of the solution) by diffusion. This concentration gradient and mass transport is described by Fick's law, which essentially describes the amount of material impinging on the electrode's surface per unit time. In particular, Fick's law states, that the flux of matter (electroactive/analyte species) (Φ) is directly proportional to the change in concentration of species as a function of the distance, x , away from the electrode surface (concentration gradient):

$$\Phi = -AD_{Ox}(\partial c_O/\partial x) \quad \mathbf{3A.4}$$

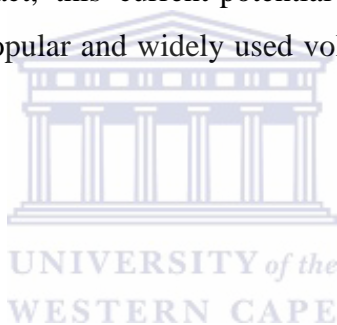
where D_O is the diffusion coefficient of Ox and x is the distance from the electrode surface. An analogous equation can be written for R. It is important to note that since voltammetric electrochemical processes always involves consumption of electroactive species and formation of product occurring at the same time that current is flowing, these processes will always be accompanied by the formation of such concentration gradients and as such, mass-transport ~~indeed~~ and flux plays a

significant role. In effect, the flux of Ox and R at the electrode surface controls the rate of reaction and thus the Faradaic current flowing through the cell. In addition to diffusion, mass-transport may also occur through migration or convection. Convection involves the movement/transport of species by a forceful physical movement, in which such fluid flow occurs with controlled-stirring or flow-through of the solution, as well as with rotation or vibration of the working electrode (i.e. forced convection), or due to density gradients. Migration on the other hand, refers to the movement of charged particles under the action of an electric field (a gradient of electrical potential). In effect, it may be simply described as the movement of charge-carrying ions in the solution during an electrode process: the positive ions are attracted by the negatively charged electrode (cathode), while the negative ions are attracted by the positively charged electrode (anode). The rate of migration depends on the charge on the ion (transference number), the size of the ion (including its full solvation spheres) and on the strength of the interaction between the ion and electric field. A stronger field will of course form at an electrode bearing a larger potential. In voltammetry, however, the effects of migration is attenuated by using an electrolyte which contains an excess of un-reactive ionic salt, known as a swamping electrolyte. More on this subject is discussed in **Section 3.3.1.2**.

From a general perspective, a voltammetric electrode reaction can be quite complex and takes place in a sequence that involves several steps. In the simplest case, only mass transport of the electroactive species to the electrode surface; the electron transfer across the interface and the transport of the product back to the bulk of the electrolyte solution is involved. More complex reactions include additional chemical and surface processes that precede or follow the actual electron transfer. The net rate of the reaction, and hence the measured current value may be limited either by the mass transport of the reactant or by the rate of electron transfer — the slower process will be the rate determining step. Overall, whether a given reaction is mass-transport or electron transfer controlled, is determined by various parameters, including the

type and concentration of the redox-active compound being measured; the size, shape and material of the electrode; the electrolyte solution resistance; operating potential; mode of mass transport; number of electrons transferred; time scale, etc. Thus, in effect, these parameters also determine the measured current signal. When the overall reaction is controlled exclusively by the rate at which the electroactive species reach the surface, the current signal is said to be mass transport limited. Such reactions are labeled Nernstian or reversible, since they obey thermodynamic relationships.

Commonly, results obtained from voltammetric analysis are displayed in terms of a voltammogram, which, in the most general form is a plot of current signal versus excitation potential. In fact, this current-potential plot is used to exhibit results obtained from the most popular and widely used voltammetric technique, i.e., cyclic voltammetry.



3A.2.1.1 Cyclic Voltammetry

Cyclic voltammetry is undoubtedly, the most widely used electroanalytical technique and is highly beneficial in diverse areas of scientific research application, mainly due its exceptional ability for providing qualitative information about redox processes. In particular, it provides rapid information with regard to the thermodynamics of redox processes, on the kinetics of heterogeneous electron-transfer reactions, and on coupled chemical reactions or adsorption processes, including understanding reaction intermediates and for obtaining stability of reaction products. In fact, cyclic voltammetry is normally the first experiment performed in an electrochemical study, since it enables rapid location of redox potentials of the electroactive species, as well as simplistic evaluation of the effect of media upon the redox process.

The technique itself is based on linearly scanning the applied potential of a stationary working electrode (in an unstirred solution) in a triangular waveform with time. The form of the potential-time impulse is exhibited in **Figure 3A.1**.

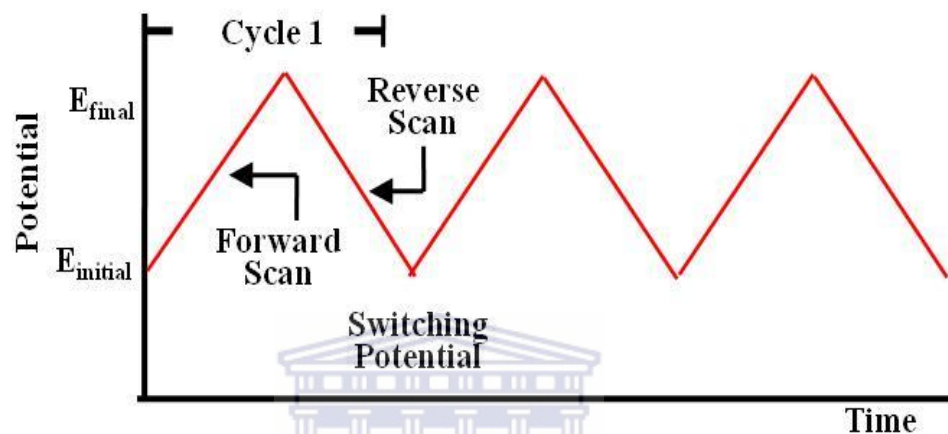


Figure 3A.1 Potential-time excitation signal in cyclic voltammetric experiment

During the process of potential scanning, the potential is varied with time, in a linear manner at a specific scan rate, up to a pre-defined limit (known as the switch potential), and then reversed to the initial value. The parameters which are of significance during the actual sweep scan, are the initial potential (E_i), the initial sweep direction, the sweep rate (v), the final potential (E_f) and the switch potential. Depending on the particular experiment being conducted, the initial/forward sweep may be in the negative or positive direction, whereas the reverse scan, being the inverted sweep, will then obviously be in the opposite direction. Moreover, depending on the information sought, such as the potential at which the redox process occur, or the concentration of the electroactive species, or the presence of preceding or following chemical complications – a partial cycle, full cycle, or multiple cycles can be performed. During the potential sweep, the current signal resulting from the applied potential is measured by the potentiostat, whereas the overall response is

collected as a resulting current versus potential plot, known as the cyclic voltammogram. An illustration of the expected typical cyclic voltammetric response of a $\text{FeCN}^{\text{III} \rightarrow \text{II}}$ redox couple during a single full potential cycle, is exhibited in **Figure 3A.2**.

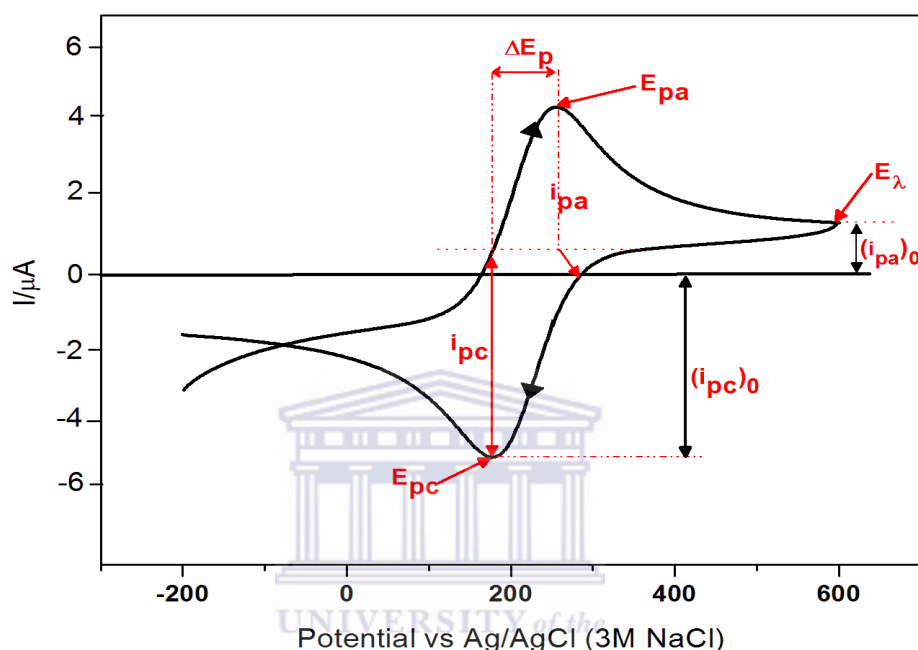


Figure 3A.2 Basic parameters for a cyclic voltammogram: E_{pa} refers to the potential of the anodic (forward) peak; E_{pc} represents the potential of the cathodic (reverse) peak; E_{λ} is the potential value at the inversion of the scan direction (switch potential); i_{pa} represents the current of the forward peak with respect to its baseline; i_{pc} is the cathodic (reverse) peak current with respect to its baseline; $(i_f)_0$ is the current at the inversion potential with respect to the zero current baseline

With the assumption that only the reduced form is present initially. Thus appropriately, a positive potential scan is chosen for the first half-cycle, which starts from a value where no oxidation occurs. As the applied potential approaches the characteristic E° for the redox process, an anodic current signal begins to increase, until a peak is reached. After passing through the potential region where the oxidation process takes, the direction of the potential sweep is reversed. During the reverse scan, Ox molecules (generated in the forward half cycle), and accrued near the electrode surface) are reduced back to R and a cathodic peak results.

Generally, as shown in **Figure 3A.2** the prominent observable parameters in a cyclic voltammogram are the peak potentials (E_{pc} , E_{pa}), the peak currents (I_{pc} , I_{pa}) of the cathodic and anodic peaks, respectively; the switch potential (E_{λ}) and the peak potential difference (ΔE_p). In terms of data interpretation in particular, of these parameters, the most important are the two peak currents and peak potentials, which, based on the theory developed by Nicholson and Shain (“the theory of stationary electrode polarography”) is used to analyze the cyclic voltammetric response. In this regard, these parameters are applied as diagnostics for determining whether the system is electrochemically reversible, quasi-reversible, or irreversible, as well as for the study and determination of other relevant aspects, such as coupled chemical reactions and adsorption processes. In a reaction which is electrochemically reversible, i.e., a reaction in which the electron transfer is fast, compared with mass transfer (such as diffusion) — the peak current is given by the Randles-Sevcik equation:

$$I_p = (2.69 \times 10^5) n^{3/2} A C D^{1/2} \nu^{1/2} \quad \mathbf{3A.5}$$

where n is the number of electrons, A is the electrode area (in cm^2), C is the concentration (in mol cm^{-3}), D is the diffusion coefficient (in $\text{cm}^2 \text{s}^{-1}$) and ν is the scan rate (in V s^{-1}). As observed in equation **3A.5**, the current is directly proportional to the concentration, and furthermore, peak current increases with square root of scan rate. What is more, for a simple reversible reaction, the ratio of the reverse-to-forward peak currents $I_{p,r}/I_{p,f}$ is unity. On the other hand, the aforementioned peak ratio can be strongly affected by chemical reactions coupled to the redox process (more on this subject will be discussed in following sections). The positions of the peaks on the potential axis is related to the formal potential of the redox process. In particular, the formal potential for a reversible couple is centred between $E_{p,a}$ and $E_{p,c}$:

$$E^{\circ} = \frac{E_{p,a} + E_{p,c}}{2} \quad \mathbf{3A.6}$$

The separation between the peak potentials (for a reversible couple) is given by:

$$\Delta E_p = |E_{p,a} - E_{p,c}| = 2.303 RT/nF \quad \mathbf{3A.7a}$$

Which at 25°C becomes:

$$\Delta E_p = \frac{0.059}{n} \quad \mathbf{3A.7b}$$

In this regard, the peak separation can be used to determine the number of electrons transferred, and as a criterion for Nernstian behaviour. Hence, a fast one-electron process exhibits a ΔE_p of about 59 mV and such value maintains constant with scan rate. Thus for reversible electrochemical reaction, both the cathodic and anodic peak potentials are independent of scan rate. It must be noted though, that in practice, a value of 59 mV ΔE_p is indeed very difficult to attain, because of small distortions caused by solution resistance, so an error variable of about 10-15 mV is still regarded as acceptable.



Unlike, the electrochemical behaviour for reversible redox processes, in “non-ideal” redox processes, such as irreversible and quasi-reversible processes, in which the electron transfer is slow, or coupled with a chemical reaction, a very different situation presents itself. Such processes are actually of greatest chemical interest and for which the investigative ingenuity of cyclic voltammetry is most valuable.

In terms of irreversible, electrochemical processes in particular (those with sluggish electron exchange), in general, the commonality is that the rate of the electron transfer is lower than the rate of the mass transport. One of the eminent characteristics features of irreversible processes is that individual peaks are smaller in size and are widely separated from each other (**Figure 3A.3, curve A**). In fact, in many cases, the separation between the forward- and reverse peak is so large that the reverse peak is undetected. This essentially happens, because the forward peak, compared to its standard thermodynamic potential, is located at potentials more negative than if it were a reversible reaction. Moreover, the forward peak potential, $E_{p,f}$ shifts with scan rate, such that for reduction processes, the shifting will be toward more cathodic

values. At 25 °C (298 K), the shift is approximately $30/\alpha n_{\alpha}$ mV for a tenfold increase of the scan rate. Overall, the precise dependence of peak potential (E_p) on scan rate, v , is expressed by:

$$E_p = E^{o'} - \frac{RT}{\alpha \cdot n_{\alpha} \cdot F} \left[0.78 - \ln \frac{k^o}{D^{1/2}} + \ln \left(\frac{\alpha n_{\alpha}^2 F v}{RT} \right)^{1/2} \right] \quad 3A.8$$

where α is the transfer coefficient and n_{α} is the number of electrons involved in the charge-transfer step. Thus, E_p occurs at potentials higher than the standard thermodynamic potential ($E^{o'}$), with the overpotential is related to the heterogeneous standard rate constant, k^o , and the transfer coefficient, α . However, independent of the value of k^o , an appropriate change in scan rate, can compensate for the displacement in peak potential. Also noteworthy, is that if the half-peak potential ($E_{p/2}$) is the value at half-height peak current, $I_{p/2}$, it holds that at 25 °C:

$$|E_p - E_{p/2}| = \frac{1.857 \cdot R \cdot T}{\alpha \cdot n_{\alpha} \cdot F} = \frac{48}{\alpha \cdot n_{\alpha}} \text{ (in mV)} \quad 3A.9$$

Thus, as observed in **equation 3A.9**, at 25 °C, the peak potential and the half-peak potential will differ by a magnitude $48/\alpha n_{\alpha}$ mV. This essentially means that the voltammogram becomes more drawn-out as αn_{α} increases. With regard to the peak current on the other hand, given by:

$$i_p = 2.99 \times 10^5 \cdot n \cdot (\alpha \cdot n_{\alpha})^{1/2} \cdot A \cdot D_{Ox}^{1/2} \cdot C \cdot v^{1/2} \quad 3A.10$$

it is still proportional to the concentration, but will be lower in magnitude, with the actual peak current height depending on the value of the α (since the relationship shown in **equation 3A.10** shows that I_p depends on the square root of α). In this regard, assuming a value of 0.5 for α , the peak current for an irreversible process has a magnitude of about 78-80% of the peak for a reversible one, which amounts to a ratio of reversible-to-irreversible current peaks of approximately 1.25-1.27. Another noteworthy aspect with regard to the peak current for irreversible processes includes the fact that no current ratio for $I_{p,r}/I_{p,f}$ exists. In this respect, however, it must also be taken into account that the lack of any reverse response is not sufficient to conclusively diagnose an electrochemically irreversible step, since the presence of

chemical reactions involving the electrogenerated species can attenuate the reverse response.

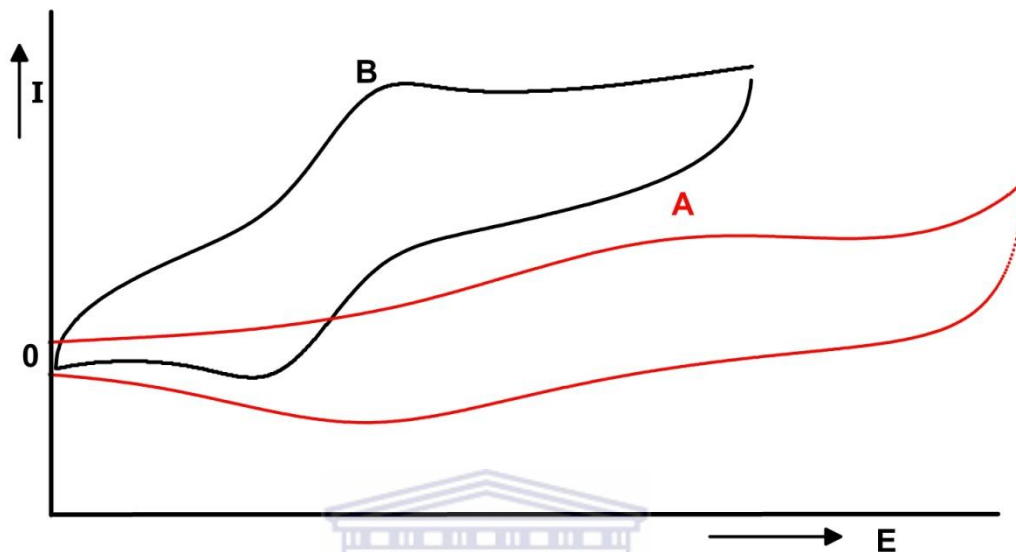


Figure 3A.3 Cyclic voltammograms for irreversible (curve A) and quasi-reversible (curve B) redox processes.

The other foreseeable type of redox electron transfer process, the quasi-reversible reaction, involves processes in the transition zone between reversible and irreversible behaviour. In such reactions, the shape of the cyclic voltammogram is a function of $k^0/\sqrt{\pi a D}$ (where $a = nFv/RT$) — thus as $k^0/\sqrt{\pi a D}$ increases (i.e., at very fast scan rates), the system portrays irreversible behaviour. Therefore, in such reactions, it is not uncommon that at low scan rates, the redox couple exhibits reversible electron transfer behaviour, whereas at high scan rates the process behaves irreversibly. Generally, quasi-reversible systems, occurs when the rate of the electron transfer (of the redox reaction) is of the same order of magnitude as the mass transport and as such, consequently, the current is controlled by both the charge transfer and the mass transport. Another point also noteworthy is that it is commonly assumed that an

electron transfer behaves quasi-reversibly when the standard rate constant lies within the values expressed as a function of the highest and lowest scan rates v , i.e.:

$$3 \times 10^{-3} \cdot v^{1/2} \geq k^o \geq 2 \times 10^{-7} \cdot v^{1/2}$$

where k^o is expressed in m s^{-1} and v in V s^{-1} . From a more practical perspective, one of the most eminent readily observable aspects of a quasi-reversible redox reaction is the separation between the forward and reverse peaks (i.e., ΔE_p) — which in this case, is much greater than that of a reversible process. Moreover, the peak height is not directly proportional to $v^{1/2}$. Also noteworthy is that the peak shapes and peak-to-peak separation (ΔE_p) depend, through a complex mathematical function Ψ (known as the rate parameter), on α , k^o and v :

$$\Psi = \frac{k^o}{\left[\frac{\alpha n F v D}{R T} \right]^{1/2}} \quad \text{3A.11}$$

The above relation holds under the assumption that $\alpha = 0.5$; $D_{\text{Ox}} = D_{\text{Red}} = D$. Considering the latter and aforementioned aspects, it becomes evident that for diagnostic characterisation of a quasi-reversible process, the parameters of relevance includes the thermodynamic parameter E^o , and the kinetic parameters α and k^o . In this regard, the parameter E^o can be efficiently calculated as the average between the forward and reverse peaks, given that $0.3 < \alpha < 0.7$; whereas k^o can be calculated if both D and α are known. In this regard, α is generally assumed to be approximately 0.5, however, one can also roughly evaluate the value of α by taking into account the effect of α on the shape of the cyclic voltammogram:

- For the case of $\alpha > 0.5$, the forward peak is sharper than the reverse peak, and as such, $I_{p,f} > I_{p,r}$;
- For $\alpha < 0.5$, the opposite is evident

Other noteworthy factors with regard to the potential and current which are also of significance in quasi-reversible processes include the following:

- The forward peak ($E_{p,f}$) shifts with v , i.e., toward more negative E_p values for reduction process;
- At 25 °C, the peak-to-peak potential difference is higher than $59.0/n$, of which the difference become much more prominent with increasing v ;

- The forward peak current $I_{p,f}$ increases with $v^{1/2}$, but the dependence may not be linear.
- The current ratio $I_{p,f}/I_{p,r}$ equals 1 only if $\alpha = 0.5$. Otherwise, if

To sum up the aspects of reversibility, irreversibility and quasi reversibility, **Table 3.2** highlights the important aspects that may be applied as diagnostic tools for the correct classification of electrochemical reactions during experimental investigations.

Table3.2 Summary of diagnostic criteria for electrochemical reversibility, irreversibility and quasi-reversibility of a redox couple, obtainable from cyclic voltammetric investigation

Property	Reversible	Quasi-Reversible	Irreversible
For Diffusion Controlled processes			
Properties of the Potential	$\Delta E_p = 57/n$ for an n-electron couple Peak potential, $E_{p,c}$ and $E_{p,a}$ are independent of v Peak-to-Peak separation, ΔE_p is independent of v ; plot of ΔE_p vs v = linear $E^{0'} = (E_{p,a} + E_{p,c})/2$	E_p varies with v $\Delta E_p \neq 57.0/n$ mV (departure from $59/n$ becomes very significant at higher v)	$E_{p,f}$ varies with v
Properties of the Current	$I_{pc} = I_{pa}$ I_p is proportional to $v^{1/2}$; plot of I_p vs $v^{1/2}$ = linear $I_{pa}/I_{pc} = 1$	$I_{p,f}$ increases with $v^{1/2}$, but the dependence may be non-linear; $I_{p,r}/I_{p,f} = 1$ only if $\alpha < 0.5$ (otherwise, if $\alpha > 0.5$: $I_{p,r}/I_{p,f} < 1$; if $\alpha < 0.5$: $I_{p,r}/I_{p,f} > 1$)	plot of I_p vs $v^{1/2}$ = linear; $I_{pa}/I_{pc} \approx I_{p,a}$ or $I_{p,c}$ (no current ratio of I_{pa}/I_{pc} exist)

So far, the application of cyclic voltammetry was discussed with respect to the response of diffusive solution systems. However, the explorative diagnostic ability of cyclic voltammetry can also be used to investigate redox processes for electron transfer across the electrode/film interface involving (electroactive) species/molecules adsorbed onto, or confined to a thin layer close to the electrode surface. For such redox-active interfacial supramolecular assemblies, a distinctly different observable electrochemical behaviour is exhibited. Firstly, for such confinement/immobilization of electroactive species, the redox-active material normally does not have to diffuse to or from the electrode surface, which concomitantly leads to changes in the shape of the cyclic voltammograms, i.e., peaks are more Gaussian in shape. Moreover, the separation between the peak potentials is also much smaller than expected for solution-phase processes, which become more evident at slow scan rates where the species is exhaustively oxidized or reduced. In fact, ideal Nernstian behaviour of surface-confined non-reacting species (species with no lateral interaction between redox centres, or in which interactions are independent of surface coverage), is characterised by symmetrical voltammetric peaks (see **Figure 3A.4**), with an ideal peak-to-peak potential difference of zero ($\Delta E_p = 0$). Moreover, the peak current is directly proportional to the potential scan rate (v), as shown in the following relation:

$$I_p = \frac{n^2 F^2}{4RT} v A \Gamma \quad \text{3A.12}$$

where n , F , R and T has its usual meanings, A is the area of the electrode and Γ is the surface coverage or concentration of the redox active molecule (in mol cm^{-2}). If one recalls from aforementioned sections, that Nernstian behaviour of diffusing species yields a $v^{1/2}$ dependence. Conversely, as shown in **Equation 3A.12**, surface confined species exhibits a linear scan rate dependence (v) and not $v^{1/2}$. Also noteworthy, as shown in the relation exhibited by the above equation, is the fact that the peak current is directly proportional to the surface coverage. Moreover, the area under the peak corresponds to the charge associated with the reduction of the adsorbed species and in

this regard, the surface coverage and the quantity of charge consumed during reduction or adsorption of the adsorbed/confined layer is related in a very useful equation:

$$Q = nFA\Gamma \quad \mathbf{3A.13}$$

In effect, the above relation shows that by measuring the Faradaic current passed during exhaustive electrolysis of the adsorbed/surface confined layer, the surface coverage of the latter can be determined, which in turn, can be used to calculate the area occupied by the adsorbed molecule. From a practical perspective, this may be done through slow scan rate voltammetry, or by using bulk electrolysis with chronocoulometry. Overall, essentially, this can be used to calculate the area occupied by the adsorbed species. Generally, for a species exhibiting an ideal Nernstian behaviour, in which there are no lateral interaction between redox centres, or where interactions are independent of surface coverage, the surface confined species will commonly adhere to the following relationships:

$$\text{FWHM} = 3.53 \cdot \frac{RT}{nF} = \frac{90.6}{n} \text{ mV}, \quad \mathbf{3A.14}$$

$$E_{p,a} = E_{p,c} \quad \mathbf{3A.15}$$

where FWHM is the full width at half maximum of the cathodic or anodic wave. On a final note, ideally, for species exhibiting the relations described by **Equations 3A.12 – 3A.15**, the type of adsorption of the adsorbed redox active species can be described by the Langmuir isotherm:

$$\Gamma = \Gamma_m \left(\frac{BC}{1+BC} \right) \quad \mathbf{3A.16}$$

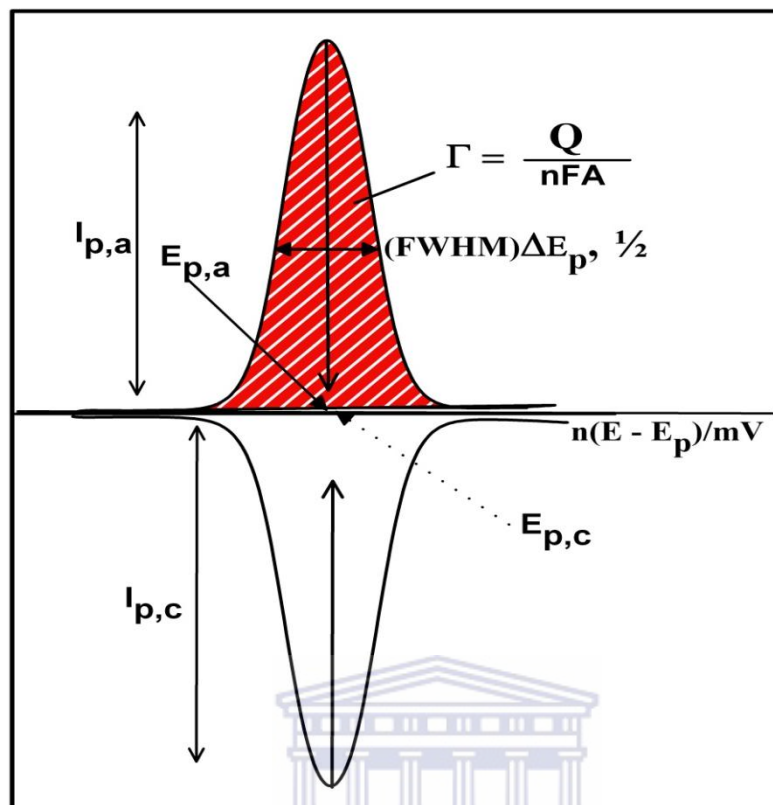


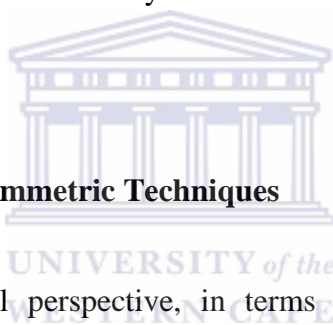
Figure 3A.4 Ideal cyclic voltammetric behaviour for reduction and oxidation of adsorbed/surface confined species. The surface coverage, Γ , can be obtained from the area under the peak

3A.2.1.1.2 Aspects of chemical reactions coupled to electron transfer

As mentioned in preceding sections, heterogeneous electron transfer processes in voltammetric reactions can be quite complex due to the common occurrence of homogenous preceding or following chemical reactions. The presence of such reactions will concomitantly affect the shape of the cyclic voltammograms, and thus will inevitably appreciably perturb the diagnostic investigations for electron transfer processes. In this regard, the chemical complications are categorized as:

- Preceding (the electron transfer) chemical reactions
- Following (the electron transfer) chemical reactions

With regard to specific classifications, these reactions may be catalytic or just coupled homogeneous chemical reactions. A specific example, with reference to catalytically coupled chemical reactions in CYP450-based electrochemical investigations in particular, the reduced product formed from the forward scan are normally, in the presence of oxygen, used up in very fast follow-up chemical reaction, hence the lack of the reverse scan, particularly evident at low scan rates. Indeed there are many aspects to consider in evaluating such reactions, however, that will not be further elaborated on at this stage. For more information regarding this subjects areas, the listed textbooks may be consulted [91-92].



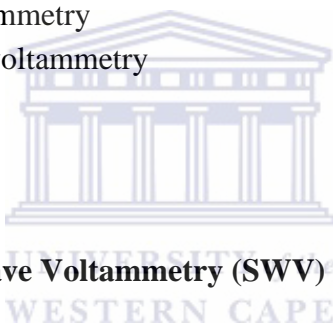
3A.2.1.2 Pulsed Voltammetric Techniques

From a general perspective, in terms of the analytical sensitivity in classical cyclic voltammetry, detection limits can go down to approximately 10^{-5} mol dm^{-3} concentration level. However, at very low concentrations of analyte, the current perturbation caused by double layer effects or other non-Faradaic sources induces a substantial compromise in the accuracy. As an example, consider the case of electron transfer processes in cyclic voltammetry complicated by consecutive electron transfer process, with the electrode potentials separated by < 100 mV — the resulting overlapping peak systems are very difficult to be resolved in order to obtain the precise formal electrode potential for each step. Moreover, during the study of catalytic electrochemical experiments, in which electron transfer processes are complicated by follow-up chemical interactions, a more accurate measure of electrode potential with preferably lower signal-to-noise ratio is required. In the latter and aforementioned cases, it is convenient to make use of pulsed techniques. These methods all ‘accentuate/amplify’ the Faradaic current, while greatly minimizing the

capacitive (charging) current. This is essentially achieved by applying a sequence of potential steps to the working electrode which enables the experimenter to exploit the variation in decaying rate of Faradaic current as opposed to the charging capacitive current. In this regard, after the potential is stepped, the charging current decays rapidly (exponentially with time) to a negligible value, while the Faradaic current decays rather slowly. Thus, after triggering the electron transfer by potential application across the working electrode, and sampling the current late in the pulse life, effectively discriminates against the charging current, and as such, the observed current is by-and-large Faradaic.

Overall, in this regard, the two techniques which are particularly useful and also as pertaining to the scope of the dissertation include:

- Square-wave voltammetry
- Differential pulse voltammetry



3A.2.1.2.1 Square-Wave Voltammetry (SWV)

Square wave voltammetry is originally invented by Ramaley and Krause and subsequently extensively further developed by Osteryoung and co-workers into the modern analytical tool which is often regarded more popular than normal- or differential pulse voltammetry. In fact, the technique itself can be viewed as a synergistic combination of the best aspects of several pulse voltammetric techniques, including background discrimination and superior sensitivity of differential pulse voltammetry, the diagnostic competence of normal pulse voltammetry and the capability of direct interrogation of products in the same manner as reverse pulse voltammetry, hence the popularity of the method.

Essentially, SWV is a large-amplitude differential technique, developed through the combination of the high-amplitude, high frequency square wave with the fast

staircase waveform, and by making use of computer-controlled electroanalytical instrument in preference to analogue hardware. With regard to practical aspects, it is normally applied to a stationary electrode, and involves the application of a potential waveform to the working electrode. In particular, the waveform composed of a symmetrical square wave, superimposed on a base staircase potential, is applied to the working electrode. With respect to the interpretation of results, it is best to consider the waveform as consisting of a staircase scan, of which each tread is superimposed by a symmetrical double pulse, one in the forward direction and one in the reverse. In general, the principle parameters associated with a square wave include a pulse height, ΔE_p , which is measured with respect to the corresponding tread of the staircase, and the pulse width, t_p . The pulse width can also be expressed in terms of the square wave frequency, $f = 1/2t_p$. The scan rate $v = \Delta E_s/2t_p = f\Delta E_s$, which is based on the fact that the staircase shifts by ΔE_s at the start of each cycle. **Figure 3A.5** exhibits the waveform and measurement scheme, including the principle parameters, for square wave voltammetry.

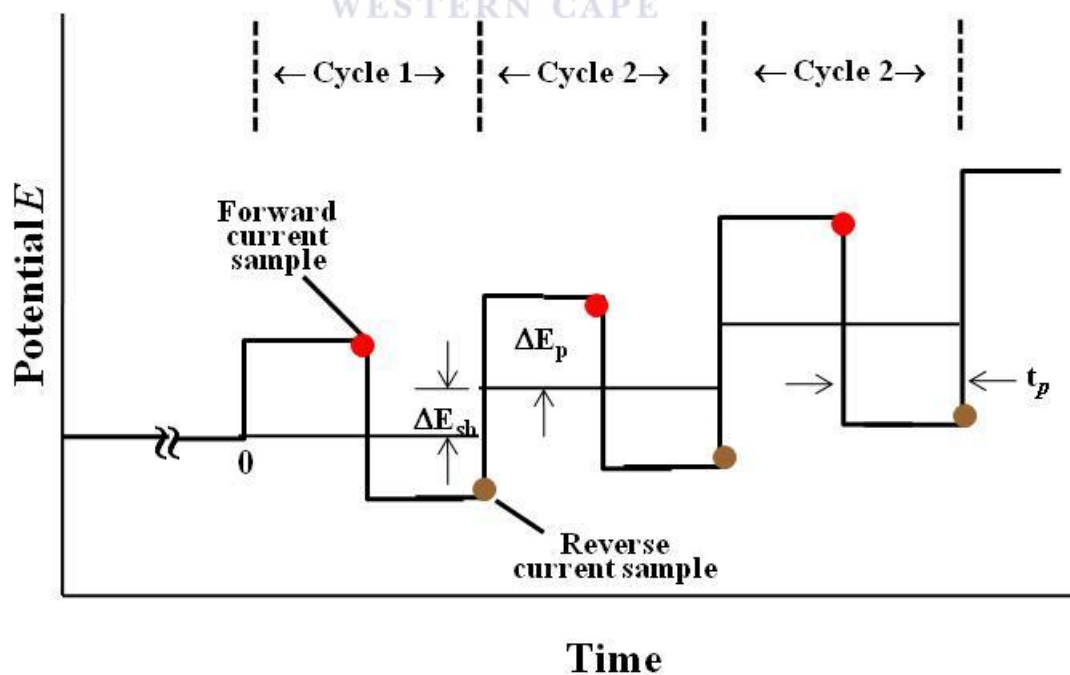


Figure 3A.5 Time-potential waveform profile for square wave voltammetry. Showing initial potential, E_i ; pulse height (amplitude), E_p ; step height, E_{sh} ; pulse width, t_p (also known as square wave period), forward current- and reverse current sample.

From **Figure 3A.5**, one can see distinguish a number of important parameters. Firstly, the square wave scan begins at an initial potential, E_i , which is applied for a subjective time to initialize the system. Another significant parameter is the pulse height/amplitude, ΔE_p , which is measured with respect to the corresponding tread of the staircase, as well as the pulse width/square wave period, t_p . During each square wave cycle, the current is sampled twice, i.e., at the end of the forward pulse (at t_f) and at the end of the reverse pulse (at t_R).

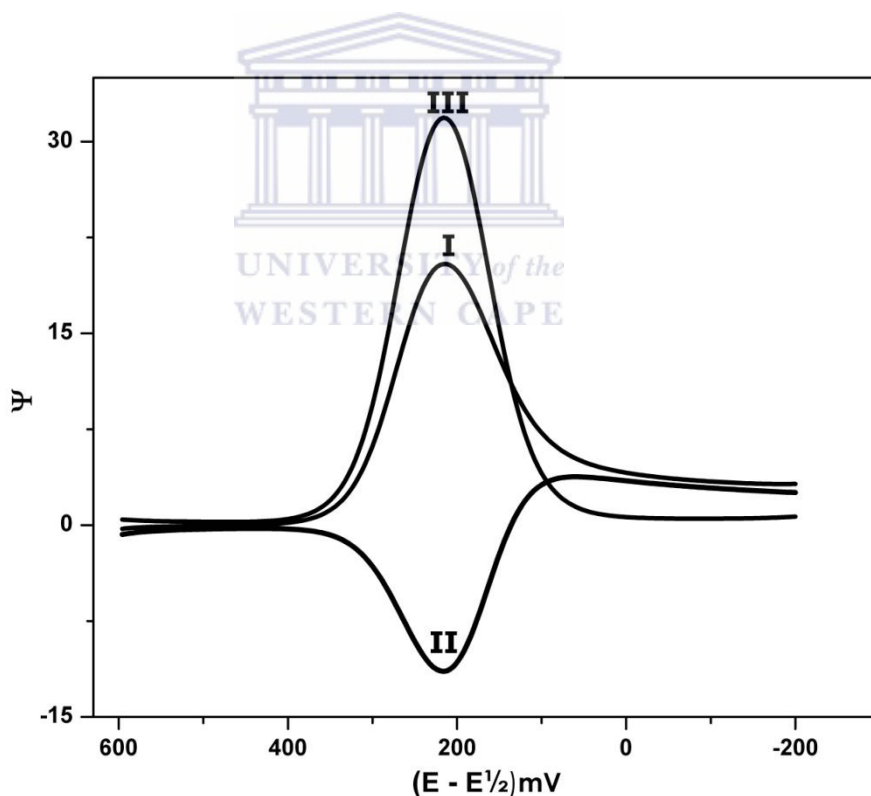


Figure 3A.6 Typical square wave voltammogram exhibiting reversible electrochemistry

3A.2.1.2.2 Differential Pulse Voltammetry (DPV)

In DPV a succession of pulses of fixed magnitude, which is superimposed on a linear potential ramp, are applied to a working electrode. Here, the current is monitored (sampled) twice per drop, i.e.: The first sample is taken just before the rise in potential, at the beginning of the pulse, whereas the second sample is taken late in the current pulse life just before it decreases back to the baseline (when the charging current is decayed). The difference between these two currents, which is instrumentally subtracted, is thus essentially ΔI_{pulse} . The differential pulse voltammogram is then subsequently plotted as a current vs potential graph. A noteworthy factor to also add, is that since the difference between the Faradaic components of the two current samples is usually negligible, in practice ΔI_{pulse} is zero, unless a legitimate redox activity occurs. From a practical perspective, during investigations involving DPV, the important parameters include:

- the *pulse amplitude* (ΔE_{pulse}), which is the magnitude (height) of the applied potential pulse;
- the *pulse width*, which is the time duration (in ms) in which the pulse is maintained;
- the *sample width*, which corresponds to the time (in ms) at which the current is measured after the application of the potential pulse;
- the *pulse period*, which is the time required to complete one cycle of variation of potential.

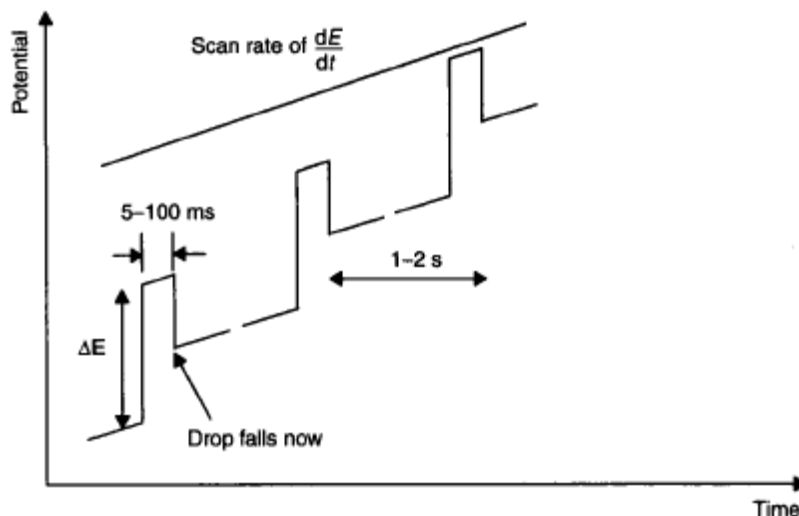


Figure 3A.7 Potential wave form and time-dependence of applied potential in differential pulse voltammetry

3A.3 Practical considerations

3A.3.1 Voltammetric investigations: Instrumentation and general practical requirements

From a general perspective, the basic requirements for the conduction of a voltammetric electrochemical investigation include an electrochemical cell – fully equipped with a three-electrode system, a voltammetric analyzer (consisting of a potentiostatic circuitry, including a voltage ramp generator), while the other component is an X-Y-t recorder/plotter (X-Y: for current-potential measurements and X-t: for current-time/concentration measurements). Also noteworthy is the fact that the complete system should be kept in a location that is free from disturbing vibrations and drastic fluctuations in temperature, since these aspects can substantially influence the obtained results.

3A.3.1.1 The electrochemical cell

Generally, voltammetric experimental investigations are commonly conducted in a glass electrochemical cell, equipped with a three electrode system. A typical electrochemical cell is exhibited in **Figure 3A.8**. The general volume capacity of such cells range from 5 to 50 mL and it is usually fitted with a teflon cover, equipped with o-ring adaptors to hold the three electrodes, which includes the working electrode (WE), the reference electrode (RE) and the counter electrode (CE) (or auxiliary electrode). In this regard, the WE is the electrode that is usually modified with the appropriately chosen interfacial enhancers and is the electrode at which the reaction of interest occurs. Various materials can be used as working electrodes, and based on origin, these may be metals, carbonaceous materials, semiconductors and organic conducting salts. With regard to the scope of this dissertation, carbonaceous WE was used. In particular, glassy carbon WE was used, the characteristics of which will be elaborated on in more details in subsequent section. The RE consist of an inner solution of constant composition of both forms of its redox couple and as such, is resistant against potential changes which enables it to provide a stable and reproducible potential, independent of sample composition. Common reference electrodes are saturated calomel ($\text{Hg}/\text{Hg}_2\text{Cl}_2$) and silver-silver chloride (Ag/AgCl) electrodes, of which the latter was used in this dissertation. With regard to the counter electrode on the other hand, an inert conducting material, usually a platinum wire is used. During the performance of the actual voltammetric experiments, these electrodes are immersed in the solvent and supporting electrolyte. In addition to this, depending on the type of voltammetric experiment, the solution may be quiescent, or may require stirring, for which a stirrer bar is included in the cell. Moreover, the tube used for bubbling the inert deoxygenating gas is also supported in the holes of the teflon cover.

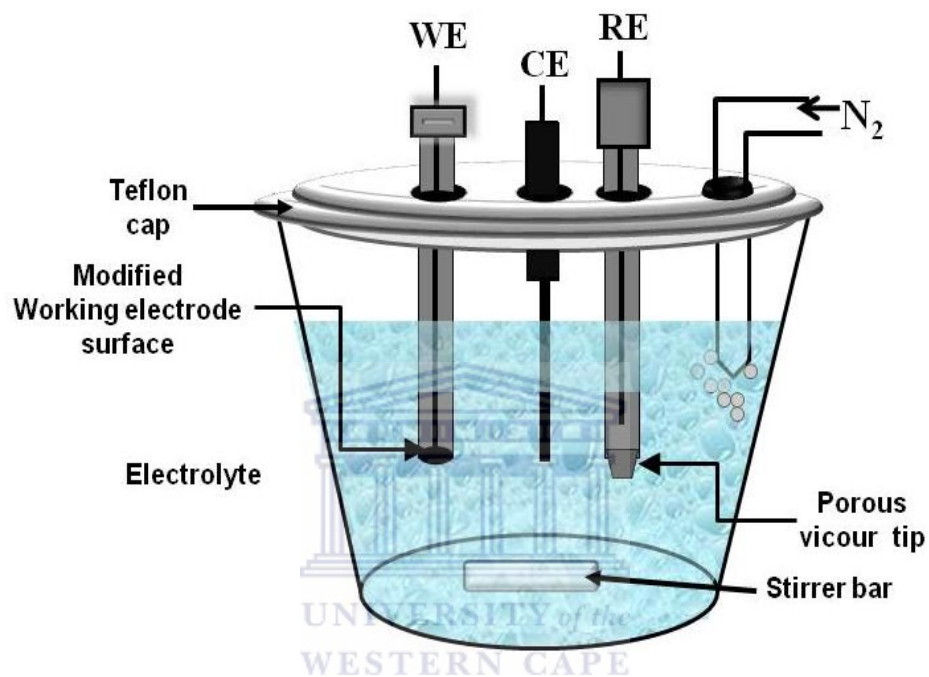


Figure 3A.8 A typical electrochemical cell used during a routine electrochemical investigation

The relative positions of the electrodes are important and should be paid close attention, while their connection to the electrochemical analyzer should also be closely monitored. Also noteworthy is the fact that in techniques where the potential for high background currents exist, such as chronoamperometry and bulk electrolysis, the CE can be separated in a glass-frit, in order to alleviate interference by electrolysis products.

3A.3.1.2 Solvents and supporting electrolytes

Akin to common chemical reactions, the electrolytic medium, which is generally constituted by the solvent and the supporting electrolyte, plays a pivotal role in the success of an electrochemical measurement [93-94]. In this regard, the choice of solvent in particular is limited by a combination of prerequisites to adequately facilitate the heterogeneous electron transfer to and from the electrode and solution. In this regard, the solvent should not react with the analyte and should not undergo electrochemical reactions over a wide potential range, but should be adequately electrically conductive. to dissolve the analyte under study, but to be chemically inert with respect to it. Other requirements with respect to the solvent include the following:

- to dissolve considerably high amounts of supporting electrolyte, with the overall aim of improving the electrical conductivity of the electrolyte solution, while concomitantly reducing its resistance;
- impurities which have the potential to interact with the analyte under study or interfere with the electrochemical process must be easily removable and as such, the solvent should be easily purified;
- since enzyme-based modified electrodes are very sensitive and susceptible to fouling, the solvent should not process any toxic constituents.

Generally, water is the most common solvent used, but, depending on the specific requirements of the electrochemical investigation, non-aqueous media may also be used. As for the supporting electrolyte on the other hand, overall, its presence in controlled-potential electrochemical investigations are required to decrease the resistance of the solution, to attenuate electro-migration effects and to maintain a constant ionic strength. It is important that the concentration of the supporting electrolyte is sufficiently high, so as to “swamp out” the effect of variable amounts of naturally occurring electrolyte (migration effects). In this regard, the usual concentration is 0.05 – 1.0 M, in other words in excess of the concentration of all

electroactive species. In terms of specific constituents, the inert supporting electrolyte may be an inorganic salt, a mineral acid, or a buffer system, of which the latter is used when a pH control is essential. With regard to the current dissertation, with specific reference to the sensitive nature of the biologically based recognition component, all supporting electrolytes were prepared with phosphate buffer systems, prepared at predetermined pH of 7.4.

3A.3.1.3 Conditions for requirement of oxygen removal

From a general perspective molecular oxygen (dioxygen, O₂) is chemically reactive with numerous substances, but more importantly, during electrochemical experiments, at cathodic potentials, O₂ is electrochemically reducible. This can be highly problematic, since the reduction of O₂ can result in series of electroactive intermediary products which of course could have dramatic effects on the electrode reaction being studied. In a more descriptive context, a detailed outline of the possible electrochemically base reactions and intermediates is subsequently discussed:

The ground state of molecular oxygen ($\cdot\text{O}_2\cdot$, $^3\Sigma_g^-$) has two unpaired electrons in degenerate $2\pi_g$ orbitals. Essentially, atmospheric dioxygen dissolves in water to a concentration of approximately 1×10^{-3} M. Thus in un-degassed supporting electrolyte solution, at sufficiently cathodic potentials, the dioxygen will be reduced by the electron transfer process, the effect of which can, via reduction, hydrolysis and disproportionation steps, result in the formation of a series of intermediate basic dioxygen and monooxygen species, that may take up one or two hydronium ions (H₃O⁺) from the electrolyte media (O₂⁻, HOO[•], H₂O₂, HOO⁻, HO[•], H₂O, HO⁻). With regard to the overall general significance on electrochemical and electrocatalysis investigations in particular, the formation of hydrogen peroxide and water is the important branching points. Considering the two main branching points in the overall

reduction of oxygen, the formation of H₂O₂ and H₂O proceeds via two well-separated two-electron steps, respectively. The first step corresponds to the formation of hydrogen peroxide:



The hydrogen peroxide formed above is essentially also electroactive and thus a second reduction step occurs:



Thus overall, since electrons are being consumed here, the associated non-Faradaic current can result in large background current accruing from this stepwise oxygen reduction, and will in effect interfere with the measurement of many reducible analytes. Moreover, the products of the oxygen reduction can affect the electrochemical process being investigated. Considering these aspects, during investigation of the electrochemical behaviour of a redox process, ideally, oxygen has to be removed/excluded, which can be done through degassing with an appropriate inert gas prior to the experiment, while a blanket of gas should also be maintained atop the solution during the experiment.

At this stage, it should also be said that in cases where the presence of dioxygen is essential, such as during normal electrocatalysis studies, particularly with regard to CYP450-based platforms, the possible formation and interference of reactive oxygen species can be limited/avoided by working at a lower operating potential and/or working under conditions of low oxygen tension. Moreover, in reagentless mediated biosensor platforms, most reduced mediating species poses the potential of reacting with oxygen resulting in the formation of H₂O₂ through dismutation of superoxide, so care has to be taken in this regard also.

3A.3.1.4 Working electrodes

Essentially, the working electrode (WE) is the electrode where the redox reaction of electroactive species takes place and where the charge transfer occurs. In this regard, from a practical perspective, the electrochemical performance aspects are influenced by the characteristics of the WE. In this context, the ideal WE should operate at a wide potential window, provide a high signal-to-noise ratio; confer low resistance and adequate conductivity, while also yielding a reproducible response. Generally, several types of materials can be used as WE, of which the most popular are those involving mercury, carbon, or noble metals (especially platinum and gold). A significant factor to consider during application of a solid WE is the dependence of the response on the surface state of the electrode. Therefore, appropriately, the application of these electrodes requires specialized pretreatment and polishing procedures to obtain reproducible results. The nature of the pretreatment protocol is highly dependent on the type of electrode material involved. To this end, mechanical polishing (to a smooth mirror-like finish) and potential cycling are common effectors, while various thermal, chemical, or electrochemical protocol steps may be added for activating surfaces. In this regard, carbon-based surfaces benefit especially from specific ‘activating’ pretreatment steps. While on the subject of carbon-based electrodes, amongst available ones, the glassy carbon electrode is the most popular and in the context of this dissertation, is the electrode used for all electrochemical investigations and prepared platforms.

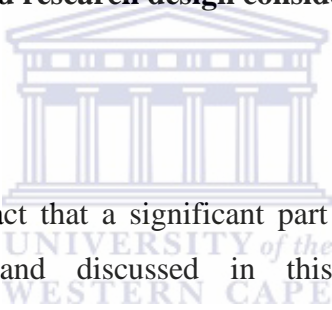
3A.3.1.4.1 Glassy carbon electrodes

Glassy carbon (GC), as does all other carbon electrode material, share the basic structure of a six-membered aromatic ring sp^2 bonding. In its full description, GC is also called vitreous carbon and is a popular choice for WE based on its wide

potential window, chemical inertness, as well as providing a relatively reproducible performance. With regard to the specific structure of GCEs, it consist thin, tangled ribbons of cross-linked graphite-like sheets. With regard to the actual use of GCEs, usually a surface pre-treatment is employed, mainly functioning to activate the electrode surface group, while also enhancing their analytical performance. In this regard, the most basic step of course involves polishing procedures. However, additional steps, have also been used to enhance performance factors.

3A.3.2 Human cytochrome P450 genetic engineering: Important theoretical pre-emptive and research design considerations

3A.3.2.1 Foreword



Based on the fact that a significant part of the success of the research investigation exhibited and discussed in this dissertation centred around understanding and physically applying the intricate process of preparing a catalytically active enzyme-based biorecognition source for the purpose of conducting successful experimental protocols, it is only appropriate to enlighten the reader's understanding with regard to this subject. This subject matter is particularly important to get a complete grasp of the experimental aspects and results interpretation of **Chapter 5B**, since the recognition component for these biosensors were prepared 'locally' by the author and not sourced from commercial domains, as in the case of recognition component used in Chapter 4 .

3A.3.2.2 The road to getting started: Important considerations

As emphasized in **Chapter 1**, for the study of enzyme-drug interactions and drug metabolic profiling investigations with cytochrome P450 enzymes and/or CYP3A4 in particular, a viable catalytically active enzyme source is a prerequisite. As already stated, these sources can be either cell cultured and tissue-based systems, liver microsomal systems, or genetically manipulated recombinant systems, expressing single CYP isoenzymes. In both the case of liver microsomal fractions and cell/tissue-based systems, the enzymes sources are directly obtained from human origin, and as such, are part of complex systems, which may contain other isoenzymes, native electron transfer mediator complex components, and these isoenzymes are largely bound to cell membranes, which, for the purpose of bioelectrochemical studies, makes the systems essentially difficult to use, since the study of a particular isoenzyme's specificity for substrates, kinetic parameters for reaction and possible means of regulation, preferentially requires the isolation of the isoenzyme. This would require extensive purification procedures, which involves disruption of the cell membranes, and other biochemical procedures, such as column chromatography, etc., of which these procedures are highly time-consuming, and expensive, while the isolated isoenzyme may be inactive in the absence of phospholipids or detergent and as such, catalytic reconstitution systems would need to contain all such additional components [95], particularly in the case of CYP3A4. Moreover these sources are highly sensitive and decay rapidly, which means that fresh supplies would have to be sourced very regularly as human liver tissues/fraction/slices are not always readily available. In addition to this, many of the isoenzymes within a family, share extensive homology with each other in their amino acid sequence identity, some of which have been shown up to 97%, and as such, their substrate selectivities overlap considerably [96], which means that additional methods of analysis would be required for the interpretation of the results in terms of one particular isoenzyme (more on this particular subject is elaborated in Chapter 1).

For the purpose of electrochemically-based, biosensor-type, enzyme-modified electrodes for drug metabolism studies in particular though, where the focus usually is on the study and investigation of the interaction of selected drug(s) with a single biorecognition component, hosted within appropriate interfacial carrier matrix, it is essential that prepared enzyme constructs be purified and isolated, rather than mixed enzyme-constructs or crude preparations, molecular impurities and/or other 'unwanted' (electrochemically active) species will interfere with electron transfer and catalytic activity. This may occur by preferential non-specific binding of impurities and/or blocking and fouling the modified electrode, or inadvertently leading to false signals which complicates the analysis and interpretation of the observed voltammetric result output. For this purpose, genetically engineered, recombinant CYP450 construct systems are highly recommended, since such methods can generate sufficient quantities of highly purified enzyme preparations, without compromising selectivity or activity. Moreover, and perhaps more importantly, these enzymes can be prepared as the heme-domain and surrounding protein, without the inclusion of the native electron transfer mediator complex (CPR: NADPH cytochrome P450 oxidoreductase) fused to the enzyme, which for the scope of the dissertation is absolutely necessary, since the purpose is using the modified electrode, with appropriately chosen interfacial enhancers as electron transfer donor, rather than the native CPR electron transfer donor system.

3A.3.2.3 Practical research design aspects and considerations for genetic engineering: cloning, purification and expression

From a very broad perspective, protein genetic engineering is generally understood to involve the use of site-directed or random mutagenesis to alter the properties of a protein or enzyme. In this regard, in terms of the scope of this

dissertation, the definition may be extended and tailored to encompass the modification of the N-terminal membrane anchor and fusion tagging of recombinant cytochrome P450 3A4 to facilitate over expression for the investigation of protein targeting with respect to enzyme- substrate interaction [97].

Generally, all human microsomal P450s are essentially membrane bound, unlike their bacterial and mitochondrial counterparts, who are soluble and thus confounded to the cytosol. In general, the expression of recombinant (human) full length, wild type CYP3A4 in particular, is quite a difficult endeavour, because the enzyme's complicated structural and catalytic requirements, based on its membrane-bound nature causes a combination of constricts. In this regard, firstly, a full length wild type CYP3A4 usually expresses at very low levels coupled with equally low activity; secondly, when considering the highly hydrophobic character of the enzyme, the host cell would require cellular organelles, because the enzyme is essentially membrane-bound and would preferentially be confounded to the endoplasmic reticulum of the host cell. Also important, is the requirement of additional monomerisation methods and reagents during application of the prepared enzyme, due to its aggregation prone nature. On the other hand, research has shown that CYP3A4 and other microsomal P450s contain a sequence of 15-25 amino acids spanning across the N-terminus, which provide the major hydrophobic interaction with the endoplasmic reticulum, and in this regard, this stretch of amino acids are the major determinant of the enzyme's membrane binding nature. Moreover, and perhaps more importantly, it was determined that this particular region does not play an active role the catalytic activity, substrate interaction, or electron-donor interaction of the enzyme, and as such, its modification holds no potential for damage to the enzyme. The significance of latter and aforementioned aspects, are that during preparation of recombinant CYP3A4, specific manipulations to this particular region has enabled the evolution of innovative techniques, based on site-directed genetic manipulation, which significantly enhanced the preparation of soluble, heterologously expressed enzyme constructs that are catalytically active. These methods can include either the

truncation of the N-terminal membrane anchor domain, or N-terminal sequence modifications, or complete removal of the hydrophobic N-terminal anchors sequence.

In terms of the practical aspects of the genetic preparation of recombinant CYP3A4 in particular, with the overall aim being the preparation of an N-terminally modified CYP3A4 construct (nCYP3A4) — the experimental protocol followed should provide the highest soluble protein expression, and in this regard a number of requirements and factors needs to be considered and addressed, in order to have a successful expression and purification process. These include the following:

- The type of host and the particular host strain which will be used for the heterologous expression of the enzyme. Available hosts, which can be used include *Escherichia coli* (E coli), yeast, mammalian cells and insect cells, of which, based on financial, time, user friendliness and potential for increased protein yield considerations, E-coli are the preferred expression host, of which available strains may be. With regard to the particular E-coli strain, the D5 α and JM109 strains are known for their increased insert stability and good yield and as such, more popular choices.
- Choosing and obtaining the host (parent) expression vector, with plasmids containing the amplified cDNA (complimentary DNA) of the particular isoenzyme, as well as promoter elements. Moreover, coding sequences for any additional fusion tag components are also cloned into these vectors, and overall, the prepared vector is then used to initiate the whole heterologous enzyme expression process.
- The choice of co-expressing charged soluble proteins tags, as fusion adducts, which functions to further enhance the soluble yield of the genetically prepared recombinant construct, by enhancing the protein targeting expression to specific cellular or extracellular compartments, and as such increasing the

cytosolic (soluble) expression. In this regard, the placement position of the tag plays a significant role. Also important, is that the tags should preferably be of a small enough nature, as to not interfere with the correct folding of the protein during expression, or enzyme-electron donor interactions during catalysis application. The most popular tags which may be used in *E. coli* expression systems are NusA (*E. coli* N-utilisation substance protein A), His (polyhistidine, usually His₆: containing 6 residues), BMP (maltose binding protein), GST (glutathione S-transferase). In this regard, his-tag is the preferable choice, since in addition to conferring increased solubility to the protein, it has reversible binding ability and a considerable affinity for Ni²⁺, of which these attributes can be used to simplify the purification step with Ni²⁺-affinity chromatography without denaturing the protein.

- Investigating/evaluating which preferred specific method to choose for modification of the N-terminal region. This is an important aspect, since without such modification; the N-terminus of the expressed construct will target the protein to be anchored into the inner endoplasmic membrane of the host cell, with only the active site facing the cytosol. The overall implications of this would obviously be at the cost of the soluble yield of the prepared enzyme, which defeats the purpose as it pertains to the scope of this dissertation.
- As CYP3A4 and other human CYP450 enzymes also contain hydrophobic amino acids at other regions of the protein, distinct from the N-terminal domain, such as areas of the catalytic domain, which is distinct from the N-terminus, addition of other reagents may be added to further increase the soluble yield of the prepared construct. In this regard, the use of detergents, particularly non-ionic detergents (at a final concentration of 0.1-0.2% (v/v) was shown to be of great benefit.

3A.3.3 Enzyme kinetics

Generally, enzymes may be regarded as biological catalysts. In effect, they possess active sites that function to bind to the substrate, which essentially leads to the catalytic production of product, P. In this regard, enzymes are able to act on substrates and produce product with the overall effect of lowering the activation energy required for product formation. In a more descriptive context, the theory behind enzyme catalysis are all based on the pioneering work of Michaelis and Menten, postulated the formation of the enzyme-substrate complex (ES), based on their studies regarding the substrate concentration dependence of enzyme reactions [98-99]. According to the Michaelis Menten (MM) theory, the rate or velocity (v) of catalysis by enzymes varies with substrate concentration. In this regard, the velocity increases with the increase in substrate concentration up to certain point and then becomes constant, thus reaching a maximum velocity V_m , as shown in **Figure 3A.9**.

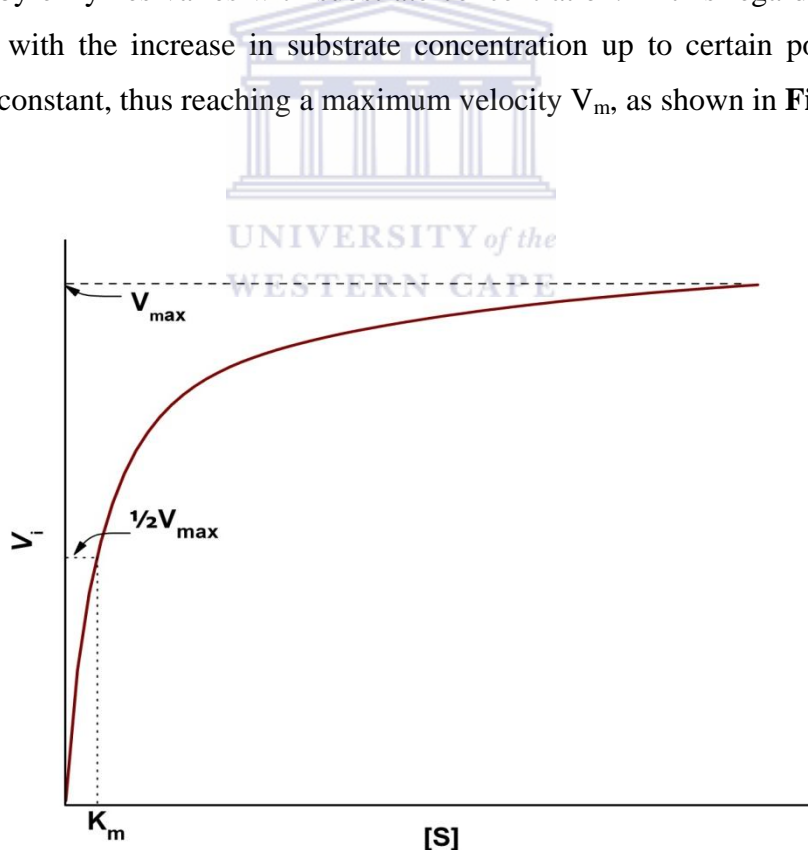
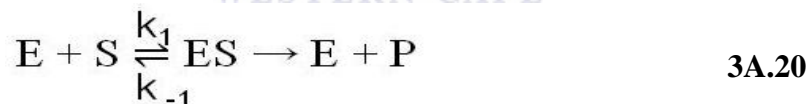


Figure 3A.9 Initial velocity v_i as a function of substrate concentration $[S]$ for enzyme-catalyzed reaction following Michaelis–Menten kinetics.

According to the plot of V_i as a function of $[S]$, the following findings is made:

- At low values of $[S]$, the initial velocity, V_i , rises in a linear fashion in association with increasing $[S]$.
- However, as $[S]$ increases, the gains V_i level off (forming what looks like a rectangular hyperbola).
- In this regard, the asymptote represents the maximum velocity of the reaction, known as V_{max} .
- The substrate concentration that produce a V_i which is one-half of V_{max} is designated the MM constant, K_m .

With regard to the K_m in particular, it is noteworthy to also add that it is an inverse measure of the affinity f strength of binding between the enzyme and its substrate. This essentially means that the lower the K_m , the greater the affinity (thus, the lower the concentration of substrate needed to achieve a given rate). Furthermore, the MM model further postulates that the ES is temporary and as such, can either dissociate back to E and S or proceed to form a product, P. The interaction, based on the MM model is shown in **Scheme 1**:



The maximum rate (V_{max}) will be observed when all the enzyme is in the form of the ES complex. The kinetics of the reaction shown in Scheme 1 can then be described by the fundamental Michaelis-Menten equation, shown as follows:

$$v = \frac{V_{max}[S]}{K + [S]} \quad 3A.21$$

where v is the initial rate (moles/time), V_{max} is the maximum rate of catalysis, K_m is the apparent Michaelis-Menten constant and $[S]$ is the substrate concentration.

3A.3.3.1 Treatment of data

Due to the difficulty of determining the limiting value of specific parameters, such as K_m directly from the plot of V vs. $[S]$, the MM equation can be rearranged in either of three different ways, to yield a linear graphical representation. These are known as the Lineweaver–Burk equation, the Eadie-Hofstee equation or the Hanse equation. In this regard, in the first case, Lineweaver and Burk converted the MM equation (3A.22) into straight line form by taking the reciprocals of each side of the equation and rearranging terms to obtain:

$$\frac{1}{v_i} = \frac{K_m}{v_m} \left[\frac{1}{[S]} \right] + \frac{1}{v_m} \quad 3A.22$$

Thus a plot of $\frac{1}{v}$ vs $\frac{1}{[S]}$ gives a straightline with a slope of $\frac{K_m}{V_m}$ and a y-intercept of $\frac{1}{V_m}$

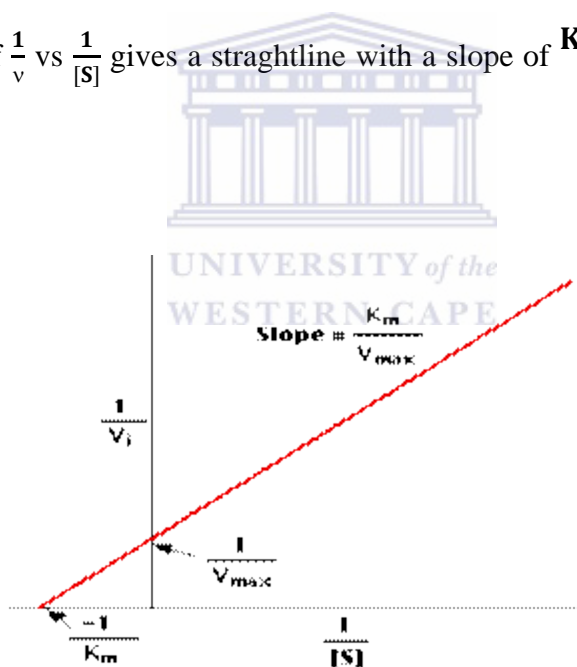


Figure 3A.10 Lineweaver-Burk double reciprocal plot of $1/v$ vs $1/[S]$ for the dependence of enzyme-catalyzed reaction velocity on substrate concentration.

3A.3.3.2 Enzyme inhibition

Noncovalent binding of inhibitors can reversibly or irreversibly decrease the activity of the enzyme. This is a particularly eminent factor in the case of CYP450 enzymes, which are known to have specific compounds that act as inhibitors of these enzymes.

3A.3.5 Biosensor performance aspects

In the context of the overall scope of this dissertation, the investigation of the electrochemical behaviour of the fabricated biosensors is the main theme, and as such, an important factor is also the evaluation of the biosensor response with respect to performance factors. In effect, the evaluated operating parameters may indicate the nature of the rate-limiting steps (e.g. transport or reaction factors), and can facilitate biosensor optimisation in a given matrix. In this regard, a list of parameters are denoted and described:

3A.3.5.1 Sensor calibration: sensitivity, working and linear concentration range, detection determination limits [52, 57]

Calibration of sensor, from a general perspective is usually done by adding standard solutions of the analyte (substrate) and by plotting the (steady-state) responses R_{rs} , possibly corrected for a blank (usually referred to as the background) signal R_{bl} , versus the substrate concentration ($[S]$). The sensitivity and linear concentration range of the calibration curves are then determined by plotting the change in concentration ($R_{rs} - R_{bl}$) versus $[S]$. Thus, in this regard, the sensitivity is determined within the linear concentration range of the biosensor calibration curve, obtained from the slope of the particular linear plot.

Electrochemical biosensors normally have an upper limit of the linear concentration range, of which this limit is directly related to the biocatalytic or biocomplexing properties of the biochemical or biological recognition component. A noteworthy aspect in this regard, is that in the case of enzyme-based biosensors that has an additional outer-layer films, the linear dynamics may be larger if the sensor response is controlled by the diffusion of substrate through the outer membrane and not by the enzyme kinetics. Having said that, the compromise for such an extension will obviously be at the cost of sensor sensitivity, with the latter showing an associated decrease. Nevertheless, still on the subject of the linear concentration range and upper limit, the parameters for Michaelis-Menten kinetics can then subsequently be determined, of which, as described in Section 3A3.3, the most notable parameters are K_m and V_{max} . In this regard, when the K_m is much larger than its value for soluble enzyme, it signifies that either a significant barrier to the diffusion of substrate is present between the sample and the reaction layer, or that the rate of reaction of the co-substrate with the enzyme is increased.

On a final note, the limit of detection (LOD) is also of significance, where determination of this parameter takes into account the blank and the signal fluctuation. The exact method used for determination of the LOD in the context of this dissertation is shown in the appropriate section in Chapter 3B.

3A.3.5.2 Reproducibility, stability and lifetime

Reproducibility may be described as a measure of the scatter or drift in a series of results performed over a period of time. The operational stability of the sensor on the other hand, can vary significantly, depending on the method of sensor preparation, the applied recognition component and the transducer used. Moreover it is also dependent on the response rate limiting factor, and furthermore, it may vary considerably depending on the operational conditions. In the case of storage stability

assessment, the parameters that requires clear distinction when reporting on this parameter, is the state of storage, i.e. dry or wet, the atmosphere composition, which usually refers to air, or under inert gas (e.g. nitrogen), pH, buffer composition and the presence of additives.

3B General Experimental: Protocols and Methods of Investigation

3B.1 Introduction

This chapter gives a succinct, but detailed overview on the following:

- **Materials:** Describing sources and preparative methods for all reagents and raw materials as pertaining to the context of the dissertation as a whole.
- **Platform(s) modification methods:** In this regard, a general flow diagram of the design for each biosensor platform used in the overall research investigation of this dissertation is given, with particular reference to highlighting the differences in overall preparation. A more in-depth description of the modification steps in research design of each enzyme-based biosensor platform is given at the end of the relevant results chapters.
- **Morphological and structural characterization methods:** Since the techniques used in the characterization methods are common to the dissertation as a whole, all morphological and structural characterization methods applied are described in terms of relevant preparative methods.
- **Voltammetric instrumentation and techniques:** All general methods and protocols used in voltammetric investigations are described.

Chapter 5 Variables of investigation and general protocols

It is noteworthy to remind the reader that this dissertation reports on results obtained from two different enzyme based biosensor platforms (i.e. biosensor platform 1 and biosensor platform 2), each based on a distinctly unique design protocol – with common features being the mediating species and category of enzyme, i.e. microsomal mammalian cytochrome P450 3A4 enzyme. In this regard, the methods and techniques described in this chapter serves as a general prelude to coincide with obtained results in the context in the relevant forthcoming chapters. However, in terms of specific step-wise sequential modifications and protocols applied — at the end of each of the results chapters (i.e. Chapter 4, Chapter 5A and Chapter 5B) a comprehensive description with relevant subsections pertaining to each procedural outline is given.



3B.2 Materials and reagents

Table 3.1 shows a list of all general materials and reagents used in the course of the research investigations of this dissertation. All reagents were of analytical grade:

Table 3B.1 A complete comprehensive list of all materials used during the conduction of this PhD research investigation; listed also are sources and specific information

Materials/Reagents	Source Information	Specific Information
Milli-Q water	Milli-Pore filter system	
Nafion	Sigma Aldrich	Supplied as a 5% (w/v) solution in lower aliphatic alcohols; Equivalent weight = 1100 g mol^{-1} ; wet density = 0.87 g cm^{-3}
Cobalt(III) sepulchrate trichloride	Sigma Aldrich	95% purity
Potassium Ferricyanide ($\text{K}_3\text{Fe}(\text{CN})_6$)	Sigma Aldrich	
Ruthenium(III) hexaamine chloride	Sigma Aldrich	
2,4-Dichlorophenol		
Potassium dihydrogen phosphahate (KH_2PO_4)	Sigma Aldrich	Analytica grade 99.99% Purity
Quantofix hydroperoxo sticks	Sigma Aldrich	

Chapter 5 Variables of investigation and general protocols

Low melting point Agarose	Hispan agar	
Ethanol		
Methanol	Merck	HPCL grade
Carbon monoxide	Specialty Gases	99% Pur, gas form
Oxygen	Specialty Gases	99+% Pure, gas
Erythromycin	Sigma Aldrich	916 $\mu\text{g mg}^{-1}$
Quinidine hydrochloride monohydrate	Sigma Aldrich	
Glutaraldehyde	Sigma Aldrich	Supplied as 25% (v/v) stock
Polyvinyl alcohol (PVA)		
Indinavir™	Crixivan	Supplied as tablets containing 400mg indinavir sulphate
Polyethylene diamine (PEI)	Sigma Aldrich	
Eastman AQ (EAQ)-55	Eastman	Supplied as pellets
L-glutamic acid	Sigma Aldrich	99.5%
L-asparagine anhydrous	Sigma Aldrich	99.5%
Bovine liver catalase	Sigma Aldrich	
Full-length wild type CYP3A4	Merck South Africa	
Glassy Carbon	Basi	Teflon shrouded; geometrical area = 0.071cm^2
Reagents and materials for Electrolyte buffer media		
Sodium phosphate buffer solution (PBS)	Na ₂ HPO ₄ , NaH ₂ PO ₄ ·H ₂ O (Sigma Aldrich) Prepared as 50 mM solution (pH7.4)	
Sodium phosphate buffer saline (PBL)	Na ₂ HPO ₄ , NaH ₂ PO ₄ ·H ₂ O Prepared as 50 mM solution containing 100 mM KCl (pH 7.4)	
Materials for enzyme expression and purification of N-terminally modified CYP34		
CYP3A4 Parent vector	pBJW102.2 and PMD004	UK
Ampicilin (Amp)		
Glycerol	Sigma Aldrich	
δ -aminolevulinic acid (ALA)		
MgCl ₂	Sigma Aldrich	
Detergents: Igepal CA-3600, { 3-[(3-cholamidopropyl)dimethylammonio-1-propanesulphonate] } (CHAPS), Triton X-100		
PD-10 Columns	GE Healthcare,	

Chapter 5 Variables of investigation and general protocols

	USA	
Polyhistidine (His ₆)		As soluble his tagg
Ni-TED resin	Macherey-Nagel, Germany	
Centriprep YM-10 columns	Millipore, Island	
Milli-Q water		
Zeba column	Pierce, USA	
Bovine serum albumin (BSA)	Sigma Aldrich	
Bio-Rad protein assay dye	Bio-Rad, USA	Based on Bradford assay
DNase I	New England Biolabs	500 Units supply stock
Mercapto ethanol	Sigma Aldrich	
Thiamine		
Isopropyl thiogalactose pyranoside (IPTG)		
Glycerol stock	It consist of the E-Coli cells containing the plasmid with the enzyme DNA-sequence . (Stored at -80 °C)	
Lysis buffer, pH 7.4	Constituents: K ₂ HPO ₄ & KH ₂ PO ₄ (20 mM), glycerol (20%, v/v), β-mercaptoethanol (10 mM)	
Terrific broth	Constituents (per litre of solution): K ₂ HPO ₄ (2.31g) & KH ₂ PO ₄ (12.54g), yeast extract (24g), tryptone (12g), glycerol (4 ml)	
Phosphate buffer saline	Constituents: Na ₂ HPO ₄ ·H ₂ O, KH ₂ PO ₄ , NaCl, KCl	
10 x phosphate buffer saline (PBL) pH 7.4	Constuents: K ₂ HPO ₄ ·2H ₂ O (4.3 mM), NaCl (147 mM), KCl (2.7 mM), KH ₂ PO ₄ (1.8 mM)	
Trace elements (per 100 mL)	Constuents: FeCl ₃ ·6H ₂ O (2.7g), ZnCl ₂ ·4H ₂ O (0.2g), CoCl ₂ ·6H ₂ O (0.2g), Na ₂ MoO ₄ ·2H ₂ O, CaCl ₂ ·2H ₂ O (0.13g), H ₃ BO ₃ (0.05g), CuCl ₂ ·6H ₂ O (0.1g), conc. HCl (10 ml)	
Luria Bertani media (LB)	Constuents (per 500 mL stock): tryptone (5 g); yeast extract (2.5 g); NaCl (2.5 g)	
Purified nCYP3A4 storage buffer: 100 mM potassium phosphate buffer storage solution (KPBST): pH 7.4	Constituents: K ₂ HPO ₄ ·2H ₂ O and KH ₂ PO ₄ (100 mM); 20% glycerol (v/v); 0.2 mM EDTA; 1 mM DTT	

3B.2.2 Solutions

All chemical solutions were prepared using ultra pure water obtained from a Milli-Q Water System (Millipore Corp., Bedford, MA, USA).

3B.2.2.1 Preparation of electrolyte buffer solutions

All biosensor investigations done throughout the course of the research investigations were conducted in aqueous solutions, with phosphate buffer as supporting electrolyte. In this regard, 50 mM sodium phosphate buffer (pH 7.45), containing AnalaR grade Na_2HPO_4 , NaH_2PO_4 was prepared with milli-Q water. These electrolyte buffers, prepared without the addition of the inorganic salt, KCl are referred to as phosphate buffer solutions (i.e. PBS). On the other hand, saline phosphate buffer solutions, prepared as above, but with the inclusion of 100 mM KCl is denoted as PBL. Generally, all electrochemically-based voltammetric experiments conducted with control and enzyme-based biosensors were either conducted in PBL or PBS. In this regard, the author specifically specifies the type of electrolyte used when describing the various experimental protocols.

3B2.2.2 Preparation of redox probes

1 mM hexaamine ruthenium(III) chloride working solution was prepared in 100 mM aqueous KCl solution, by dissolving the appropriate mass in the KCl solution in a suitably calibrated volumetric flask. In addition to this, the Ferricyanide [$\text{K}_3\text{Fe}(\text{CN})_6$] redox probe was prepared as a 1mM working solution in an aqueous KCl solution, by dissolving the appropriate amount in a calibrated volumetric flask

3B.2.2.3 Preparation of working solutions for casting components for biosensor platform 1 and biosensor platform 2

3B.2.2.3.1 Preparation of Nafion casting solution

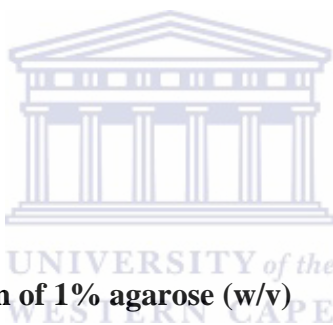
1% nafion solution (v/v) was prepared by diluting the appropriate volume of a 5% nafion[®] stock [supplied as a 5% solution (w/v) in lower aliphatic alcohols] with milli-Q water in a calibrated volumetric flask. The pH of the so prepared nafion solution was adjusted to prepare a working solution of pH 7.45. This was done by adding approximately 2-3 drops of a previously prepared pH 12.0 potassium phosphate buffer solution (of concentration 100 mM), with intermediate pH measurements until the desired pH of 7.45 was obtained. The final nafion solution, was then subsequently used for casting. Care was taken not to store the nafion casting solutions for long periods, since evaporation of alcohol may change the concentration, as well as precipitation reactions that may take place.

3B.2.2.3.2 Preparation of electrolyte solution of cobalt(III) sepulchrate species for electrodeposition (for preparation of biosensor platform 2)

1 mM Cobalt(III) sepulchrate [$\text{Co}(\text{Sep})^{3+}$] was prepared as an aqueous buffered saline saline solution, by dissolving the appropriate amount of cobalt(III) sepulchrate trichloride in 100 mM potassium phosphate buffer (pH 7.45, containing 100 mM KCl) in a calibrated volumetric flask. The prepared electrolyte solution was then subsequently used for the formation of the nafion-El-Co(Sep)³⁺ carrier matrix, as well as for the preparation of the nCYP3A4-based biosensor platform.

3B.2.2.3.3 Preparation of Eastman-AQ casting aqueous dispersion

A EAQ concentrated aqueous dispersion (15%, w/v) stock was prepared according established methods [100-101]. In this regard, stock was prepared by treating the appropriate amount of as obtained Eastman-AQ 55 in H₂O at 45 °C, under vigorous stirring, until a transparent, colourless and homogeneous phase was obtained. A 3% EAQ working aqueous dispersion was then subsequently prepared by appropriate dilution of the stock. When required, the 3% solution was used for casting during biosensor construction, but before use, the aqueous dispersion was always sonicated for at least ± 20 min, to obtain a smooth consistency for better film preparation.



3B.2.2.3.4 Preparation of 1% agarose (w/v)

The preparation for the agarose working solution was done according to standard methods [102]. In this regard, 100 mL Milli-Q water was brought to boiling point on a temperature controlled hotplate, equipped with an inbuilt magnetic stirrer. The appropriate amount of low melting agarose was then weighed out, after which the agarose powder was very slowly added to the boiling water. This was done while vigorously stirring the solution, and after all the agarose was added, the solution was stirred at the same temperature until complete dissolving of the agarose, at which point a solution with a clear consistency was obtained. The formed agarose solution was then removed from the heat and stored at 4 °C when not in use. It is noteworthy to add that working solutions of agarose was strictly only used for a maximum of two or three times, after which fresh solutions were prepared.

3B.2.2.3.5 Preparation of aqueous poly(vinyl alcohol) solution

A concentrated stock solution of PVA was prepared according to standard methods [103]. Milli-Q water was heated to 70 °C on a thermostated hotplate, after which an appropriate amount of PVA was slowly added to obtain a final stock concentration of 25% (w/v). The addition was done with vigorous stirring and the stirring was continued until complete dissolution of the PVA, at which time a clear colourless solution was obtained. The next step, involved the preparation of the working solution of PVA, which was subsequently used in the casting outer-layer composite solution preparation. In this regard, a 5% PVA solution in 0.1 M potassium phosphate buffer (pH 7.4) was prepared by appropriate dilution of the 25% stock.

3B.2.2.3.6 Preparation of aqueous polyethyleneimine solution

A working solution of PEI was prepared by dissolving 2 g of PEI in 20 mL of 0.1 M potassium phosphate buffer solution. The solution was thoroughly mixed and stored at room temperature until required.

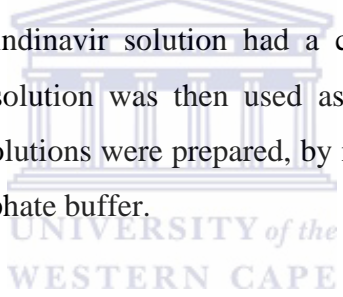
3B.2.2.3.6 Preparation of outer-film polymer blend casting solution for biosensor platform 2 (Results and discussion: Chapter 5B)

Equal volumes of the 5% PVA working solution and the 1% agrs solution placed in a pre-heated eppendorf tube and blended together by hand-mixing. The so-formed solution may be referred to as solution A. Following this, a volume of the prepared PEI solution was added to solution A, such that the final ratio of PEI to

PVA-Agrs (PEI:PVA-Agrs) was 0.2 : 1. This solution was then subsequently used for casting.

3B.2.2.4.3 Preparation of Indinavir stock and working solutions

1 Capsule of indinavir, as obtained from the manufacturers was opened up and placed in a 25 mL volumetric flask, made up to the mark with 50 mM sodium phosphate buffer solution. The active ingredient was attracted and undissolved components removed by filtering the formed suspension through a Whatman polytetrafluoroethylene syringe filter (pore size 0.3 μm) into a clean glass storage bottle. The so prepared indinavir solution had a concentration of 28,095 μM of indinavir sulphate. This solution was then used as stock indinavir solution, from which all other working solutions were prepared, by making the appropriate dilutions with 50 mM sodium phosphate buffer.



3B.3 Voltametric investigations

3B.3.1 Instrumentation, apparatus and general procedures

Generally, all of the voltammetric experiments in this dissertation were conducted in a 20 mL volume capacity glass electrochemical cell containing the required volume of supporting electrolyte and a conventional three electrode system, consisting of a glassy carbon working electrode (GCE, 0.33 cm diameter), a Ag/AgCl (3 M NaCl) as pseudo reference electrode, and a platinum wire as counter electrode (CE). Unless otherwise stated, all experiments conducted in the three-electrode electrochemical cells were done at at 25 $^{\circ}\text{C}$.

All voltammetric experiments and measurements, including cyclic voltammetric (CV), Osteryoung square wave voltammetry (OSWV) and differential pulse voltammetric (DPV) measurements were obtained with a BioAnalytical System (BAS) 100 B/W Electrochemical Workstation. During substrate interaction experiments, conducted with OSWV, convective transport during measurements was achieved with the use of a magnetic stirrer bar, and stirring was done at predetermined rate.

3B.3.1.1 Pre-treatment of the glassy-carbon working electrode

Prior to all electrochemical investigations, all working electrodes (modified and unmodified) were activated by following a specific protocol in accordance with selected literature procedures — modified and customized for the requirements of the practical aspects of the current dissertation. Generally, this entailed the polishing of the GCE with 3 μm diamond paste for 1 min, followed by rinsing with methanol and water, respectively. The polished electrode was then ultrasonicated for 2 min. Then the electrode was polished consecutively, with aqueous slurries of 1.0, 0.3 and 0.05 μm alumina, for 1 min on a microcloth pad (Buehler). Residual polishing material was removed by ultrasonication for 3 min after each polishing step. Finally, the pre-treated GCE was sonicated in absolute ethanol for 2–3 min, rinsed with water, dried for 5min and immediately used. Surface cleanliness and electro-analytical reproducibility was always verified for all cleaned electrodes by standardization and calibration with ‘universal’ redox probe, 1mM $\text{Fe}(\text{CN})_6^{3-}$, and known standard solutions. It is also noteworthy to add that, when additional cleaning or polishing of the surfaces were required, a more vigorous cleaning was done with diamond paste polishing kit, by following the same general procedure as described above.

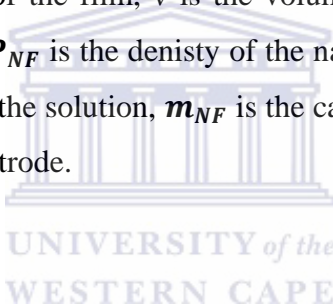
3B.4 Specific methods for important calculations of electrochemical parameters

3B.4.1 Determination of film thickness

In the context of this dissertation, the approach for the determination of film thickness was based on taking into consideration the volume of the drop of nafion-solution, the density of the Nafion® solution and the area of the electrode, according to the following equation [104-105]:

$$h = v/s = m_{NF}/P_{NF} \times S = m_{drop} \times \omega/P_{NF} \times S \quad \text{3B-1}$$

where h is the thickness of the film, v is the volume of the solution applied to the surface of the electrode, P_{NF} is the density of the nafion (g cm^{-3}), ω is the fractional concentration of nafion in the solution, m_{NF} is the calculated mass of nafion, and S is the surface area of the electrode.



3B.5 Complimentary ex-situ characterisation analysis

3B.5.1 Scanning Electron Microscopy (SEM)

Scanning electron microscopy was used to characterize the morphology of the prepared films, including the following:

- the unmodified nafion film prepared for each biosensor platform;
- the naf-CME-Co(Sep)³⁺ composite film;
- the naf-EI-Co(Sep)³⁺

The SEM images were captured with an Hitachi X-650 analyzer employing the secondary electron (SE) mode with interchangeable accelerating voltages of 25

kV electron microscope All samples prepared for SEM characterization were adequately dried before analysis. Screen printed carbon electrodes were used for preparation of films for SEM analysis. The modified electrodes were fixed onto a SEM mounting stage with low resistance carbon transfer adhesive. For cross-sectional views, electrodes were fractured with a sharp surgical blade. Prior to SEM analysis, each sample was gold-coated with a Polaron sputter coater. As a control, for comparison purposes, a blank screen printed electrode was always analysed in addition to the modified electrodes.

3B.5.2 Fourier Transform Infrared Spectroscopy (FTIR)

All the FTIR spectra of samples were recorded on a PerkinElmer Spectrum 100, FT-IR spectrometer. All FTIR spectra recordings were done with small amount of dried, or wet samples without KBR mixing. Moreover, all spectra were obtained against the air background spectrum. With regard to the specific methods used: In the case of the spectral analysis for the prepared films, the samples were first prepared on the electrode surface, following the specific procedures for the particular platform (as outlined in the methodology section of the relevant results chapters), after which the samples were gently scraped off the surface, followed by desiccator drying. The dried samples were then used for recording of the spectra, as shown in Figure 3B.1. In the case of FTIR spectral analysis for the enzyme solutions on the other hand, the wet samples were used, as described in the experimental section of the relevant results chapter.

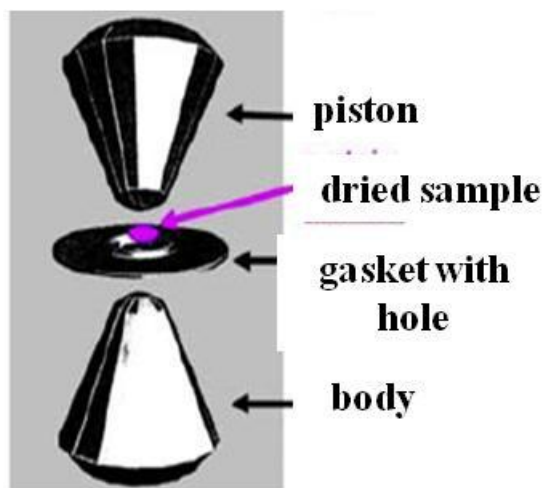


Figure 3B.1 Showing method of FTIR analysis with high-pressure anvil cell for dry samples

3B.5.3 UV-Vis Absorption Spectroscopy

All UV-Vis absorption spectroscopic analysis were done with a Nicolet-Evolution UV-visible scanning spectrophotometer (Thermo Electron Corporation, UK) using 1-cm path length quartz cells. The exact protocols followed for the specific analysis experiments are discussed in the Experimental outline of the relevant results chapter.

CHAPTER 4

RESULTS AND DISCUSSION: Biosensor Platform 1

Chapter Prelude

The results presented in the current chapter were published in *Electrochimica Acta*, 2009, 54, 1925-1931. In the context of the dissertation as a whole, the biosensor platform presented and discussed in this chapter, serves as a portrayal of an initial attempt in the creation of a reagentless biosensor mediated by the electroactive cage-type mediating species, cobalt(III) sepulchrates, in which the mediator was integrated into the reagent layer. Generally, this initial approach was more ‘unrefined’, consisting of casting and mixing was applied in creating this particular biosensor platform — the main focus here was to observe the electrocatalytic behaviour of the of the immobilized enzyme with its co-substrate (molecular oxygen) and selected substrates. This could also be done, since the commercially sourced, wild type, full-length CYP450 3A4 used on the current platform, is more stable than their N-terminally modified genetically engineered counter-parts, which was used as recognition component in the platform presented and discussed in Chapter 5A and B.

CHAPTER 4

Microsomal cytochrome P450-3A4 (CYP3A4) biosensor for the determination of 2,4-dichlorophenol — An endocrine disruptor compound

Abstract

Cytochrome P450-3A4 (CYP3A4) is a monooxygenase enzyme that plays a major role in the detoxification of bioactive compounds and hydrophobic xenobiotics (e.g. medicines, drugs, environmental pollutants, food supplements and steroids). A unique CYP3A4 biosensor system that essentially simplified the enzymatic redox processes by allowing electron transfer between the electrode and the enzyme redox centre to occur, without any need for the enzyme's natural physiological redox partners, was developed and tested with respect to analyte detection, by using 2,4-dichlorophenol (2,4-DCP), a priority environmental pollutant and an endocrine disruptor as substrate. The biosensor, GCE||Naf|CMECo(Sep)³⁺|fCYP3A4|Naf, was constructed by entrapping commercially obtained wild type full length cytochrome P450 3A4 (fCYP3A4) on a pre-formed electroactive carrier matrix, consisting of a Cobalt(III) sepulchrates-modified nafion membrane on a glassy carbon (GC) electrode. The responses of the biosensor to 2,4-dichlorophenol, erythromycin (CYP3A4 native substrate) and ketoconazole (CYP 3A4 natural inhibitor) were studied by cyclic and square wave voltammetric techniques. The detection limit (DL) of the biosensor for 2,4-dichlorophenol was 0.043 μgL^{-1} , which is by an order of magnitude lower than the EU limit (0.3 μgL^{-1}) for any pesticide compound in ground water. The biosensor's DL is lower than the U.S. Environmental Protection Agency's drinking water equivalent level (DWEL) value for 2,4-DCP, which is 2 μgL^{-1} .

4.1 Introduction

The pervasiveness and incapacitatingly negative impact of 2,4-dichlorophenol (2,4-DCP) both on the environment (particularly our waterways), as well as on human beings are well known and exhaustively documented in many peer reviewed literature [32-36, 41, 44]. Most of these aspects were already discussed in Chapter 1, **Section 1.2.3**, and as such need not be elaborated on in its entirety this time. However, it will be said, that in terms of the multiple catastrophic effects of this pollutant, it is the endocrine disrupting properties that poses the biggest threat, affecting not only the exposed person, but also their generational offspring [32]. Overall, with regard to curbing the effects of 2,4-DCP, safety limits have been set, as 50 – 100 μgL^{-1} , 1 – 5 μgL^{-1} and 100 – 500 ngL^{-1} for river water, pre-treatment potable water and drinking water, respectively (WHO, EPA, EU). Conventional analytical methods, used for determination of 2,4-DCP and other chlorophenols indeed have high accuracy – obtaining detection limits ranging from 0.01 to 0.5 $\mu\text{g L}^{-1}$, and linearity of up to 2–3 orders of magnitude [32], but all fall short in terms of the requirement of extensive sample preparation and time-consuming pre-concentration steps. Moreover, onsite real-time measurements are out of the question. In contrast, it is known that biosensor devices based on electrochemical principles can offer analytical solutions with low cost, simplicity and fast sample throughputs, while being suitable for on-the-spot testing of environmental samples [53-54, 106]. The biosensors reported so far for the determination of chlorinated phenols are mostly based on indirect recognition of the analyte, and rely on the inhibition of enzymes such as horseradish peroxidase, tyrosinase or cholinesterase immobilized over an electrode surface [32, 43, 107]. This preference may be due to limitations in the availability of oxido-reductase enzymes which can act on these pollutants. Nevertheless, biosensors based on enzyme catalysis would operate on “signal-on” transduction basis and, thus, possess better detection limits. Amongst the possible enzyme ‘candidates’, the cytochrome P450 iso-enzyme, CYP3A4, is the most catalytically versatile, having the ability to catalyze the oxidative metabolism of various lipophilic xenobiotic compounds which includes

chlorophenols, pesticides, carcinogens, etc. [3, 64, 66, 108] and thus can be used for the development of non-inhibition based biosensor for these pollutants. In fact, based on the ability of CYP3A4 and many other microsomal CYP450s to break down highly toxic hydrophobic compounds to harmless water soluble products, such as aromatic hydrocarbons, aflatoxins, etc., their proposed future significance in industrial applications have long been predicted [109]. Notwithstanding all these factors, to this end, no biosensors have been reported for 2,4-DCP and/or other chlorophenols using CYP3A4 as the enzymatic recognition component. Nevertheless, in considering such an endeavor, based on the unique and highly complex nature of CYP3A4 enzymes, very versatile and innovative electron transfer mechanisms is required support this membrane bound, microsomal mammalian heme thiolate protein chemistry – the overall challenge being designing a system that has a good electrode-enzyme electronic coupling that, in turn, would drive catalytic turnover at relatively high rates. In this regard, the integration of a mediator into the reagent layer has proven highly beneficial in functioning as electron transfer shuttle to and from the deeply buried enzyme active site. Amongst available mediating species, with specific reference to microsomal CYP450 enzymes, cobalt(III) sepulchrate $[(\text{Co}(\text{Sep})^{3+})]$ is shown to be the better choice.

In this study, firstly, wild type full-length CYP3A4 was monomerized through treatment with nonionic 3-[(3-chloramidopropyl)dimethylammonio]-1-propanesulphonate (CHAPS), which prevented aggregation of the enzyme units and enabled simplified casting of the enzyme. The biosensor was constructed by immobilizing the enzyme on a carrier matrix consisting of a nafion-cobalt (III) sepulchrate composite film. The choice of nafion as base matrix, was due to the multifaceted inherent features of the ionomer, including its unique cation pre-concentration ability that is distinct from most other ionic polymers and conventional ion exchanges, its high chemical stability, as well as its microscopic hydrophobic/hydrophilic phase segregation. These qualities was applied to firstly extract and stably pre-concentrated the mediating species in the overall carrier matrix,

while secondly providing the suitable platform in which the immobilized flCYP3A4 could interact with the pseudo-donor electron platform through its required hydrophobic/hydrophilic interactions that it normally use in native in-vitro and in-vivo systems. In order to re-enforce the stability of the reagent-layer film and protect the underlying components, an additional thin layer of nafion was used as outer film throughout all experimental investigations.

4.2 Morphological and structural characterization of the nafion-CMECo(Sep)³⁺ film (carrier matrix) formed on the GCE [GCE (GCE||naf|CMECo(Sep)³⁺]

Before the application of the carrier matrix in the fabrication of the flCYP3A4-based biosensor, some morphological and structural analysis of the formed film was done. In this regard, morphological studies were done through Scanning Electron Microscopic (SEM) analysis, while the structural analysis of the films was done with Fourier Transform Infrared (FTIR) Spectroscopy.

4.2.1 Morphological characterization: Scanning Electron Microscopy (SEM)

Figure 4.1 a – c shows the top sectional view of the blank, un-modified electrode (bl-E), the nafion-modified electrode, as well as the nafion-modified electrode containing the incorporated Co(Sep)³⁺ species. The nafion film displays more of an island-type feature, containing random void-type areas, thus overall not does not really have a smooth consistency. This may probably be due to the argon flow used during the drying of the nafion film, which could have possibly slightly perturbed the nafion during film formation. On the other hand, one must bear in mind

that nafion is known for its high chemical stability and in this regard, is still expected to provide an acceptable inner-film for the incorporation and/or immobilization of the other reagent-layer constituents. Moreover, according to documented literature, actual decomposition of a nafion film is signified by visible pore holes which is evident in cross-sectional views [110]. In this regard, the cross sectional images taken of the formed film, exhibited an intact film, devoid of any such pores. The Co(Sep)³⁺-modified nafion film, of which the SEM image is shown in **Figure (c)** also exhibits an island-like film, which does not really have a smooth consistency, but rather resembles a ‘cauliflower-type’ surface.



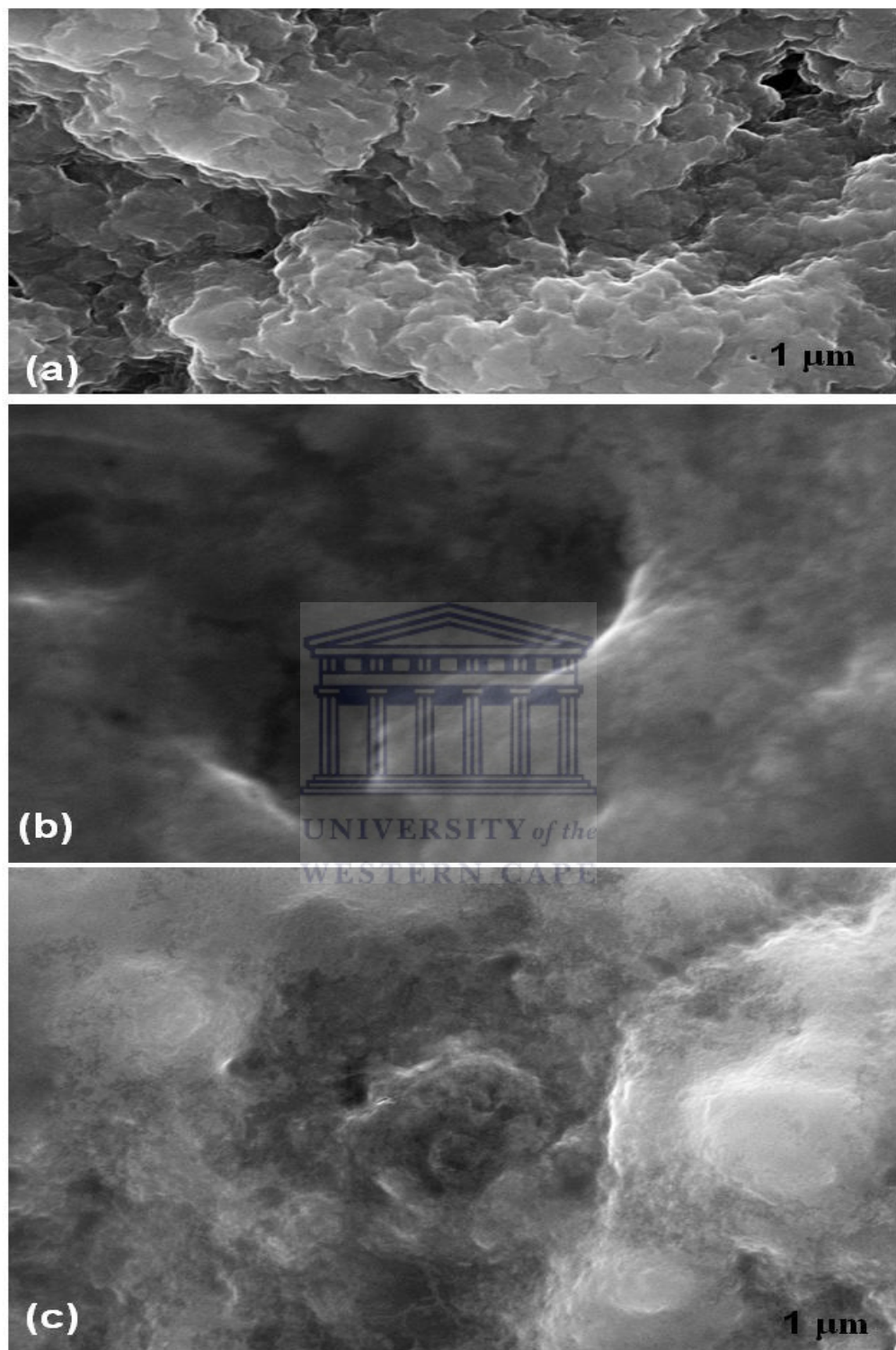


Figure 4.1 Top scanning electrochemical image of electrode (a) blank electrode (bl-E); (b) nafion modified electrode (Naf-E); (c) Naf-E with pre-concentrated Co(Sep)^{3+}

4.2.2 Structural characterization: Fourier Transform Infrared (FTIR) Spectroscopy

Figure 4.2 a – c exhibits the FTIR spectra of the nafion membrane, commercially attained pure cobalt(III) sepulchrate trichloride, and the chemically prepared naf[CMECo(Sep)³⁺] composite film, respectively. In this regard it shows the structural features, exhibited as vibrational fingerprints, associated with each component within an analyzed film. The assignment of vibrational bands thus assists in identification of species. In terms of the nafion membrane, in particular, shown in Spectra a, characteristic bands associated with the structure of pure nafion, identified as the CF₂ asymmetric stretching (1207 cm⁻¹), CF₂ symmetric stretching (11490 cm⁻¹), S-O symmetric stretching (1058 cm⁻¹), C-O-C stretching (981, 862 cm⁻¹), and C-F stretching (630 cm⁻¹) are shown and appropriately highlighted [110-114]. With regard to the pure un-modified cobalt(III) sepulchrate [Co(Sep)³⁺], shown in Spectra b, the exhibited absorption bands, associated with the associated with methylene groups (733, 834, 2850, 3034 cm⁻¹), and secondary amines (1055, 1130, 1168, 1335, 1366, 1444, 3415, 3520 cm⁻¹) are in fact characteristic functional groups in the structure of Co(Sep)³⁺ [115], and as such, may be regarded as an efficient fingerprint identification of the unique structural features of the compound. With regard to the chemically prepared nafion-Co(Sep)³⁺ composite film on the other hand, shown in Spectra c, from a general perspective, most of the characteristic fingerprint bands associated with the structural features of nafion can be seen. However, closer evaluation of the spectra revealed the presence of new vibrational bands, as well as slight positional shifts in some of the original bands as seen in Spectra a. Cumulatively, these observations of course suggest the modification of the microstructure of nafion, which in the current case is due to the pre-concentration of the chemically deposited Co(Sep)³⁺ within the pre-formed nafion membrane. Thus appropriately, the changes in vibrational absorption bands associated with the incorporation of the Co(Sep)³⁺ have been indicated by coloured arrows on the

spectrum, with the likely functional group involved in the change also suitably marked on Spectra b. In this regard, in the modified nafion membrane, the appearance of vibrational band located at 854 cm^{-1} (indicated by the magenta colour arrow) may be ascribed to methylene groups associated with the $\text{Co}(\text{Sep})^{3+}$ structure. Moreover, the appearance of bands in association with secondary amines, located at 1240 and 1462 cm^{-1} , (indicated by the blue and green arrows, respectively) also signify the presence of $\text{Co}(\text{Sep})^{3+}$ within the nafion membrane. Also, it is notable that the peaks centred at 2892 - and 2997 cm^{-1} , associated with methylene functional groups of the $\text{Co}(\text{Sep})^{3+}$ structure. Interestingly, it is noteworthy that the water content of the modified nafion membrane, signified by the broad peak for stretching vibration of water molecules centred at between $\approx 2630 - 3740\text{ cm}^{-1}$, is still very high, as compared to the untreated nafion membrane. On the one hand, to some extent, this phenomenon may be partly ascribed to the blending vibration of molecularly adsorbed water in the membrane [116]. On the other hand, since the $\text{Co}(\text{Sep})^{3+}$ was manually casted and allowed to mix with the pre-formed nafion membrane, which in itself is known to contain an appreciable amount of water molecules, which functions as plasticizer around the sulphonic cluster region [117] – this could indicate that while some of the $\text{Co}(\text{Sep})^{3+}$ molecules were indeed taken up within the lower density ionic cluster phase, some were probably still concentrated near the surface of the bulk polymer phase. The reasoning for the school of thought here is based on the fact that from a general perspective, the water of hydration contained within the nafion is normally reduced in direct association with the increase in the uptake of the amount of counter ions, particularly in the case of counter ion species which contains hydrophobic ligands, such as is the case with $\text{Co}(\text{Sep})^{3+}$ [117-118]. Nevertheless, overall, the results shown in the FTIR spectra does indeed confirm the existence of the electroactive $\text{Co}(\text{Sep})^{3+}$ mediating species in the nafion membrane, which of course is the more important factor. Moreover, due to nafion's unique method of extraction of cationic species that, as described in Chapter 2, Section is quite distinct from other ionic polymers and/or conventional cation exchangers, and as such, is known to stably retain these species for much longer time frames [119]. (More on the

subject of the aforementioned aspects surrounding the water molecules etc., is comprehensively discussed in Chapter 5A.)

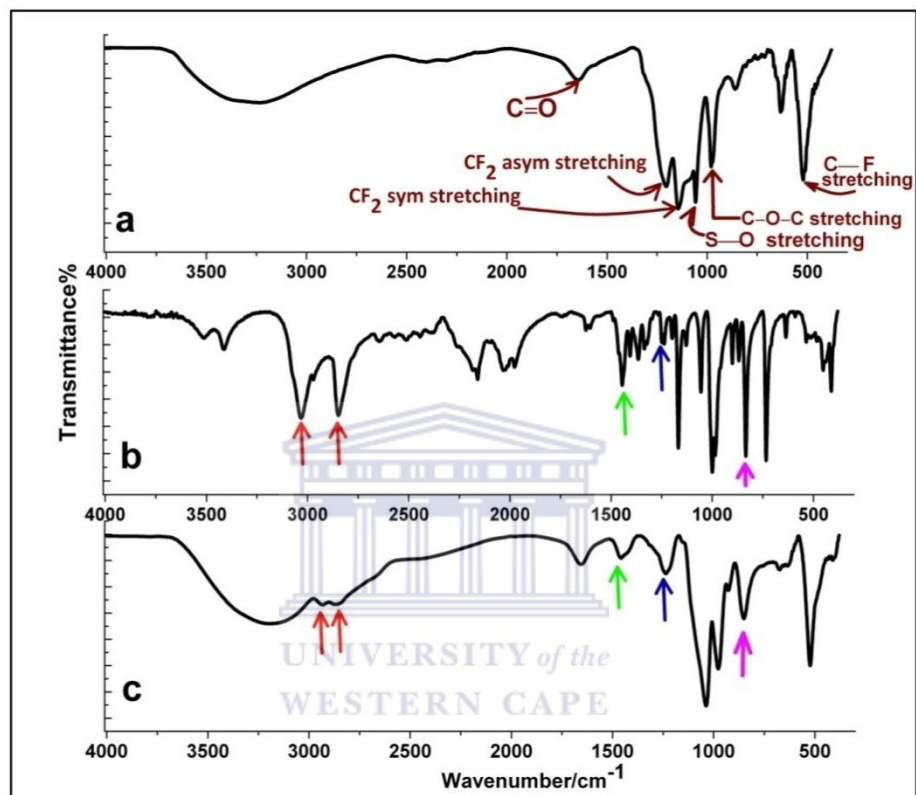


Figure 4.2 Fourier Transform Infrared Spectroscopic (FTIR) spectra of (a) unmodified nafion membrane; (b) commercially obtained, pure cobalt (III) sepulchrate only; the nafion membrane modified with the chemically deposited Naf-Co(Sep)³⁺-composite film naf|CMECo(Sep)³⁺

On a final note, regarding the latter and afore-showed characterization results: Although the morphology of the formed films were not exactly visually ideal, the structural analysis of the formed films still showed the presence of the expected functional groups and as such, the method of preparation may be regarded as acceptable.

4.3 Voltammetric characterization of the modified electrode

Before commencing with the electrochemical results, it is noteworthy to bring to the reader's attention that to reinforce the stability of the carrier matrix and/or enzyme-based reagent layer, a thin layer of nafion film was used as outer film.

4.3.1 Electrode Assembly

In order to ascertain whether the proposed electroactive compound, i.e., $\text{Co}(\text{Sep})^{3+}$, can effectively function as mediating species within the fICYP3A4-derivatized biosensor platform, background studies first have to be conducted. The specific aim here being the determination of whether the mediator exhibits a redox response at a sufficiently negative potential to be able to, in turn, reduce the enzyme ferric iron (Fe^{3+}) for the initiation of its catalytic reaction cycle and concomitant electrocatalytic interaction with its co-substrate, molecular oxygen, and/or selected analytes (substrates) [74, 120]. The results for these studies are shown in **Figure 4.1**. In particular, **Figure 4.1** shows the cyclic voltammogram of 1 mM cobalt sepulchrate on a bare GCE working electrode performed at 10mVs^{-1} in argon-degassed PBL. The voltammogram exhibited a cathodic peak ($E_{p,c} = -640\text{mV}/\text{Ag}/\text{AgCl}$, $I_{p,c} = -3.74\mu\text{A}$) and an anodic peak ($E_{p,a} = -579$, $I_{p,a} = 3.54\mu\text{A}$). Moreover, both the cathodic and anodic waves consisted of one peak each, which is indicative of only one redox species, and can thus be ascribed to the metal-centred, one-electron process due to $\text{Co}^{3+}/\text{Co}^{2+}$ with a E° determined as $610 (\pm 10)$ mV. The peak separation (ΔE_p) value was $61\text{mV} \pm 3\text{mV}$, whereas the $I_{p,a}/I_{p,c}$ value was 0.95 ± 0.05 . In this regard, in terms of theoretically based values, the aforementioned ΔE_p and $I_{p,a}/I_{p,c}$ values are well within the range for fast diffusion controlled reversible one electron cyclic voltammetric processes (i.e. $\Delta E_p = 59$ and $I_{p,a}/I_{p,c} = 1$) [74, 121] and as such, imply

rapid electron transfer. In addition to this, the inset in **Figure 4.1** exhibits the square wave response of the GCE in the 1 mM Co(Sep)³⁺, shown as the difference square wave, for which a signal was obtained at -640 ± 5 mV. In this regard, as compared to the E° obtained for the CV, there is approximately 30 mV difference between the values obtained from the two respective voltammetric techniques. However, as explained in Chapter 3A, **Section 3A.2.1.2.1**, square wave voltammetry is eminent for its lower signal-to-noise ratio and as such, variation in obtained results from the two techniques are indeed expected. Nevertheless, in terms of specific assessment, both of these values are sufficiently cathodic, to be able to, in turn, reduce the enzyme heme ferric ion (Fe^{3+}) to its active Fe^{2+} form for its electro-catalytic function.

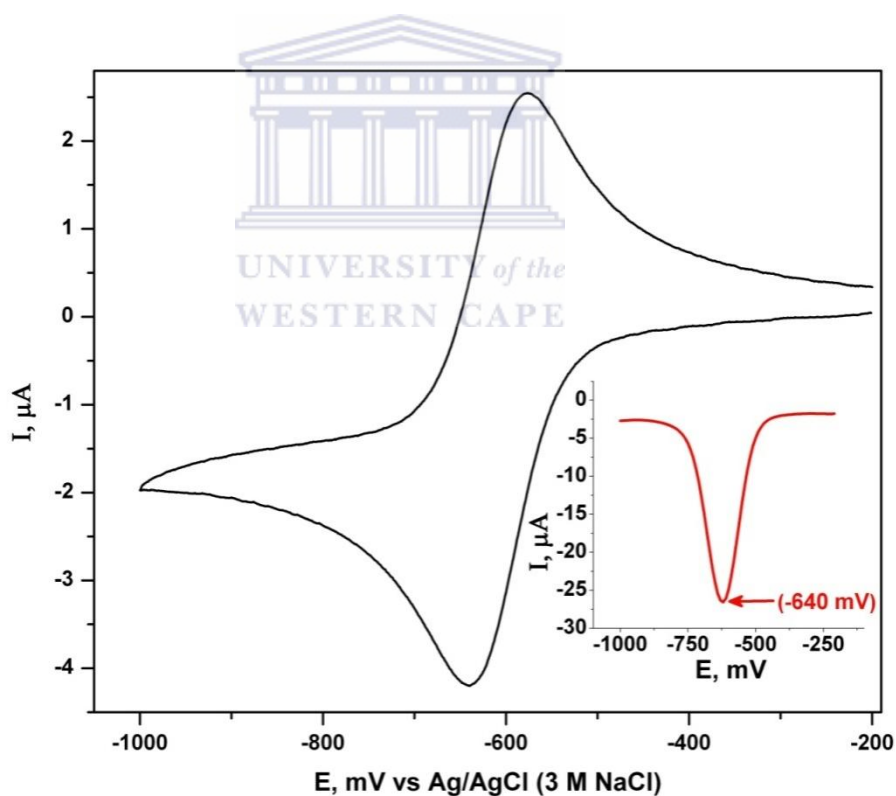
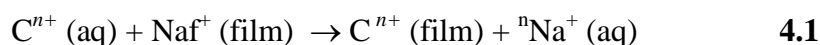


Figure 4.3: Cyclic voltammogram of bare GCE in phosphate buffer saline (PBL, pH 7.4) containing 1 mM Co(Sep)³⁺. Inset shows the square wave (SW) voltammetric response of the GCE in 1 mM Co(Sep)³⁺, exhibited as the difference SW.

The stepwise modification of the GCE was monitored by electrochemical studies in order to investigate the variation in the voltammetric characteristics in association with the progression from the nafion-modified GCE, to the reagentless, mediator-containing fCYP3A4-derivatized biosensor platform (GC||naf|CMECo(Sep)³⁺|fCYP3A4|naf). A major main aim here, was also to confirm electron flow from the electrode to the fCYP3A4 via the(nafion pre-concentrated) Co(Sep)³⁺ mediator. In this regard, **Figure 4.4(a)** shows the cyclic voltammograms of the nafion-modified GCE (GCE||naf) and the Co(Sep)³⁺-entrapped nafion film (GCE||naf|Co(Sep)³⁺). In addition to this, the difference SW voltammogram of the GCE||naf|Co(Sep)³⁺ is shown in **Figure 4.4(b)**. With regard to evaluation of the CVs exhibited in **Figure 4.4(a)**, the nafion-modified electrode did not exhibit any discernable electrochemistry. Essentially, this is not an unexpected phenomenon, since nafion is not itself electroactive but due to its unusually high ion-exchange ability and/or affinity for large (hydrophobic) cations it may be used to pre-concentrate [52, 122], or simply physically absorb electroactive cationic molecules in a thin membrane-layer, onto a suitable electrode, as is the case in the current study. This usually done by contacting a pre-formed nafion film with an aqueous solution containing the specific counter ion species, in accordance with the following equation [52]:



On the other hand, in biosensor preparation in particular, based on its unique physical and structural characteristics, nafion may be used as an electrode coating for the stable incorporation and immobilization of biomolecules, while simultaneously preventing biofouling [52, 122-123]. Considering aforementioned characteristics of nafion with regard to its superior counter-ion pre-concentration ability, it is thus not surprising that in the CV for the GC||Naf|CMECo(Sep)³⁺ electrode, a pair of well defined symmetrically shaped redox peaks can be observed. In terms of the context of the current research investigation, the peaks can be ascribed to the reversible one electron transfer reaction of the metal-centred surface-confined redox species

Co(Sep)³⁺/Co(Sep)²⁺ and as such, also exhibits fast electron tunnelling process through the Nafion layer, to and from the underlying GCE. Closer evaluation of the redox couple showed that they consist of cathodic peak ($E_{p,c} = -609$ mV (vs Ag/AgCl), $I_{p,c} = -1.048$ μ A) and an anodic peak ($E_{p,a} = -534$ mV (vs Ag/AgCl), $I_{p,a} = 0.848$ μ A) with a midpoint potential, E_m of -571 ± 5 mV. Compared to the electrochemistry of Co(Sep)³⁺ on bare GCE, GC||Naf-Co(Sep)³⁺ showed a decrease in the magnitude of the $I_{p,c}$ and $I_{p,a}$ and an anodic shift in the $E_{p,a}$ value by approximately 23mV. Interestingly, in previously documented literature, other researchers report a cathodic potential shift in the E_m value of GC|Naf-Co(Sep)³⁺ as compared to that observed for the bare electrode [124]. In this regard, unlike the physical casting/mixing technique of Co(Sep)³⁺-nafion interaction used in the current investigation, in the aforementioned study, incorporation of Co(Sep)³⁺ within the pre-formed nafion membrane was done through potentiodynamic cycling in the contacting solution. The significant difference in applied technique could thus possibly confer a variation in the interaction and/or distribution of the Co(Sep)³⁺ counter ion species within the microstructure of the nafion film. Moreover, considering that the redox potential of Co(Sep)³⁺ depends on the specific experimental conditions, such as the nature of the film, pH, supporting electrolyte, etc., the results are well within experimental variability. Another noteworthy factor with regard to the exhibited CV for the GC||Naf|CMEECo(Sep)³⁺ is that the anodic peak current is slightly smaller in magnitude than the corresponding cathodic peak current, by a value of about 0.20 μ A. This is not an uncommon phenomenon and can be ascribed to the fact that the electroactive species was entrapped in the Nafion film in its oxidized form Co(Sep)³⁺ [91]. With regard to the difference SW voltammogram shown in **Figure 4.4(b)** for the GC|Naf-Co(Sep)³⁺ electrode, the signal is observed at -570 mV, which, as in the case of the results obtained for the CVs, shows an anodic shift as compared to the obtained E_p observed for the difference SW of the bare GCE, by a magnitude of approximately 70 mV.

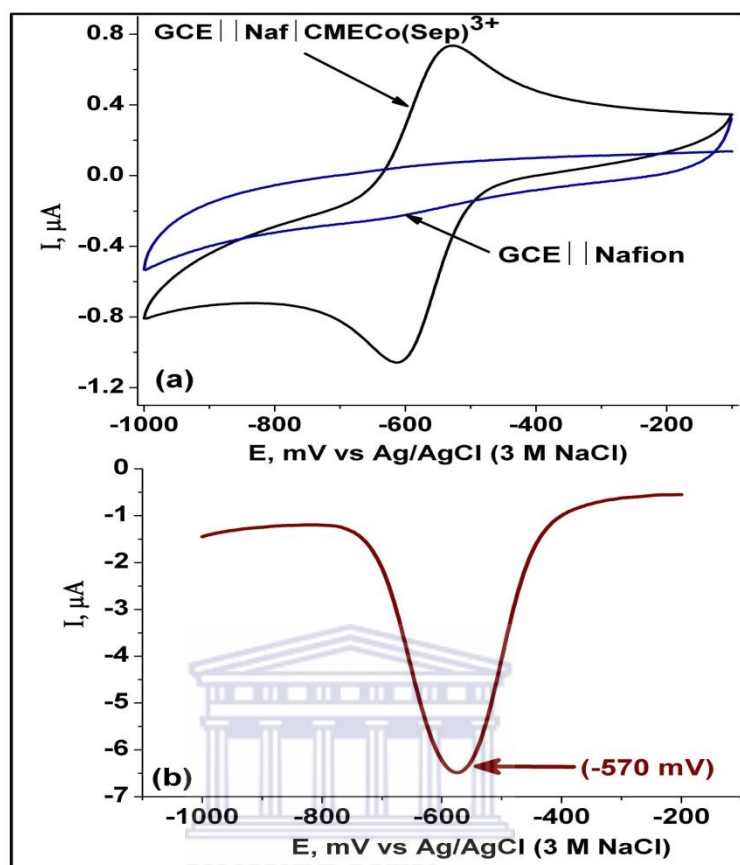


Figure 4.4: (a) Cyclic voltammetric response for the nafion-coated GCE (GCE|naf), and the cobalt(III)sepulchrates modified- GCE|naf (i.e., GC|naf|CMECo(Sep)³⁺|naf) for experiments conducted in argon-degassed (Ar) 50 mM PBL at 10 mV s⁻¹. (b) Square wave voltammetric response of the GC|naf|CMECo(Sep)³⁺|naf also in ArPBL, presented as the difference spectrum. Experimental conditions: StepE = 4 mV; amplitude = 75 mV;

In terms of the fabricated biosensor, the results for the cyclic and square-wave voltammetric responses for the GC|naf|CMECo(Sep)³⁺|fICYP3A4|naf electrode for an experiment conducted in ArPBL, is shown in **Figure 4.5 (a)** and **(b)**, respectively. In the absence of substrate (indinavir), and/or co-substrate (molecular oxygen), the immobilized enzyme gives no catalytic response, and as such, the electrochemistry observed is essentially dictated by the the Co(Sep)³⁺ mediator [125]. In this regard, with respect to the CV in particular, the anodic and cathodic peak potentials for the

reaction was -555 and -625 mV, respectively, corresponding to the $\text{Co}^{3+} + 1e^- \rightleftharpoons \text{Co}^{2+}$ redox system. Moreover, the cathodic and anodic peak currents ($I_{p,c} = -1.322$ μA ; $I_{p,a} = 0.717$ μA), were fairly symmetrical, with the $I_{p,c}$ exhibited for the fabricated biosensor (GCE|naf|CMECo(Sep)³⁺|fCYP3A4|naf) shown to be higher in magnitude, than the $I_{p,c}$ of the Nafion-entrapped CMECo(Sep)³⁺ modified GCE (i.e. GCE||naf|CMECo(Sep)³⁺) [Figure 4.4(a)], by almost 2 orders of magnitude. Prior research has established Nafion as a perfluorinated polymer with a micellar pore structure, that is able to stably bind or incorporate surfactants and other molecules to and/or into its bulk membrane through coulombic and/or hydrophobic interactions, depending on the charge and hydrophobic nature of the compound [122, 126]. Thus, the increase in $I_{p,c}$, may be ascribed to the favourable interaction between the Nafion and the CHAPS monomerized-fCYP3A4 without the need for any additional coupling reagents and/or bifunctional linking molecules to re-enforce stable enzyme immobilization. The overall result is effective electron shuttling between the reduced mediator and the enzyme heme group yielding $I_{p,a}/I_{p,c}$ and ΔE_p values of 0.9 and 70 mV, respectively. The ΔE_p value is close to 65mV indicating the presence of a surface-bound electroactive species undergoing fast reversible electron transfer at the electrode [74]. In this context, the GC||Naf|CMECo(Sep)³⁺ is therefore a better electrode system than the Nafion-entrapped mediators reported by some other researchers. For example, Nafion-entrapped [cobalt(II)phthalocyanine-cobalt(II)tetra(5-phenoxy-10,15,20-triphenylporphyrin)] — pentamer, also done through a casting/mixing technique, showed a ΔE_p value of 200mV [127]. **Figure 4.5(b)** shows the squarewave response of the GC|naf|CMECo(Sep)³⁺|fCYP3A4|naf electrode, for which signals was obtained at -600 ± 5 mV. Compared to the results shown for the nafion-entrapped CMECo(Sep)³⁺ and the bare GCE in $\text{Co}(\text{Sep})^{3+}$, the signal shifted anodically by approximately 40 mV and 30 mV, respectively. These results are comparable with those obtained in cyclic voltammetric studies and thus corroborate those findings.

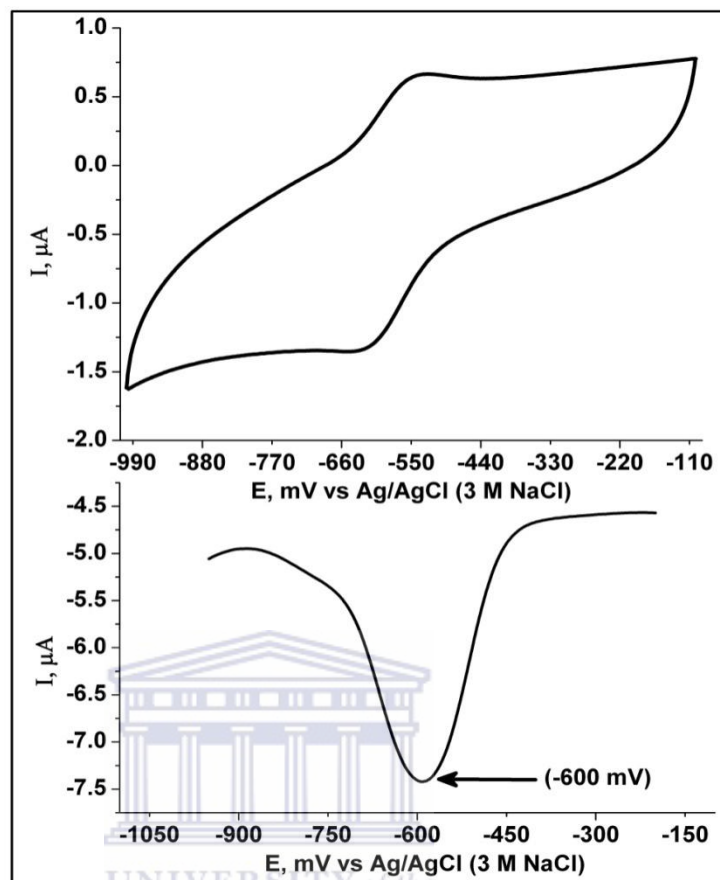


Figure 4.5: (a) Cyclic voltammetric response for the fICYP3A4 based biosensor, i.e., naf|fICYP3A4|Co(Sep)³⁺|naf||GC electrode, for experiment conducted in argon-degassed (Ar) 50 mM PBL at 10 mV s⁻¹. (b) Square wave voltammetric response of the naf|fICYP3A4|Co(Sep)³⁺|naf||GC electrode in ArPBL, presented as the difference spectrum. (Plot shows the net current of the forward and reverse SWV response for a scan that was done cathodically). Experimental conditions are: square-wave amplitude 75 mV; potential step 4 mV. Step E = 4 mV; amplitude = 75 mV;

4.3.2 Electrochemical behaviour of the GCE|Naf|CMECo(Sep)³⁺|CYP3A4|Naf biosensor

To ascertain and identify the type of current involved in the redox process, the dependence of the peak current on scan rate was investigated over the potential range scanned (-350 → -850 mV). In this regard, scan rate studies for the GCE||Naf|Co(Sep)³⁺|CYP3A4|Naf biosensor was conducted in argon-degassed PBS (50 mM, pH 7.4), from which the obtained voltammetric results were fitted by linear regression analysis, of which the results are shown in **Figure 4.6**. In this regard, the current function, $I_p/v^{1/2}$ exhibited a constant value for all the scan rates within the range of 20→1500mV, essentially implying that the charge transfer at the electrode-film interface, in the absence of oxygen and substrate in the higher scan rate region (20–1500 mVs⁻¹), is diffusion-kinetic-controlled and as such, governed by semi-infinite conditions at all the scan rates employed [119, 125, 128-129]. In the context of electrochemical characteristics, generally, this behaviour suggest the possibility of kinetic effects for bulk and/or surface processes. However, according to documented literature, the unique phase segregation in the micro-domain of nafion membranes, confer electron transfer and/or charge transport in such membranes to be equivalent to a diffusion process. As such, these results does not necessarily reflect kinetic limitations, but more on the subject on the type of charge transport and electron transfer in nafion membranes is comprehensively discussed in Chapter 5A, which will give the reader a more in depth view on this subject. Nevertheless, as is common with many films showing diffusion controlled current, a region of monolayer behaviour may be exhibited at low scan rates, in which thin layer electrochemistry behaviour is mimicked and exhaustive electrolysis of the electroactive species is possible. In this regard, at low scan rates, $v < 9 \text{ mV s}^{-1}$, the surface coverage of the Co(Sep)³⁺, Γ (mol cm⁻²), was determined by measuring the Faradaic charge (Q) passed during exhaustive electrolysis of the assembly, using slow scan rate voltammetry [91, 119, 129]. This is based on the equation [92, 129-130]:

$$\Gamma = Q/nFA \quad 4-1$$

where n is the number of electrons transferred and F is Faraday's constant, A is the area of the electrode. The surface coverage was calculated to be $9.8 \times 10^{-8} \text{ mol cm}^{-2}$. On the other hand, with regard to the least squares regression results shown for the higher scan regions (**Figure 4.6 Inset**), the linear regression equations for the cathodic and anodic peaks, based on peak current versus $v^{1/2}$ plots for diffusion kinetically-controlled scan rates were determined as: $I_p = -0.1593 v^{1/2} - 0.07335$ ($r = 0.996$) and $I_p = 0.1148 v^{1/2} - 0.2027$ ($r = 0.99854$), respectively. Concomitantly, the slopes of these graphs could then be used to determine the charge transfer diffusion coefficient, D_{ct} ($\text{cm}^2 \text{ s}^{-1}$), in the films by Randle Sevcik analysis, as shown in equation:

$$I_p = (2.69 \times 10^5) v^{1/2} D_{ct} \frac{Fr}{l} \quad 4-2$$

The volume of the film ($l \times A$) was determined from the molecular volumes and amounts of Nafion and $\text{Co}(\text{Sep})^{3+}$ deposited in the film [128, 131]. The electron diffusion coefficient, D_{ct} for the electroactive film was estimated as $3.6 \times 10^{-8} \text{ cm}^2 \text{ s}^{-1}$. The D_{ct} value is subject to error of $0.5 \times 10^{-8} \text{ cm}^2 \text{ s}^{-1}$ due to the uncertainty in film thickness [130, 132].

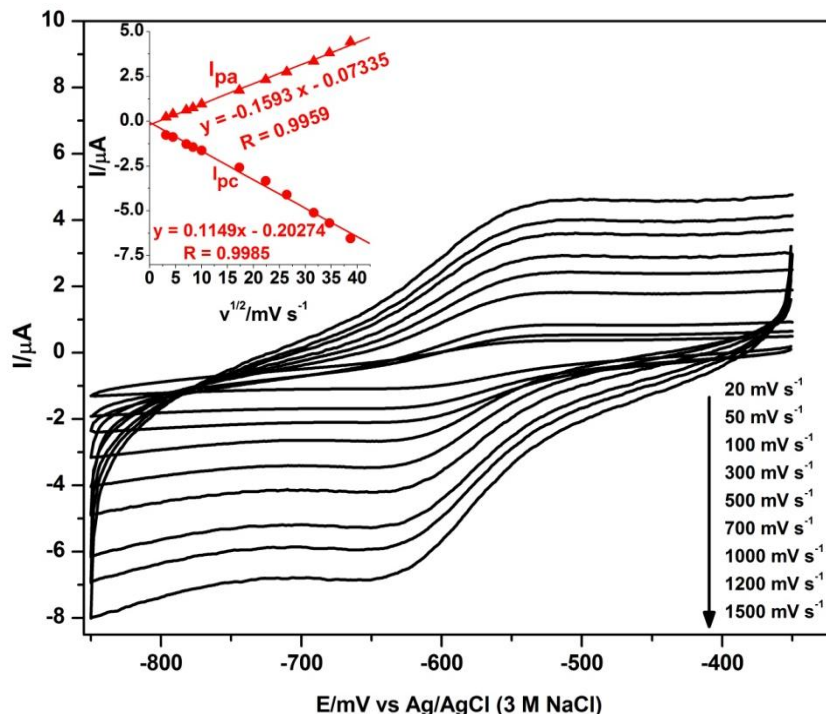


Figure 4.6 Cyclic voltammograms of Naf|CYP3A4|Co(III)Sep-Naf-film in phosphate buffer saline (pH 7.4) at scan rates 20 – 1500 mVs⁻¹. Inset: Plot of cathodic and anodic peak current vs $v^{1/2}$.

With regard to the operational stability of the film within the context of an experimental setup, when the GC|Naf|CMECo(Sep)³⁺|CYP3A4|Naf electrode (biosensor) was scanned continuously in 50mMPBL (pH 7.4), the voltammetric response decreased gradually with increasing cycles. The peak current remained approximately 90% of the initial response after 20–30 cycles. In terms of storage stability, on the other hand: Upon storage of the biosensor in buffer solution, followed by subsequent electrochemical cycling in fresh PBL, under the same experimental conditions used in the study, a gradual decline in signal, equivalent to approximately 6-10% per day could be observed. The decline is an indication of gradual leaching of the mediator species from the reagent layer, since as discussed earlier, in argon-degassed PBL, in the absence of substrate and/or oxygen, the observed electrochemistry is essentially dominated by the Co(Sep)³⁺ mediator.

4.3.3 Electrocatalytic investigations of the fabricated biosensor (GCE||naf|CMECo(Sep)³⁺|f|CYP3A4|naf)

4.3.3.1 (Electro)catalytic responses to co-substrate (oxygen) and substrate 2,4-dichlorophenol (2,4-DCP)

One of the major disadvantages of nafion is its extremely acidic nature which usually limits its usefulness as an enzyme immobilization agent. However, in

this study the pH of Nafion was adjusted to 7.4 before the incorporation of CYP3A4. The responses of the biosensor under anaerobic or aerobic conditions are shown in **Fig. 4.7** for experiments carried out at a potential scan rate of 10mVs^{-1} in PBL. The biosensor response in argon-degassed substrate-free PBL (voltammogram **(a)** of **Figure 4.7**) shows that in the absence of substrate, the observed charge transfer is by-and-large dictated by the $\text{Co}(\text{Sep})^{3+}/\text{Co}(\text{Sep})^{2+}$ electrochemistry. In the presence of $11.04\ \mu\text{M}$ 2,4-DCP in anaerobic PBS (voltammogram **(b)**), there was an increase in the cathodic peak current ($I_{p,c}$) and a small cathodic shift in reduction potential. Compared to the substrate-free CV in anaerobic PBS, the $I_{p,c}$ in the presence of the substrate (2,4-DCP) increased by $317\ \text{nA}$ ($0.317\ \mu\text{A}$) and the $E_{p,c}$ shifted cathodically by approximately $5\ \text{mV}$. The increase in $I_{p,c}$ value upon substrate binding illustrates the typical response of ferri-heme-containing enzyme biosensors, in which the reduction of the heme group ($\text{Fe}^{3+} + 1\text{e}^{-} \rightarrow \text{Fe}^{2+}$) is coupled to monooxygenation (hydroxylation) of the substrate. Oxygen binding to ferrous P-450 enzymes are known to be very rapid, even at low oxygen tension, such as found in the liver [12]. With regard to CYP3A4 in particular, according to documented findings, binding of oxygen to the reduced heme iron, Fe^{II} occurs at an estimated rate of $350 - 400\ \text{s}^{-1}$ [67]. Considering the latter and aforementioned aspects, it may be concluded that the residual oxygen contained in the injected substrate containing solution, was sufficient for the formation of the activated ferro-oxo complex, which in turn functioned in substrate metabolism. In fact, the observed $I_{p,c}$ increase in the presence of substrate under anaerobic conditions, is in agreement with previous findings involving P450_{cam} reported by Iwuoha et al.. [74]. The shift in peak potential on the other hand, may be attributed to substrate docking via weak hydrophilic interactions between distant prosthetic group amino acids, followed by binding to active site functional groups [25]. In this regard, substrate binding is accompanied by the displacement of water (originally bound to CYP3A4 as the sixth axial ligand), concomitantly resulting in the conversion of the heme to high spin, while sufficient oxygen was present for substrate hydroxylation. However, with limited residual oxygen present, only the partial displacement of water at the enzyme active site was possible, hence the small shift in

$E_{p,c}$ [25, 74, 133]. It is noteworthy though, that the absence of cathodic shift in the $E_{p,c}$ values on changing from substrate-free sensor to substrate-bound sensor under anaerobic conditions does not necessarily imply a lack of heme–substrate interaction [73, 134]. Previous studies suggested that in the absence of oxygen, the effect of substrate on the heme electronic environment may be negligible. This, however, in turn depends on the nature of the substrate [133]. The voltammetric response of the biosensor in substrate-free oxygenated PBS is shown in voltammogram (c) of **Fig. 4.7**. Oxygen is the natural co-substrate of CYP3A4 and binds to the ferrous iron (Fe^{2+}) at a very fast rate, usually more rapid than substrate binding ($> 10^6 \text{ M}^{-1}\text{s}^{-1}$) [74, 77, 135]. Therefore, voltammogram (c) is essentially the electrocatalytic response of the enzyme heme redox centre to dioxygen. In this regard, the most likely equation which can adequately describe the aforementioned oxygen interaction is as follows:



Figure 4.7 CV (d) on the other hand, shows the biosensor response to $11.04 \mu\text{M}$ 2,4-DCP in oxygenated PBL. The presence of substrate, in this case 2,4-DCP, increases the rate of dioxygen binding to the heme, which is exemplified by the increase in the electro-reduction current ($I_{p,c}$) shown in the cyclic voltammogram. Moreover, the flCYP3A4-oxygen and/or flCYP3A4-oxygen/substrate interaction is essentially a chemical reaction and as such, irreversible. In terms of an electrochemical perspective this means that the heme- Fe^{II} of the flCYP3A4 produced during the cathodic scan, was consumed in the fast follow-up chemical reaction, thus making it unavailable for re-oxidation during the anodic scan. In this regard, the background capacitive-current subtracted CVs specifically showing the electrocatalytic response of the enzyme based biosensor to substrate and/or oxygen exhibited in **Figure 4.8**, essentially shows that this was accompanied by a complete attenuation of the anodic peak current ($I_{p,a}$).

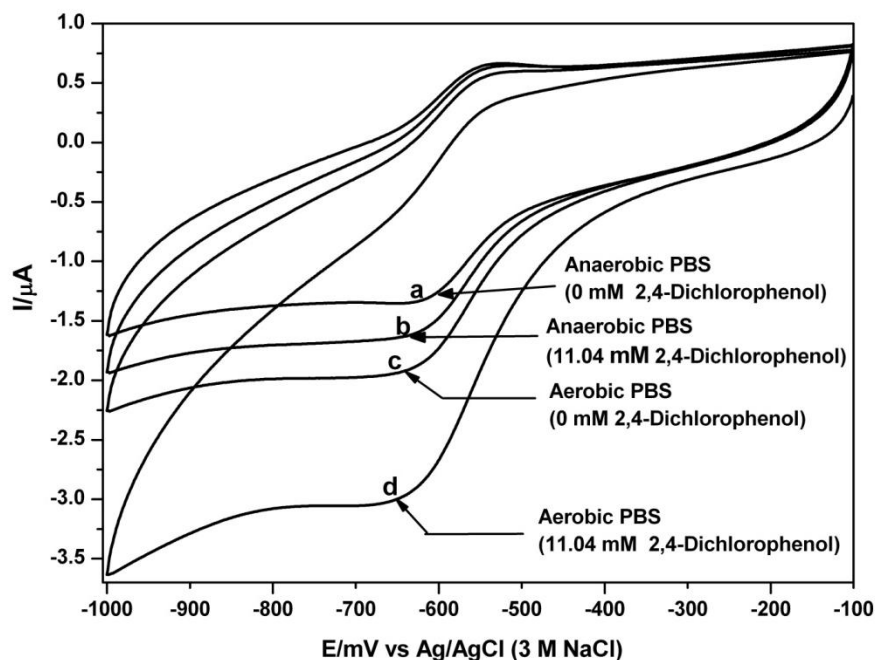


Figure 4.7: Cyclic voltammograms of GCE||naf|CMECo(Sep)³⁺|naf (biosensor) in 50 mM PBS at 10 mV s⁻¹, showing: (a) biosensor in anaerobic PBS with 0 μM 2,4-DCP; (b) anaerobic PBL with 11.04 μM 2,4-DCP; (c) air-saturated PBS containing 0 μM 2,4-DCP; (d) air-saturated PBL containing 11.04 μM 2,4-DCP

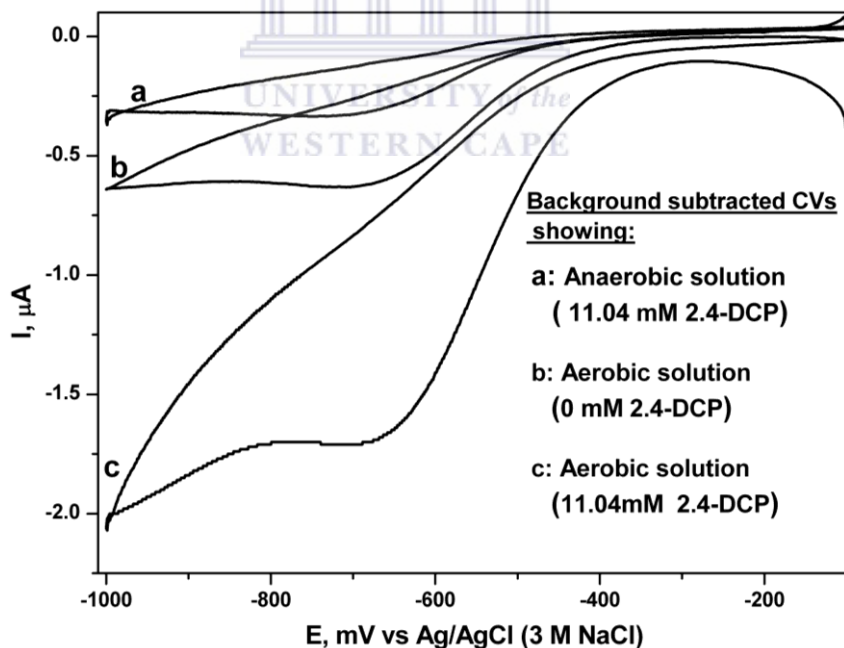


Figure 4.8 Voltammetric response of the GCE||naf|CMECo(Sep)³⁺|naf biosensor, showing background capacitive current-subtracted CVs in: (a) the presence of 11.04

μM 2,4-DCP in argon-degassed PBS; (b) substrate-free un-degassed PBL; (c) in un-degassed PBL in the presence of $11.04 \mu\text{M}$ 2,4-DCP.

On a final note, with regard to the catalytic response profile of the biosensor exhibited in **Figure 4.7 CV(d) and Figure 4.8** – this is typical of cytochrome P450 enzymes in particular, and heme enzymes in general, thereby suggesting the metabolism of 2,4-DCP by CYP3A4 [74, 135]. It is noteworthy though to also add that, as discussed in **Chapter 2, Section 2.2.3**, the catalytic cycle of P450 enzymes are frequently complicated by uncoupling reactions, such as the formation of superoxide and concomitantly produced peroxide, which of course can complicate the interpretation of exhibited results. However, based on documented literature, it has been shown that the substrate has a stabilizing effect on the oxygenated P450 enzyme, which in turn could minimize side reactions that could generate superoxide and peroxide [67]. Having said that, however, this does not preclude the possible contribution of peroxide to the observed electrocatalytic response, especially considering the large difference between the catalytic oxygen reduction current in the absence and in the presence of 2,4-DCP, of which such a phenomenon has been thought to indicate the possibility of the contribution of what is known as the peroxide shunt pathway [77, 136]. On this note, **Section 4.3.2.5**, gives more insight into the enzyme-substrate interaction, with inclusion of some perspective of reactive oxygen species. On the other hand, it is also noteworthy to bring to the reader's attention that **Section 5B.3.3.1.1**, in **Chapter 5B** gives an even more comprehensive overview all of the possible envisaged reaction pathways in relation to electrocatalytic investigations with this category of enzyme, including the effects of reactive oxygen species, both with specific reference to the enzyme, as well as in consideration of the mediating species. In this regard, detailed equations are also provided.

The response of the $\text{GCE}|\text{naf}|\text{CMECo}(\text{Sep})^{3+}|\text{naf}$ biosensor in the presence of increasing concentrations of 2,4-DCP was subsequently investigated and the

results recorded with square wave voltammetry. In the presence of increasing 2,4-DCP concentrations, an eminent increase in peak catalytic current, in a linear fashion, with each consecutive addition, up to a final concentration of 1600 μM was observed. These results are shown in **Figure 4.9**. In addition to this, the calibration curve for 2,4-DCP was also constructed, by the plot of I_p of 2,4-DCP versus their concentrations, of which the results are shown in **Figure 4.10**. Also shown in the inset of **Figure 4.10**, is the linear range of the biosensor. In this regard, the dynamic linear range for 2,4-DCP had an upper limit of 45 μA and a sensitivity of 0.038 $\mu\text{A } \mu\text{M}^{-1}$. Moreover, the corresponding detection limit, calculated as the concentration giving a signal equal to three times the standard deviation of the blank signal divided by the sensitivity [$3(S/N) = 3\sigma$], was determined as 0.043 $\mu\text{g L}^{-1}$.

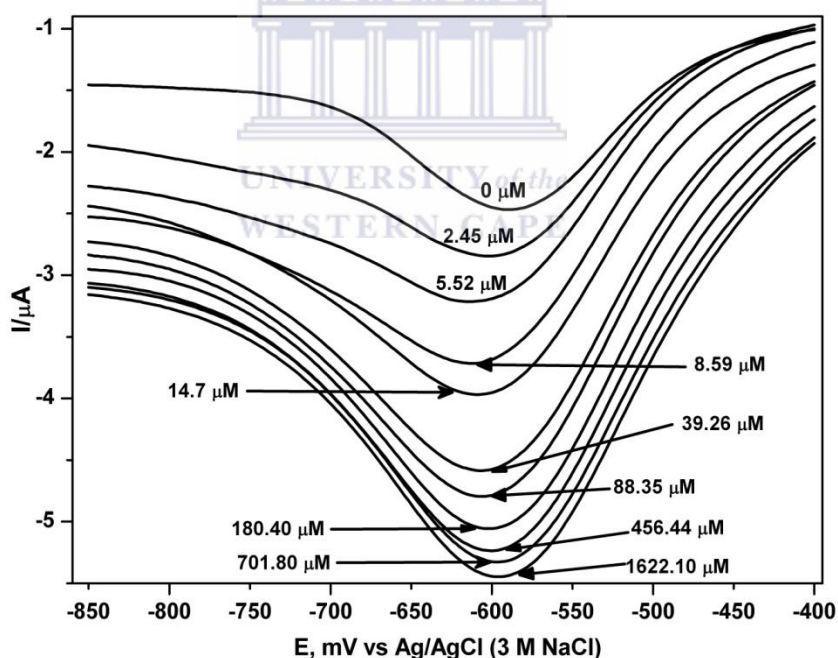


Figure 4.9 Square wave voltammetric response of GCE||naf|CMECo(Sep)³⁺|CYP3A4|naf biosensor in 50 mM un-degassed PBL containing 0 → 264 μM 2,4-DCP

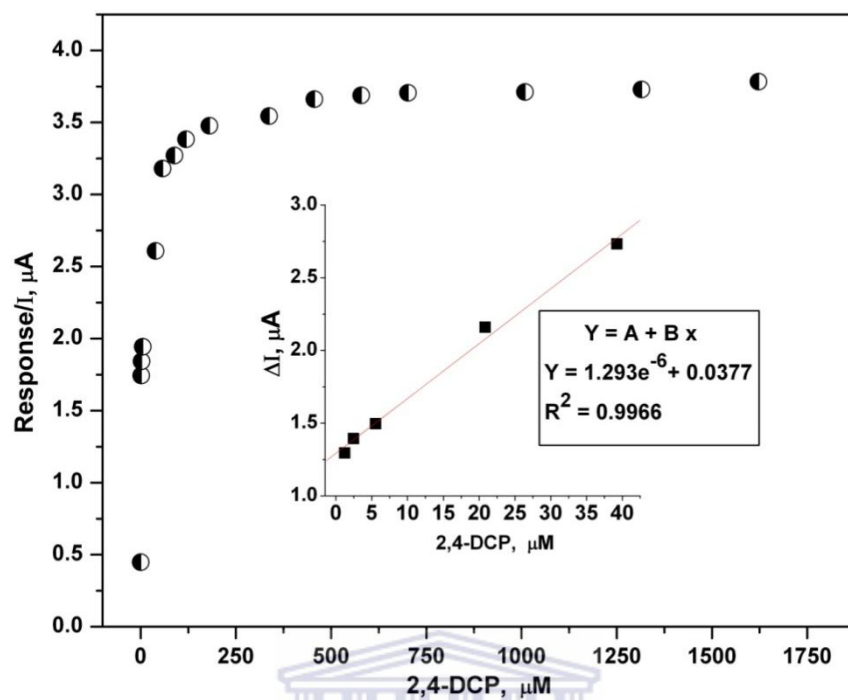


Figure 4.10 (b) Dependence of catalytic peak current GCE||naf|CMECo(Sep)³⁺|flCYP3A4|naf biosensor for 2,4-DCP for experiment performed in un-degassed 50 mM PBL.

UNIVERSITY of the
WESTERN CAPE

4.3.3.2 (Electro)catalytic response to native marker CYP450 3A4 substrate: Erythromycin

In order to re-affirm and corroborate that the response of GCE||naf|CMECo(Sep)³⁺|flCYP3A4|naf biosensor is due to flCYP3A4 enzyme, experiments were carried out with erythromycin, which is a macrolide antibiotic that is frequently used in in-vitro studies as standard substrate for testing and confirming CYP3A4 activity [12]. The responses of the biosensor under anaerobic and aerobic conditions, in the presence and absence of erythromycin (ERM) are shown in voltammograms (a)–(d) of **Fig. 4.11**, for experiments carried out at a potential scan rate of 10 mVs⁻¹ in 50mM PBL, pH 7.4. The cyclic voltammetric responses in the

absence and presence of 2.18 mM ERM under anaerobic conditions are shown in CVs (a) and (b) of **Fig. 4.11**, respectively. CVs (c) and (d) on the other hand, shows the cyclic voltammetric responses of biosensor in the absence or presence of 2.18 mM ERM, in the presence of dissolved oxygen. The sensing of ERM in anaerobic PBS caused an increase in $I_{p,c}$ value (by 0.1462 μA) and an anodic shift (by 14mV) $E_{p,c}$ value. The voltammetric response of the biosensor in substrate-free oxygenated PBS is shown in **Fig. 4.11 CV (c)**. The CV portraying the biosensor response in oxygenated PBL (**Fig. 4.11 c**) displays a distinct increase in $I_{p,c}$ value due to the coupling of the ferri-/ferro-heme reaction to the binding of dioxygen to the reduced heme (Fe^{II}) [74, 135]. Biosensor response to 2.18 mM ERM in oxygenated PBL is shown in **Fig. 4.11 CV (d)**. The $I_{p,c}$ value increased by 0.64 μA over the response of erythromycin-free oxygenated solution. The results for the voltammetric studies with ERM exemplify a response profile which is in complete agreement with those obtained for 2,4-DCP, thus corroborating and confirming the latter as a substrate of fICYP3A4.

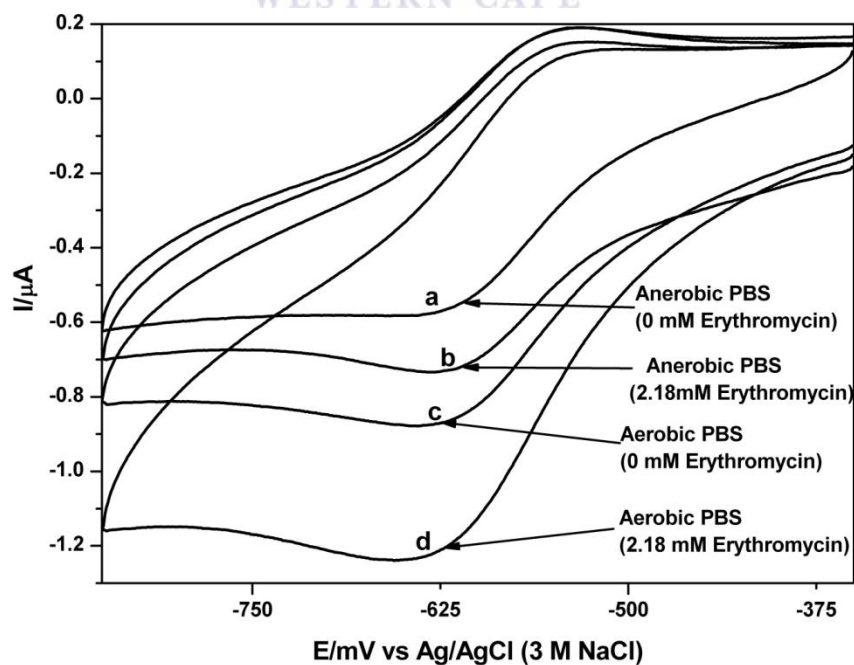


Figure 4.11 Cyclic voltammograms of GCE||naf|CMECo(Sep)³⁺|f|CYP3A4|naf biosensor in 50 mM PBS at 10 mV s⁻¹, showing: (a) biosensor in anaerobic PBS with 0 mM erythromycin (ERM); (b) anaerobic PBS with 2.18 mM ERM; (c) air-saturated PBS containing 0 mM ERM; (d) air-saturated PBS containing 2.18 mM ERM

As in the case of 2,4-DCP, response of the GCE||naf|CMECo(Sep)³⁺|f|CYP3A4|naf biosensor to increasing ERM concentrations was also investigated. This was done by successively adding ERM in conjunction with intermittent stirring of the solution in un-degassed PBL under optimized conditions followed by subsequent voltammetric recording of the response. The results showing the SW voltammetric response of the biosensor to ERM up to 164.0 μM is shown in **Figure 4.12**. The voltammograms shown represent the difference SWVs, for scans done cathodically. Overall, a periodic increase in peak current in conjunction with each consecutive addition of ERM up to a final concentration of 164 μM can be observed. A full calibration curve was then subsequently constructed. In this regard, **Figure, 4.13** exhibits the dependence of catalytic peak current on ERM concentration (0 → 292 μM), showing an upper limit for the dynamic linear range of 53.7 μA. A linear plot was obtained for ERM over the 4.63 → 26.4 μM concentration range, ($R^2 = 0.9987$, slope = 0.0323 μA μM; intercept = 1.9212 μA. The limit of detection for ERM, was determined as 1.271×10^{-5} M.

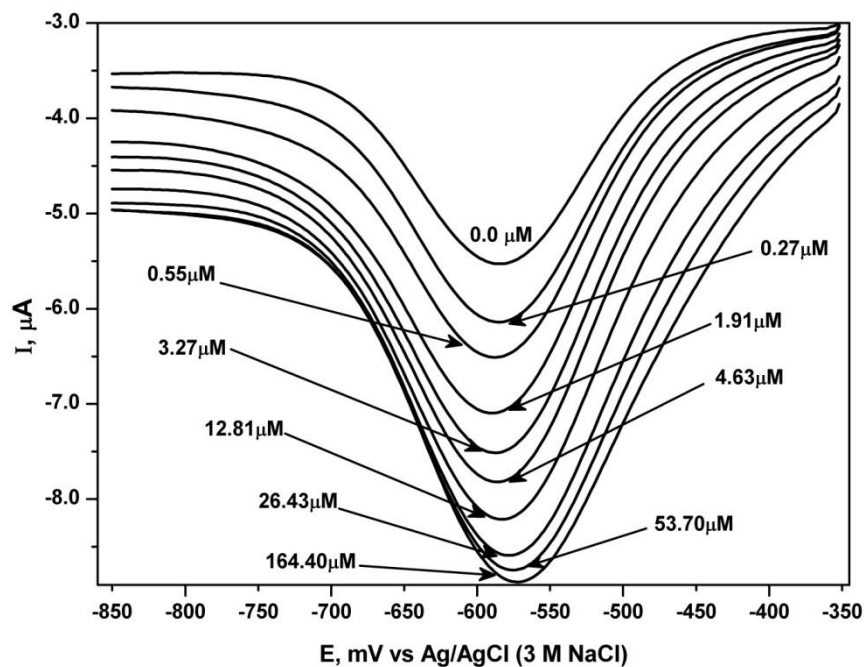


Figure 4.12 Square wave voltammetric response of GCE||naf|CMECo(Sep)³⁺|ficYP3A4|naf biosensor in 50 mM un-degassed PBS containing 0 → 164.4 μM erythromycin.

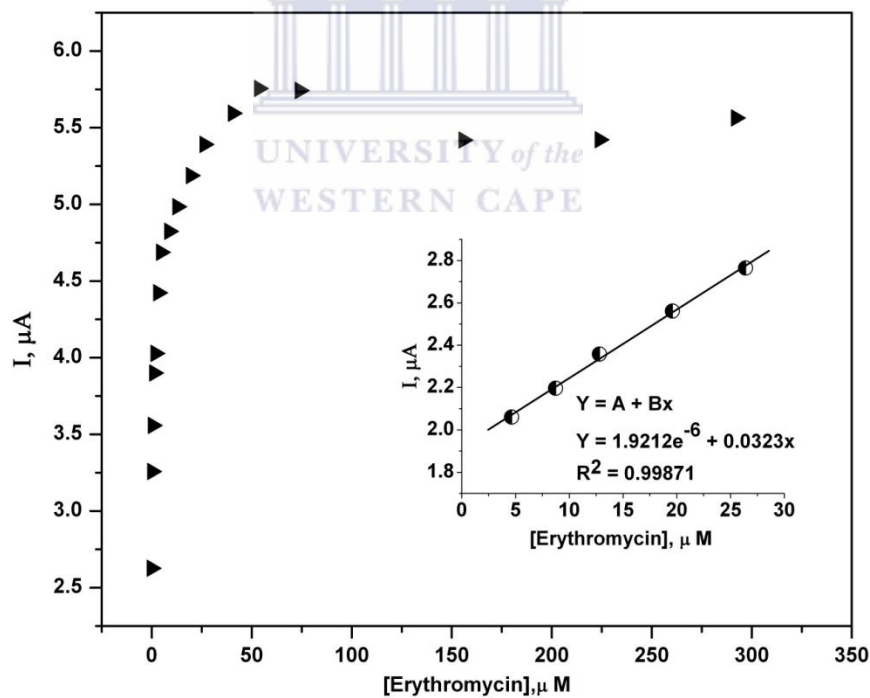


Figure 4.13 Full calibration plot for response of GCE||naf|CMECo(Sep)³⁺|naf biosensor to ERM for experiment performed in un-degassed 50 mM PBS. Inset: Linear curve for 2,4-DCP.

4.3.2.3 Electrocatalytic behaviour in the presence of inhibitor: ketoconazole

Voltammetric experiments were conducted to ascertain the effect of heme-inhibitor interactions on the electro-catalytic metabolism of 2,4-DCP. In this regard, the effect of ketoconazole, a known CYP3A4 inhibitor, on the response of the CYP3A4 biosensor to 2,4-DCP was studied by square-wave voltammetry. Voltammogram (a) of **Fig. 4.14** depicts the SWV of the fCYP3A4 biosensor in PBL containing 245 μM DCP, with no ketoconazole present. The peak cathodic current for this SWV was determined as 11.8 μA . After 15 min incubation with 94 μM ketoconazole, the square wave voltammetric signal was reduced by 12% (voltammogram (b)). 188 μM ketoconazole decreased the response by 27% (voltammogram (c)) and 36% for 15 and 30 min incubation periods, respectively. These results agree with the finding of Joseph et al. [135] for which 500 μM ketoconazole induced an 80% decrease in CYP3A4 activity.

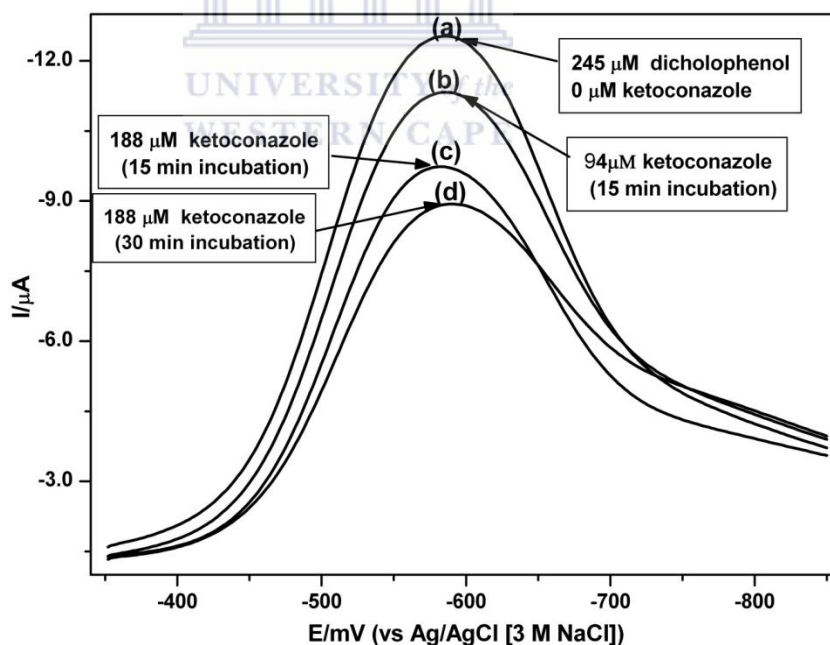


Figure 4.14 Square wave voltammograms of GCE||naf|CMECo(Sep)³⁺|fCYP3A4|naf biosensor in 50 mM air-saturated PBS: showing biosensor response to 2,4-DCP before (a) and after incubations with enzyme inhibitor, ketoconazole (b – d) .

4.3.2.5 Critical assessment and additional observations of electrocatalytic behaviour of biosensor: A closer look at the bio-electrocatalytic response

The results obtained for the electrocatalytic response of the GCE||naf|CMECo(Sep)³⁺|flCYP3A4|naf biosensor with respect to oxygen, as well as the investigated substrates, i.e., 2,4-DCP and ERM were comprehensively compared and assessed, to reveal additional findings which may contribute to the overall understanding of the dynamic mechanism of the enzyme-based detection process. In this regard, the following findings were made: Firstly, with respect to the cyclic voltammetric studies exhibiting the biosensor response in the absence and presence of 2,4-DCP or ERM, as shown in **Figure 4.7** and **4.11**, respectively, a peculiar phenomenon presents itself: The augmentation of the $I_{p,c}$ by the additional catalytic response to ERM was accompanied by a marked anodic (positive) shift in $E_{p,c}$, corresponding to a magnitude of 17 mV, whereas the in the case of 2,4-DCP a small cathodic $E_{p,c}$ shift was found. These results, seemingly contradictory can actually be moderately well explained by understanding particular aspects of the unique nature of the structure and substrate interaction aspects of CYP3A4 active site. Firstly, from a general perspective, the metabolism of CYP3A4 and/or P450 isoenzymes is governed by three generic rules [25]:

- The topography of the active site.
- The measure of steric hindrance of the access of the iron-oxygen complex to the possible sites for metabolism on the substrate.
- The possible ease of hydrogen or electron abstraction from the various carbons or heteroatoms of the substrate.

In view of the aforementioned aspects, with regard to the more specific characteristics and specifications of CYP3A4 in particular, firstly the initial motion of substrates to within the vicinity of the enzyme's active site is enabled by weak hydrophilic interactions. However, actual substrate binding to the enzyme's active site, which consist mainly of hydrophobic residues is by-and-large governed by highly lipophilic

forces, and as such, also requires the removal/stripping of any water molecules associated with any of the functional groups on the substrate molecule, a process which requires a considerable amount of energy. Moreover, favourable substrate binding governed by lipophilic forces results in the preferential expulsion of water from the active site, which in turn provides the driving force for the enzyme spin state change and hence the formation of the catalytic oxy-complex, $[(\text{FeO})^{3+}]$, unit. Also noteworthy is the fact that the substrate can adopt more than one orientation in the active site, of which, the eventual product is governed by the interaction between one of these orientations and the enzyme catalytic $(\text{FeO})^{3+}$ unit. In addition to the above aspects, with specific reference to substrate-turnover and the formation of the catalytically-active oxy-complex of the enzyme, important documented findings have been made [67]: From a general perspective, in bacterial P450 counterparts, such as P450cam, substrate turn-over rates are typically much faster than the autoxidation of the catalytic oxy-complex, $[(\text{FeO})^{3+}]$ in substrate-free oxygenated solution. Conversely, in human CYP450s, the catalytically active oxy-complex is highly unstable and, once formed can decompose at a rapid rate. In fact, product formation, particularly in the case of CYP3A4, is much more slower and significantly lower than the rates for spontaneous decomposition of the $(\text{FeO})^{3+}$, which decomposes at a rate of 2-3 orders of magnitude faster than in other CYP450s. This poses the potential threat of rapid uncoupling reactions during catalytic studies with this enzyme. On the other hand, saturation of CYP3A4 with substrate, confer a marked stabilization of the catalytically active oxy-ferrous intermediate of the enzyme. This unique stabilization ability of CYP3A4 substrates presumably occurs through modulating the escape of superoxide or hydroperoxyl radical from the distal binding pocket of the enzyme. Cumulatively, the unique stabilization ability of substrates can result in the acceleration of the reduction rate, concomitantly attributing to a positive shift of the redox potential in response to substrate binding to the enzyme. On this note, it must also be remembered though, that the percent contribution of stabilization and/or increased reduction, is highly dependent on the type of substrate.

Keeping in mind all of the aforementioned aspects, both these compounds are essentially hydrophobic in nature, however ERM holds the additional advantage of being a significantly large molecule, thus avoiding the possible occurrence of randomly unfavourable oriented conformations within the enzyme active site, while being large enough to possibly effectively confer the expulsion of the sixth water ligand from the active site, thus effectively driving the required spin state change of the enzyme to rapidly drive the formation of the catalytic $(\text{FeO})^{3+}$ unit. Moreover, during phase I reaction with CYP3A4, this compound is known to undergo N-dealkylation. This requires the abstraction of an electron from the ERM molecule, a phenomenon which could have a synergistic effect on the transfer of the second electron required in the catalytic cycle of the enzyme. In addition to this, the fact that this particular electrocatalytic interaction of substrate addition was investigated in argon degassed- PBL, coupled with the fairly high injected concentration of ERM, held an advantage: In this regard, binding of the substrate probably occurred at a fast rate, thus essentially stabilizing the enzyme, while the undegassed substrate solution provided sufficient residual oxygen to effectively drive the required oxygen activation and subsequent substrate turnover. Moreover, ERM being the larger substrate probably enabled a ERM-CYP3A4 complex that minimized available active site volume to any uncoupling intermediates. The cumulative effects of these attributes would of course favourably affect the metabolism of ERM, which, from an electrochemical point of view, can greatly contribute to the observed positive potential shift in association with the electrochemically-based substrate interaction. The small nature of the 2,4-DCP molecule on the other hand, could induce random orientations of the substrate in the enzyme active site, which, in turn, could confer an initial unfavourable orientation, thus slightly impeding interaction with the catalytic $(\text{FeO})^{3+}$ unit, while also resulting in partial expulsion of water from the active site.

4.3.4 Performance aspects: reproducibility and stability

Some selected aspects regarding the repeatability and stability of the GCE||naf|CMECo(Sep)³⁺|f|CYP3A4|naf biosensor with respect to 2,4-DCP was considered. Firstly, the repeatability of the measurements of the biosensor-based electrocatalytic response was evaluated by measuring the response of freshly prepared biosensor to 24 μM 2,4-DCP within the first six hours of preparation, consecutively, at ± 1 hr time intervals, with intermittent rinsing and storing of the biosensor at 4 °C after each measurement. In this regard, **Figure 4.15**, exhibits the obtained current responses for the biosensor for five consecutive measurements taken within the first five hours. Assessment of the results reveals that a fairly consistent response was obtained, declining very gradually, by a magnitude of approximately 5% with each measurement, up to the fourth measurement, after which a much more eminent decline, corresponding to a magnitude of about 44% was observed. Overall, in its completeness, the evaluation of the repeatability of measurements exhibited a relative standard deviation (R.S.D) value of 5.5%, indicating good repeatability. In another evaluation, the biosensor's storage lifetime (storage stability) was investigated, by monitoring its response to 2,4-DCP at pre-determined time-intervals. In this regard cyclic and square wave voltammograms were recorded using the same biosensor after storing in PBS at 4 °C for 0h, 12h, 24h, 2 days, 4 days and 1 week. The peak current decreased with increase in storage time; however, the biosensor still retained 65% of its initial response after 1 week of storage. A R.D.S. value of 5.2% for $n = 3$ was obtained for the 1 week stability study (where n is the number of biosensors tested).

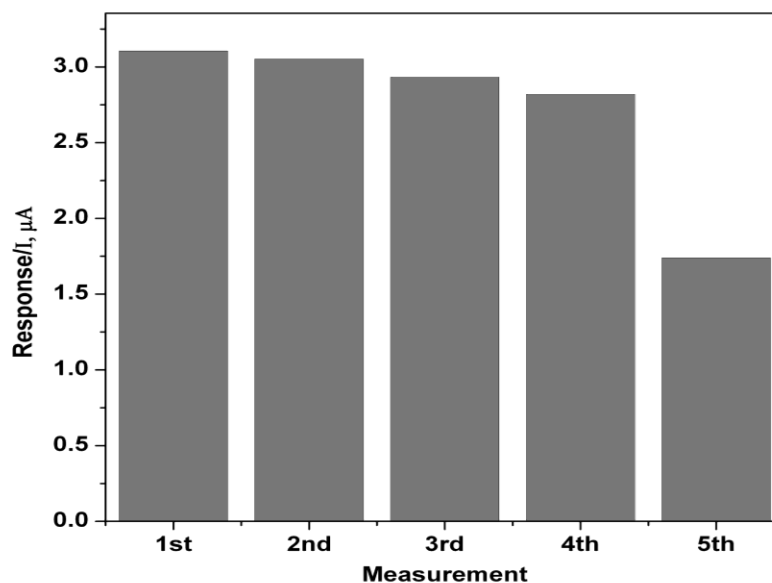
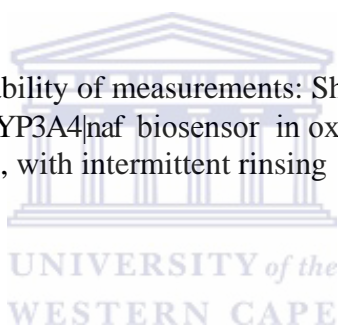


Figure 4.15 Repeatability of measurements: Showing response of GCE||naf|CMCo(Sep)³⁺|f|CYP3A4|naf biosensor in oxygenated PBS to 24 μM for five consecutive measurements, with intermittent rinsing



4.4 Conclusions

Nafion-entrapped cobalt (III) sepulchrate provided stable matrix for the immobilized CYP3A4. The film permitted fast reversible electrochemistry of Co(Sep)³⁺ which was coupled to the reduction of ferri-heme to ferro-heme and the resultant monooxygenation reaction steps responsible for the amperometric detection and quantification of 2,4-DCP. The proposed reaction scheme is shown in **Fig. 4.16**. The sensor exhibits high sensitivity and a detection limit for 2,4-dichlorophenol far below the EU requirement for pesticides in ground water. The sensitivity, detection limit, as well as the wide dynamic linear range associated with this sensor system makes it very promising for environmental monitoring. With an upper linear range

value of 45mM the biosensor may, in future be used to determine and thereby control the amount of 2,4-DCP in industrial effluents from pesticide plants where the concentration of the compound is expected to be high. Since exposure to 2,4-DCP contamination can only occur through drinking water it is important to compare our results with the USA Environmental Protection Agency's (EPA) drinking water equivalent level (DWEL) [44,45]. The DWEL value is the daily intake that will not cause any deleterious effect to a 70- kg adult exposed over a lifetime period and drinking 2 L of water per day, which for 2,4-DCP is $2 \mu\text{g L}^{-1}$. The detection limit calculated for the GC/Naf-Co(Sep)³⁺/CYP3A4/Naf biosensor system reported in this study is $0.043 \mu\text{g L}^{-1}$. This demonstrates the potential of the sensor as an easy to use device for possible regular testing of drinking water since it can detect concentrations of 2,4-DCP well below the DWEL value.



4.5 Experimental protocols

4.5.1 Reagents and Materials

Wild type genetically engineered cytochrome P450-3A4 (CYP3A4), purified from a full length human CYP3A4 cDNA clone and over expressed in *Escherichia coli* cells [137], consisting of only the terminal oxidase (heme domain) and surrounding protein, was purchased from Merck South Africa. Upon receipt, the original enzyme stock, supplied as a 38 μM suspension, was immediately aliquoted into 5 μL portions, each of which was always stored at $-70\text{ }^\circ\text{C}$ until used. Nafion (5% (w/v) alcoholic solution), cobalt(III)sephalchrate trichloride $\{\text{Co}(\text{Sep})^{3+}\}$ and 3-[(3-chloramidopropyl)dimethylammonio]-1-propanesulphonate (CHAPS) were the products of Sigma–Aldrich. Di-potassium hydrogen phosphate (K_2HPO_4), potassium dihydrogen phosphate (KH_2PO_4) monohydrate salts, and KCl were purchased from Sigma and used to prepare phosphate buffer saline (PBS) (50mM, pH 7.4, 100mMKCl) used as supporting electrolyte. All solutions were prepared with water obtained from a Millipore Milli-Q purification system.

4.5.2 Preparation of biosensor for voltammetric analysis

4.5.2.1 Pre-treatment of working electrode

The conditioning and pre-treatment of the WE were done exactly as outlined in the general experimental Chapter, i.e. Chapter 3B, **Section 3B2.2**.

4.5.2.2 Preparation of GCE||naf|CMECo(Sep)³⁺|f|CYP3A4|naf biosensor

Nafion stock solution was diluted to 1% (w/v) and the pH adjusted with PBS, yielding a 1% solution (pH 7.4) or solution **A**. This was followed by the preparation of a 1-mM solution of Co(Sep)³⁺ in PBS, yielding solution **B**. 5 μ L of the 38 μ M CYP3A4 enzyme stock suspension was solubilised in CDPS followed by the addition of 100mM PBS to give solution **C** containing 3.8 μ M monomeric CYP3A4 enzyme and 0.8mM CDPS. The following coating procedure yielded the best electrochemical reversibility for the Co³⁺/Co²⁺ process: 4 μ L of solution **A** was drop-coated onto the clean GCE and dried for 10 min under a gentle flow of argon, in order to evaporate the excess ethanol. Care was taken to avoid the complete drying out of the Nafion layer. Then 4 μ L of solution **B** was drop-coated onto the Nafion-modified GCE and allowed to stand for 20 min under argon, during which time Co(Sep)³⁺ diffused into the Nafion layer to form Nafion-entrapped cobalt(III)sepulchrate-modified GCE (GC/Naf-Co(Sep)³⁺). The next step involved the drop-coating of 5 μ L of solution **C** onto the Nafion-entrapped Co(Sep)³⁺ layer, and argon-dried for 20 min. Finally, approximately 2 μ L of solution **A** was drop-coated onto the enzyme-modified GCE, to keep the enzyme film stable, whilst protecting the enzyme from biofouling. The resultant enzyme-modified electrode is denoted as GCE||naf|CMECo(Sep)³⁺|f|CYP3A4|naf.

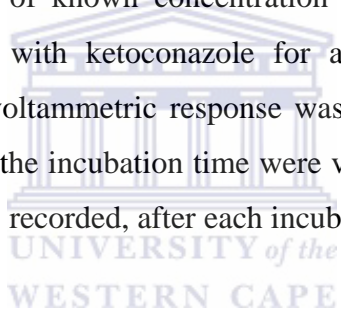
4.5.3 Biosensor response experiments

Biosensor responses to 2,4-DCP (analyte of interest), ketoconazole (a CYP3A4 inhibitor) and erythromycin, ERM (a native CYP3A4 substrate) were studied by cyclic and square wave voltammetry in the presence and absence of the substances. All the electrochemical measurements with the biosensor were carried out at 25 °C in either degassed or un-degassed 50mM potassium phosphate buffer solution pH 7.4, 100mM KCl. Anaerobic condition was ensured by passing argon gas through the

electrolyte for at least 15min before measurements and maintaining an argon atmosphere atop the solution throughout the duration of the particular experiment. Cyclic voltammetry (CV) and Osteryoung-type square-wave voltammetry (SWV) were run in the presence and absence of oxygen and/or substrate to probe the enzyme–oxygen–substrate interaction.

4.5.3.1 Inhibition Experiments with Ketoconazole

The inhibitory experiments were performed with 250 μM 2,4-DCP. In the method, 250 μM 2,4-DCP was added to the PBS, under aerobic conditions and the voltammetric response of the CYP3A4 biosensor was recorded. This was then followed by the addition of known concentration of ketoconazole. The CYP3A4 biosensor was incubated with ketoconazole for a specific time, under constant stirring, after which the voltammetric response was again taken. The ketoconazole concentrations, as well as the incubation time were varied and the cyclic and square-wave voltammetric signals recorded, after each incubation session.



CHAPTER 5

RESULTS AND DISCUSSION: Biosensor Platform 2



Chapter prelude

In the context of the dissertation as a whole, the current chapter serves as an improved version of the biosensor platform presented and discussed in Chapter 4, in which the platform was up-scaled and customized for the current purpose. Particular attention was focussed on a more sophisticated and reproducible method of preparation of the carrier matrix, while simultaneously pre-concentrating a larger percentile of the mediating species deep within the microstructure of the nafion film, thus attenuating potential pre-mature and/or long term leaching of the small mediating species from the reagent layer. The other important focus points were lowering of the operating potential, as well as down-scaling on financial burden of expensive commercially sourced biosensor components, such as nafion and biological recognition component. In terms of layout, this chapter consists of two parts: In the first part, Chapter 5A, the results for the synthesis and characterization of the base-composite film (carrier matrix for enzyme-derivatised platform) are presented and discussed. In the second part, Chapter 5B, the results for the preparation, optimisation, electrochemical and catalytic performance of the enzyme-derivatised biosensor platform is presented and discussed. From a panoramic perspective, overall, platform improvement was done with a multifaceted approach: Firstly, 34.8 μg was casted in the current platform, instead of 34 μg , as used in the platform presented in Chapter 4. Moreover, dried nafion film formation was done under vacuum conditions, rather than under argon-flow as used in Chapter 4. In addition to this, the $\text{Co}(\text{Sep})^{3+}$ mediator was not immobilized through manual casting technique, but rather, was incorporated within the base-nafion film through electrochemical deposition method. Secondly, the enzyme used for this particular biosensor platform, is the heme-domain of the N-terminally modified, human recombinant microsomal CYP3A4 isoenzyme (nCYP3A4), expressed as a catalytically-active His-tagged enzyme construct, prepared in-house, by the investigator, through genetic engineering; unlike the full-length hydrophobically-based, commercially attained counter-part used in Chapter 4. In the third aspect, unlike the biosensor used in Chapter 4, where an additional nafion-layer was used as outer membrane, in this particular biosensor, a hydrogel-film based on a biocompatible hydrogel-type composite membrane was used as outer layer. Lastly, the analyte detected in this study is a pharmaceutical drug, extensively used as part of the HAART treatment regime.

CHAPTER 5A

Assembly and characterization of composite film consisting of nafion and electrochemically deposited cobalt(III) sepulchrate [El-Co(sep)³⁺]

Abstract

In the current chapter, the incorporation of electrochemically active transition metal complex, cobalt (III)sepulchrate (Co(Sep)³⁺) into preformed ionomer nafion polymer film, prepared on a glassy carbon electrode surface is presented and discussed. Based on the hydrophobic nature of the sepulchrate ligand and nafion's exceptional affinity for hydrophobic compounds, pre-concentration of Co(Sep)³⁺ was easily achieved through potentiostatic electrodeposition method, by applying a constant potential of 450 mV for 1200 seconds (20 min) in aqueous solution, with cobalt (III) sepulchrate trichloride (1,3,6,8,10,13,16,19-octaazabicyclo[6.6.6]eicosaine cobalt trichloride) as starting material. In this regard, the nafion base-film, of thickness 3.1 μm , provided an efficient matrix for the incorporation of Co(Sep)³⁺ and a stable functional electroactive composite (Naf|El-Co(Sep)³⁺) film was prepared, for which the surface concentration (Γ) of the Co(Sep)³⁺ was determined as $1.537 \times 10^{-5} \text{ mol cm}^{-2}$. Thus, the Co(Sep)³⁺ species was preferentially incorporated into the ionic cluster microdomain of the polymer, and the formed Naf|El-Co(Sep)³⁺ film exhibited, diffusion controlled electrochemistry with a formal potential (E°) of -615 mV. Moreover, electrochemical behaviour exhibited by the electroactive film was in line with the unique inherent charge transfer characteristics of nafion, while the obtained charge transfer coefficient determined as $2.63 \times 10^{-7} \text{ cm}^2 \text{ s}^{-1}$. In addition to this, the composite film was highly stable.

5A.1 Introduction

Although polymers, particularly of the ion exchange type, are popular choices for fabrication of composite electroactive platforms for electrocatalytic studies and/or creation of carrier matrices for mediated biosensor construction, a major limitation is their short lifetime caused by low ionic mobility in the polymer film and/or easy loss of electroactive species from the inner phase of the membrane [117-118]. Attempts have been made to fix such problems through covalent attachment of selective ligands to polymers, however, these techniques require the addition of plastizers which tend to leach and thus leads to demise of the formed films. On the contrary, the non-electroactive, ion-containing polymer, nafion, have the ability to circumvent such problems, based on its very unique characteristics, which includes phase segregation, with phases consisting of components which are highly hydrophilic in nature; containing no water leachable components; having an inherent ability for charge-exclusion and being chemically inert; and also having unparalleled affinity for cation species, particularly of hydrophobic nature, as well as unique cation pre-concentration features. In this context, the unique features of nafion is combined with novel electrocatalytic technique, to afford an electroactive coating that is highly chemically stable, and preoperatively easily reproducible, while also subsequently serving as effective carrier matrix for the coupling of the prepared enzyme to the electrode in the creation of biosensor platform 2.

As for the overall aim of the current investigation, the emphasis was on the creation of a stable $\text{Co}(\text{Sep})^{3+}$ -modified, electroactive nafion membrane which, as mentioned in the prelude to Chapter 5 A and B, would subsequently serve as carrier matrix for fabrication of an enzyme-based biosensor. On the other hand, notwithstanding the fact that the composite film is based on the same starting components as in Chapter 4, a major focus point of the current study was the improvement of the matrix, particularly in terms of repeatability, structural morphology and ease of preparation.

This required a multifaceted approach and in this regard – firstly, 0.045 mg cm^{-2} nafion was used as the base layer, as opposed to the 0.35 mg cm^{-2} used in the platform prepared in Chapter 4. This was done in an overall quest to provide better coverage on the underlying GCE. Secondly, a more evenly dispersed nafion layer was formed by using a specialized short-structured micro-tip for casting, while drying of the nafion film was not done under argon flow, but rather under a tightly fitted cover which provided a vacuum effect. Lastly, and perhaps more importantly, as already elaborated, a potentiostatic technique was used for $\text{Co}(\text{Sep})^{3+}$ incorporation, rather than the manual casting/mixing method used in the previous chapter. In addition to voltammetric characterization, the assembly of the prepared matrix was characterized with selected ex-situ methods, of which the results are subsequently shown and comprehensively discussed.



5A.2 Assembly: Electrochemical characterisation of the $\text{GCE}|\text{Naf}|\text{El-Co}(\text{Sep})^{3+}$

As explained in the outline of the experimental protocols described in **Section 5A.5**, the cobalt(III) sepulchrate was deposited on a pre-formed nafion matrix on a glassy carbon working electrode. The step-wise modification of the GCE was monitored with voltammetry and in this regard, the findings are appropriately exhibited and discussed. In this context, an important noteworthy aspect to emphasize is that all cyclic voltammetric results are obtained from scans taken after repeated cycling when a steady state response was attained. Moreover, all reported values, for determined parameters, such as formal potential (E°), are reported as mean \pm standard deviation for 3-4 experiments. In addition to this, the results presented and discussed in this chapter are all based on an optimized nafion-cobalt(III) sepulchrate composite $[\text{GCE}|\text{Naf}|\text{El-Co}(\text{Sep})^{3+}]$ film, in which optimisation was done with

respect to electrocatalytic response of the CYP450 enzyme-modified electrode [138], since the Co(Sep)³⁺-modified nafion platform was created with the overall aim to eventually fabricate a nCYP3A4-based biosensor for detection of HAART associated drug, indinavir. In this regard, results for optimisation is not shown in this Chapter, but are exhibited and comprehensively discussed in **Chapter 5B**.

The cyclic voltammogram of the nafion-modified GCE, GCE||naf, in anaerobic PBS (50 mM; pH 7.4) is shown in **Figure 5A.1**, for an experiment conducted at a scan rate of 10 mV s⁻¹. Essentially, the voltammogram obtained for the nafion-modified GCE is similar to that for bare GCE (not shown), with the fundamental difference being that the background current is appreciably reduced, which indicates that some active sites have been filled in by the smooth nafion film. In fact, according to literature findings, the proportion of active sites blocked by nafion ranges from 15 to 20% [139]. Moreover, the lack of observable electrochemistry is in complete agreement with studies based on nafion modified electrodes [104, 122, 140]. The important fact here is that the presence of the nafion does not substantially modify or block electron transfer with respect to the underlying electrode, and as such the nafion film may be effectively used as matrix for subsequent incorporation of cationic (mediating) species, as well as additional layers.

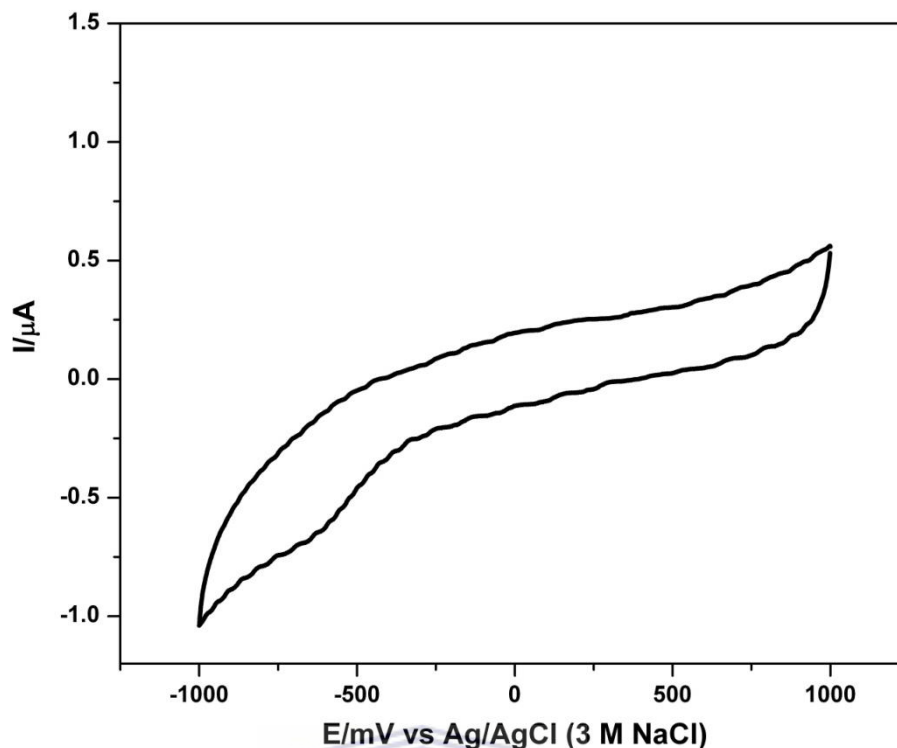


Figure 5A.1 Cyclic voltammogram of GCE|Naf at 10 mV s^{-1} in argon-degassed phosphate buffer (50 mM, pH 7.45)

The thickness of the nafion film was also determined, of which the calculations were done according to established methods, in conjunction with relevant theoretically based equations, from already published data [104-105, 128, 132]. In particular, calculations were done according to methodology outlined by **equation 3B-1** in Chapter 3B. In short, however, essentially, the relation takes into consideration the fractional concentration of the nafion added, the density of the Nafion[®] stock solution, as well as the density of the dry film and the area of the electrode. The nafion film thickness estimated by this method, was determined as $3.1 \mu\text{m}$. In this regard, considering that the nafion film essentially served as inner layer, for the eventual assembly of an enzyme-based biosensor, the thickness value is in fairly good agreement with other research investigations which utilized nafion for similar purpose [122].

The cobalt(III) sepulchrate, which was loaded into the nafion membrane through potentiostatic deposition, on the other hand, exhibited a completely different electrochemical behaviour. **Figure 5A.2** displays the voltammetric response of the GC|naf|El-Co(Sep)³, for scans taken in argon-degassed PBS. In particular, the cyclic voltammogram for the GC|naf|El-Co(Sep)³⁺ shown in **Figure 5A.2(a)**, for an experiment conducted at scan rate of 3 mV s⁻¹ shows a pair of well-defined symmetrically shaped redox peaks, consisting of a cathodic and anodic wave. In this regard, considering that an oxygen-free medium was used and that fact that only one pair of redox waves, the cathodic and anodic peak of the CV can be ascribed to the Co(Sep)³⁺/Co(Sep)²⁺ redox couple. The reduction (cathodic, E_{p,c}) and oxidation (anodic, E_{p,a}) peak potential values were determined as -654 and -575 mV, respectively, while a peak separation, ΔE_p, of 79 (± 3) mV was determined. The formal potential (E^o), determined as the midpoint potential (E_{mid}), estimated from the cyclic voltammetric data, was found to be -615 mV, and in addition to this, the ratio of anodic to cathodic peak current (I_{p,a}/I_{p,c}) was estimated to be 1.2. In fact, the values of E_{mid}, ΔE_p and I_{p,a}/I_{p,c}, from CVs between 2 and 10 mV s⁻¹, determined as averaged values corresponded to -611 mV, 77 and 1.1. Moreover, the variation in ΔE_p for these scan rates were negligible. In this regard, in terms of the theoretical aspects of electrochemical reversibility, a value of 1.0 for I_{p,a}/I_{p,c} corroborates the reversibility of the electron transfer reaction at the electrode surface, while a value of lower than 65 mV for ΔE_p is an indication of a surface-bound electroactive species which undergo fast reversible electron transfer at the electrode [74]. In practice however, the exact values for these parameters are difficult to attain, and as such, room is made for experimental error of approximately ± 10%, which essentially means that the results obtained for the current electrochemical system shows adequate promise in terms of ideal proximity. Another noteworthy point to emphasize at this stage, is that repeated CV scans recorded at half hour or one hour intervals, up to three/four hours after assembly of the GC|Naf|El-Co(Sep)³ exhibited stable background currents, with no indication of instability or reduction of peak current — a factor which also corroborates the findings of the stability and reversibility of the prepared film. The

total surface coverage/concentration (Γ) of the $\text{Co}(\text{Sep})^{3+}$ cationic species in the nafion film was calculated by measuring the Faradaic charge (Q) passed at slow scan rate, where exhaustive electrolysis of the film occurs [129, 141]. In particular, the Γ was calculated by integrating the cathodic charge under the voltammetric peak recorded at $v = 2 \text{ mV s}^{-1}$, by using the equation, $\Gamma = \frac{Q}{nFA}$, where n is the number of electrons of the redox reaction, A is the geometric electrode area (0.071 cm^2), and F is the Faraday constant ($96\,500 \text{ C mol}^{-1}$). Considering $n = 1$, Γ of the $\text{Co}(\text{Sep})^{3+}$ was calculated to be $1.537 \times 10^{-5} \text{ mol cm}^{-2}$. Since the Γ of the electroactive $\text{Co}(\text{Sep})^{3+}$ species may be regarded as a reflection of the amount of cationic species incorporated into the pre-formed nafion film it is important to accentuate that, the technique used in the current study enabled the incorporation of the highest possible percentile of electroactive species within the nafion membrane in the shortest possible time. In fact, it is highly comparable to previously published studies involving metal centred and/or cage complexes, for example, in a study conducted by Dewald et al. [124], the maximum loading for $\text{Co}(\text{Sep})^{3+}$ into a $36 \mu\text{m}$ pre-formed nafion film, was only $2 \times 10^{-4} \text{ mol cm}^{-2}$, obtained by potentiodynamic cycling method over a two hour period. In this regard, the method used in the current study (i.e. potentiostatic deposition) may be revered as an effective technique for pre-concentration of counter-ion species in nafion and/or other ion-based polymer films.

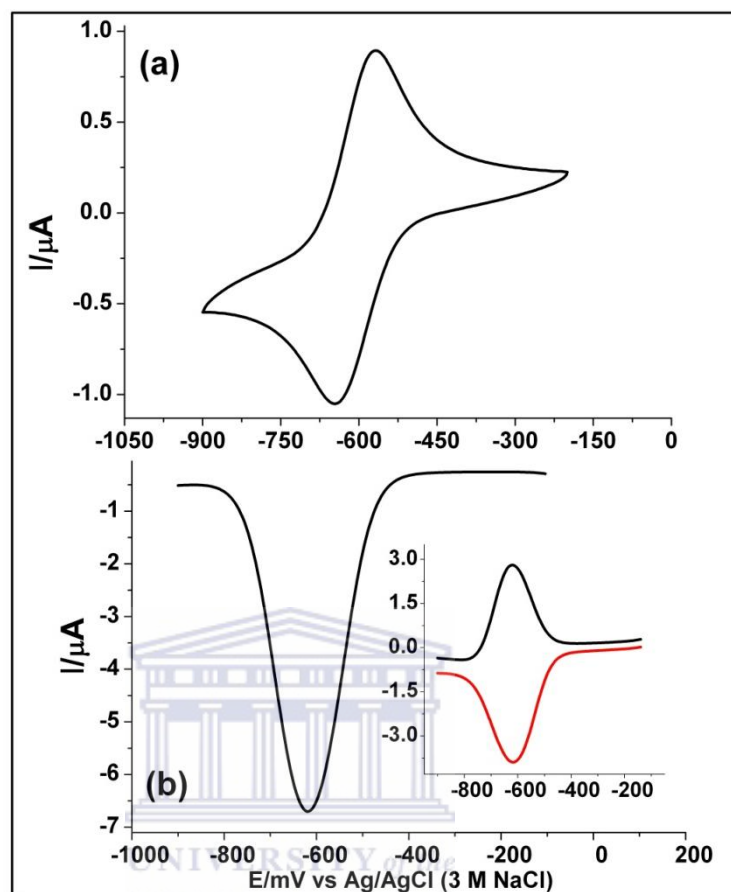


Figure 5A.2 Voltammetric response of the nafion-cobalt(III) sepulchrate composite film, GC|Naf|El-Co(Sep)³ in argon-degassed PBS. Cyclic voltammogram taken at 3 mV s^{-1} , with cathodic and anodic waves indicated by negative and positive currents, respectively. Experimental conditions for square wave: StepE = 4 mV; S.W. amplitude = 25 mV; frequency = 1 Hz

The effectiveness of pulsed techniques such as square wave voltammetry to accentuate the Faradaic current while discriminating against capacitive (charging) current cannot be over estimated. In this regard, Osteryoung square wave (OSW) voltammetry was employed to compliment cyclic voltammetry, particularly in terms of a more accurate measure of the E° for the $\text{Co(Sep)}^{3+}/\text{Co(Sep)}^{2+}$ redox couple. Thus appropriately, **Figure 5A.2 (b)** depicts the SWV responses of the GC|Naf|El-Co(Sep)³, with the main graph showing the net (difference) SWV response and the inset showing the forward (negative wave) and reverse (positive) SW responses. The

value of the net SW response as determined from SW data is $-620 (\pm 5)$ mV, while the forward and reverse potential values was determined as -616 and $-624 (\pm 5)$ mV, respectively. Moreover, these results revealed a small ΔE_p , corresponding to a value of only 8 mV. On the other hand, the forward and reverse waves, although fairly symmetric in shape, revealed that, the magnitude of the reduction SW is higher than that of the anodic SW, by approximately one order of magnitude. In fact, these findings, although with a smaller difference, was also found in CV and this essentially means that the metal centred electroactive species was incorporated into the nafion film in its Co(Sep)^{3+} form. This is indeed a true representation of the electrode reaction, since the Co(Sep)^{3+} was potentiostatically deposited at a sufficiently anodic potential (i.e. $+450$ mV), which means it was taken up into the nafion layer in its original Co(Sep)^{3+} form. Overall, the E° , as determined from the aforementioned results shows values that are significantly more cathodic in magnitude (by at least ± 65 mV) as compared to results obtained for Co(Sep)^{3+} at bare electrodes in similar aqueous solution and potential scan conditions. This finding was also reported in some previous research investigations [124, 142], involving the incorporation of other metal-centred cationic electroactive species, into nafion films. In fact, it has been determined by prior research investigations, that this type of cathodic potential shift suggest a strong affinity of nafion for the particular cationic species [143], and as such incurs uptake and retention of the cobalt(III) sepulchrate species within the nafion structure, through strong hydrophobic interactions between the two species. In this regard, to substantiate the aforementioned proposed method of retention, it is noteworthy to some of the structural unique attributes of nafion [117, 119, 143]:

- Firstly, unlike conventional ion exchange resins which are all 100% sulphonated, in nafion, only about one in every eight monomer units is sulphonated, and consequently, the large segments of uncharged chain material enable an enhanced ability of hydrophobic interaction, and these hydrophobic interactions dominate ion exchange reactions for cation species in nafion membranes/films.

- Secondly, unlike other ion exchange polymers, such as PVP⁺, nafion has a very low dielectric constant, as well as a low charge density and the implications of these factors is that hydrophobic interactions dominate retention in nafion polymers, whereas electrostatic forces are the critical component in other ion exchange polymers.
- Thirdly, unlike Co(Sep)³⁺, nafion has very little affinity for many other trivalent species, such as Fe³⁺, Eu³⁺ and Ru(bpy)₃³⁺, which essentially indicate that enhanced electrostatic interaction based on charge, is not the only or dominant factor responsible for nafion's strong retention of any particular cationic species. In fact, it has been shown that solvation of the hydrophobic parts of a cationic complex by nafion's organic chain material is a major determining factor for uptake and retention of cations, and considering the hydrophobic nature of the sepulchrate ligand (containing at least > 3 methylene groups, see Figure 2.5(a)), this type of interaction is definitely highly possible.
- Fourthly, nafion is eminent for its microscopic phase segregation, which is mainly constituted by the bulk polymer phase and the much lower density ionic cluster phase. Electroactive counter ions are present in the ionic cluster phase and charge-based ion-pair formation, although present to some extent, is not significant in these polymers. In fact, it has been proposed that due to nafion's high preference for organic cations, the ionic cluster regions must be regarded as a rather lipophilic environment, while the water contained within these regions acts a plasticizer, functioning to increase the free volume of and decrease the polymer chain concentration in the ionic cluster.

Considering all the aforementioned unique structural attributes of nafion, the most fundamental conclusion that can be drawn at this stage is that the mechanism of retention of electroactive ions in nafion membranes are significantly different, as compared to conventional ion exchange polymers — nafion being largely dominated

by hydrophobic interactions, rather than the normal electrostatic forces. This also confirms and reiterates the proposed mechanism of uptake and retention for $\text{Co}(\text{Sep})^{3+}$ as described above.

Another noteworthy finding, as determined from the voltammetric results exhibited for the GC|Naf|El-Co(Sep)³⁺ in the current study, is that the $E_p^{o'}$, determined as $-615 (\pm 5)$ mV, varies quite significantly from the value determined for the previous platform presented in **Chapter 4** (-571 ± 5 mV) but is quite similar to previously reported value obtained for a different investigation, conducted by Dewald and Chen (i.e., $(\pm) -600$ mV), which also involved a nafion-cobalt(III) sepulchrate composite film. In this regard, the composite film presented and discussed in **Chapter 4**, involved chemical preparation methods, in which the $\text{Co}(\text{Sep})^{3+}$ was manually mixed with the pre-formed nafion film, whereas the protocol used by Dewald and Chen, on the other hand was based on potentiodynamic technique, in which $\text{Co}(\text{Sep})^{3+}$ was incorporated into the nafion film through electrochemical cycling in a contacting solution, containing the electroactive species. The overall fundamental deduction that can possibly be made from these findings is that electrochemical pre-concentration of cobalt(III) sepulchrate and/or other metal centred electroactive species in ion-containing polymer films, such as nafion is a more effective method for producing stable composite films, as opposed to chemically preparative methods.

Overall, a critical evaluation of the above presented and discussed voltammetric results for the GC|Naf|El-Co(Sep)³⁺ system, in terms of the determined $I_{p,a}/I_{p,c}$ (± 1); ΔE_p (close to $65/n$ mV); ΔE_p and variation with scan rates (negligible for $v = 3 \rightarrow 10$ mV), corresponds to a reversible system [74, 131]. On the other hand, for ideal Nernstian electrochemical reversibility of a surface-confined electroactive species, the relationship, $E_{p,c} = E_{p,a}$ should be satisfied and in this regard, the difference in

peak potential, which was determined as an average value of $77 (\pm 5)$ mV, is consistent with semi-infinite linear diffusion, and not with ideal Nernstian electrochemical surface confined species for which peak potentials should coincide [130, 144]. In fact, the results obtained for the investigation of peak current on scan rate, of which the results are exhibited in **Figure 5A.3**, revealed a perfectly linear relation for the $I_p/v^{1/2}$ for both the cathodic and anodic peak currents, as shown in the inset of **Figure 5A.3**, with correlation coefficients obtained from linear regression for both $I_{p,c}/v^{1/2}$ and $I_{p,a}/v^{1/2}$ functions determined as 0.9994. This finding essentially corroborates diffusion controlled electrochemistry for the GCE|Naf|EI-Co(Sep)³⁺ system. On the other hand, when looking at the cyclic voltammograms shown in **Figure 5A.3**, the reduction and oxidation waves were fairly symmetrically shaped and increased gradually with the scan rates studied ($v = 4 \rightarrow 50 \text{ mV s}^{-1}$), with no visible tailing observed. Such results, would normally indicate thin layer electrochemistry, usually accompanied by a linear $I_{p,c}/v$ function, which is not the case here, as shown by the linear relation between peak current and square root of scan rate. These results, although seemingly baffling, can be perfectly explained and envisaged if one understands the peculiar nature of the mechanism of charge transport in ion-containing nafion films: Unlike conventional polymers, containing electroactive sites along their polymer backbone, for which charge transport is a one dimensional process (Donnan equilibrium), mainly constituted by electron hopping in which electrons are transferred from reduced to oxidized sites in the film, play a major role in charge transfer within the films — in ion-containing polymers such as nafion, for which phase segregation and water of hydration in microdomains are the characteristic features, a significantly different model for charge transport has been shown [117-119]. Electroactive counter ions taken up by nafion, is by-and-large present in the randomly distributed low density ion cluster regions in nafion films. These clusters are inter-connected by small channels, and as such charge transport within such films in the absence of any chemical kinetic complications actually occurs through a three dimensional process, consisting of diffusional mass transport

of species through these channels, largely controlled by what is known as the percolation effect, which proposes that the short channels connecting two neighboring clusters are thermodynamically stable. In fact, it has been documented that in nafion membranes, all electron hopping processes has been shown to be equivalent to a diffusion process and as such the overall rate of charge transport can be described in terms of an apparent diffusion coefficient [119]. What is more, in a previously documented study conducted by a different research group [124], in which $\text{Co}(\text{Sep})^{3+}$ was pre-concentrated through potentiodynamic cycling into a pre-formed nafion film, the current function, $I_p/v^{1/2}$ also exhibited a constant value at different scan rates, which essentially corroborates the results obtained in the current research investigation.

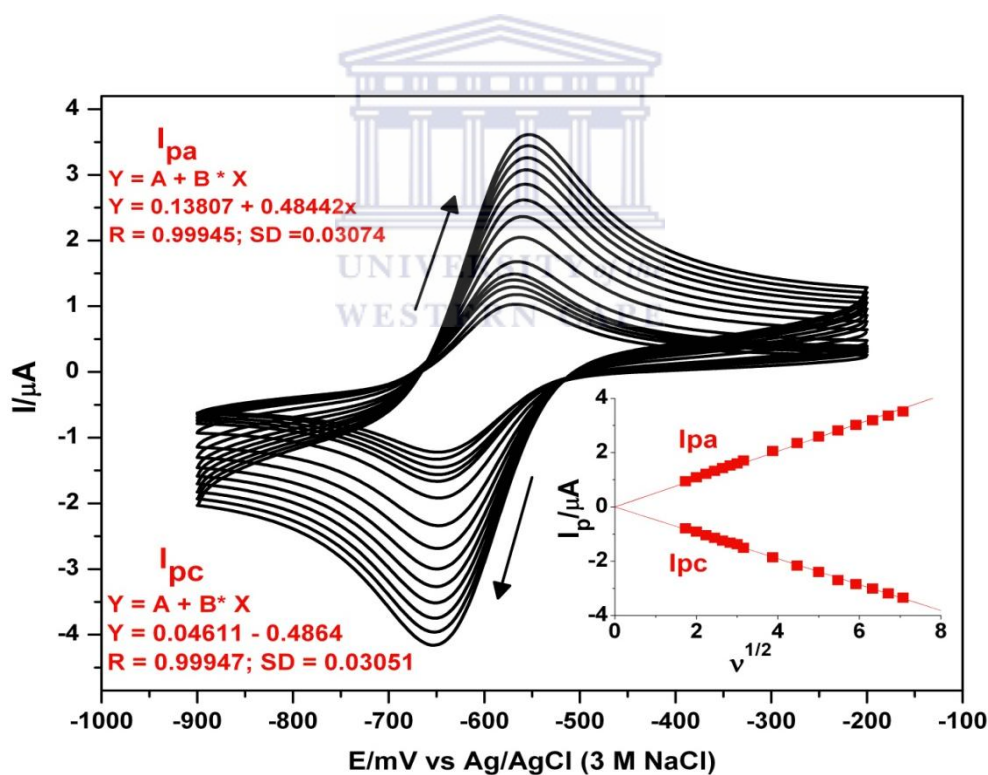


Figure 5A.3: Cyclic voltammograms of $\text{GC|Naf|EI-Co}(\text{Sep})^3$ showing voltammetric response in argon-degassed PB with increasing scan rate ($4 - 50 \text{ mV s}^{-1}$). Inset: Influence of scan rate on cathodic ($I_{p,c}$) and anodic ($I_{p,c}$) peak current

With regard to the charge transfer diffusion coefficient (D_{ct}) for this study in particular, the Randle Sevcik behaviour of the cyclic voltammetric peak currents, as exhibited in **Figure 5A.3**, was used to evaluate D_{ct} from the slope of the straight line obtained from the $I_{p,c}$ vs $v^{1/2}$ plot [129, 131], by using the equation, $\frac{i_p}{v^{1/2}} = \frac{(2.69 \times 10^5) \cdot D_{ct}^{1/2} \cdot \Gamma \cdot A}{L}$ = slope, where A is the geometric surface area of the electrode, Γ is the surface concentration of the Et-Co(Sep)^{3+} ($1.537 \times 10^{-5} \text{ mol cm}^{-2}$) and L is the thickness of the film ($3.10 \times 10^{-3} \text{ cm}$). Based on this method, using the already calculated aforementioned values for Γ and L, the $D_{c,t}$ for this study was determined as $2.64 \times 10^{-7} \text{ cm}^2 \text{ s}^{-1}$. Compared to other metal-centred cationic species incorporated within nafion films of similar thickness, i.e. Ru(bpy)_3^{2+} [119] [141]; $\text{Ru(NH}_3)_6^{3+}$ [143]; $[\text{Os(bpy)}_2(\text{PVP})_{10}\text{Cl}]\text{Cl}$ [145], the aforementioned value of $D_{c,t}$ obtained in the current study is in the higher region. In fact, it is comparable to previously reported values obtained for smaller counter-ion species, Na^+ ($9 \times 10^{-7} \text{ cm}^2 \text{ s}^{-1}$) [143], which is eminently known for its fast diffusion through nafion films, as compared to many other pre-concentrated cationic counter-ion species. Moreover, it has been documented that a larger $D_{c,t}$ is a reflection of a more homogeneous distribution of the cationic species within the microstructure of the polymer film [119]. The cumulative significance of the latter and aforementioned findings, once again is of course to exemplify and reiterate the effectiveness of the technique used in the current study for pre-concentration of the cationic species within the nafion film.

In addition to the above results exhibited for scan rate studies, the plot of $\log I_p$ vs $\log v$ for both anodic and cathodic peak currents, revealed slopes of 0.47 and 0.52 for $\log I_{p,a}/\log v$ and $\log I_{p,c}/\log v$ respectively. Both these values are close to the theoretical value of 0.5 for diffusion controlled electrode processes [122] and as such, corroborates the above findings. The results for these plots are shown in **Figure 5A.4**.

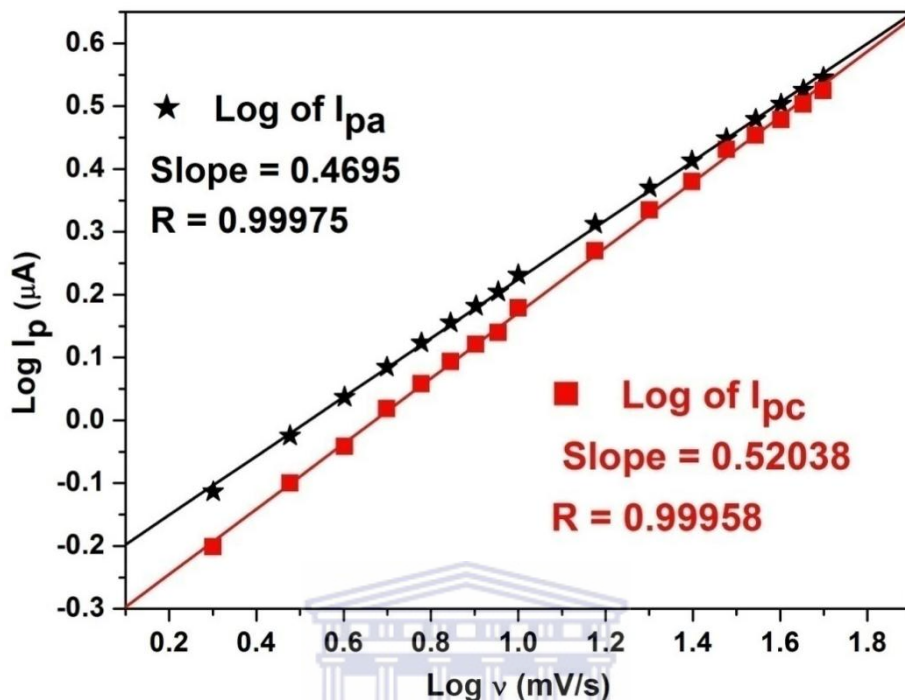


Figure 5A.4: Plots of $\log I_p$ vs $\log v$ for cathodic and anodic peak currents, to show influence of scan rate on peak current for GC|Naf|El-Co(Sep)³⁺ films

5A.2.1 Long-term stability of the GC|Naf|El-Co(Sep)³⁺ film

Due to nafion's unique method of cation extraction and uptake, which, as described in aforementioned and preceding sections is distinctly different and more effective than conventional ion-exchange resins and/or electrostatic binding polymers [118-119], combined with its phase segregation enabled three-dimensional charge transport network, providing molecular accessibility and rapid diffusional mass transport of electroactive species [104-105, 118, 143], as well as its renowned superior chemical and thermal stability [146-147], a factor that remains, even in the presence of strong oxidants at elevated temperatures — nafion-based electrodes has

been shown to have a greater lifetime, while retaining electroactive species for longer times than other ionic polymer and/or coordinating polymer based electrodes. In this regard, to illustrate long term stability, the storage stability of the nafion–El-Co(Sep)³⁺ film was investigated, of which the results are exhibited in **Figure 5A.5**, in which Day 0, refers to the day of fabrication of the GC|Naf|El-Co(Sep)³⁺ film, and as such, considered as time 0. A close evaluation of the results depicted in **Figure 5A.5** revealed the following:

- On the third day, there was a 13% and 8.8% decline in the magnitude of $I_{p,c}$ and $I_{p,a}$, respectively. This was accompanied by a cathodic peak potential shift for both $E_{p,c}$ and $E_{p,a}$ by a magnitude of 16 mV and 9 mV, respectively. In addition to this, the formal potential (E°) for GC|Naf|El-Co(Sep)³⁺ shifted cathodically by ± 13 mV, as compared to the original CV exhibited for Day 0.
- On the fifth day of storage, there was a 14.3% decline in the magnitude of $I_{p,c}$. On the other hand, the no measurable change in $I_{p,a}$ was observed, as compared to what was determined for the third day. As for $E_{p,c}$ and $E_{p,a}$, once again a cathodic shift was observed corresponding to a magnitude of 30 mV and 24 mV for $E_{p,c}$ and $E_{p,a}$, respectively. Similarly, the E° shifted cathodically by a magnitude of 27 mV, as compared to the original results for the GC|Naf|El-Co(Sep)³⁺ film observed on Day 0.

Overall, the above electrochemical results for the GC|naf|El-Co(Sep)³⁺ system showed that, upon storage for up to one week in dry conditions at ambient temperature (23 ± 3 °C), the film still retained 73% of its original electrochemical signal, without the need for storage and/or physical contact with the Co(Sep)³⁺-containing supporting electrolyte. Moreover, the presented CVs were recorded after repeated cycling, when a steady state in $I_{p,c}$ and $I_{p,a}$ were attained, in which these cycles were completely identical and showed no loss of signal, which are all indications of a stable film.

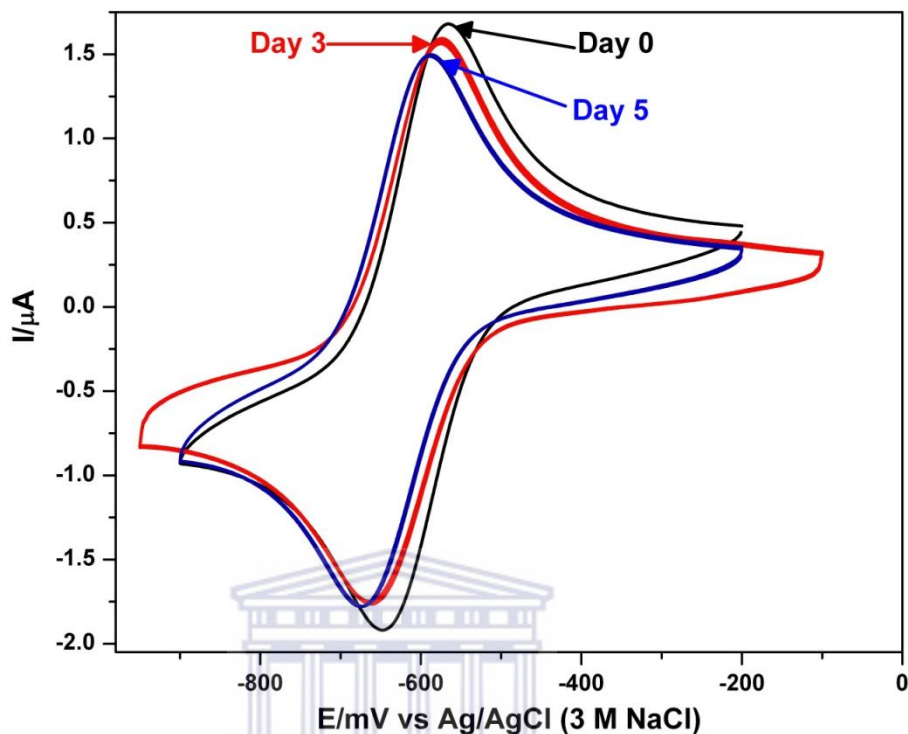


Figure 5A.5 Cyclic voltammetric response showing variation in Faradaic current and peak parameters ($I_{p,c}$; $I_{p,a}$; $E_{p,c}$; $E_{p,a}$) of the GC|Naf|EI-Co(Sep)³⁺ films with numbers on the curves denoting days elapsed after fabrication. The voltammograms were recorded in anaerobic PB (50 mM; pH 7.45)

The cumulative implications of all the preceding and aforementioned results with regard to the Co(Sep)³⁺ loading, voltammetric behaviour, as well as the stability of the composite nafion-EI-Co(Sep)³⁺, is quite significant, since it not only accentuates improvement as compared to techniques applied in numerous previously conducted research investigations involving incorporation of metal-centred cationic species into nafion films, but also exhibits enhancement in terms of long term stability, as opposed to some of these studies:

- Firstly, loading methods used by most previously conducted research investigations involved either physical equilibration with the solution, which were usually done from a few hours up to 24 hours to ensure adequate loading or in some cases, potentiodynamic techniques using potential cycling for up to 2-3 hours in the supporting electrolyte containing the metal centred cationic species (analyte solution) [124, 143]. To recall, the technique applied in the current study on the other hand, involved potentiostatic deposition of the $\text{Co}(\text{Sep})^{3+}$ at +450 mV for 20 min, which overall, resulted in a highly stable composite film. In this context, with regard to $\text{Co}(\text{Sep})^{3+}$ in particular, the rate of loading for the current research investigation was considerably faster (by a factor of 6), as compared to rate observed for $\text{Co}(\text{Sep})^{3+}$ loading for a study conducted by Dewald and Chen [124] who used the potential cycling pre-concentration technique.
- Secondly, the composite nafion-El- $\text{Co}(\text{Sep})^{3+}$ - (GC|naf|El- $\text{Co}(\text{Sep})^{3+}$) film exhibited well defined, stable voltammetric behaviour, upon repeated cycling in the PB supporting electrolyte containing no $\text{Co}(\text{Sep})^{3+}$ analyte. In some other studies, conducted by other research investigators involving composite nafion/metal centred cation species, however, stable CVs were only possible in electrolyte solutions containing the cationic analyte [143, 148].
- Thirdly, under the experimental conditions applied for the current study, the GC|naf|El- $\text{Co}(\text{Sep})^{3+}$ film maintained at least 73% of its original signal after five days of storage, whereas for methods based on pre-concentration of metal centred cationic species (analyte) through physical equilibration techniques especially — maintaining adequate signal response of the composite film was only possible in conjunction with storage in the supporting electrolyte [119].

Before commencing with subsequent discussions, a final important subject to also address, is the implications of the exhibited voltammetric behaviour of the naf|El- $\text{Co}(\text{Sep})^{3+}$ composite film with regard to its proposed application, i.e., as

mediating-carrier matrix platform for amperometric biosensor construction with the synthesized n-terminally modified recombinant CYP3A4 (n-CYP3A4). As already accentuated and discussed in **Section 2.2.4** in **Chapter 2**, creating a successful reagentless amperometric mediated biosensor requires effective retention of the mediator at the electrode surface, and, perhaps more importantly, allowing simultaneous free diffusional movement of the mediating species, as well as rapid electrochemical communication to-and-from the electrode surface. In fact, according to relevant literature survey, it has been recorded that the diffusional movement of the mediator is an essential prerequisite for a productive electron transfer [65, 149] in mediated biosensors. Taking into consideration the latter and aforementioned criteria: Based on the results exhibited and discussed in terms of electrochemical performance factors of the composite film, as well as critical comparisons to relevant literature findings, the suitability of the prepared naf-El-Co(Sep)³⁺ film with regard to suitability for biosensor construction was critically assessed and the findings summarized. In this regard, firstly, as corroborated by previous findings, nafion was shown to retain and incorporate the electroactive cation mediator distinctly different from other ion exchange polymers/resins, which resulted in a more stable film, exhibiting good reversible electrochemistry. Secondly, also as corroborated by previous findings, in the absence of any kinetic complications, the electrochemistry of the film is dominated by diffusional movement, which as elaborated above, is fundamental for productive electron transfer. Thirdly, due to nafion's considerably lipophilic nature, essentially containing no water leachable components, formed membranes/films consequently should have much longer lifetime, particularly with regard to incorporated electroactive counter-ion species [118] [117]. In fact, research has shown that unlike conventional polymer membrane ion selective electrodes (PMISEs), which require plasticizers and covalently attached ligands to increase ionic mobility in the polymer membrane, as well as preventing loss of electroactive species from the membranes, ion containing polymers, like nafion, requires no additional components and films containing ionic species have shown stability for up to six months [117]. In this context, as evaluated by the results exhibited and discussed for

long term stability, the Naf|El-Co(Sep)³⁺ film corroborated the aforementioned findings and thus maintained a high electronic signal after storage for up to one week.

5A.2.2 Electrochemical behaviour of GCE|Naf|Co(Sep)³⁺ with Ruthenium(III) hexamine redox probe

It is an eminent fact that nafion has an unusually high affinity for ruthenium(III) hexamine. In this regard, thus it seemed appropriate to further investigate the integrity and charge-transfer behaviour of the naf|Co(Sep)³⁺ film by using Ru(NH₃)₆Cl₃ as a redox probe, for which the studies were done in PB containing 1 mM Ru(NH₃)₆Cl₃. Upon initial potentiodynamic cycling in the Ru(NH₃)₆Cl₃ containing PB with the GCE|naf|Co(Sep)³⁺ electrode, there was a gradual increase in I_{p,c} and I_{p,a} with time, of which steady state background current was obtained after approximately five hours. The CVs are shown in **Figure 5A.6**, for 0 – 5 hour equilibration time. The results, in terms of increasing I_{p,c} and I_{p,a} is completely in accordance with previous findings, and in this regard, usually signifies the extraction and pre-concentration of the Ru(NH₃)₆³⁺ into the film — a process which, for a 1 μm thick nafion film, normally takes up to one day for completion. However, the uptake of the Ru(NH₃)₆³⁺ into the film can only be conclusively deduced, with the aid of additional investigations, such as determination of distribution coefficients (k_D), etc., however such parameters were not determined at this stage, since it is not required for the scope of the dissertation. With regard to further evaluation of the CVs presented in **Figure 5A.6**, a fairly well-defined redox couple can be observed, which corresponds to the oxidation and reduction of the Ru(NH₃)₆³⁺/Ru(NH₃)₆²⁺ couple. The specific peak parameter values for E_{p,c}; E_{p,a}; E^o, for the redox couple were determined as -210 mV; -145 mV and -176 mV (± 5 mV) respectively. These were determined as mean standard deviation at low scan rates, where exhaustive electrolysis were possible, as such converting all of the Ru(NH₃)₆³⁺

to $\text{Ru}(\text{NH}_3)_6^{2+}$. Furthermore, $|\text{I}_{p,c}/\text{I}_{p,a}|$ was determined as 1.4, while a peak potential difference (ΔE_p) of $60 (\pm 2)$ mV signified semi-infinite linear diffusion, as it is close to the theoretical value of 57 mV for a diffusion controlled system. Diffusion control was confirmed by varying the scan rate, as shown in **Figure 5A.7** which exhibits the cyclic voltammometric responses, as well as a linear relationship of $\text{I}_{p,c}$ and $\text{I}_{p,a}$ with $v^{1/2}$ of $\text{Ru}(\text{NH}_3)_6\text{Cl}_3$ at the GC|Naf|El-Co(Sep)³⁺ electrode for scan rates from 10 to 150 mV s^{-1} . A closer evaluation of the exhibited CVs, shows a gradual increase in both $\text{I}_{p,c}$ and $\text{I}_{p,a}$ with each scan rate, up to 150 mV s^{-1} , coupled with a very small cathodic and anodic peak shifts for the cathodic wave and anodic wave, respectively, with each scan rate (by a magnitude of ± 5 mV). The Randles-Sevcik relation for a one-electron reaction was applied to determine the apparent diffusion coefficient, based on the following equation:

$$I_p = (2.687 \times 10^5) n^{3/2} v^{1/2} D_{\text{app}}^{1/2} AC$$

Where I_p is the peak current, n is the number of electrons transferred, v is the scan rate (V s^{-1}), A is the electrode area (cm^2), C is the bulk concentration D_{app} is the $\text{Ru}^{3+}/\text{Ru}^{2+}$ diffusion coefficient (mol cm^{-3}). In this regard, by using the slope of the straight line obtained from the $\text{I}_{p,a}$ vs $v^{1/2}$ plot, and applying it in the Randles-Sevcik equation (Equation), D_{app} was determined as $7.982 \times 10^{-10} \text{ cm}^2 \text{ s}^{-1}$. It is noteworthy to add though, that the obtained D_{app} is slightly on the low side, but is not entirely unexpected, since usually smaller ions like Na have, is expected and indeed does exhibited larger diffusion coefficients [143]; on the other hand, research has shown that diffusion of $\text{Ru}(\text{NH}_3)_6^{3+}$ into pre-formed nafion films can take up to 24 hours to reach equilibrium, while equilibration for $\text{Ru}(\text{NH}_3)_6^{2+}$ uptake can take up to one week [117, 143], which essentially translates into corresponding generally lower D_{app} values. That being said, considering the preformed nafion film already contained a counter-ion ($\text{Co}(\text{Sep})^{3+}$), which were quite stably retained,, as well as the fairly good charge transfer/electrochemical behaviour of the film with respect to the $\text{Ru}(\text{NH}_3)_6\text{Cl}_3$ redox probe, including the fact that equilibration with $\text{Ru}(\text{NH}_3)_6^{3+}$ took ± 5

h to attain a steady state – the obtained D_{app} are well within reason. Moreover, the value obtained for D_{app} for Ru^{3+}/Ru^{2+} in this study is actually completely in line with literature reported values for nafion film of similar thickness (i.e. $\approx 1 \times 10^{-10} - 25 \times 10^{-10} \text{ cm}^2 \text{ s}^{-1}$).

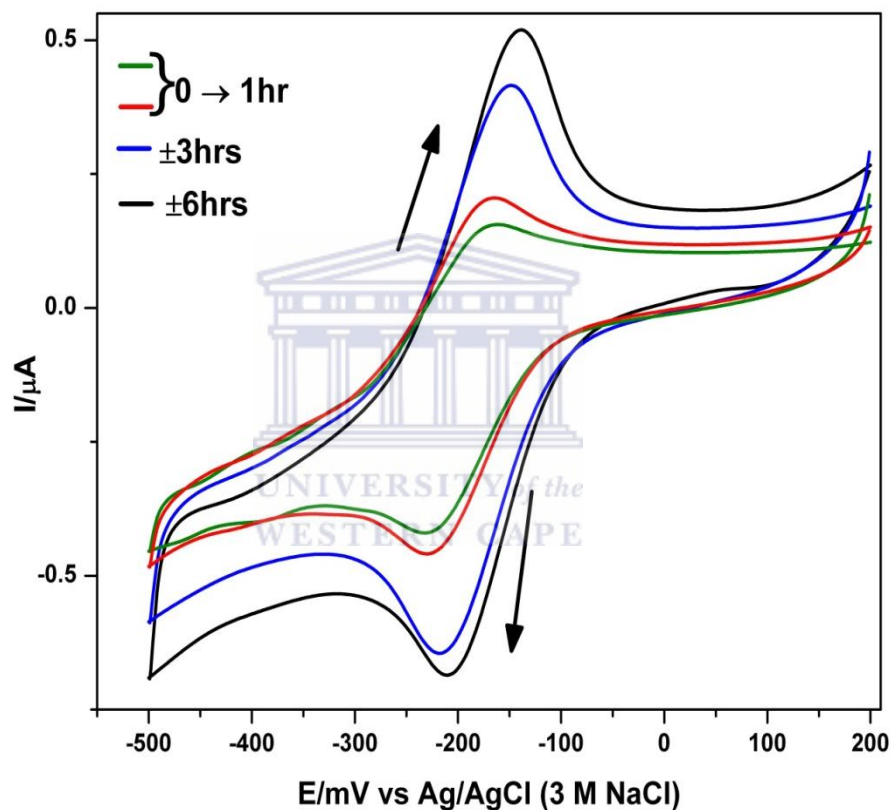


Figure 5A.6 Cyclic voltammograms (5 mV s^{-1}) of the $GC|Naf|EI-Co(Sep)^{3+}$ electrode in anaerobic PB containing 1 mM ruthenium(III) hexamine chloride $[Ru(NH_3)_6Cl_3]$. Voltammograms at 0-, 1-, 3-, and 6 hours are shown

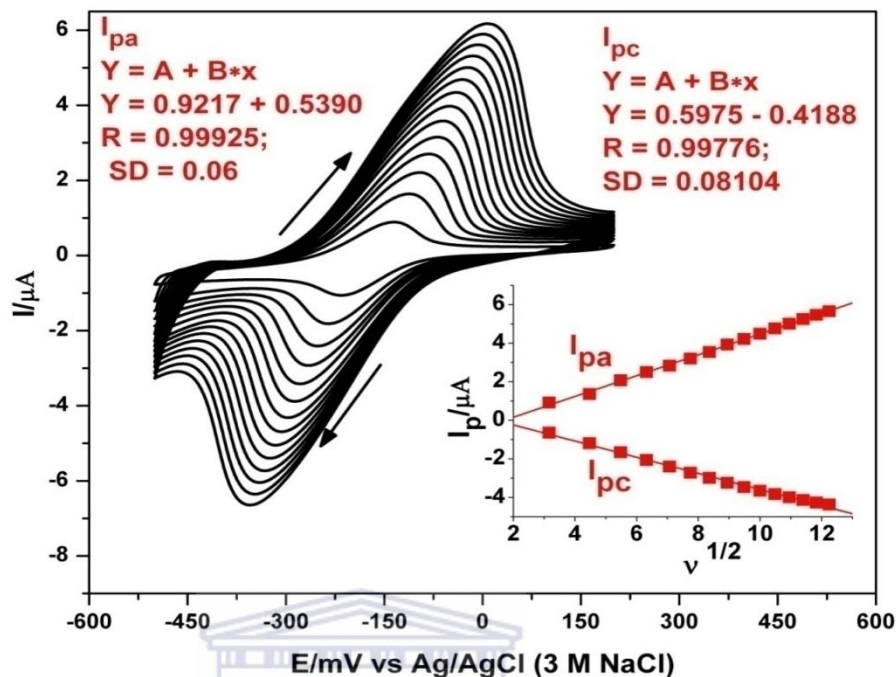


Figure 5A.7 Cyclic voltammograms showing the influence of scan rate on oxidation and reduction peak current for 1 mM ruthenium(III) hexamine chloride $[\text{Ru}(\text{NH}_3)_6\text{Cl}_3]$, in 50 mM PBS (pH 7.4) at the $\text{GC}|\text{Naf}|\text{El-Co}(\text{Sep})^{3+}$ electrode. Scan rates in order of increasing peak height are 10, 20, 30, 40, 50, 60, 70, 80, 90, 100, 110, 120, 130, 140 and 150 mV s^{-1} . In set shows the linear relationship between peak current ($I_{p,c}$ and $I_{p,a}$) and $v^{1/2}$, with determined slopes

5A.3 Morphological and structural characterization of the $\text{Naf-El-Co}(\text{Sep})^{3+}$ film

To get a complete comprehensive overview of a prepared platform, morphological and structural investigation of the film is also required, of which these investigations may be conducted through various spectroscopic and microscopic techniques, but the most eminent being, normally done through Scanning Electron Microscopic (SEM) analysis and Fourier Transform Infrared (FTIR) Spectroscopy, respectively. In this

regard, obtained FTIR spectra enables the assignment of unique characteristic vibrational signals, which allows for easy structural analysis of compounds. Similarly, changes in chemical environments due to incorporated chemical components, etc. induces vibrational peak shifts, which may aid in structural characterization of composite material. On the other hand, SEM analysis allows for top-sectional and/or cross-sectional views, revealing more detailed information on film morphology, and integrity of film constituents.

5A.3.1 Morphological characterization: Scanning Electron Microscopy (SEM)

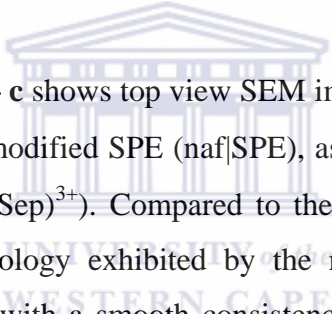


Figure 5A.8 a – c shows top view SEM images of the blank screen printed electrode (bSPE), nafion-modified SPE (naf|SPE), as well as the $\text{Co}(\text{Sep})^{3+}$ modified electrode (SPE||naf|El- $\text{Co}(\text{Sep})^{3+}$). Compared to the rough surface observed for the bSPE, the surface morphology exhibited by the nafion film on the other hand, revealed a microstructure with a smooth consistency, which indicates a chemically stable membrane that covers and protects the underlying electrode. In this regard, according to research findings, nafion is known to maintain its chemical stability under extreme conditions – proven to maintain characteristic structural bonds even when exposed to radical producing H_2 or O_2 environment for up to 1000 hours [111]. The incorporated $\text{Co}(\text{Sep})^{3+}$ cation species did not induce any noticeably visible changes to the nafion-derivatised film, but rather also exhibited a fairly smooth film, as shown in **Figure 5A.8 (c)**. The notable similarity of the composite naf|El- $\text{Co}(\text{Sep})^{3+}$ -film to the film consisting only of nafion is indeed an interesting feature, not an entirely unexpected phenomenon, since as described in preceding sections within this chapter, once exposed to the $\text{Co}(\text{Sep})^{3+}$, the nafion extracts the cation species and it subsequently taken up within the nafion microstructure, which essentially means that, although inherent structural changes within the nafion

microstructure occur, this does not necessarily translate into visible changes and as such, not much visible changes of the film surface is really expected.

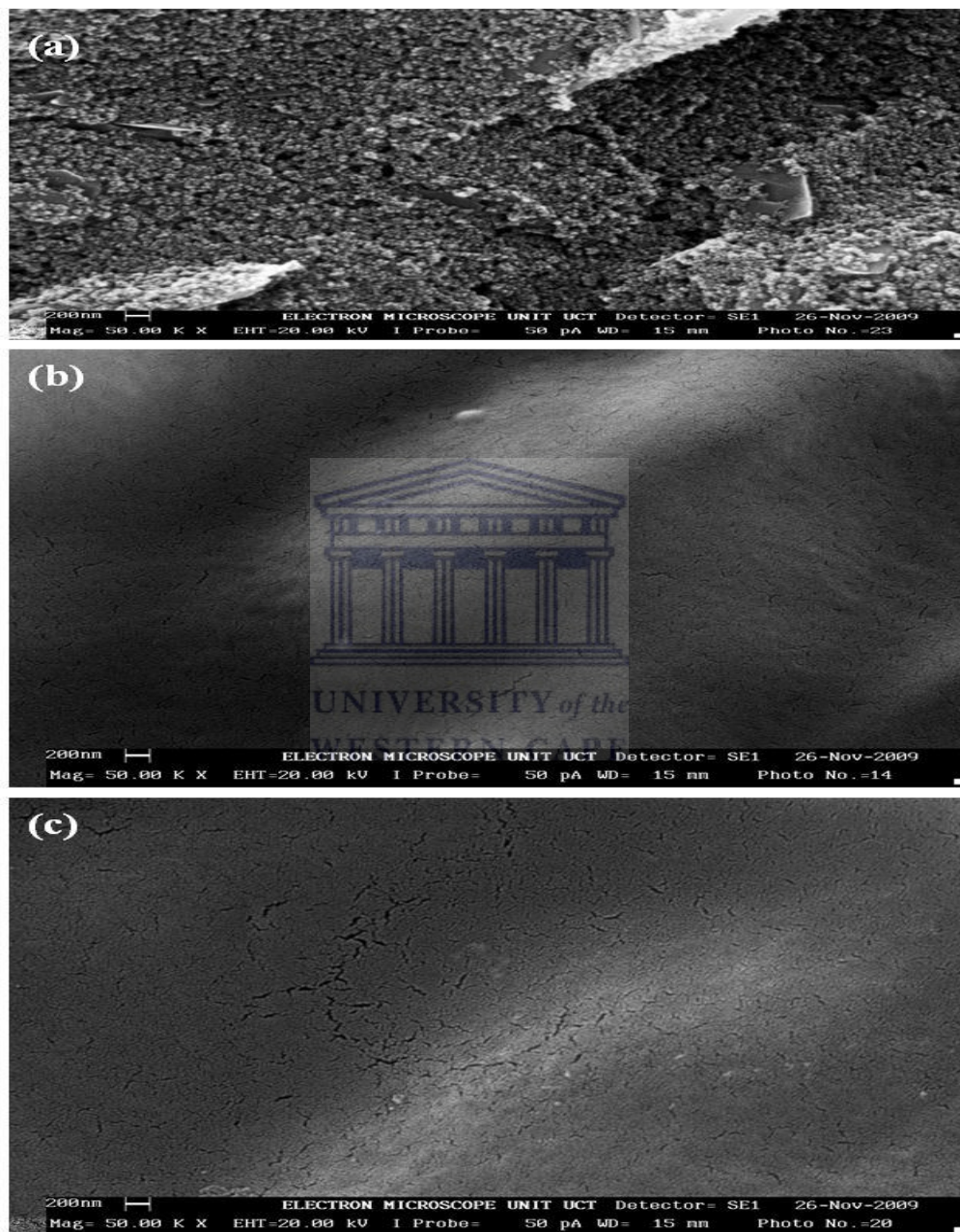


Figure 5A.8: Top Scanning electrochemical microscopy images of electrode and films: (a) blank screen printed electrode (bSPE); (b) Naf modified SPE (nafSPE); (c) nafSPE with pre-concentrated $\text{Co}(\text{Sep})^{3+}$ ($\text{SPE}||\text{naf}|\text{El}-\text{Co}(\text{Sep})^{3+}$)

At this stage, still on the subject of the exhibited SEM-images, an important aspect to bring to the reader's attention, is the fundamentally unequivocal dissimilarity in the surface morphology with respect to the pre-formed nafion membrane, as well as the Co(Sep)³⁺-modified nafion membrane in the current study, as compared to what was observed for the study presented and discussed in Chapter 4. In this regard, for the current study, both films exhibited a compact nature with a highly smooth consistency, whereas those observed in the previous chapter was highly unevenly distributed films with very little signs of compactness. This finding is quite significant, since firstly, the compact nature and smooth consistency of the nafion film, in turn allows for a better coverage and/or protection of the underlying electrode. Secondly, the marked similarity of the modified and un-modified nafion films, essentially portrays a good extraction and uptake of the incorporated Co(Sep)³⁺ within the nafion microstructure. The cumulative sub-conclusion which may be drawn from these findings point to the improvement in technique used for film preparation, as compared to the experimenter's initial approach used for the design of biosensor platform 1 in Chapter 4. The observed improvement may be attributed to the different approach taken in terms of design parameters, with particular reference to the amount of nafion cast, the technique used for nafion film formation, as well as the specific technique used for incorporation of the Co(sep)³⁺ species, as compared to the design path used in the preparation of the carrier matrix for the preparation of biosensor platform 1.

5A3.2 Structural characterization: Fourier Transform Infrared Spectroscopy (FTIR)

Figure 5A.9 a – c shows the FTIR spectra of nafion used in this study, commercially obtained cobalt(III) sepulchrates trichloride, as well as the electrochemically prepared nafion/EI-Co(Sep)³⁺ composite membrane, respectively.

In this regard, the spectra exhibits the major vibrational fingerprints associated with each singular and/or composite compound, of which the assignment of vibrational bands was based on relevant already published data, as well as theoretically established IR correlation charts. With regard to the un-modified ‘pure’ nafion membrane exhibited in **Spectra a**, characteristic absorption bands associated with CF₂ asymmetric stretching (1207 cm⁻¹), CF₂ symmetric stretching (11490 cm⁻¹), S-O symmetric stretching (1058 cm⁻¹), C-O-C stretching (981, 862 cm⁻¹), and C-F stretching (630 cm⁻¹) are shown and identified within the graph [111-114, 116, 150]. In terms of the pure Co(Sep)³⁺ exhibited in **Spectra b**, absorption bands associated with methylene groups (733, 834, 2850, 3034 cm⁻¹), and secondary amines (1055, 1130, 1168, 1335, 1366, 1444, 3415, 3520 cm⁻¹), associated with the characteristic structural features of Co(Sep)³⁺ (see **Figure 2.5**, Chapter 2) is shown [115].

With regard to the Co(Sep)³⁺-modified nafion film (naf|EI-Co(Sep)³⁺), shown in **Figure 5A.9 (c)**, most of the major vibrational fingerprint bands associated with the nafion are also exhibited; however, positional shifts in vibrational bands, as well as new vibrational bands is exhibited in the FTIR spectra. This is an unequivocal indication of structural changes within the microstructure of the nafion membrane and can broadly be ascribed to the incorporation of the electrochemically deposited Co(Sep)³⁺ within the membrane. In this regard, vibrational absorption bands associated with the structure of Co(Sep)³⁺ are indicated/highlighted by differently coloured arrows in **Spectra b and c** of **Figure 5A.9**. Thus, in a more descriptive context regarding **Spectra c**, in terms of a more in-depth investigation of the presence of Co(Sep)³⁺ in the modified nafion membrane in particular, firstly, the appearance of vibrational bands located at 735-, 835 and 971 cm⁻¹ (highlighted by the red arrows) can be ascribed to the methylene groups associated with the structure of Co(Sep)³⁺. Secondly, the appearance of absorption peaks for secondary amine groups, located at 1367 and 1448 cm⁻¹, indicated by green arrows as shown in **Spectra c**, once again signifying and confirming the presence of Co(Sep)³⁺ within the nafion membrane.

Another very noteworthy aspect is that the FTIR spectra for the unmodified nafion membrane (**Spectra a**) exhibited a notable amount of inherent water content signified by the broad peak for stretching vibration of water molecules ranging from $\approx 2620 - 3740 \text{ cm}^{-1}$, whereas no such observable peaks in this region for the $\text{Co}(\text{Sep})^{3+}$ -modified nafion membrane can be seen in **Spectra c**. This is not unexpected, since un-evacuated/un-heat-treated, pure nafion membranes are known to contain an appreciable amount of water, constituted by hydrogen bonded, partially hydrogen bonded and non-hydrogen bonded water molecules [114] — of which these water molecules decreases relative to the increase in concentration of and/or size of counter-ion species (particularly hydrophobic cation species) [118] and considering that on average, each prepared nafion membrane used in the current research investigation (thickness $\approx 3.1 \text{ }\mu\text{m}$) contained at least $\pm 1.5 \times 10^{-5} \text{ mol cm}^{-2}$ extracted/pre-concentrated $\text{Co}(\text{Sep})^{3+}$ counter-ion species, a significant decrease of water content are within experimental expectancy. Moreover the intensity of the $-\text{CF}_2$ absorption bands, as well as for the sulphonic group (1055 cm^{-1}) in the $\text{Co}(\text{Sep})^{3+}$ modified nafion membrane shown in **Spectra c** are more intense and slightly shifted as compared to the bands observed for the unmodified nafion membrane shown in **Spectra a**. Considering the afore-discussed visibly reduced water content associated with the modified nafion membrane, this is certainly not an unexpected phenomenon: Generally each sulphonic cluster region in an unmodified nafion membrane contains water filled pockets consisting of approximately 1000 water molecules and the ensuing interaction of the sulphonate ion groups with these water molecules results in less intense $\text{S}-\text{O}$ (SO_3^-) absorption bands (as seen in **Spectra a** $\approx 1058 \text{ cm}^{-1}$). Moreover, these water molecules is known to function as a plasticiser, thus increasing the free volume (and decreases the concentration of the polymer chain) in the sulphonic clusters [117]. However, as the concentration and/or size of the counter-ion species increases during ion pre-concentration and/or modification of the nafion membrane, a the cumulative effect concomitantly results in loss of water molecules (dehydration) from the sulphonic cluster regions, with a simultaneous increase in the role of the CF_2 groups, thus leading to more intense

FTIR absorption bands for these groups. Furthermore, another prominent finding as observed from the current spectra, is the appearance of a new absorption band of quite strong intensity at 1742 cm^{-1} which is likely to also be associated with the structural changes due to the blending vibration of the incorporated cationic $\text{Co}(\text{Sep})^{3+}$ species, which, based on the upward shift of the frequency as compared to position of absorption band observed in that vicinity (see **Spectra a**) for the unmodified nafion membrane, this may be attributed to the resultant effect of specific interactions such as strong hydrogen bond interactions between the $\text{Co}(\text{Sep})^{3+}$ and structural groups in the nafion microstructure [114, 118].

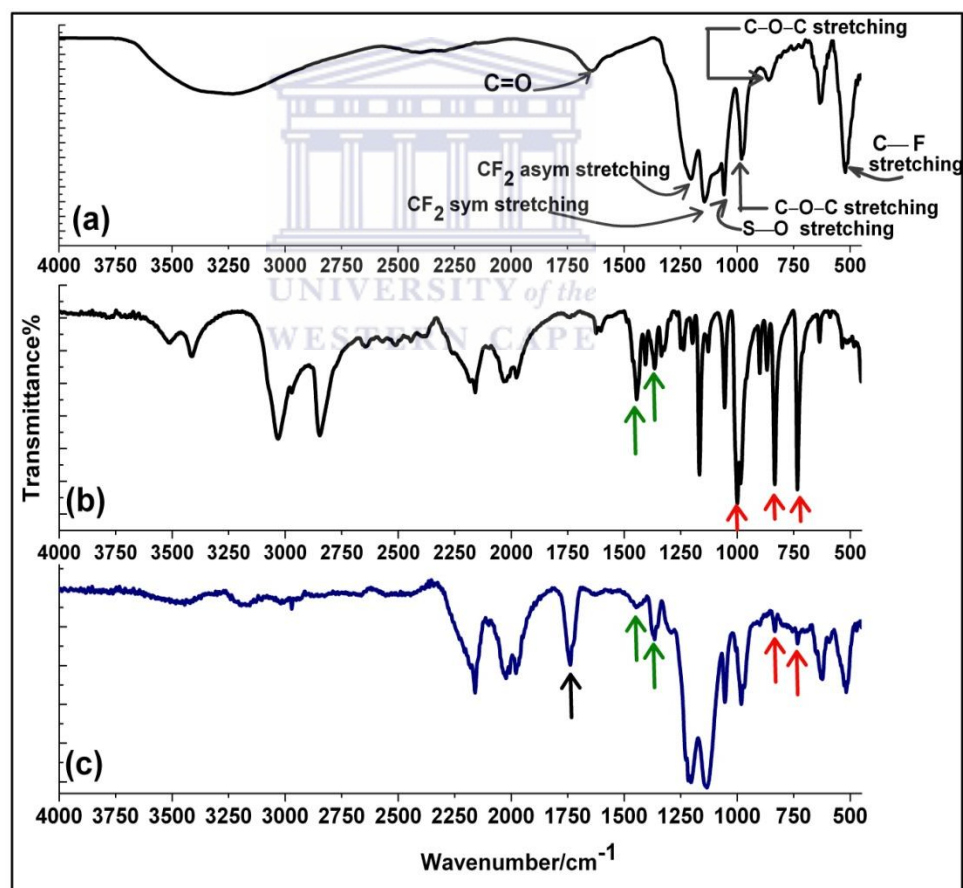


Figure 5A.9: Fourier Transform Infrared Spectroscopy (FTIR) spectra of (a) unmodified nafion membrane; (b) commercially obtained cobalt sepulchrate

On a sub-conclusive note, in a conclusive observation regarding the afore-presented and discussed FTIR results, an interesting feature to once again bring to the reader's attention, is the conspicuous variation in the microstructure of the Co(Sep)³⁺ modified nafion membrane, compared to that observed for 'pure' nafion, particularly with regard to the marked difference in water molecules and associated structural vibrations. In a critical comparative evaluation, with specific reference to the FTIR results exhibited for the nafion-CMECo(Sep)³⁺ carrier matrix in Chapter 4, for which a chemically-based modification technique was applied, the results were significantly different. In the context of the explanative significance of these findings, the reader's attention is drawn to the following facts: Generally, the change in the chemical nature of the ionic domains associated with the nafion structure, is caused by the increasing uptake and incorporation of the cationic species, particularly in the case of compounds with hydrophobic ligands. This behaviour is caused by a change in polarity of the microenvironment surrounding a portion of the sulphonate groups from hydrated, inverted micelle type domains to a more hydrophobic, low dielectric medium. As the content of the counter-ion species increases, the ionic clusters become increasingly dehydrated and the quantity of the other linkages which penetrate into the polar interior of the ionic clusters decreases while the quantity of ether groups surrounded by the less polar regions of the ionomer increases. Hence, in this regard, the fundamental structural changes observed in accordance with the modified nafion microstructure, is in fact a good indication of the effective uptake of the counter-ion mediator species, which in turn signify the superior efficiency of the electrochemically-based technique, as opposed to the chemically-based, manual casting/mixing technique used in Chapter 4.

5A.4 Conclusions

The cationic species, $\text{Co}(\text{Sep})^{3+}$, was successfully incorporated into the microstructure of the pre-formed nafion film through potentiostatic electrochemical deposition method. Moreover, FTIR spectroscopic studies confirmed the incorporation of the $\text{Co}(\text{Sep})^{3+}$ species deep within the microstructure of the nafion membrane. In addition to this SEM analysis revealed that the formed composite has a exceedingly smooth consistency with a highly compact structure. In addition to this, results obtained from electrochemical investigations all pointed to a stably prepared electroactive film, which exhibited excellent electrochemical characteristics, particularly in terms of fast reversible electron transfer with the underlying electrode as well as stability and reproducibility. Compared to other pre-concentration methods involving metal-centred electroactive species, the technique applied in this study enabled the incorporation of the highest possible percentile of electroactive counter-ion species within the shortest possible time, with a Γ value of the incorporated counter ion species. Similarly, a fairly high obtained charge transfer diffusion coefficient, 2.64×10^{-7} , was evidence of a fast uptake of cationic species, as well as the ease of preparation using the proposed method.

CHAPTER 5B

N-terminally modified genetically engineered human recombinant P450-3A4 (nCYP3A4) biosensor for the determination of protease inhibitor ARV drug, Indinavir:



Abstract

A catalytically active N-terminally modified human recombinant CYP3A4 isoenzyme was successfully prepared through genetic engineering, as a catalytically active histidine-tagged N-terminally modified soluble construct. The active P450 content was corroborated with The catalytically active P450 content was confirmed by the absorption maximum of the reduced CO-bound complex at 450 nm. A reagentless mediated biosensor was constructed with cobalt(III) sepulchrate [Co(Sep)³⁺] as mediating species, integrated within the microstructure of a pre-formed nafion base film by potentiostatic deposition, and the prepared enzyme was used as the bio-recognition component. Stable enzyme immobilization was ensured by a combination of entrapment and encapsulation. In this regard, to ensure enzyme stabilization and retention of catalytic activity, the immobilized enzyme was encapsulated with a ionic hydrogel-composite membrane. The hydrogel was prepared through pre-blending, via the combination of agarose (Agrs) hydrogel with hydrophilic polymer, poly(vinyl alcohol) (PVA) and cationic polyelectrolyte, polyethylene amine (PEI). The combination of PVA and agarose, while the addition of PEI enabled the ionic cross linking of the biocompatible Agrs-PVA composite hydrogel, and thus confirming reduction in the swelling index of both polymers, while also inducing ionic cross linking of the polymers, thus ensuring a more stable insoluble hydrogel blend, with a porous meshwork that still freely allowed the diffusion of the substrates into the reagent layer. The prepared biosensor, GCE||naf|EI-Co(Sep)³⁺|nCYP3A4|Agrs-PEI-PVA, exhibited a low operating potential for oxygen reduction, determined as -365 mV. The biosensor successfully detected and quantified the selected model substrate, indinavir. In this regard, the biosensor showed a linear range between 2.183 x10⁻⁶ — 3.552 x 10⁻⁶ M, a sensitivity of 0.0349 $\mu\text{A } \mu\text{M}^{-1}$, while the LOD was determined as 59.72 mg L⁻¹. The LOD was shown to be of significance in the C_{Max} of the ritonavir-boosted regimen, as well as for poor metabolisers. Control experiments corroborated the bio-electrocatalytic response from the active enzyme.

5B.1 Introduction

The PI ARV, indinavir is given either by itself, or in association with booster-PI ARV, ritonavir. An important problem associated with the standard singular and/or boosted regimen is the manifold side effects, which is in direct relation to drug-induced toxicity, in association with the P450 3A4 first pass biotransformation pathway. Therefore, therapeutic drug monitoring (TDM) is always a highly recommended fundamental aspect of indinavir treatment, which normally involves blood samples taken and sent for analysis with standard centralized techniques by trained personnel — in effect boiling down to a tedious and expensive endeavour. However, the often overlooked, but clearly pivotal subject-area during such treatment regimes, is finding alternative, cheaper, decentralized techniques for TDM of indinavir and/or other HAART associated drugs. In fact, during the initial comprehensive literature survey, approximately one journal, focussing on cheaper alternative detection/quantification method for selected HAART drug, nevirapine, based on the development of a immunochromatographic (IC) strip test, was found [16]. In contrast, all other available literature focussed on enhancing centralized methods of detection and analysis, particularly, HPLC — a technique which in spite of its precision, is highly expensive, requiring tedious sample preparation with trained personnel. In this regard, biosensors is the only analytical device that have the potential to parallel the detection and quantification ability of these centralized methods, the difference here of course being a much more simplified analysis technique and real-time analysis. Moreover, due to the complexity and unique nature of CYP3A4 enzymes, substantially multifaceted electron transfer machinery is required to support this membrane bound, microsomal mammalian heme thiolate enzyme chemistry, and in this regard, the electrochemical platform provided by biosensor configurations can substitute for many of these needed components. On the other hand, genetically manipulated cells expressing single CYP genes/isoenzymes, can be an effective way of providing a continuous supply of biological recognition component for these biosensor platforms. In such configurations, an important

aspects is enzyme immobilization. In this regard, although immobilization methods for mammalian microsomal P450 isoenzymes are not as yet entirely well established, gel-entrapment has been documented as the least damaging to such enzymes and can even be used in methods when reusable enzyme-based sensor platforms are required. The high preference for hydrogel material is based on collective inherent favourable attributes, of which the most eminent include their considerable water imbibing ability, and soft consistency which is similar to natural tissue. In fact, hydrogels resemble natural living tissue more than any other class of (synthetic) biomaterials, and are thus considered highly biocompatible

In this study, the favourable interaction between the ionomer, nafion, and the $\text{Co}(\text{Sep})^{3+}$ mediating species was further explored and harnessed for utilization in the creation of alternative analytic tool for decentralized method of therapeutic drug monitoring, specifically aimed at selected HAART associated drug components. This was done through the creation of a sophisticated, robust reagentless-type mediated biosensor, prepared through the innovative combination of potentiostatic deposition technique, combined with genetic engineering technology and complimented by the application of three-dimensional biocompatible hydrogel blend-membrane creativity. In this regard, firstly a highly stable and reproducible electroactive carrier matrix was prepared through potentiostatic electrodeposition of $\text{Co}(\text{Sep})^{3+}$ onto a pre-formed nafion membrane, for which the results were presented and comprehensively discussed in Chapter 5A. Secondly, a reagentless, mediated enzyme-based biosensor was constructed, by using the heme domain of mammalian microsomal CYP3A4 (expressed as a catalytically-active histidine-tagged, N-terminally modified soluble construct) as bio-recognition component. In addition to this, stable enzyme immobilisation was ensured by its mild entrapment in an ionically-based three-dimensional hydrogel blend, consisting of agarose, polyvinyl alcohol and polyethyleneimine. In keeping with the main aim of the biosensor, the HAART associated protease inhibitor ARV drug, indinavir, was used as model substrate, in order to evaluate its performance in the detection and quantification of ARV drug

components. As elaborated in the **Prelude** of Chapter 5, a major aim of the current biosensor was to improve the characteristics of the $\text{Co}(\text{Sep})^{3+}$ biosensor (designed and created in the research investigation presented and discussed in Chapter 4), with particular reference to pre-determined aspects, of which the most fundamental was the following:

- Designing a reproducible method of preparation of the carrier matrix, especially in terms of preventing/alleviating pre-mature and/or long-term leaching of mediating species;
- Pre-concentrating a larger percentile of mediating species in the nafion microstructure to allow faster enzyme/electrode interaction at the shortest distance;
- Lowering the operating potential (to a less cathodic value), especially in terms of the reduction of dioxygen, which plays a pivotal role in the reaction cycle of nCYP3A4's electrocatalytic response to the substrate. Moreover a less negative oxygen reduction potential would also considerably alleviate any air-sensitivity/reactivity of the $\text{Co}(\text{Sep})^{3+}$ mediating species within the nCYP3A4-based biosensor configuration, a process that would strongly curtail the potential formation of reactive intermediate species that could affect the efficiency of the bio-electrocatalytic activity of the enzyme to oxygen and selected substrates ;
- Incorporating cheaper alternatives for selected reagent-layer components, sourced commercially.

On the subject of improving the operating potential with respect of reduction of dioxygen in particular — the results obtained for biosensor-platform1, presented and discussed in Chapter 4, was used as primary reference point, and as such obtained results on this factor was comparatively evaluated. Thus, with all the proposed criteria in mind, design and optimisation of the nCYP3A4-based biosensor with regard to major objectives and sub-problems were conducted accordingly.

5B.2 Structural aspects of the genetically engineered his₆-tagged N-terminally modified recombinant CYP3A4 (nCYP3A4)

Before commencing with presentation and discussion of the electrochemical results, the synthesized nCYP3A4 enzyme was subject to specific characterization studies, to verify and corroborate certain characteristics associated with CYP450 enzymes, for which the results are subsequently presented and discussed.

In general, cytochrome P450 (CYP450) enzymes, in their naturally oxidised resting state, portray inherently unique trait-specific conformational and/or structural features, which are easily distinguishable by specific complimentary in-situ/ex-situ spectrophotometric, spectroscopic and/or biophysical techniques. Moreover, in their reduced and/or excited state, these enzymes undergo characteristic conformational changes which are also discernible through the application of such complimentary methods. The significance of such techniques also allows experimenter to assess the success of expression/synthesis methods used for preparation of these enzymes with genetic engineering, since secondary/tertiary enzyme structure exhibit unique characteristics, which are easily determined by these methods. In this regard, depending on the specific purpose, there are a number of possible techniques that can and have been applied, which include Fourier transform infrared (FTIR) spectroscopy, Ultraviolet-Visible (UV-Vis) absorption spectroscopy, Circular dichroism (CD), Resonance Raman spectroscopy. In the interest of the scope of this dissertation however, only results for FTIR and UV-Vis spectroscopic analysis are shown and discussed, since these two techniques are basic exploration methods which can provide sufficient information regarding the secondary structure of CYP450 enzymes. For a more comprehensive outline regarding the structure-function and other biophysical properties of these enzymes, the reader is encouraged to read the PhD dissertation of Natasha Beeton-Kempton .

5B.2.1 Fourier transform infrared spectroscopy (FTIR) characterization [151-152]

The characteristic shape and positions of amide and/or other bands observed in FTIR spectrum can be used as fingerprint identification of enzymes/proteins, while simultaneously providing information on the secondary structure of the polypeptide chains of these compounds, and as such, is an age-old, invaluable tool for studying their structure-function relationships. In this regard, FTIR spectroscopy was used for conformational studies of the prepared enzyme (nCYP3A4), of which the results are exhibited in the spectrum shown in **Figure 5B.1**. Before commencing with the discussion of the observed results, an important noteworthy factor should first be brought to the reader's attention: Generally, in principle, in FTIR analysis of CYP450 and/or other heme proteins, all of the components in the sample contribute to the observed spectrum. This essentially means that the full spectrum, as obtained from the original FTIR scan, consist of absorption bands from (i) the surrounding apo-protein part; (ii) the heme (prothetic group) component and heme ligands; (iii) interactions between the heme and the surrounding apo-protein; and (iv) the water and other components of the buffer solution, particularly those from the phosphate group. Thus considering the aforementioned aspects, with regard to the results exhibited in **Figure 5B.1** — the inset shows the full spectrum as obtained from the original FTIR scan, whereas the main graph is an enhanced graphical presentation of the relevant absorption bands restricted to the components of enzyme itself, i.e., the spectral region of 2200 cm^{-1} to 1300 cm^{-1} .

In terms of specific band assignments, firstly, the distinctive absorption band marked as $\pm 1630\text{ cm}^{-1}$, may be attributed to overlapping contributions from the surrounding apo-protein groups (protein component), as well as heme associated groups. With regard to the protein component in particular, it may be ascribed to the Amide I band, primarily from the stretch vibration of the peptide C=O. With regard to the

contribution from the heme, on the other hand, it may be ascribed to the C=C stretching from the vinyl group in the protoporphyrin IX (Normally, distinctive porphoryn vibrational modes are difficult to detect in isolation, because of their low intensity and their overlap with amide bands from the surrounding apo-protein). Secondly, the smaller and much less distinctive band, highlighted at position $\pm 1459 \text{ cm}^{-1}$ may be attributed to the Amide II absorption band, of which the latter arises from N-H bending coupled with C-N stretching. According to documented reviews, the positioning of this particular band is normally centred around $\pm 1550 \text{ cm}^{-1}$, however, FTIR reflects the degree and strength of hydrogen bonding, a phenomenon which is known to be strongly influenced by sources other than changes in the protein secondary structure, including different sampling techniques, the surrounding water- and other molecules from the protein storage solution; stress factors such as lyophilisation of the protein, etc. These constricts, thus essentially shifts the modes to higher/lower frequencies, and as such, the results within this research investigation are well within experimental variability. The absorption band positioned at $\pm 1328 \text{ cm}^{-1}$ may be ascribed to the protein-associated Amide III band, while the other bands of equally small intensity in the surrounding area (highlighted by red arrows), can be ascribed to the α -helices and β -sheets as induced by the protein secondary structure, as well as the infrared absorption of amino acid side chains.

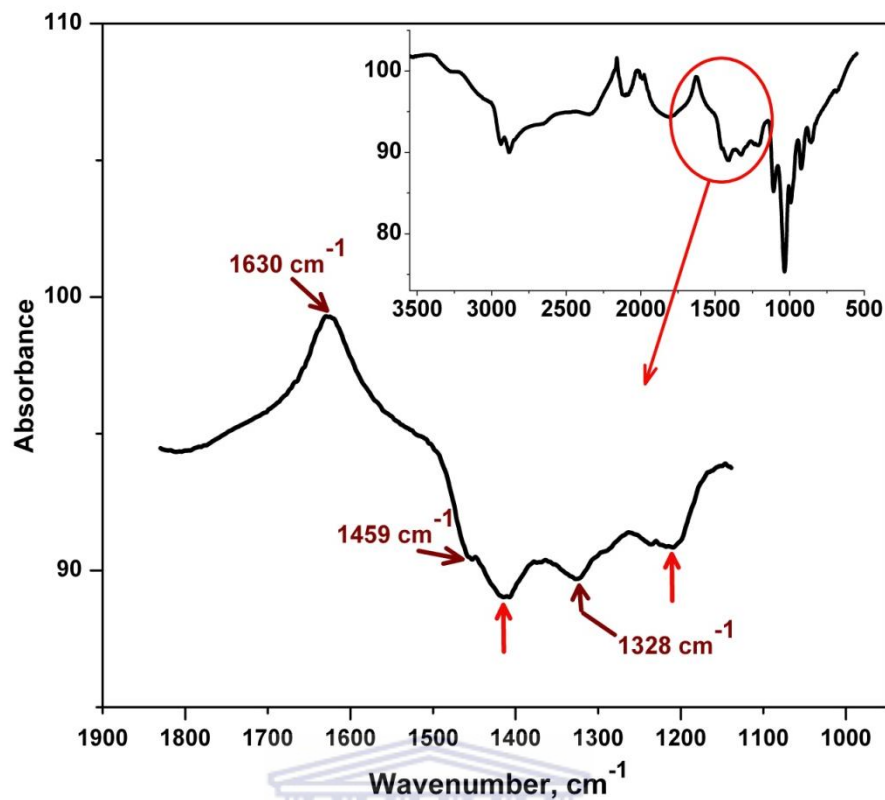


Figure 5B.1 Fourier transform infrared (FTIR) spectra of the pure synthesized N-terminally modified CYP3A4 construct (nCYP3A4). Inset shows full spectrum as obtained directly from FTIR analysis. Main spectrum shows the relevant spectral range for bands associated solely from nCYP3A4, restricted to the region of 1830 cm⁻¹ – 1140 cm⁻¹.

5B.2.2 Spectrophotometric characterization: UV-Vis Spectroscopy

The inherent advantage of the presence of the spectroscopically rich heme in the active site of CYP450 enzymes can easily serve as an in situ probe – exhibiting characteristic visible and near-ultraviolet absorption band changes for recognition of protein, and in association with interaction of the protein/enzyme with various effectors [153-154]. In this regard, the results of the UV-Vis analysis of the synthesized CYP450 3A4 enzyme (nCYP3A4), are shown in **Figure 5B.2(a) and (b)**. **Figure 5B.2 (a)** in particular, is the absolute UV-Vis absorption spectrum of the pure, substrate-free nCYP3A4, from which a distinct peak with a Soret maximum (λ_{\max}) at

424 nm is observed. This is essentially characteristic of P450 enzymes in their resting state and as such, exhibits a low-spin state of the water-ligated six-coordinate heme, in which the heme-iron is in its ferric (Fe^{III}) oxidation state [83, 155-156]. No additional shoulder peak at ~ 390 nm can be observed, which, if present, would have indicated a mixed spin heme, of which a proportion would be in the high-spin state. Moreover, the smaller shoulder peak and two slightly broad troughs, located at ± 358 , 536 and 570 nm, respectively, exhibits spectral properties typical for members of the P450 enzyme class, and as such, are always observed in $\text{CYP450}_{3\text{A}4}\text{-Fe}^{\text{III}}$ absolute spectra [153, 155-156]. Moreover, these peaks may be attributed to the intrinsic apoprotein absorbance of the surrounding protein molecule, thus confirming the overall structural integrity of the synthesized enzyme construct. In terms of specific classification, these peaks may be ascribed to the δ -band (358 nm), α -band (570 nm) and the β -band (536 nm), respectively. Reduction of the $n\text{CYP3A4}$ enzyme and addition of carbon monoxide (CO) gave the characteristic $\text{CYP450}_{n3\text{A}4}\text{Fe}^{\text{II}}\text{-CO}$ band, exhibited in the difference spectrum with a Soret maximum at ± 449 nm, as shown in **Figure 5B.2 (b)**. With regard to the displayed $\text{CYP450}_{n3\text{A}4}\text{Fe}^{\text{II}}\text{-CO}$ complex, the structure of CYP450 enzymes is such that, in general, the enzyme's prosthetic group is constituted of an iron(III), protoporphyrin-IX which is covalently linked to the surrounding apoprotein by the sulphur atom of a proximal cysteine (see **Figure 1.2 a and b, Chapter 1**) [22-24, 72]. Moreover, the catalytically active conformational state of these enzymes are guaranteed/corroborated by the presence of the aforementioned specific thiolate bond between the heme iron and the highly conserved cysteine residue (the fifth ligand of the heme), of which such an active state may be spectroscopically identified as a reduced $\text{CYP450Fe}^{\text{II}}\text{-CO}$ complex [21, 23-24, 137] (formed upon reduction of the heme iron and exposure to CO gas), as shown in **Figure 5B.2 b**. Thus in essence, the UV-Vis absorption spectrum shown for the reduced CO-complex of the prepared enzyme is very significant, since it contributes to the corroboration of the success of the preparation of a catalytically active enzyme construct [72, 156-158].

On the other hand, still on the subject of the CO-difference spectrum, it is noteworthy to also add, that the full spectrum (shown in **Figure A-1, Appendix A**) also exhibited an additional absorbance peak at ± 419 nm, albeit a peak maxima of smaller intensity, as compared to the P450 peak. This is also a finding that requires its own merit of attention, since ideally, the carbon-monoxide difference spectrum produced from reduction and CO treatment of pure catalytically active; CYP450 enzymes should produce an ‘abrupt’ absorption maximum, with no additional peaks at 420 nm [24, 72, 159]. Observation of a peak at 420 nm in this context, would thus imply a proportion of the protein being denatured [24, 72, 83, 156]. Based on the aforementioned criteria, such a result, as it stands, imply that the synthesized enzyme contains a mixture of spectral species – with a proportion being in its native catalytically active state, and a proportion being denatured. That being said, based on documented findings regarding genetically engineered N-terminally modified soluble CYP450 constructs and other constricts known to contribute to trouble shooting in this area in such enzymes, the reader is cautioned to consider the following [24, 158-159]:

- Prior research has shown that mammalian microsomal P450s, particularly CYP3A4 has a rather unstable conformational nature, with the enzyme easily being denatured during treatment with various effectors. In fact, it has been shown that research has shown that the P450-complex in these enzymes are unstable, with P450 very easily converting to the inactive P420 form within minutes of formation of the complex. Similarly, the agitation brought about by excess dithionite treatment and/or CO bubbling also can cause distortion/loss of the heme-thiolate ligation, which in effect will cause denaturing of the protein.
- The sensitivity of N-terminally modified CYP450s as compared to their full-length wild-type enzyme equivalents are generally well known – the protein structure being easily disconcerted, and as such, easy loss of cystein ligation could be an artefact of the genetic engineering process.

- To obtain sufficient yields of soluble purified protein, the application of detergents during the genetic engineering process is crucial, however, it has been documented that they do have a percentile of destabilising effect on the so produced enzymes, thus once again enzyme sensitivity with loss of cyteinate could be an artefact of the preparation process.

Based on the preceding facts, it is evident that the number of constricts could have contributed to the inactive 'P420 form' during CO studies. Nevertheless, the results does indeed show structurally intact, catalytically active native enzyme construct. Moreover, the sensitivity of the so produced enzyme construct is not uncommon, since all proteins/enzyme suffer a percentile of this fate, which is always taken into consideration during biosensor construction, particularly in terms of optimum immobilization and coupling efficiency.

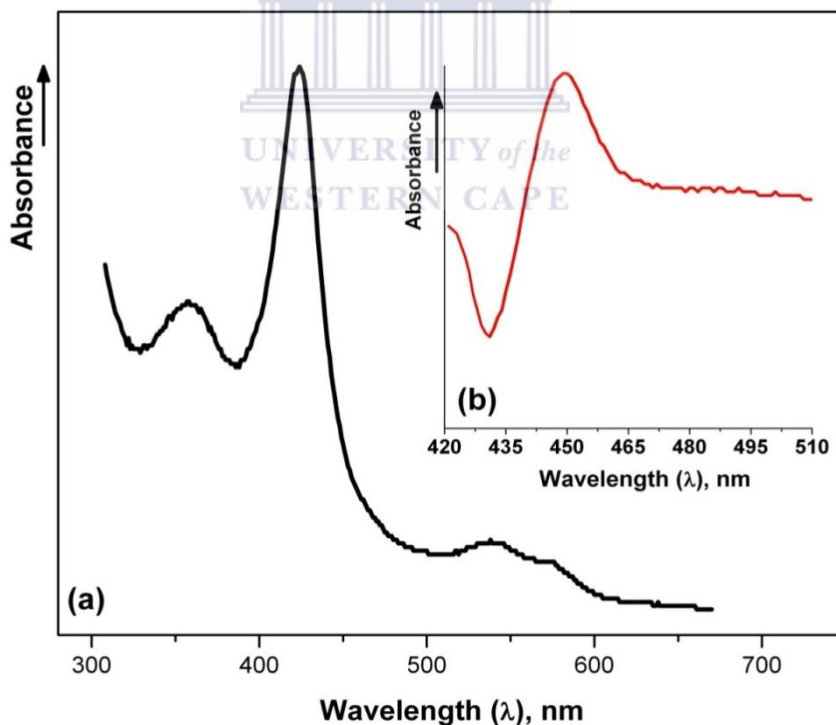


Figure 5B.2 Electronic absorption spectra for the synthesized, N-terminally modified CYP450 3A4 (nCYP3A4). The UV-Vis absorption spectrum for pure nCYP3A4 (concentration μM) showing (a) nCYP3A4 in its resting low-spin Fe^{III}

state; inset (b) nCYP3A4-Fe^{II}-carbon monoxide, prepared by reducing nCYP3A4Fe^{III} with excess sodium dithionite and saturating with CO by bubbling for 2 min. Spectra in (b) were difference spectra taken against references of reduced nCYP3A4 before addition of CO. Working solution of nCYP3A4 was 20 mM potassium phosphate buffer, pH 7.40, 20% glycerol, EDTA, DTT.

5B.3 Assembly and electrochemical characterization of the hydrogel-based enzyme biosensors prepared on glassy carbon electrode

5B.3.1 Electrode Assembly: Optimisation of the variables concerning the indinavir amperometric biosensor assembly and behaviour

5B.3.1.1 The effect of carrier matrix assembly: Optimisation of constituents and method of preparation

With the ‘research spotlight’ on the main objectives and sub-problems for the current investigation, as elaborated in the Prelude of Chapter 5, as well as the aspects highlighted in the introduction of the current chapter — the investigation in the initial studies were focussed on three important aspects during the biosensor construction. Firstly, the feasibility of using the poly(ester sulphonic acid) cation exchanger, Eastman-AQ55 (EAQ), as cheaper alternative to the more expensive nafion membrane as base film was explored. Secondly, in the quest to design a more, reproducible method of preparing the electroactive carrier matrix composite, the Co(Sep)³⁺ mediating species was incorporated into the EAQ through electrochemical deposition. With regard, to the time aspect of the potentiostatic deposition process in particular, an electro deposition time of 1200 s was regarded as an optimal period to

accumulate sufficient mediating species within the pre-formed polymer film. The selection was based on a series of experimental trial investigations in which the stability of the background signal was evaluated. In the third aspect, the investigation of a suitable aqueous biocompatible hydrogel as outer layer, instead of the more expensive nafion film was conducted. In this regard, as an initial possible replacement, the hydrophilic, non-toxic, biocompatible polymer, poly(vinyl alcohol) (PVA) was evaluated. However, PVA has a considerably high swelling index and dissolves readily in water when not cross-linked, and as such, during the fabrication of the biosensor, the PVA was cross-linked with glutaraldehyde (GA) under acid catalysis, denoted cIPVA. (A comprehensive step-wise description of the experimental protocols used in the preparation of the biosensor is elaborated in **Section 5B** in the current chapter.) As a sensitivity criterion, the prepared biosensor, denoted GCE||EAQ|Co(Sep)³⁺|nCYP3A4|cIPVA, was evaluated with regard to the stability of the prepared platform, as well as electrocatalytic response both in terms of the enzyme's co-substrate (i.e. molecular oxygen, O₂) and the substrate (indinavir), paying particular attention to the operating potential for electrocatalysis.

The obtained results for the GCE||EAQ|Co(Sep)³⁺|nCYP3A4|cIPVA biosensor is exhibited in **Figure 5B.3**. In the first aspect, the stability of the reagent-layer coating was evaluated both visually (i.e. by observing the integrity of the coating in the aqueous buffer electrolyte) and voltammetrically (i.e. by observing the stability and reproducibility of the obtained voltammetric signals). When the prepared biosensor was placed in the argon-degassed electrolyte buffer, the film took on an opaque appearance, also exhibiting a substantial amount of swelling, a finding which is characteristic of EAQ-coatings and in agreement with previous studies. However, upon close visual examination, a sizeable percentage of reagent-layer component leaching could be seen after initial placing of the biosensor in the electrolyte solution. Moreover, the film appeared unstable. These observations were in fact mirrored by the voltammetric behaviour exhibited by the biosensor, as shown in **plot I** of **Figure**

5B.3. In this regard, the obtained cyclic voltammograms showed a distinct decrease in $I_{p,c}$ and $I_{p,a}$ in direct accordance with increased equilibration time, observed during repeated cycling, a phenomenon which lasted at least 50-60 min after initial placing in the electrolyte. In terms of magnitude, the highest decrease in I_p was seen in terms of the cathodic peak current, and thus points to the loss of electroactive $\text{Co}(\text{Sep})^{3+}$ species from the reagent layer (which is pre-concentrated in the oxidized form) — essentially meaning that with each scan, there are less available $\text{Co}(\text{Sep})^{3+}$ for reduction. Similar observations and findings regarding leaching behaviour and instability of EAQ-films have been observed in previous research investigations [160]. In terms of a plausible explanation for the current investigation, these observations can perhaps be explained in terms of the literature-based unique structural aspects of Eastman AQ. Firstly, EAQ is known to take up huge amounts of water, swelling to 4-5 times its original dry volume after hydration [161-162]. In fact EAS films with or without electroactive and/or enzyme species have been shown to contain at least 87% water, following hydration after being placed in electrolyte solutions. Moreover, EAS films, in their characteristics, have been compared to biomembrane-like surfactant-based films, of which the latter is known to exhibit fragility in aqueous solutions, while also showing a certain degree of leaching behaviour after initial equilibration. In a comparative context, swelling in nafion membranes are not that extensive, with dry films shown to contain only up to approximately 28% after soaking in aqueous solutions [161]. In addition to this, and perhaps more importantly, with regard to the uptake and pre-concentration of cation species, research has shown that, EAQ has other inherent structure-functional features that are distinctly different from those observed for nafion: Firstly, AES's method of cationic retention/pre-concentration, occurs largely in accordance with the Gibbs-Donnan equation, which essentially means that ionic charge, and as such electrostatic binding, rather than hydrophobic interactions plays the determinant role in cationic retention [163]. With nafion on the other hand, counter ion retention/pre-concentration is dictated by hydrophobic interactions, whereas the Gibbs-Donnan equation does not play a role with this polymer [118-119]. Moreover, based on

documented literature, transport in accordance with the Donnan equilibrium is a one dimensional process, which would be the case in EAS, whereas in the case of nafion, who does not comply to the Donnan equilibrium, transport is a three dimensional process [118-119]. This of course has highly significant implications, since it would mean faster charge transport in the case of electroactive platforms created with nafion, as compared to the use of EAQ. The general implications of these factors, points to nafion being far more superior for application in the current purpose, as opposed to EAQ. Thus, cumulatively, all of aforementioned literature-based factors gives some insight into the observed instability with regard to the GCE||EAQ|Co(Sep)³⁺|nCYP3A4|cIPVA biosensor.

The next aspect was of course the evaluation of the electrocatalytic response of the GCE||EAQ|Co(Sep)³⁺|nCYP3A4|cIPVA biosensor, the results of which is shown in **plots II and III** of **Figure 5B.3**. In this regard, plot II shows the cyclic voltammetric responses of the prepared biosensor in argon-degassed phosphate buffer solution (pH 7.45) (a); in response to dissolved oxygen (b); and in response to 0.5 μM indinavir (c). Indeed in the presence of molecular dioxygen, the reduction peak was distinctly augmented by the marked increase in peak current caused by the catalytic response of the immobilized enzyme to its co-substrate oxygen, and a concomitant decrease in $I_{p,a}$. Similarly, the response to indinavir was signified by a further increase in the $I_{p,c}$ and accompanied by a further decline in the $I_{p,a}$. These results were corroborated by the square wave voltammetric response of the biosensor in the presence of oxygen and indinavir, as shown in **plot III** of **Figure 5B.3**. These results are characteristic behaviour of CYP450 enzymes, and thus suggest the reduction of oxygen by the reduced heme iron (i.e. Fe^{II}), a reaction which is increased in the presence of the substrate, as shown by the additional $I_{p,c}$ increase in response to indinavir. Having said, analysis of the obtained voltammetric results revealed that oxygen reduction occurred at an average operating potential of -650 ± 10 mV, while, average response to indinavir occurred at $-630 (\pm 15)$ mV. In this regard, the operating potential attained with this biosensor is quite high, in fact, reduction of oxygen and substrate

detection both occurred at more cathodic potentials, as compared the results obtained for biosensor platform1, presented in Chapter 4 (CGE|naf|CMECo(Sep)³⁺|flCYP3A4|naf), for which reduction of oxygen occurred at an average E_p of $-600 (\pm 5\text{mV})$, while the average operating E_p for the substrates was -585 mV for erythromycin and $-590 (\pm 5\text{mV})$ for 2,4-dochlorophenol (as determined from SWV), respectively. Moreover, a more cathodic potential can increase the likelihood of reactive oxygen intermediate species, such as superoxide anion and H_2O_2 , through a process known as uncoupling reaction, which in itself could have contributed to the observed increase in $I_{p,c}$. (More on this subject and a deeper insight into the process of oxygen reduction is given in **Section 5B.3.3.1.1** of the current chapter). Moreover, the obtained electrochemical and electrocatalytic response did not exhibit sufficient reproducibility, which could be due to a combination of the instability and leaching incurred by using the EAQ as base layer, as well as the acid-catalyzed cross-linking of the PVA, of which the latter could have negatively impacted the integrity of the delicate enzyme. With regard to the latter constrict, CYP3A4 constructs produced through N-terminal modification is generally known to be more sensitive than its wild type full-length counterpart, and as such, reagent layer preparation methods needs to be mild enough as to ensure the absolute integrity of the immobilized enzyme, as to obtain the highest possible activity for the longest possible time. In this regard, a more stable crosslinked PVA film was only possible if the acid-catalyzed glutaraldehyde crosslinking was done after casting of the PVA on the electrode surface, so it is possible that, although extreme care was taken, some of the active cast enzyme units could have been affected by the residual traces of acid.

On a final note, in keeping with the original objectives, as outlined in preceding sections in this chapter, in light of the instability and leaching behaviour incurred by the fragile nature of the EAQ-film, as well as the high operating potential, and the non-reproducibility of the signal obtained, the method of biosensor preparation based on the using EAQ in creating the current platform was not taken forward.

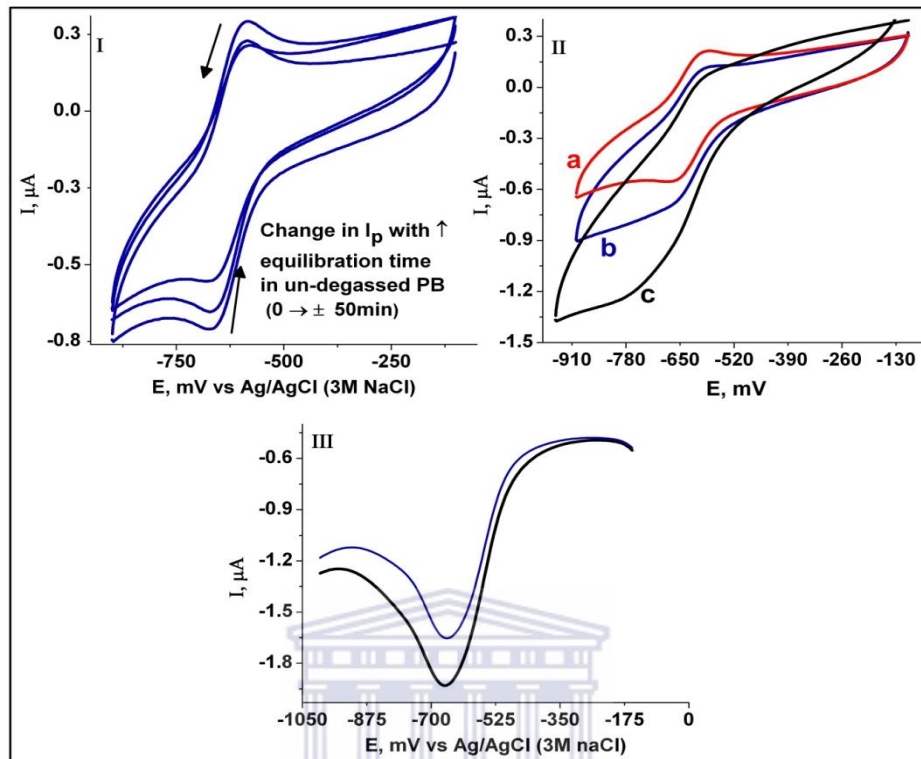


Figure 5B.3(I-III) Voltammetric behaviour and electrocatalytic response of the nCYP3A4-based biosensor, fabricated from Eastman AQ(EAQ)-Co(Sep)³⁺ carrier matrix (i.e. GCE||EAQ|Co(Sep)³⁺|nCYP3A4): plot I: CVs illustrating the biosensor in argon-degassed phosphate buffer solution (ArPBS) with increased equilibration time; plot II: cyclic voltammetric response of the biosensor in ArPBS (a), in the presence of dissolved oxygen (b), in the presence of 0.5 μM indinavir in un-degassed PBS (c); plot III: square wave voltammetric response to dissolved oxygen (b) and indinavir (c). Co(Sep)³⁺ was pre-concentrated on pre-formed ionomer ionic polymer (nafion or EAQ film, respectively) by potentiostatic deposition at +450 mV. Arrows show the trend of the variation in peak current.

With it now clear that the compromise on nafion as base layer may not be a suitable route for improving on the Co(Sep)³⁺-mediated biosensor, the next step was to re-strategize the biosensor design to further explore and optimize on this variable. In this regard, the biosensor was fabricated by following the same general protocol as used for the EAQ-Co(Sep)³⁺ platform, but with nafion as base matrix. The fabricated biosensor is denoted, GCE|naf|EI-Co(Sep)³⁺|nCYP3A4|cIPVA. Indeed, the obtained

results, both in terms of general voltammetric response, particularly with regard to the stability of the signal response showed by the biosensor, as well as electrocatalytic response, proved to be a definite improvement as compared to the results obtained for the EAS-platform. **Figure 5B.4** shows the voltammetric response of the GCE||naf|E|Co(Sep)³⁺|nCYP3A4|cIPVA biosensor, prepared with the electroactive nafion-Co(Sep)³⁺ composite as carrier matrix, in which Co(Sep)³⁺ potentiostatic electrodeposition was done for 1200 sec. The results presented are for an experiment conducted in argon-degassed PBS, at 5 mV s⁻¹. Thus, when the GCE, coated with the complete reagent-layer film components were placed in argon-degassed buffer solution, repetitive scanning revealed a single redox couple, exhibiting a stable background current, consisting of a cathodic and anodic peak, with an overall E° determined as -600 (± 3) mV. Moreover, the integrity of the coating remained stable in the aqueous electrolyte buffer, exhibiting negligible leaching behaviour. In addition to this, the stability of the background I_{p,c} and I_{p,a} signal remained stable throughout the equilibration time, i.e., from initial placing in the buffer up to 60 min, exhibiting a very small, almost negligible increase in I_{p,c} and I_{p,a} in association with increased equilibration time.

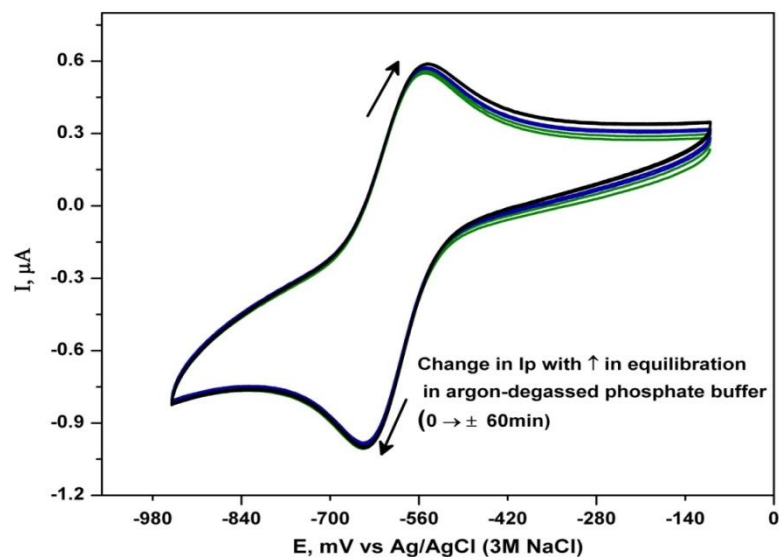


Figure 5B.4 Cyclic voltammetric response of the GCE|naf|Ei-Co(Sep)³⁺|nCYP3A4|cIPVA biosensor in argon-degassed PBS, showing $E_{p,c}$ and $I_{p,a}$ variation with increased equilibration time, from 0 up to 60 min. Arrows show the trend of the variation in I_p .

The electrocatalytic response of the biosensor was also investigated, of which the results are shown in **Figure 5B.5 I–II**. In this regard, in **graph I, plot (a) – (c)** shows the cyclic voltammetric response of the biosensor in argon-degassed PBS; in the presence of dissolved oxygen in the PBS containing no indinavir; and in un-degassed PBS containing 22.45 μM indinavir, respectively. Thus as shown in **plot (b)**, the interaction with dissolved oxygen is signified by a marked increase in the cathodic peak current ($I_{p,c}$) and associated decrease in the anodic peak current. In this regard, these results therefore suggest the rapid interaction of the electrochemically generated CYP3A4Fe^{II} with dioxygen, followed by the reduction of the CYP3A4^{II}-O₂, as such, leaving a very small amount of the reduced heme Fe^{II} species available for re-oxidation, during the reverse scan, hence the significant decrease in $I_{p,a}$ in the reverse scan.

The presence of indinavir, increases the rate of oxygen binding and subsequent reduction, as shown by the dramatic increase in $I_{p,c}$ in response to 22.45 μM indinavir. In terms of the specific operating potential, the biosensor response to

molecularly dissolved oxygen was determined to occur at an average E_p of $-615 (\pm 10)$ mV, whereas the response to indinavir occurred at an average of $-595 (\pm 10)$ mV. The response of the biosensor to increasing indinavir concentrations was also evaluated and in this regard, **Figure 5B.5 II** shows the dependence of current change on increasing concentrations from 0.05 up to 96.95 μM indinavir. A linear calibration curve was also constructed, as shown in the **inset of Figure 5B.5 II**, which reveals a linear concentration range from $2.15 \times 10^{-6} - 18.25 \times 10^{-6}$ M ($r = 0.9903$) and a sensitivity of $0.02932 \mu\text{A} \mu\text{M}^{-1}$.

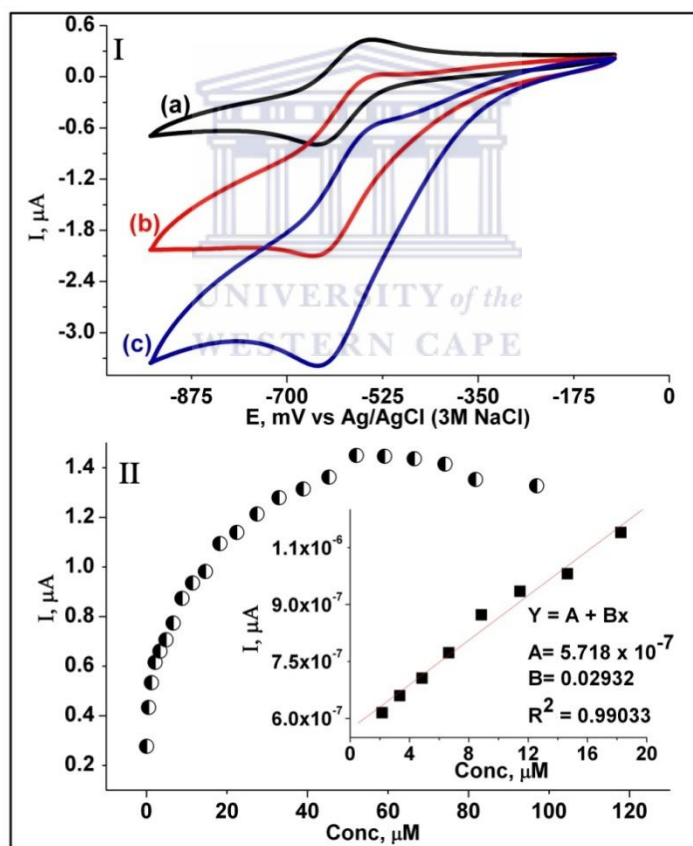


Figure 5B.5 (I): Voltammetric response of GC[naf]E1-Co(Sep)³⁺[nCYP3A4|Cl-PVA electrode in (a) argon-degassed PBS; (b) un-degassed PBS; OxPBS containing 22.45 μM indinavir. **(II):** Biosensor response to indinavir at concentrations ranging from 0.05 up to 96.95 μM . Inset shows the linear calibration curve for the biosensor.

5B.3.1.2 Outer layer optimisation: Effect of film constituents and/or ratio

The school of thought here, was to create a biocompatible composite film, for which low-melting point agarose served as the base component, while polyvinyl alcohol (PVA) and polyethyleneimine (PEI) functioned as enhancing/supporting components. The overall emphasis was to provide a mild entrapment-based outer layer for the nCYP3A4-derivatized biosensor platform. These components were comprehensively evaluated in terms of their own merit, as well as their contributory factor in combination, paying particular attention to their optimum working-performance- ratio. The evaluation criterion for optimisation on this particular variable was done firstly, with regard to efficient reduction of oxygen, and secondly, in terms of substrate interaction, paying particular attention to achieving the lowest operating potential. With regard to PEI in particular, its inclusion in hydrogel blend membranes enables the effective formation of polyion complex membranes, which exhibit a high degree of stability and structural strength [164-165]. In fact, according to documented findings, it has been shown to improve the sensitivity and other enzyme-based biosensor performance factors, by favourable modification of the electrochemical properties, as well as the stability and activity of the biocomponents, if included in the reagent-layer film preparation [74, 121]. However, establishing the correct ratio of PEI in association with the other components of the outer layer film was a critical aspect. In the initial evaluation, a ratio for PEI:PVA-Agrs of above 0.2 : 1, substantially impeded the electrochemical interaction of the mediating species with the underlying electrode, as well as its concomitant interaction with the immobilized nCYP3A4 in the reagent layer. In this regard, **Figure 5B.6** shows the obtained voltammetric response for a biosensor, based on a 0.25 : 1 ratio of PEI:PVA-Agrs. In argon-degassed PBS shown in plot (a), a CV consisting of only an oxidation peak centred at -560 mV, while no observable reduction peak could be seen. This essentially suggests the difficulty of the required electrochemical reduction of the

Co^{III} metal ion within the mediating species to the required Co^{II} , which in turn, is necessary to effectually reduce the heme iron of the immobilized enzyme ($\text{Fe}^{\text{III}}/\text{Fe}^{\text{II}}$). In effect, this phenomenon will of course concomitantly negatively affect the bioelectrocatalytic ability of the immobilized enzyme, due to the inability of generating the necessary active oxidation-state conformation in order to initiate its catalytic reaction cycle. Indeed as shown in **Figure 5B.6 (b)**, which represents the response of the biosensor to molecular oxygen in un-degassed PBS, for a scan taken after a 60 min equilibration time in oxygenated PBS, no observable reduction peak current is seen. Oxygen is the co-substrate of CYP450 enzymes, and interaction of the reduced enzyme with molecular oxygen encompass a catalytic-type interaction, a phenomenon which, from an electrochemical perspective, is signified by an additional cathodically-based catalytic current [74, 83]. Moreover, still on this subject, an observable electrocatalytic response to molecular oxygen could only be seen after an equilibration time of at least ± 210 min (i.e. ± 3.5 h) in un-degassed PBS, as shown in the inset in **Figure 5B.6**. The implications of these results of course points to the impracticality of applying this particular ratio of PEI in the blend hydrogel outer-layer membrane, and as such, the ratio had to be appropriately adjusted. On the other hand, let us draw our attention to the providing a plausible explanation for the aforementioned exhibited unfavourable biosensor responses. PEI is a cationic hydrophilic polymer, which essentially contains a high density of reactive primary, secondary and tertiary amine functional groups. In this regard, within the right setting, under optimized conditions, these reactive groups can confirm ionic cross-linking with the functional groups of PVA through ionic complexation between the cationic group (NH_3^+C) of PEI and anionic group ($-\text{CO}^{2-}$) of PVA and/or other hydrogel-blend membrane co-constituents, to form a structurally stable hydrophilic blend membrane, that effectively allows the permeation of water molecules and associated analyte/ions contained within the surrounding solution. Moreover, the presence of PEI can induce a small degree of plasticisation of the polymers within the blend [164], a factor that can prove favourable, particularly in terms of increasing selectivity of fabricated biosensor.

On the other hand, if the ratio of PEI is too high, as compared to that of the other components, the cross-linking reaction may be intensified by the multifold increase in available functional moieties, resulting in excessive reduction in the proximity of the polymer chains with respect to each other, thus producing a very rigid membrane, which in turn highly restricts movement of reagent-layer constituents, as well as impeding diffusion of analyte species.

Interestingly, upon interaction of the biosensor with indinavir, the electrocatalytic response was dominated at operating potential in the region of -660 mV, which was accompanied by a measurable concentration of H_2O_2 , as determined from the reagent layer through *quantofix* peroxide sticks. The significance of this finding is quite pivotal, since as will be shown in subsequent sections (electrocatalysis section), this is in fact related to the autooxidation of the enzyme and the formation of uncoupling reactions.

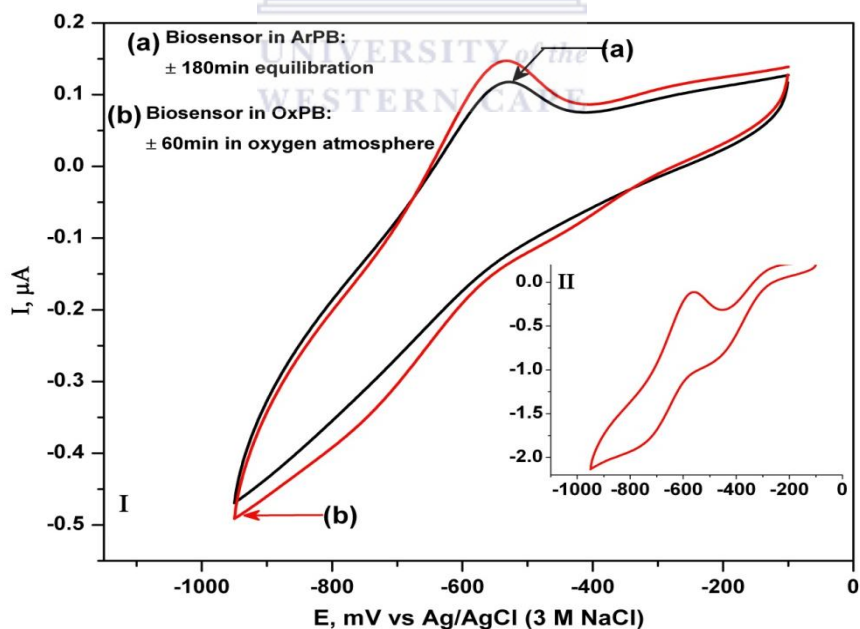


Figure 5B.6 Voltammetric response of GC|naf|El-Co(Sep)³⁺|nCYP3A4|PVA-PEI-Agrs electrode in: (a) argon-degassed PBS (ArPBS); (b) response after 60min equilibration in aerobic conditions (OxPBS); and after ± 210 min in OxPBS (II). Note: The outer layer of the biosensor is prepared with a ratio of PEI : PVA-Agrs of

0.25 : 1 (v/v). Experimental conditions: CVs taken in PB, pH 7.4 at 10 mV s^{-1} ; reductively scanned: $E_i = -100 \text{ mV}$, $E_f = -950 \text{ mV}$.

Figure 5B.7 shows the obtained voltammetric response for a biosensor, based on a 0.1 : 1 ratio of PEI:PVA-Agrs. Indeed, the exhibited electrochemical behaviour is distinctly different from that observed previously in **Figure 5B.6**. In this regard, in argon-degassed PBS, a cyclic voltammogram consisting of a single set of fairly symmetric cathodic and anodic peak currents, with an average E_m of approximately $-617 (\pm 5) \text{ mV}$ is observed. Moreover, the $I_{p,c}$ and $I_{p,a}$ increases gradually with increasing equilibration time, up to about 50 min, after which a steady state CVs were obtained, as observed with subsequent cycling. The electrocatalytic response of the biosensor to dissolved molecular oxygen was also investigated, from which the results are shown in the inset of **Figure 5B.7**. As can be seen, the presence of oxygen, signified by a dramatic increase in $I_{p,c}$. Moreover, this is accompanied by a fundamental augmentation of the $I_{p,c}$, due to the appearance of a single new peak centred at $-445 (\pm 5) \text{ mV}$, while the $I_{p,a}$ completely disappeared. These results suggest the rapid binding and reduction of dioxygen, catalyzed by the reduced immobilized nCYP3A4. When compared to the results obtained for bio-electrocatalysis exhibited by the biosensor platform in Chapter 4, the overpotential was reduced by at least 135 mV, whereas in terms of the results shown in aforementioned sections within the current chapter, the overpotential for oxygen reduction was reduced by between 180 – 200 mV. Thus, based on the favourable results shown by the biosensor, this fabrication method was taken forward.

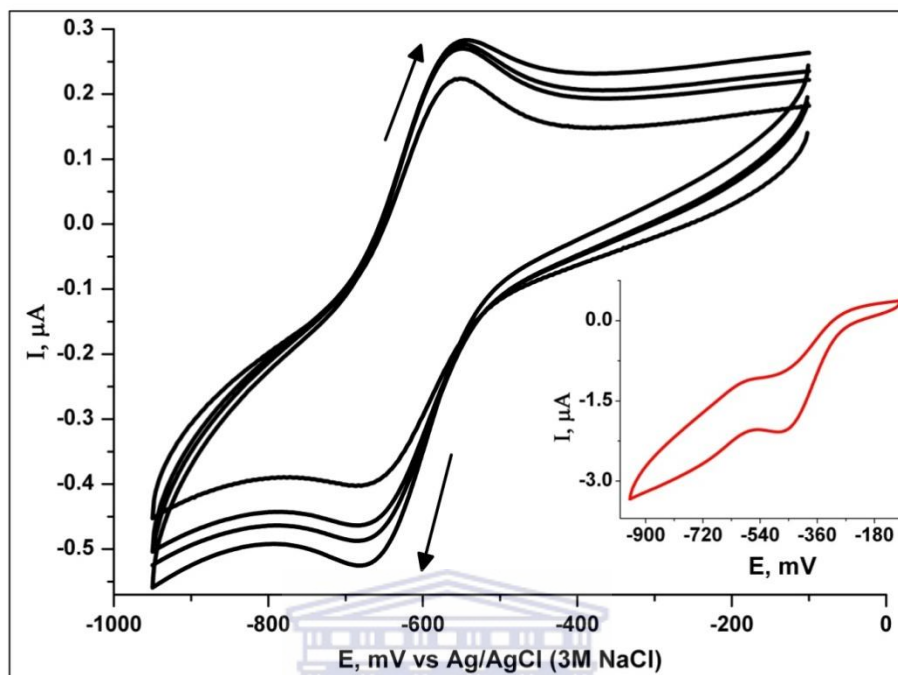


Figure 5B.7 Voltammetric response of GC|naf|EI-Co(Sep)³⁺|nCYP3A4|PVA-PEI-Agrs electrode in: (a) argon-degassed PBS (ArPBS); inset: response to dissolved molecular oxygen in aerobic conditions; Parameters: Ratio of biosensor outer-layer (PEI:PVA-Agrs) = 0.1 : 1 (v/v). Experimental conditions: CVs taken in PB, pH 7.4 at 10 mV s⁻¹; reductively scanned: E_i = -100 mV, E_f = -950 mV.

With protocol now in place, the next step was just to optimize on the specific minor variables, such as the enzyme loading amount and the potentiodynamic deposition time.

5B.3.1.3 Optimisation of Enzyme (nCYP3A4) loading

From a general perspective, for optimal analytical performance in biosensors and/or bio-electrochemical platforms in general, the enzyme concentration needs to be sufficiently high, so as to ensure that neither the rate of the enzymatic reaction, nor the electrode kinetics is the limiting step in the overall detection scheme. In this regard, too low enzyme loading can concomitantly result in high sensitivity to

small variations in activity, which in effect can lead to poor analytical performance. On the other hand, too high enzyme loading may induce an effect in which the enzyme layer itself becomes a barrier for the diffusional movement of both the substrate and the mediating species, while simultaneously affecting rates of mass transfer to the electrode. In this context, the cumulative effects of these constricts can inadvertently cause delaying in biosensor response time. With all such and other aspects in mind, the enzyme loading amount for the indinavir amperometric biosensor was investigated, by varying the amount of the enzyme per unit area (i.e. $\mu\text{g nCYP3A4 cm}^{-2}$), while keeping all other variables constant. Regarding the practical aspects – for this particular variable, the calibration plot for indinavir in the 0.05–82.8 μM concentration range was selected, with the resulting sensitivity obtained as slope from overall regression analysis obtained and comparatively assessed. **Figure 5B.3** exhibits the slopes ($\mu\text{A } \mu\text{M}^{-1}$) as a function of amount of nCYP3A4 loaded ($\mu\text{g cm}^{-2}$). Evaluation of the graph reveals that the slope of the indinavir calibration plot increased with enzyme loading up to 5.58 $\mu\text{g nCYP3A4 cm}^{-2}$, after which the slope value levelled off. With regard to relating the aforementioned obtained amount to units of enzyme cm^{-2} : Considering that, 1 mg of nCYP3A4 contains approximately 0.828×10^{-4} units of enzyme, thus 5.58 μg (i.e. 5.58×10^{-3} mg) nCYP3A4 is determined to contain 4.61×10^{-7} units cm^{-2} . The school of thought regarding the determination of the units of nCYP3A4 in 1 mg of enzyme is in relation with the established standard unit for expression of enzyme, according to the International Union of Biochemistry. In this regard, in terms of a definitive context, one international unit (IU) of enzyme activity is defined as “the amount of enzyme necessary to produce one μmol of product per minute, under specified standardized conditions of substrate concentration, pH and temperature” [99]. Thus, the unit factor here, is in specific reference to the amount of active enzyme per unit area. The plot showing the slopes as a function of enzyme units as a function of amount of nCYP3A4 loaded in particular is shown in **Appendix A1-2(b)**.

The individual calibration graphs and all obtained parameters for each enzyme loading amount is exhibited in **Appendix B1-2 a-b**.

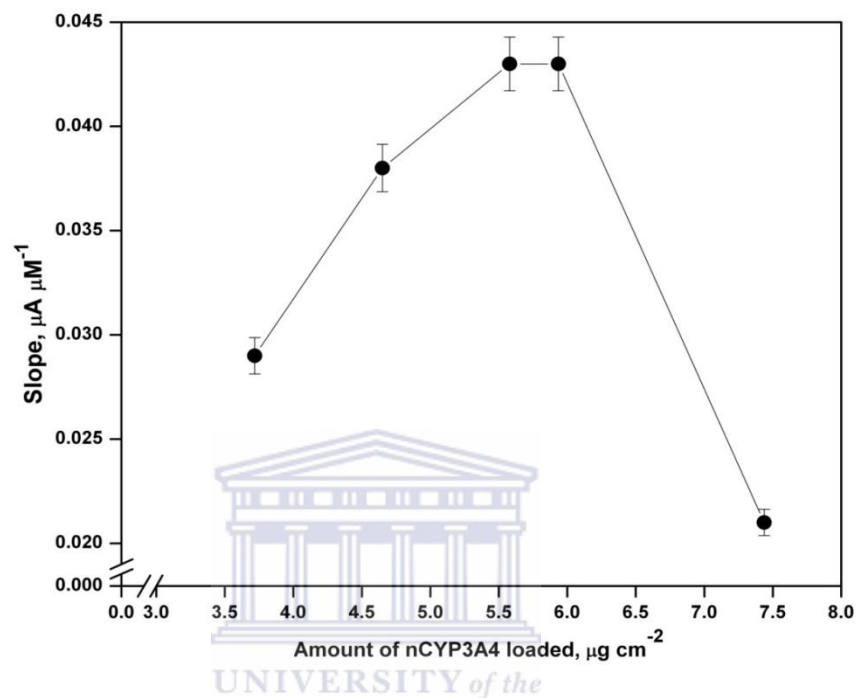


Figure 5B.8 Effect of nCYP3A4 loading amount on the bio-electrocatalytic response of the nCYP3A4-based biosensor [GCE||naf|Et-Co(Sep)³⁺|nCYP3A4|Agrs-PEI-PVA]. Slopes obtained from indinavir calibration plots in the 0.05 – 25.60 μM concentration range. Supporting electrolyte: 0.05 M aerobic PB (pH 7.4).

5B.3.1.4 Optimisation of potentiostatic electro-deposition time for Co(Sep)³⁺

The optimisation on the deposition time of Co(Sep)³⁺ is a subject area that required the judicious all-inclusive consideration of a range of different, but equally fundamental aspects:

- Firstly, from a general perspective, physiological reconstitution of microsomal P450-mediated monooxygenase activity requires a relationship with its NADPH-based electron transfer donor-component, such that a 1:1 complex is

formed. In terms of a bioelectrochemical setup on the other hand, although no actual complex is formed — as exhibited in **Equation 2.1(c)**, enzyme reduction proceeds via a chemically-based interaction between the reduced mediator (M_R) and the oxidized enzyme (E_{Ox}). In this regard, diffusion of the mediating species to and from the underlying electrode needs to be sufficiently swift in order to ensure fast, continuous regeneration of enzyme active site. Moreover, the percentile of available electroactive mediating species needs to be sufficient as to provide optimally favourable interactions with all catalytically active immobilized enzyme units per unit electrode area.

- Due to the inherent susceptibility to denaturation of microsomal mammalian heme thiolate CYP450s, particularly in the case of N-terminally modified constructs, as a precautionary measure to maintain the functional integrity of the enzyme during immobilization, no exchange of buffer for glycerol-free casting solution was made, resulting in casting solutions containing 20% glycerol. However, considering glycerol's hydrophobic nature, coupled with its low dielectric constant (as compared to water, i.e. 43) and high viscosity, the overall effect of its presence on the electrode would of course confer a substantial degree of electronic resistance. Moreover, according to documented findings, the buried cofactor of the enzyme, which is normally encased in a fairly hydrophobic intervening peptide shell, normally results in moderately weak electronic coupling between the prosthetic group and the external reluctant (the GC | naf | El-Co(Sep)³⁺). The cumulative effect of the aforementioned constricts, generally translates into lowered electronic conductivity, and in this regard, it is essential that the carrier matrix contains a sufficient percentile of electroactive species, in order to effectively recompense these constricts.
- In terms of the specific activity of the synthesized recombinant enzymes (\pm 66 kDa), on average, they have been determined to contain 0.828×10^{-4} (catalytically active) units per mg of protein, which is essentially on the low side. Moreover, from a general perspective, in a bio-electrochemical setting,

enzyme immobilization always occurs at the expense of denaturalization of a small percentage of active enzyme [87]. The cumulative effect of these constricts results in the requirement of higher amount of enzyme per unit surface area (cm^2) in order to drive a sufficiently productive catalytic turnover. On the other hand, based on documented literature, as stated in Chapter 2 **Section 2.24**, the diffusional movement of the mediator is an absolute prerequisite for productive and successful electron transfer in amperometric biosensor configurations. Considering the aforementioned aspects, including the fact that as shown in **Section 5B.3.1.2**, the enzyme sample used in the current research investigation contains a small percentile of inactive P420 component, it is essential that sufficient mediator species is pre-concentrated within the carrier matrix, such as to ensure optimum interaction with the active immobilized enzyme units at the shortest distance possible.

In view all the preceding aspects, the primary objective during the investigation of the effects of $\text{Co}(\text{Sep})^{3+}$ loading time, the focus was on providing the highest fraction of electroactive mediating species within the base-nafion matrix to ensure that all available exchange sites are filled, while not exceeding an amount that may actively block electron transfer, as too high fractions of mediating species has been shown to incur blockage effects. With regard to the actual experiments, as a sensitivity criterion for the optimisation on this particular variable, the slope for the calibration plot for indinavir in the 0.05 – 25.60 μM concentration range was chosen, and as such, mediator loading time was varied (from 300 s – 2000 s), while keeping all other variables constant, of which the results are shown in **Figure 5B.8**. In particular, the graph shows the obtained slopes for the aforementioned indinavir concentration range obtained by the Agrs-PEI-PVA|nCYP3A4| $\text{Co}(\text{Sep})^{3+}$ |naf||GC electrode (nCYP3A4-based biosensor), as a function of $\text{Co}(\text{Sep})^{3+}$ loading time. As can be seen from the graph, 300 s resulted in the poorest performance, while optimum response was observed for deposition times between 600 and up to 1200 s, thus exhibiting an

upper-limit within this region. Potentiostatic loading times exceeding 1200sec, on the other hand, resulted in drastic reduction in biosensor response to the selected concentration range – in fact, the value obtained for a loading time of 2000sec, fell completely out of the range of the points shown in **Figure 5B.8** and, as such, could not be included in the graph. This phenomenon has been encountered before in mediated biosensor systems, and as such, can probably be attributed to non-conductivity, caused by hindrance of electron transfer in the presence of too high fraction of pre-concentrated $\text{Co}(\text{Sep})^{3+}$ [138]. Although 600 sec, fell within the starting range of the upper slope value limit for this particular variable, 1200 sec was selected as the formal $\text{Co}(\text{Sep})^{3+}$ loading time, since it enabled the highest mediator pre-concentration without exhibiting any visible kinetic limitations to electron transfer in terms of blocking interactions. Moreover, this particular deposition time resulted in highly stable and reproducible results observed, for the electroactive naf- $\text{Co}(\text{Sep})^{3+}$ carrier matrix in particular. Still on this subject of the carrier matrix, a comprehensive morphological, structural and electrochemical investigation on the nafion- $\text{Co}(\text{Sep})^{3+}$ was conducted, the results of which have been exhibited and discussed in **Chapter 5A**.

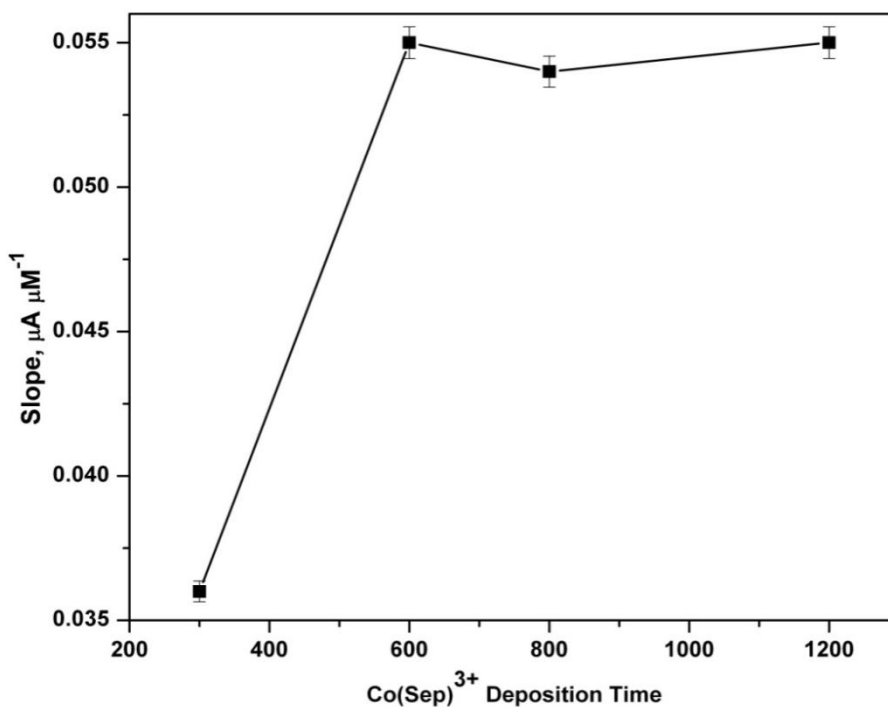


Figure 5B.9 Effect of $\text{Co}(\text{Sep})^{3+}$ electrostatic deposition loading time on bio-electrocatalytic response of the $\text{GCE}|\text{naf}|\text{El-Co}(\text{Sep})^{3+}|\text{nCYP3A4}|\text{Aargs-PEI-PVA}$ biosensor. Showing slopes of indinavir calibration plots in the 0.05 – 25.60 μM concentration range. Supporting electrolyte: 0.05 M aerobic PB (pH 7.4).

The typical calibration curves obtained for each $\text{Co}(\text{Sep})^{3+}$ loading time is exhibited in **Appendix B.1**.



UNIVERSITY of the
WESTERN CAPE

5B.3.2 Voltammetric characterization of the fabricated biosensor (prepared under optimized conditions): General electrochemical behaviour in anaerobic conditions

Figure 5B.10 exhibits the voltammetric response of the fabricated biosensor, both in terms of the biosensor un-mediated biosensor [plot (a)], denoted $\text{GCE}|\text{naf}|\text{nCYP3A4}|\text{Aargs-PEI-PVA}$, as well as the mediated biosensor [i.e. plot (b)], denoted $\text{GCE}|\text{naf}|\text{El-Co}(\text{Sep})^{3+}|\text{nCYP3A4}|\text{Aargs-PEI-PVA}$. The cyclic voltammograms were obtained for a typical experiment conducted in argon-degassed phosphate buffer, for a scan done cathodically, at 3 mV s^{-1} in (pH 7.45). In this

regard, in the absence of the $\text{Co}(\text{Sep})^{3+}$ the obtained CVs were defined by ill-formed cathodic and anodic waves, with no observable $I_{p,c}$ and $I_{p,a}$ maxima, and as such the E° could not be determined. Similarly, complimentary techniques, with inherently higher signal-noise ratio, such as SWV also did not show an observable or $I_{p,c}$ and $I_{p,a}$ maxima. This phenomenon has been observed before, in particular, attempts to observe cytochrome C electroactive signals in nafion films were shown to be unsuccessful [101], while, in a separate study conducted with myoglobin, the presence of surfactants were required to observe electroactivity signals with hemoglobin, since no observable signals could be obtained with unmodified nafion films [122]. Similarly, in yet another study, HRP could not be incorporated into unmodified nafion films [160]. Based on these documented findings and the results, as shown in **Figure 5B.10** of the current study, this phenomenon observed here can probably be ascribed to somewhat weak electronic coupling of the immobilized enzyme with the underlying nafion-modified GCE, which may be due to a combination of factors: Firstly, the enzyme prosthetic group is buried within a fairly hydrophobic intervening peptide shell and as such will not readily exchange electrons with the modified electrode [64, 87]. Moreover, in terms of nafion in particular, it has a small micellar pore structure [122, 160], with small water-filled volume, due to its limited water imbibing ability (dry nafion films, was shown to absorb up to 28% water upon rehydration) [161-162], and as such cannot incorporated large molecular weight biological molecules into its porous microstructure. In fact, according to documented literature, nafion is not able to incorporate species with a molecular mass higher than $10\ 000\ \text{g mol}^{-1}$ into its microstructure [160]. Therefore in the current study, with nCYP3A4 having an average MW of $\approx 46\ 500\ \text{g mol}^{-1}$, such an endeavour would also prove difficult. In addition to this, nafion's phase segregation, which confers it a substantial degree of heterogeneity, exhibiting a large percentage of hydrophobic regions, can in turn result in the formation highly hydrophobic interactions with immobilized biological molecules [101], as it would probably do in the present platform, which in turn would be unfavourable for electron transfer due to

enhanced electronic resistance, and as such, exhibiting moderately weak electronic coupling between the enzyme and the modified electrode.

In terms of the $\text{Co}(\text{Sep})^{3+}$ mediated biosensor, on the other hand, the results were significantly different, as shown by the CV in **Figure 5B.10 (b)**. The voltammogram exhibits a typical electroactive signal of the fabricated biosensor, and essentially consists of a reduction and oxidation wave, typical of a single redox couple. Considering that substrate- and oxygen-free electrolyte reaction medium was used, the observed anodic and cathodic waves were attributed to the $\text{Co}(\text{Sep})^{3+}/\text{Co}(\text{Sep})^{2+}$ redox species contained within the reagent layer. In this regard, the electrochemistry under anaerobic conditions are normally dominated by the mediating species [74]. The $E_{p,c}$ and $E_{p,a}$, determined as average values from four different biosensors at scan rates between 2- and 10 mV s^{-1} , was determined as $-670 (\pm 5) \text{ mV}$ and $-565 (\pm 5) \text{ mV}$, respectively. The average $E^{\circ'}$, as determined from cyclic voltammetry was $-617 (\pm 5) \text{ mV}$. Moreover the ΔE_p was determined as $100 (\pm 10) \text{ mV}$. As far as the peak shapes are concerned, they are roughly symmetric, however, the $I_{p,c}$ was larger than the $I_{p,a}$, a phenomenon that was observed at all scan rates studied, by on average, 1.2 orders of magnitude. As compared to the results obtained for the peak analysis of the nafion- $\text{Co}(\text{Sep})^{3+}$ carrier matrix platform and that obtained for the control sensor (containing all reagent-layer components, but with BSA instead of nCYP3A4) in particular, variations in all parameters was observed. In this regard, **Table 5B.1**, lists comparatively enlists the obtained values for $E_{p,c}$, $E_{p,a}$, ΔE_p and $E^{\circ'}$.

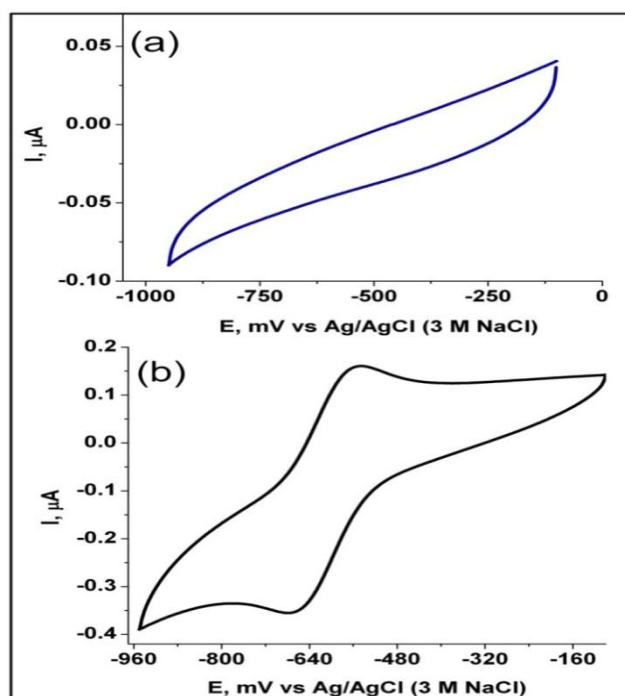


Figure 5B.10 Cyclic voltammetric response of (a) GC|naf|nCYP3A4|Agrs-PEI-PVA electrode; (b) GCE|naf|Co(Sep)³⁺|nCYP3A4|Agrs-PEI-PVA biosensor. Scans taken in substrate-free argon-degassed PB solution at $v = 3 \text{ mV s}^{-1}$. Scans done reductively, thus negative scan represent $I_{p,c}$ (cathodic).

Table 5B.1 Peak parameters as obtained from GCE|naf|EI-Co(Sep)³⁺; GCE|naf|EI-Co(Sep)³⁺|BSA|Agrs-PEI-PVA (control sensor); GCE|naf|EI-Co(Sep)³⁺|nCYP3A4|Agrs-PEI-PVA

	$E_{p,c}(\text{mV})$	$E_{p,a}(\text{mV})$	E^0	ΔE_p
GCE naf EI-Co(Sep) ³⁺	-654	-575	-615	79
GCE naf EI-Co(Sep) ³⁺ BSA Agrs-PEI-PVA	-703	-547	-625	156
GCE naf EI-Co(Sep) ³⁺ nCYP3A4 Agrs-PEI-PVA	-670	-565	-617	100

With regard to the aforementioned results, it is also noteworthy to add that the CV of the control sensor, denoted GCE|naf|EI-Co(Sep)³⁺|BSA|Agrs-PEI-PVA, is shown in **Appendix C (Figure C-1)**.

In addition to cyclic voltammetry, other complimentary voltammetric techniques, known for their low signal-to-noise ratio and particular exclusion of charging current,

was also used explored, the results of which was compared to that obtained for the biosensor from CV. In this regard, the square wave voltammetric response for the GCE||naf|E1-Co(Sep)³⁺|nCYP3A4|Agris-PEI-PVA biosensor in substrate-free argon-degassed PBS — exhibited as the difference SW, for a scan done cathodically, is shown in **Figure 5B.11 (a)**. Moreover, **plot (b)** shows the cathodic- (red) and anodic (black) differential pulse waves as obtained for the biosensor in argon-degassed PBS. With respect to the SWV results, the $E^{\circ'}$, obtained as an average from the evaluation of at least four biosensors, was determined as $-616 (\pm 5)$ mV. Results obtained from DPV on the other hand, exhibited cathodic and anodic waves showing good symmetry. Close evaluation of the scans, revealed a $E_{p,c}$ of -600 mV and $E_{p,a}$ corresponding to a value of -610 mV respectively, thus showing an overall ΔE_p of 10 mV. Moreover, the $I_{p,a}/I_{p,c}$ ratio was determined to be 0.97 , which is close to the theoretical value of 1 , for electrochemically reversible system. These results, with respect to both SWV, as well as DPV are in fact in good agreement with that obtained from cyclic voltammetry. Moreover, the small ΔE_p suggest rapid electron transfer between the electroactive species in the reagent layer film and the underlying GCE .

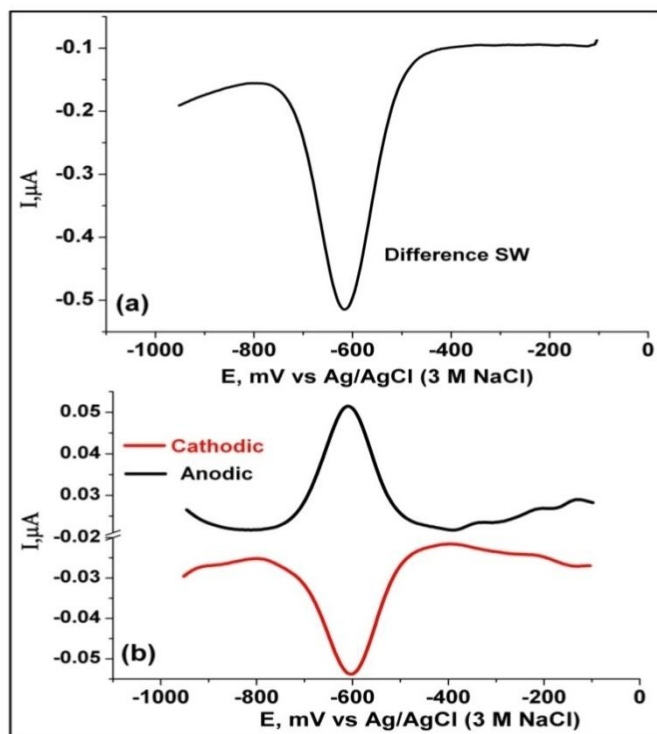


Figure 5B.11 (a) Square wave (SW) voltammetry response of the GCE|naf|E|Co(Sep)³⁺|nCYP3A4|Agrs-PEI-PVA biosensor (plot shows the difference SW current obtained for a cathodic scan). (b) Differential pulse waves, showing cathodic (red) and anodic scans for the GCE|naf|Co(Sep)³⁺|nCYP3A4|Agrs-PEI-PVA biosensor. Experimental conditions: All scans were taken in substrate-free, argon-degassed PBS (pH 7.45). SWV: square wave amplitude 25 mV; potential step 4 mV. DPV: pulse amplitude 25 mV; sample width of 15 ms; pulse period of 200 ms.

On a final note, the background-subtracted CV of the GCE|naf|E|Co(Sep)³⁺|nCYP3A4|Agrs-PEI-PVA biosensor is exhibited in **Appendix C (Figure C-2)**.

The next factor involved the determination of the type of current involved in the redox reaction of electroactive film of the nCYP3A4-based biosensor. In this regard, the dependence of peak current on the scan rate was investigated in order to identify the type of current, from which it was shown that the current function ($I_p/v^{1/2}$) has a constant value at the different scan rates studied (i.e. 3 – 10 mV s^{-1}), the results of which is depicted in **Figure 5B.13**. The electrochemical behaviour, as it presents

itself here, is in accordance with the unique structural aspects of nafion membranes, since as explained in **Chapter 5A (Section 5A.2)**, according to documented literature, in general, electron transfer in nafion membranes has been shown to be equivalent to a diffusion process. On the subject of scan rates and electron transfer, it is noteworthy to also add that at scan rates up to 10 mV s^{-1} , peak potentials for the $\text{Co}(\text{Sep})^{3+}$ mediated biosensor were nearly constant in the film. However, as the scan rate increased beyond 10 mVs^{-1} , a marked negative shift in peak potentials could be observed. This behaviour has been depicted in **Figure 5B.14**, which exhibits $E_{p,c}$ as a function of $\log v$. This suggests the onset of limiting kinetic effects in association with increase in scan rate. Nevertheless, overall, in a critical comparison of the electrochemical behaviour (which includes all determined parameters) of the enzyme-based biosensor, as compared to that exhibited by the $\text{naf-El-Co}(\text{Sep})^{3+}$ film (the results of which was presented and comprehensively discussed in Chapter 5A) — based on the exhibited and afore-discussed results, as well as data shown in **Table 5B.1**, the key aspects including $I_{p,a}/I_{p,c}$; E° ; ΔE_p ; $I_p/v^{1/2}$; $E_p/\text{Log } v$ all exhibit an unambiguous similarity. The cumulative implications of this finding suggest that, indeed, in substrate-free argon-degassed electrolyte medium, the observed electrochemistry is dictated by the electroactive $\text{Co}(\text{Sep})^{3+}$ mediating species, and as such, the observed redox waves may be ascribed to the $\text{Co}^{3+} + 1e^- \rightleftharpoons \text{Co}^{2+}$ redox system.

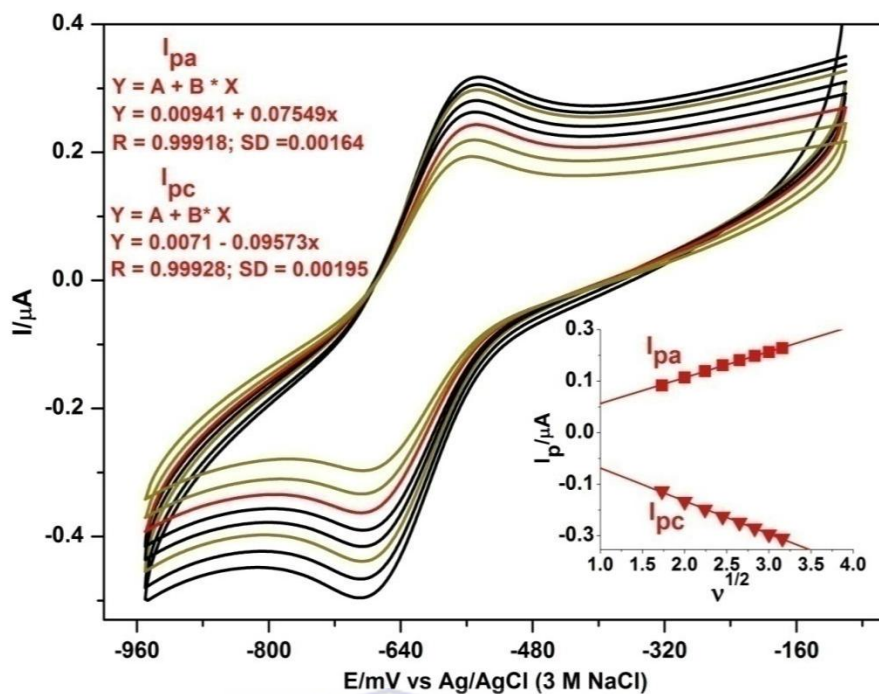


Figure 5B.12 Influence of scan rate on peak current. Inset: $I_{p,c}$ and $I_{p,a}$ as a function of $v^{1/2}$ for scan rates of 3 – 10 mV s^{-1} .

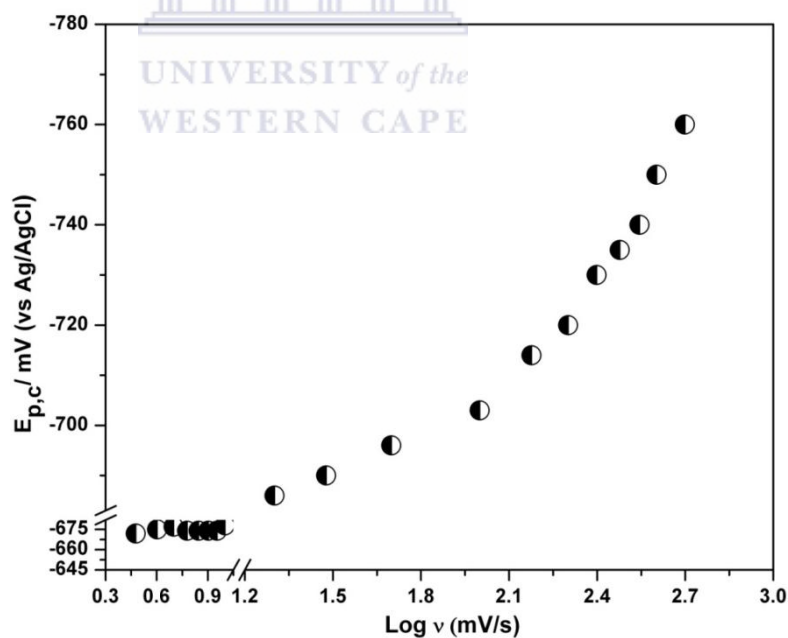


Figure 5B.13 Influence of scan rate on cathodic peak potential for a GC||naf|EI-Co(Sep)³⁺|nCYP3A4|Agra-PEI-PVA electrode

5.B.3.3 Bio-electrocatalytic activity of the GCE||naf-El-Co(Sep)³⁺|nCYP3A4|-PVA-PEI-Agrs biosensor

According to documented literature, with reference to the quest for preventing the futile cycling of electrons and for curtailing/attenuating the formation of reactive oxygen species, it has been proposed that electrocatalytic investigations involving Co(Sep)³⁺ mediated systems with P450 enzymes are best done under conditions of low oxygen tension, by gentle blanketing of the reaction mixture with an inert gas [120]. However, due to the possible associated constraints with regard to diffusional rate limiting of dioxygen within the reagent layer under conditions of low oxygen tension — in the current research investigation, catalytic studies were done in ambient conditions in the presence of molecular oxygen, while other additional steps were taken to help to maintain the catalytic integrity of the enzyme-based recognition component. With regard to the latter constrict, maintaining a 15–20% glycerol presence within the reagent layer, proved to be an important factor, the reasons of which will become apparent in the discussion involving a more comprehensive overview of the reaction steps in the bio-electrocatalytic process (**Section 5B.3.3.1.1**). In addition to this, due to the fairly low small amount of active CYP450 units per mg of protein (as determined by standard reconstitution methods) and the known liability of these enzyme constructs, all electrochemical investigations with the prepared biosensor platforms were done in a salt-free phosphate buffer solution (PBS), as supporting electrolyte, rather than the phosphate buffer saline (PBL), which according to documented findings may induce possible inhibitory effects due to ionic competition [166].

5B.3.3.1 Bio-electrocatalytic response to molecular oxygen and substrate (indinavir)

Under optimized biosensor fabrication conditions, voltammetric experiments were undertaken to ascertain the effect of heme-co-substrate/substrate interactions on the redox properties of the immobilized nCYP3A4, without the presence of the electroactive Co(Sep)³⁺ mediator species. This was done in order to observe the effect of the absence and/or presence of the mediator on the bio-electrocatalytic response of the enzyme-based biosensor, with particular reference to observing any changes in the obtained overpotential. **Figure 5B.14** exhibits the voltammetric results obtained from the bio-electrocatalytic studies with the mediatorless nCYP3A4-based biosensor, which was fabricated by immobilizing the enzyme directly on the unmodified nafion membrane, denoted GCE||naf|nCYP3A4|Agrs-PEI-PVA. In this regard, **plot I (a)** exhibits the cyclic voltammetric response of the biosensor in substrate-free, argon-degassed PBS, whereas **plot I (b)** shows the cyclic voltammetric response of the nCYP3A4-based biosensor in substrate-free oxygen in air-saturated PBS, and **plot I (c)** depicts the biosensor response in oxygen-saturated PBS containing 14 μM indinavir. The voltammetric response of the biosensor in substrate-free argon-degassed PBS was already discussed in previous sections and thus need not be further elaborated now. Compared to the ill-defined redox waves seen in substrate-free, argon-degassed, the presence of dissolved molecular oxygen (O_2), however, was signified by a dramatic augmentation of the cathodic peak current, which was simultaneously accompanied by a marked increase in $I_{p,c}$. From a general perspective, in an electrode-based electrochemical setting, the observation of additional catalytic current is in effect the classic voltammetric signature for electrochemical catalysis [85, 167]. In the current situation it reflects the reaction of the reduced nCYP3A4 heme iron, i.e. nCYP3A4- Fe^{II} , with dioxygen followed by the reduction of the nCYP3A4- Fe^{II} - O_2 complex (known as the oxy-ferrous complex), a reaction which within the context of the current experimental conditions, occurred at a determined $E_{p,c}$ of $-650 (\pm 10)$ mV.

Direct reduction of oxygen on these electrodes (prepared without enzyme) occurs at potentials significantly more negative than observed for the enzyme-based electrode. Nevertheless, under aerobic conditions, in the presence of 14 μM indinavir, as shown in **plot (c)** of **Figure 5B.14**, a further increase in the cathodic peak current was observed, which in effect reflects the increase in turnover of dioxygen induced by the presence of the substrate, suggesting the metabolism of the substrate by nCYP3A4, which is in turn regenerated for the next catalytic cycle. Indeed, based on documented findings regarding the catalytic interactions of CYP450 enzymes, it has been shown that the presence of substrate favourably affects the enzyme-oxygen interaction, by significantly increasing the rate of oxygen binding to the heme redox centre, a factor that has been observed in numerous studies involving CYP450 and/or heme-containing enzymes [74, 77, 85, 135]. A closer evaluation of the exhibited CV showed that the bio-electrocatalytic response to indinavir occurred at a potential of -687 mV, which, compared to the operating potential determined for oxygen reduction, shifted negatively by a value of 36 mV. Normally, in the context of electrochemical systems, and with regard to CYP450 enzymes in general, a positive shift in E_p in association with substrate interaction signifies the thermodynamic favourability of the interactions, which in terms of specifics portrays the expulsion of a water molecule (bound as a sixth axial ligand) from the heme centre, in association with the change in heme iron from six co-ordinate, low spin to five co-ordinate high spin state. On the other hand, as explained in **Chapter 2 (Section 2.2.3.2)**, according to the Marcus theory for biological electron transfer [65, 70], the kinetic effects of electron transfer is between two redox species is directly dependent on the driving force (i.e. the potential difference), as well as the reorganizational energy. Having said that, a cathodic (negative) potential shift, in this context, signifies a larger reorganization energy in association with a slower rate of electron transfer [134]. In this context, on a microscopic level, due to nafion's small micellar pore size, it cannot incorporate the large enzyme into its structure. However, based on its inherent phase-related heterogeneity (consisting of the bulk hydrophobic phase and the much lower density hydrophilic ionic cluster region), it can form strong interactions with

compounds largely dominated by lipophilic forces, which is probably the case between the pre-formed nafion and the nCYP3A4 in the current investigation, the results of which would be unfavourable for electron transfer with the underlying electrode. Indeed, this phenomenon has been observed with other enzymes immobilised on nafion matrices [101]. Moreover, this in itself could also constrict the accessibility to the enzyme's deeply-buried prosthetic group, the overall effect which would be an increase in reorganization energy in association with co-substrate and/or substrate interaction, thus resulting in a negative shift in E_p . In addition to this, the enzyme stabilizing effect of glycerol, by-and-large operating by slowing down the conformational changes of the enzyme required for electron transfer, to minimize enzyme denaturation and/or unwanted harmful side reactions, could also contribute to the observed negative shifts in potential, as well as the high operating potential. Nevertheless, the presence of the $\text{Co}(\text{Sep})^{3+}$ mediating species would thus play a significant role in enhancing the electron transfer reactions and as such, the overall bioelectrocatalytic response of the enzyme-based biosensor. In addition to cyclic voltammetry, the bioelectrocatalytic response was also studied with SW voltammetry, the results of which are shown in **plot II** of **Figure 5B.14**. The scans were done cathodically, and as such, the difference SWs shown here represents the net reduction process. Evaluation of these results showed that once again, as in the case of the cyclic voltammetric study, the presence of dioxygen (**scan b**) and substrate (**scan c – e**) results in a marked increase in catalytic peak current. In the case of the plots showing the substrate (indinavir) interaction in particular, a concentration dependent increase in peak current up to the final concentration (i.e. 14 μM) can be seen. Moreover, with regard to the peak potentials observed from SW voltammetric studies in particular, oxygen reduction occurred at approximately -678 mV, whereas the catalytic response to indinavir occurred at a more negative potential, corresponding to a value of -706 mV, thus coinciding with results observed from cyclic voltammetric studies. At this stage it must also be emphasized that the high operating potential with regard to reduction of dioxygen, as well as substrate detection and monooxygenation, as observed from both cyclic voltammetric and square wave voltammetric results,

holds the potential consequence of a much higher likelihood of the formation of reactive oxygen species and associated uncoupling reactions, and as such, as earlier stated, the presence of the mediator will greatly aid the bio-electrocatalytic response to effective substrate turnover.

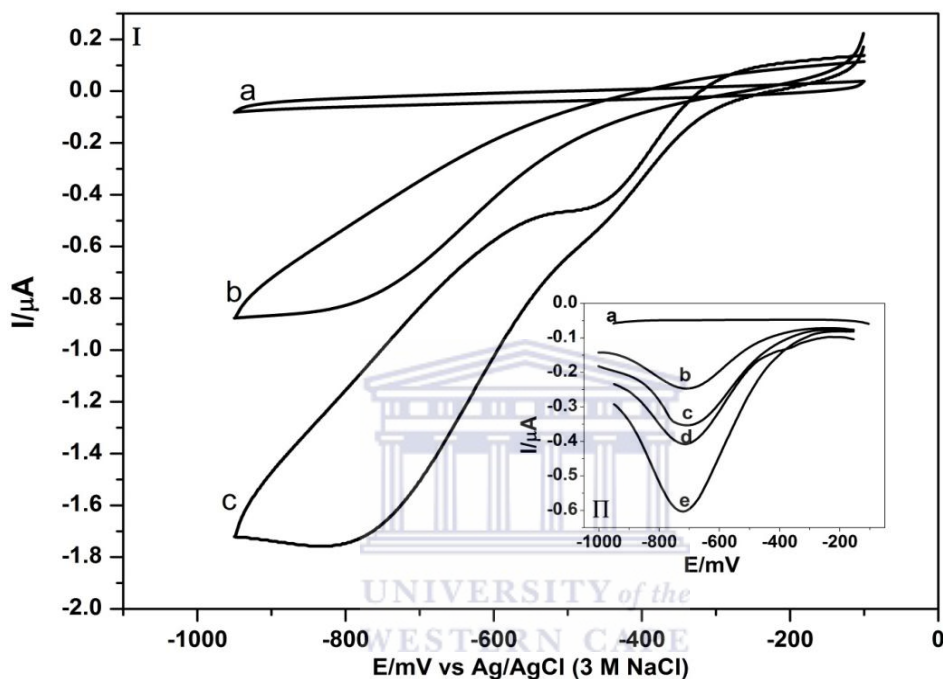


Figure 5B.14 I: Cyclic voltammograms of the GC|n-CYP3A4|Agris-PEI-PVA electrode in 50 mM PBS, showing biosensor response in (a) substrate-free argon-degassed PBS; (b) air-saturated PBS with 0 μM indinavir; (c) air-saturated PBS with 14 μM indinavir. **II:** square wave voltammograms of the GC|n-CYP3A4|Agris-PEI-PVA electrode, showing response in (a) substrate-free argon-degassed PBS; (b) air-saturated PBS with 0 μM indinavir; air-saturated PBS with (c) 1 μM , (d) 2 μM and (e) 14 μM indinavir, respectively. Experimental conditions are: CVs scanned cathodically at 5 mV s^{-1} . SWVs: square wave amplitude 25 mV; potential step 4 mV (showing difference SWs)

The results as observed for the $\text{Co}(\text{Sep})^{3+}$ -mediated electrochemically driven catalysis of nCYP3A4 in the presence of dissolved molecular dioxygen and indinavir was markedly different. In this regard, the voltammetric response of the GC|n-CYP3A4|Agris-PEI-PVA electrode (biosensor) in the presence of O_2 , as

well indinavir was investigated with cyclic voltammetry and square wave voltammetry, for which the results are exhibited in **Figure 5B.15 I**, (**plot b, c**) and **Figure 5B.16 I** (**plot a, b**). With regard to the cyclic voltammetric results in particular, **Figure 5B.15 I, plot b and c** exhibits the response of the GC||naf-EI-Co(Sep)³⁺|nCYP3A4|-Agrs-PEI-PVA electrode in substrate-free air-saturated phosphate buffer solution (PBS) and air-saturated PBS containing 5 μ M indinavir, respectively. **Plot a** on the other hand depicts the cyclic voltammetric behaviour of the biosensor in substrate-free argon-degassed PBS. These plots show results for an experiment conducted at 5 mV s^{-1} for which scans were done cathodically. Evaluation of the exhibited results revealed that the presence of molecular oxygen caused a dramatic augmentation of the CV as compared to the cyclic voltammetric response observed from the biosensor in substrate-free, argon-degassed PBS [**plot a**]. In a more descriptive context, the presence of oxygen was signified by a distinct increase in the cathodic current, which was accompanied by the emergence of a new peak, centred at an average potential of $-440 (\pm 10)$ mV ($n = 10$), and also accompanied by a considerable decline of the anodic current. Moreover, as compared to the CV in argon atmosphere, for which the cathodic wave exhibited a single peak centred at approximately -670 mV, the response in the cathodic wave of the CV in oxygen on the other hand, was dominated by the new peak, centred at -440 mV, while the peak in the region of -670 mV became almost ‘featureless’ and thus its exact parameters could not be determined. When indinavir was added to the air-saturated PBS there was a further increase in the cathodic current, in specific association with the peak centred in the region of that observed for the response to oxygen. Moreover, the small increase in reduction (cathodic) peak current, in association with indinavir addition, coupled with the negligible amount of H_2O_2 formation (as measured by Quantofix hydrogen peroxide sticks), suggest the minimal occurrence of “futile” redox cycling of the system and associated concomitant production of reactive oxygen species [86, 89, 168]. Considering the latter, including the fact that oxygen is the co-substrate of nCYP3A4, and in view of the exhibited voltammetric responses, as well as the absence in catalytic response of the enzyme in substrate-free argon-degassed PBS (of

which the observed redox process is dominated by the $\text{Co}(\text{Sep})^{3+}$ mediating species), these results suggest the bio-electrocatalytic reduction of oxygen by the mediator-reduced nCYP3A4, (i.e. nCYP3A4- Fe^{II}), in the substrate-free aerated buffer and the increase in turnover of dioxygen affected by indinavir in the substrate-containing aerated buffer (shown in **plot b**) [77-78, 136, 142]. With regard to the square wave voltammetric results, a more well-defined indication of the position and magnitude of the peak response for the $\text{GC}||\text{naf-EI-Co}(\text{Sep})^{3+}|\text{nCYP3A4}|\text{-Agrs-PEI-PVA}$ electrode in the presence of oxygen, and in the presence of indinavir can be observed. In this regard, **Figure 5B.16 I plot a** and **b** depicts the response of the $\text{GC}||\text{naf-EI-Co}(\text{Sep})^{3+}|\text{nCYP3A4}|\text{-Agrs-PEI-PVA}$ electrode in substrate-free air-saturated phosphate buffer solution (PBS) and air-saturated PBS containing indinavir, respectively. The voltammograms represent the net (difference between forward and reverse scans) SWV responses when the modified electrode was scanned cathodically. Evaluation of the observed plots revealed that these results coincide with that exhibited for cyclic voltammetry and as such, the presence of both O_2 and indinavir was signified by a distinct response, centred in the potential region where the new peak emerged [as compared to the SWV observed in substrate-free, argon-degassed PBS (see inset in **Figure 5B.16, i.e. plot II**)]. It must also be emphasized at this stage that although the exhibited SWs are characterized by two peaks, no discernible response was observed at the other peak position (i.e. ≈ -637 mV), which can be evidenced by the noticeable lack of catalytic-type increase in I_p in association with indinavir/ O_2 addition. Moreover, at the same time, an increase in net current in association with the response of the biosensor to both O_2 and indinavir, as compared to that observed for the biosensor in substrate-free argon-degassed PBS (**plot II**) was also observable. With regard to the exact position of the emerged peak in association with the bio-electrocatalytic response to O_2 , the peak potential was determined as $-365 (\pm 5)$ mV, while the addition of the indinavir resulted in a small cathodic shift of approximately 4 mV, thus yielding a final response potential of $-369 (\pm 10, n=10)$ mV. In terms of current magnitude on the other hand, the I_p^{nCYP3A4} in the presence of indinavir was significantly higher than that observed in the presence

of dioxygen (containing no indinavir), thus showing an increase in the value of $I_p^{nCYP3A4}$ (≈ -369 mV) of approximately 1.6 orders of magnitude. Still on the subject of the observed bio-electrocatalytic results, it is noteworthy to emphasize the fact that the presence of the $\text{Co}(\text{Sep})^{3+}$ mediator has enabled an unequivocal reduction in the overpotential for the bio-electrocatalytic reduction of O_2 , as well as for the bio-electrocatalytic substrate turnover, as compared to the results observed for the unmediated biosensor (i.e., $\text{GCE}|\text{naf}|nCYP3A4|\text{Agrs-PEI-PVA}$). In particular, the overpotential for the reduction of O_2 was reduced by at least 210 mV, while the overpotential for indinavir detection/metabolism was reduced approximately 240 mV. Moreover, with specific reference to the reduction of O_2 , as compared to the results obtained for the **biosensor platform1**, presented and discussed in **Chapter 4**, (i.e. $\text{CGE}|\text{naf}|\text{CMCo}(\text{Sep})^{3+}|nCYP3A4|\text{naf}$), the operating potential was reduced by approximately 215 mV. This observation also holds for previous investigations involving CYP3A4-based biosensor platforms — in particular, compared to the study involving full-length human recombinant CYP3A4 in a PDDA-polyelectrolyte platform [135], the overpotential for the bioelectrocatalytic reduction of dioxygen was reduced by ≈ 250 mV; and as compared to another study also involving full-length microsomal CYP3A4, in a DDAB liquid crystal vesicular system [136], the overpotential was reduced by ≈ 270 mV. It is also noteworthy to again point out the effectiveness of the design path used in this biosensor platform, as compared to that used for biosensor platform 1, with particular reference of the technique used in the fabrication of the electroactive carrier matrix. In this regard, the design path used in biosensor platform 2 probably enabled a better coupling efficiency between the immobilised enzyme and the transducer material.

In the interest of negative control measures, the behaviour of the control sensor, fabricated with the exclusion of nCYP3A4, by using the pseudo carrier enzyme, bovine serum albumin (BSA), in the presence of oxygen and in the presence of indinavir was also investigated with cyclic voltammetry, as well as square wave

voltammetry. In this regard, with reference to the CV results in particular, **plot b** of **Figure 5B.15 II** depicts the cyclic voltammetric response of the control sensor (i.e. GCE||naf|E1-Co(Sep)³⁺|BSA|Agrs-PEI-PVA) in substrate-free air-saturated PBS, while **plot c** exhibits the behaviour of the control sensor in air-saturated PBS in the presence of indinavir. In addition to this, **plot a** (in **Figure 5B.15 II**), which depicts the redox reactivity of the control sensor in substrate-free argon-degassed PBS is also showed. In terms of the SWV results on the other hand, **Figure 5B.16**, **plot c** depicts the reactivity of the GC||naf|E1-Co(Sep)³⁺|BSA|Agrs-PEI-PVA in substrate-free aerated-PBS, whereas **plot d** shows the reactivity of the control sensor in aerated-PBS containing 5 μM indinavir. Evaluation of the CV results in particular, showed that indeed, the presence of molecular dioxygen, as well as indinavir (in air-saturated PBS) were both accompanied by a measurable increase in cathodic current, as compared to the CV in substrate-free argon-degassed PBS, and although the cathodic wave was not entirely featureless/ill-formed, the exact positions of the observed small cathodic peaks (minima) could not be determined. Moreover, unlike in the results observed for the nCYP3A4-based biosensor, where a clear response at ≈ -440 mV could be observed, no clear E_p could be observed in this region with the BSA-based control sensor. In terms of the SWVs, in the presence of oxygen, a small, but measurable increase in net current could be observed, while the introduction of indinavir resulted in another small measurable increase in net SW current. However, the reactivity in the presence of both O_2 and indinavir was indistinct, with current increase in both cases observed to be at two peak potentials, i.e. ≈ -410 mV and -645 mV. This was contrary to the clear response as exhibited by the nCYP3A4-based biosensor, for which a distinct current increase centred on a single potential was observed, typical of a catalytically active enzyme containing a single prosthetic group. Nevertheless, in terms of the observed increase in cathodic current as seen from CV and SW voltammetric studies for the BSA-based control electrode — based on documented literature findings regarding catalytic electrochemical studies, this type of phenomenon is in fact not uncommon. On the other hand, the observed ‘double-peak increase behaviour’ is

characteristic of the reduction of two species at different potentials [169], which, in the current case, suggest with relative certainty, the effect of reactive oxygen species, particularly H_2O_2 , formed in association with two electrochemically driven processes. In this regard, the first process most probably involved the direct reduction of dioxygen in the film at the GCE, while the other process may be attributed to the coupling of the $1e^-$ reduction of the mediating species with a fast follow-up chemical process, which involves the interaction of the reduced species with dioxygen [85, 120, 135, 169]. A comprehensive description of the details of these interactions and their concomitant implications are given in **Section 5B.3.3.1.1**.

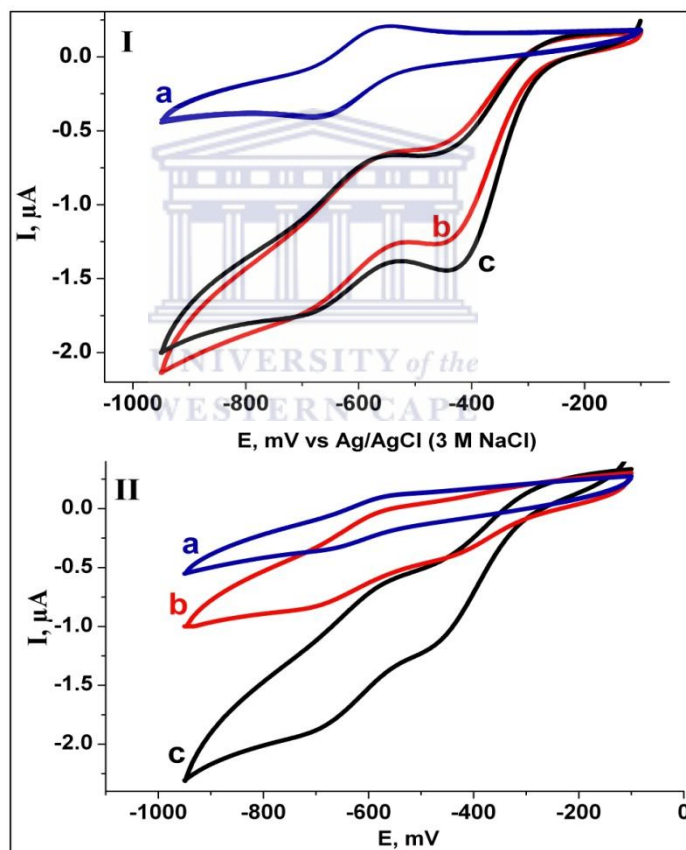


Figure 5B.15 Cyclic voltammograms showing: (a) response of nCYP3A4-based biosensor, (GCE||naf|El-Co(Sep)³⁺|nCYP3A4|Agrs-PEI-PVA) in argon-degassed PBS containing 0 μM indinavir; (b) response of nCYP3A4-based biosensor in air-saturated PBS containing 0 μM indinavir; (c) response of nCYP3A4-based biosensor in air-saturated PBS containing 5 μM indinavir. (d – e): negative control, showing BSA-based control sensor (i.e. GCE||naf|El-Co(Sep)³⁺|BSA|Agrs-

PEI-PVA in (d) air-saturated PBS containing 0 μM indinavir; (e) air-saturated PBS containing indinavir

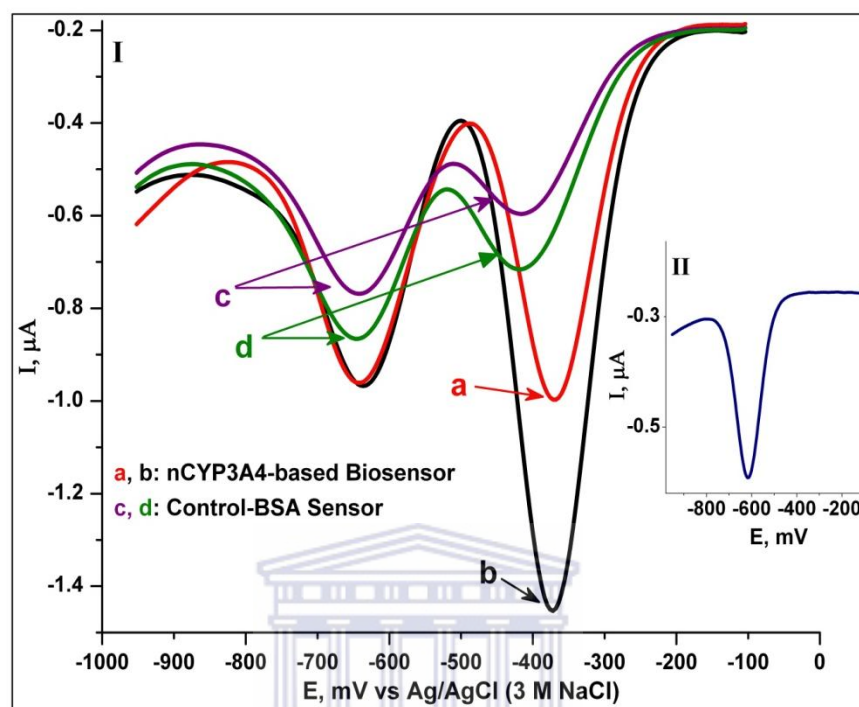


Figure 5B.16 Square wave voltammograms showing: (a) response of nCYP3A4-based biosensor, (GCE||naf|El-Co(Sep)³⁺|nCYP3A4|Agrs-PEI-PVA) in air-saturated PBS containing 0 μM indinavir; (b) response of nCYP3A4-based biosensor in air-saturated PBS containing 5 μM indinavir; (d) – (e) negative control showing: reactivity of BSA-based control sensor (GCE||naf|El-Co(Sep)³⁺|BSA|Agrs-PEI-PVA) in air-saturated PBS containing 0 μM indinavir [i.e. (a)] and reactivity of BSA-based control sensor in air-saturated PBS containing 5 μM indinavir. Experimental conditions are: square wave amplitude 25 mV; potential step 4 mV; plots show net currents for forward and reverse SW currents for scans done cathodically.

To further explore the catalytic response of the nCYP3A4-based, Co(Sep)³⁺-mediated biosensor with respect to indinavir — the voltammetric response of the GC||naf|El-Co(Sep)³⁺|nCYP3A4|Agrs-PEI-PVA electrode in the presence of increasing indinavir concentrations in the potential region where the afore-discussed biosensor response was observed was investigated. In this regard, **Figure 5B.17**

exhibits the dependence of the square wave voltammetric current (response) as a function of concentration, for indinavir. The depicted plots represent the net (difference between forward and reverse scans) SWV responses for scans done cathodically. Moreover, the voltammograms showed a measurable increase in the $I_p^{nCYP3A4}$ upon subsequent addition of indinavir to the air-saturated PBS up to the final concentration of 73 μM . In addition to this, in the interest of corroborating the lack of bio-electrocatalytic response of the GC||naf|El-Co(Sep)³⁺|nCYP3A4|Agrs-PEI-PVA electrode in the potential region where the second peak was shown in the afore-discussed results, (i.e. ≈ -637 mV, for **plots a and b of Figure 5B.16**), the reactivity of the GC||naf|El-Co(Sep)³⁺|nCYP3A4|Agrs-PEI-PVA electrode to increasing indinavir concentrations in the region of that potential was also investigated with respect to this particular potential region. In this regard, as exhibited in **Figure 5B.17**, other than the normal redox reactive peak seen, no additional discernible catalytic response in this region could be observed.

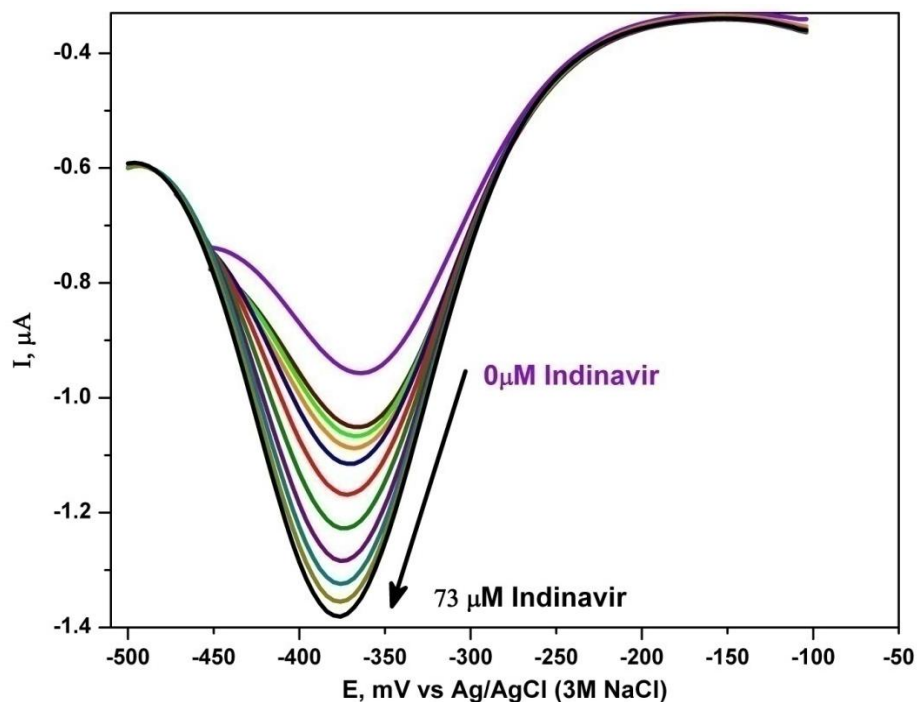


Figure 5B.17 Square wave voltammograms showing response of GC||naf|El-Co(Sep)³⁺|nCYP3A4|Agrs-PEI-PVA electrode to increasing indinavir concentrations, from 0 μM up to a final concentration of 73 μM . Experimental conditions are: square wave amplitude 25 mV; potential step 4 mV. (Plots show the net currents obtained from scans done cathodically)

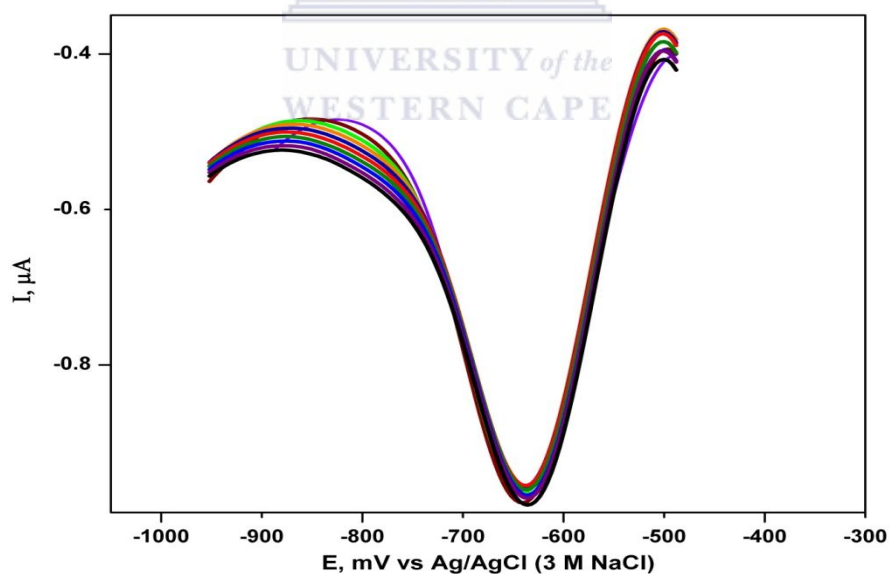


Figure 5B.18 Square wave voltammograms for the potential region of -490 \rightarrow -950 mV for the GC||naf|El-Co(Sep)³⁺|nCYP3A4|Agrs-PEI-PVA electrode, for an experiment done with increasing indinavir concentrations (0 \rightarrow 73 μM).

Experimental conditions are: square wave amplitude 25 mV; potential step 4 mV. (Plots show the net currents obtained from scans done cathodically)

Once again, with the focus on negative-control measures, the reactivity of the BSA-based control sensor to increasing indinavir concentrations were also investigated, with SWV. In this regard, Figure 5B.19 shows exhibits the dependence of the square wave voltammetric current as a function of concentration of indinavir. The depicted plots represent the net (difference between forward and reverse scans) SWV responses for scans done cathodically. Indeed, an increase in current in the presence of both O₂ and indinavir as compared to the background current observed for the substrate-free argon-degassed PBS (see inset, i.e. **plot II**) could be seen. However further evaluation of the voltammograms showed that the results for the GCE||naf|Ei-Co(Sep)³⁺|BSA|Agrs-PEI-PVA control electrode was irrefutably different from the results showed for the nCYP3A4-based biosensor (GC||naf|Ei-Co(Sep)³⁺|nCYP3A4|Agrs-PEI-PVA). In this regard, with particular reference to the results showed for indinavir, other than the initial peak current increase with the initial indinavir addition, no clearly discernible subsequent increase in peak current (I_p) in association with consecutive indinavir additions could be seen, which essentially means that for all subsequent indinavir additions, up to the final 16 μM, the magnitude of I_p stayed the same. Moreover, the observed initial I_p increase presented itself as a double-peak increase, thus mirroring and corroborating what was seen in the afore-discussed results for control studies exhibited **Figure 5B.16** (plot c,d).

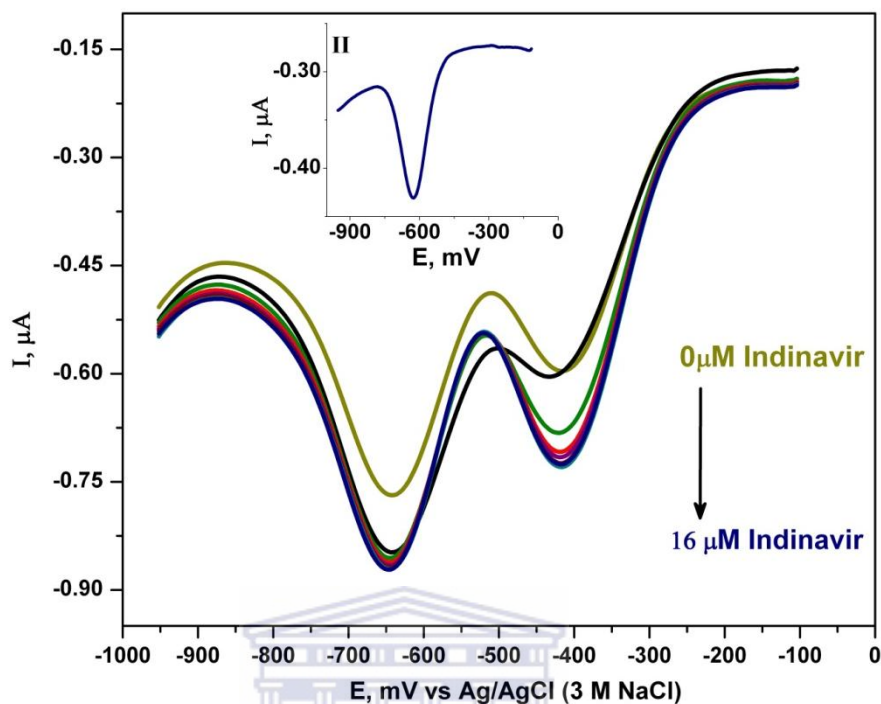


Figure 5B.19 Negative control: square wave voltammograms showing reactivity of BSA-based control sensor ($\text{GCE}|\text{naf}|\text{El-Co}(\text{Sep})^{3+}|\text{BSA}|\text{Agrs-PEI-PVA}$) with increasing indinavir concentrations from $0 \rightarrow 16 \mu\text{M}$ in air-saturated PBS. Inset (i.e. II) shows the redox behaviour of the $\text{GC}|\text{naf}|\text{El-Co}(\text{Sep})^{3+}|\text{BSA}|\text{Agrs-PEI-PVA}$ electrode in substrate-free argon-degassed PBS. Experimental conditions are: square wave amplitude 25 mV; potential step 4 mV. (Plots show the net currents obtained from scans done cathodically)

Still on the subject of electrocatalysis investigations, it is noteworthy to also show an interesting, but not unexpected phenomenon that became apparent during the these studies. In this regard, **Figure 5B.20 (a — c)** exhibits the electrocatalytic reactivity in air-saturated PBS, of (a) the $\text{GC}|\text{naf}|\text{El-Co}(\text{Sep})^{3+}|\text{nCYP3A4}|\text{Agrs-PEI-PVA}$ electrode, containing freshly expressed nCYP3A4 (**biosensor-n1**); (b) $\text{GC}|\text{naf}|\text{El-Co}(\text{Sep})^{3+}|\text{nCYP3A4}|\text{Agrs-PEI-PVA}$ electrode containing nCYP3A4 which have been stored for > six-eight months (**biosensor-n2**); and (c) the ($\text{GCE}|\text{naf}|\text{El-Co}(\text{Sep})^{3+}|\text{BSA}|\text{Agrs-PEI-PVA}$) containing the pseudo-enzyme, BSA (BSA-based control). From an evaluation of the results, it became apparent that the biosensor containing the freshly expressed enzyme (biosensr-n1) responded unequivocally

different to dioxygen as compared to the biosensor in which the old stored enzyme was used as recognition component (biosensor-n2). In this regard, biosensor-n1 exhibited the classic signature of dioxygen reduction for an enzyme containing a single active centre, comprised by a characteristic increase in cathodic peak current, with an almost complete attenuation of the anodic peak current [73-74, 82-83, 135], the implications of which, essentially suggest the coupling of the $\text{Co}(\text{Sep})^{3+/2+}$ -mediated $\text{Fe}^{3+}/\text{Fe}^{2+}$ reduction event to fast binding of oxygen to the ferro-heme. Moreover, the exhibited results corroborate the afore-shown and discussed results for the $\text{GCE}|\text{naf}|\text{EI-Co}(\text{Sep})^{3+}|\text{nCYP3A4}|\text{Agris-PEI-PVA}$ biosensor. On the other hand, the results as exhibited for biosensor-n2 showed a rather vague reactivity to dioxygen, which was in fact similar to what was observed in the case of the BSA-based control electrode, the difference being just a slightly more pronounced intensity in the cathodic peak currents in the case of biosensor-n2 as compared to that seen for the BSA-based control. The reason for this seemingly reprehensible behaviour in the case of biosensor-n2, may be attributed to the fact that since it contained very little catalytically active nCYP3A4, the results were essentially a very weak interaction between the enzyme and the mediator-containing carrier matrix, resulting in the formation of a large percentage of reactive oxygen species, particularly H_2O_2 , due to unspecific interaction of $\text{Co}(\text{Sep})^{2+}$ with dioxygen, as well as uncoupling reactions in association with the small percent of enzyme that engaged in reductive dioxygen activation [77-78, 86]. In fact, the latter is a known possible branching point in observed uncoupling reactions involving CYP450 enzymes [23, 67]. Moreover, with the BSA-control, as well as biosensor-n2, a measurable amount of H_2O_2 was formed in association with electrocatalytic studies ($10 - 25 \text{ mg L}^{-1}$) as measured by *quantofix*-peroxide sticks, whereas in the case of biosensor-n1 which contained the fresh active nCYP3A4 H_2O_2 formation was more-or-less negligible. In this regard, it suggests that the reduction of oxygen competes poorly with the reduction processes involving $\text{Co}(\text{Sep})^{3+/2+}$ and $\text{nCYP3A4-Fe}^{3+/2+}$, and as such, much less H_2O_2 peroxide is formed with fresh enzyme samples. Similar results have been seen before with CYP450 3A4 enzymes using reductase as electron transfer mediator [86].

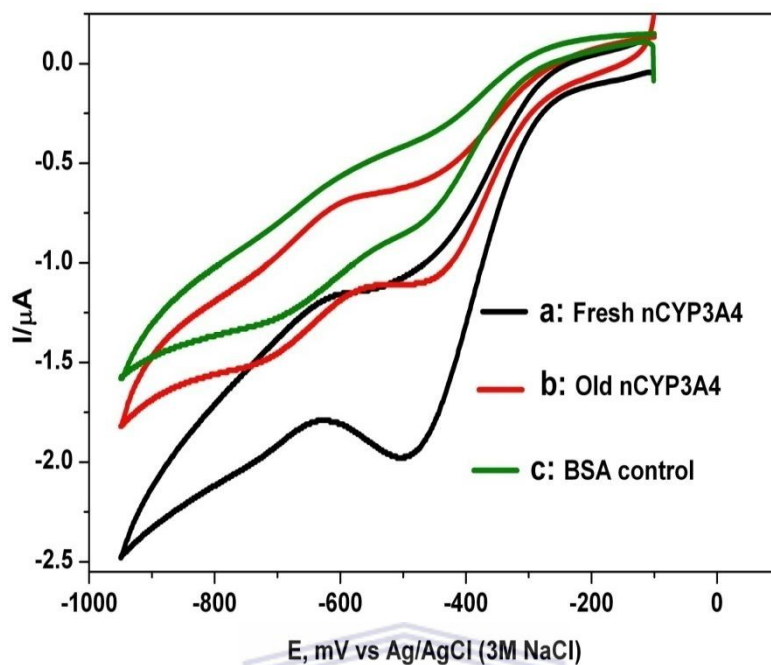


Figure 5B.20 Comparisons of effect of oxygen : Cyclic voltammograms showing: (a) (GC||naf|El-Co(Sep)³⁺|nCYP3A4|Agrs-PEI-PVA) electrode containing fresh nCYP3A4, (b) (GC||naf|El-Co(Sep)³⁺|nCYP3A4|Agrs-PEI-PVA) electrode containing nCYP3A4 which have been stored for > six-eight months; (c) (GC||naf|El-Co(Sep)³⁺|BSA|Agrs-PEI-PVA) electrode (BSA-control) in substrate-free air-saturated PBS.

On a sub-conclusive note, in the context of the collective implications of the afore-exhibited and discussed results regarding the catalytic investigations for the GC||naf|El-Co(Sep)³⁺|nCYP3A4|Agrs-PEI-PVA electrode, a few noteworthy sub-conclusions may be drawn at this stage. Firstly, with regard to the response of dioxygen in particular, these results are consistent with catalytic reduction involving nCYP3A4-Fe²⁺-O₂, and as such, suggest that the electrochemically-based reduction of the nCYP3A4 ferric heme, through the Co(Sep)³⁺ mediating species, is followed by rapid binding of dioxygen with the subsequent formation of the ferrous-dioxygen complex. Secondly, the results obtained in association with indinavir addition, all in turn coincides with previously documented findings, and as such suggests that the

presence of substrate increases the rate of the reduction of dioxygen [74, 77-78, 135-136, 142]. In addition to this, comparative evaluations between response behaviour of the $\text{Co}(\text{Sep})^{3+}$ mediated nCYP3A4-based biosensor, and that observed in the case of the BSA-based control was fundamentally different, in all electrocatalytic investigations done. Thus cumulatively, these results all suggest, that firstly, the enzyme may be activated along a similar pathway utilized in its physiological reaction cycle the overall response of the $\text{GCE}||\text{naf}|\text{El-Co}(\text{Sep})^{3+}|\text{nCYP3A4}|\text{Agrs-PEI-PVA}$ biosensor upon substrate addition to the air-saturated PBS is due to bio-electrocatalytic substrate turnover,

Evaluation of the voltammograms exhibited in the presence and absence of indinavir all suggest that indinavir increases the rate of oxygenation of nCYP3A4. The significance of this observation is the implication that the $\text{GC}||\text{naf}|\text{El-Co}(\text{Sep})^{3+}|\text{nCYP3A4}|\text{Agrs-PEI-PV}$ electrode can be used for varying the indinavir concentration in the construction of a calibration curve for indinavir. In this regard, **Figure 5B.21** shows the full calibration curve obtained from experimental studies with increasing indinavir concentrations up to a final concentration of 147.5 μM . A linear calibration curve was also constructed, as shown in the **inset** of **Figure 5B.21**, from which it was shown that the biosensor response to indinavir exhibited a linear concentration range from 2.183×10^{-6} to 3.552×10^{-6} M ($r = 0.99501$). Moreover, the accompanied sensitivity value was determined as $0.00349 \mu\text{A} \mu\text{M}^{-1}$. In addition to this, the value for the LOD, (calculated as the concentration giving a signal equal to three times the standard deviation of the blank signal divided by the sensitivity) was determined as 59.72 mg L^{-1} . This value is markedly higher than the documented maximum plasma drug concentration range (C_{Max}) for indinavir (i.e. 5 – 11 mg L^{-1}) [2, 170], however, according to the Handbook for HIV Medicine [14], as well as other documented literature [4, 7, 170-171], there is a high degree of variability in terms of plasma levels among individuals. Moreover, the quoted literature-based

value showed above, is based on the in-vitro model for the unboosted indinavir dose regiment, and secondly, is recorded in association with standard prediction in-vitro models, which are in effect based on animal studies and/or intermediate to extensive metabolisers. The effect of ritonavir-boosting on the other hand can lead to up to a 3–5 fold increase in indinavir C_{Max} value, since it results in a significant increase in the most important pharmacokinetic parameters, including C_{Max} , trough levels and half life [14]. The implications of these factors, essentially means that in poor metabolisers (as are most HIV/AIDS patients), as well as within the context of the multi-drug based HAART associated regiments, the C_{Max} value for indinavir and/or any other PI ARV may in reality rise to markedly higher values, therefore, within the context of these criteria, a higher LOD does not necessarily reflect an out of range detection rating. Still on the subject of the obtained LOD, it is also noteworthy to add that the value is higher than the value published for indinavir, based on a biosensor platform developed during the course of this research investigation, with wild type full length microsomal CYP3A4 in a vesicle dispersion of DDAB [136]. In this regard, vesicular dispersions/liquid crystal film environments are known to have a distinct effect on the heme environment of the immobilized enzyme, mostly through dehydration, which very effectually leads to more positive shifts in potential, and as such can significantly influence the obtained results. On the other hand, full-length wild-type CYP450s are known to be more stable than the N-terminally truncated enzymes (which are easily perturbed), while the use of detergents (which are necessary to obtain acceptable yields of soluble N-terminally modified constructs during the process of genetic engineering) is also known to have a destabilizing effect on the prepared CYP450s. The implications of these factors may have also contributed to the observed variance in results.

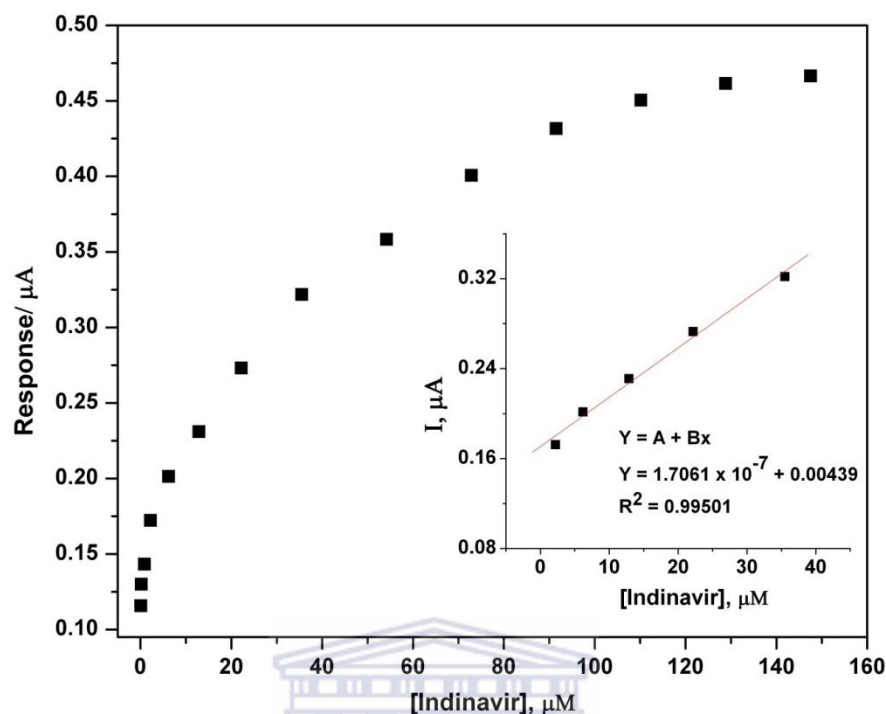


Figure 5B.21 Calibration curves for GCE||naf|El-Co(Sep)³⁺|nCYP3A4|Agrs-PEI-PVA biosensor response to indinavir: Main plot shows increasing concentration of indinavir up to a final concentration of 147.5 μM. Inset shows the linear calibration plot for indinavir.

With regard to the plot shown in **Figure 5B.21**, at high indinavir concentration a current plateau can be observed. In this regard, the curvature from the initial straight line represents the characteristics of Michaelis-Menten (MM) kinetics (see Chapter 3A, Section for a comprehensive overview of the MM theory aspects). The apparent Michaelis-Menten constant, K_M^{app} , which essentially gives an indication of the enzyme-substrate kinetics for the biosensor, i.e. GC||naf|El-Co(Sep)³⁺|nCYP3A4|Agrs-PEI-PVA electrode can then be calculated from the electrochemical version of the Lineweaver-Burk equation:

$$\frac{1}{I_{ss}} = \frac{K_M^{app}}{I_{Max}} \frac{1}{C} + \frac{1}{I_{Max}} \quad \text{5B-1}$$

where I_{ss} the steady-state current after the addition of the substrate, I_{Max} the maximum current measured under conditions of substrate saturation, and C is the concentration

of the substrate. In this regard, the slope (K_M^{app}/I_{Max}) and intercept ($1/I_{Max}$) from the plot of the reciprocal current versus the reciprocal indinavir concentration was used to calculate K_M^{app} . With regard to the general implication of determined K_M^{app} — it gives an indication of the kinetics of the enzyme-substrate system [74, 77, 172]. A low K_M^{app} shows that the E–S complex is stable, thus indicating that the saturation of the enzyme active site is a fast process. Moreover, a smaller K_M^{app} implies that the proposed electrode exhibits a higher affinity for indinavir. Having said that, the K_M^{app} value for the GC||naf|El-Co(Sep)³⁺|nCYP3A4|Agrs-PEI-PVA electrode was determined as 17.539 μ M.

5B.3.3.1.1 A deeper insight into the specifics of the electrocatalytic interactions with dioxygen and with the substrate, indinavir

This section serves to provide a deeper insight into the specific interactions pertaining to the results as observed from the afore-exhibited (bio)electrocatalytic studies. On this subject, the common phenomenon that was apparent in all catalytic interaction studies was the distinct increase in cathodic current. In this regard, through the comprehensive discussions provided in this section, as well as the schematic information shown, the common role in reactive dioxygen in the observed results will become apparent and collectively, will help explain the observed results, both with regard to the control electrodes, as well as the Co(Sep)³⁺-mediated nCYP3A4-based biosensor.

With oxygen shown to be the important factor here, to grasp the significance of the fundamental role of the biosensor's interaction with oxygen, one needs to firstly understand the effect of oxygen in the context of general electrochemically based studies; secondly, its role in the physiological reaction cycle of CYP3A4; and thirdly,

the possible implication of oxygen interaction with the mediating species in mediated biosensor systems. Let us first divert our attention to oxygen in general electrode-based interactions in particular. Generally, oxygen is chemically reactive with numerous substances and also electrochemically reducible, therefore, unless catalytic studies are being conducted, electrochemical work is best done with the exclusion of oxygen. Having said that, according to documented literature, at unmodified or modified electrodes, the overall electrochemical reduction of dioxygen with electron transfer, results in the production of H₂O, with the complete process consuming a total of 4e⁻. In a more descriptive context, the reduction usually occurs through two well separated steps, the first of which corresponds to the formation of hydrogen peroxide:



While the second step corresponds to the reduction of peroxide:



Moreover, while the latter two equations gives a broad description of the overall process, on a microscopic level, the formation of H₂O₂ and H₂O, may generally be preceded and/or accompanied by a series of other intermediate basic reactive dioxygen and monooxygen species, including $\text{O}_2^{\bullet-}$, $\text{HOO}\bullet$, HOO^- , $\bullet\text{O}^-$, HO^- , that may take up one or two hydronium ions (H₃O⁺) from the electrolyte media. Generally, the large background current accrued from this stepwise oxygen reduction, can interfere with the measurements of many reducible analytes. Moreover, the products of the oxygen reduction may affect the electrochemical process under investigation.

With regard to the role of oxygen in CYP450 enzymes and CYP3A4 on the other hand, the binding and reduction of dioxygen plays a pivotal role in the reaction cycle of CYP3A4 and CYP450 enzymes in general. In fact, according to documented literature, the oxy-ferrous/ferrous-dioxygen complex (CYP3A4-Fe^{II}-O₂) has been

labelled the first and most fundamental intermediate for successful monooxygenation of substrate in the catalytic reaction cycle of the enzyme. In this regard, from a general perspective, for catalytic reactions involving P450 isoenzymes, the reduction of molecular oxygen to reactive oxygen species, such as H_2O_2 , is preferably an unwanted occurrence, since it can essentially curtail the electron transfer between the reducing equivalents and the isoenzyme under study. In this regard, once formed, the oxy-ferrous complex rapidly binds dioxygen, but the catalytic reduction to H_2O_2 rapidly follows. Moreover, the introduction of the second electron thus can result in H_2O_2 dissociation, and the overall process is known as autooxidation. Therefore, the oxy-complex is believed to be the primary source of such reactive species (radicals), i.e. superoxide/peroxide, and the resultant challenge thus is getting the second electron to be used in peroxoiron complex formation and not in H_2O_2 dissociation. Considering these factors, it is not surprising that, according to documented literature, the oxy-ferrous complex has also been categorized “the first major branching intermediate in the catalytic cycle of CYP450 in which the total efficiency of the substrate monooxygenation may be curtailed by the uncoupling reaction of autooxidation”. On the other hand, as in the case of physiological reducing equivalents, in catalytic systems utilizing electroactive pseudo-mediating species, the formation of H_2O_2 due to non-specific inadvertent reactions between the reduced mediator and dioxygen can result in catalytic activities of P450s that are uncoupled from the natural enzyme-based consumption of dioxygen. Moreover, this reaction pathway does not consume electrons, and as such, occurs in association with uncoupling of the mediator-based electron transfer to the enzyme. This can essentially divert the sequence of CYP3A4’s reaction cycle through what is known as the peroxide shunt pathway, which can also contribute to substrate turnover, but may come at the cost of enzyme longevity. In this regard, the stability of the biosensor is more inclined to the envisaged realization of a disposable platform, as opposed to reusable platform. Considering all of these aspects, the electrocatalytic response of the CYP3A4-based biosensor ($\text{GCE}|\text{naf}|\text{EI-Co}(\text{Sep})^{3+}|\text{nCYP3A4}|\text{Agris-PEI-PVA}$), to dioxygen may be regarded as a key juncture in the overall evaluation of the biosensor

dynamics and thus merits due consideration with regard to its own plausible reaction pathways, in tandem with substrate-related electrocatalytic discussions.

Bearing in mind all of the above aspects, we will now take a closer look at the electrocatalytic dynamics of the biosensor platform in the current study, essentially providing a comprehensive overview of all reactions taking place at the modified GC working electrode. In this regard, **Figure 5B** gives a schematic representation of all envisaged reactions, occurring during typical voltammetric catalytic experiments, with reference to both the nCYP3A4-based biosensor, as well as the BSA-based control electrode, as done according to the context of the experimental for the current research investigation. With regard to the reactions outlined in **Figure 5B**, reactions **A** and **C** refers to reaction pathways which may typically occur in the GC||naf|El-Co(Sep)³⁺|BSA|Agrs-PEI-PVA electrode, i.e., the BSA-based control sensor, whereas reaction **B** and **D** exhibits the reaction pathway typically occurring in the context of the GC||naf|El-Co(Sep)³⁺|nCYP3A4|Agrs-PEI-PVA electrode, i.e., the Co(Sep)³⁺-mediated, nCYP3A4-based biosensor. Let us start with the GC||naf|El-Co(Sep)³⁺|BSA|Agrs-PEI-PVA electrode: In this regard, no nCYP3A4 is present to initiate the substrate monooxygenation pathway, and as such the futile redox cycling of the system can lead to the reactive oxygen species. Firstly, as shown in **reaction A**, a small amount of dioxygen may be reduced in the film at the underlying GCE, forming the reactive dioxygen species, superoxide ($O_2^{\bullet-}$), which, when formed dismutates to H₂O₂ through another reduction process. Secondly, according to **equation 5B-4**



the electroactive mediator, Co(Sep)³⁺ is reduced to Co(Sep)²⁺, and with no nCYP3A4 present, the reaction of the reduced species with dioxygen is highly probable, a

process which also produces superoxide that dismutates to H_2O_2 , according to the following equation:



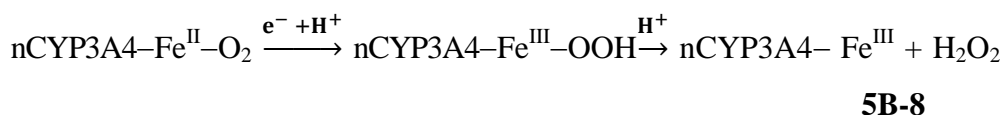
The produced H_2O_2 can of course be further reduced in the formation of H_2O as by-product, according to **equation 5B-3**. The general implications of these processes is that the accrued current associated with the produced reactive oxygen species adds to the catalytic oxygen reduction current, i.e. in the reverse scan in the cyclic voltammetric studies, and in the overall difference current in the square wave voltammetric studies, in air-saturated electrolyte media (i.e. PBS). Needless to say, this then explains the catalytic current, as observed from the results in association with the response of the GC||naf|EI-Co(Sep)³⁺|BSA|Agrs-PEI-PVA electrode in the presence of dioxygen in substrate-free air-saturated PBS (see Figure **5B.15**, **5B.16**). Moreover, the reaction associated with the GCE and with the $\text{Co}(\text{Sep})^{3+}$ occurs at separate potentials, hence the increase at two separate peak currents, as shown from the voltammograms. On the other hand, with reference to the formed H_2O_2 particular, during electrocatalytic substrate interaction studies, it is known induce the formation of small amounts of minor metabolites, a reaction path that occurs through a non-enzymatic reaction of the selected substrate with the formed H_2O_2 . In fact, this phenomenon has been documented for numerous studies involving enzyme-based electrocatalytic investigations conducted in the presence of oxygen, for which negative control-electrode studies with the occlusion of active enzyme was done [85-86, 135]. However, it must be emphasized that this reaction pathway is completely distinct from the catalytic pathway followed by the active enzyme-based electrode/biosensor, and as such, no main metabolites can form through this reaction path. Moreover, no characteristic increase with each consecutive substrate addition is seen, as opposed to the case for the active enzyme-based electrocatalysis, hence the distinctly different voltammetric reactivity exhibited by the control-electrode in the presence of increasing indinavir concentration, as shown in **Figure 5B.19**.

We can now focus our attention to the electrocatalytic reactions as occurring at the GC||naf|E|Co(Sep)³⁺|nCYP3A4|Agrs-PEI-PVA electrode (i.e. the Co(Sep)-mediated nCYP3A4-based biosensor). The reaction pathways in **Figure 5B.22** that are of significance in the case of the active-enzyme based electrode include **reaction B** and **D**. It is important to emphasize the fact that while the indinavir is the selected substrate, dioxygen is the co-substrate of nCYP3A4, and as such the reaction pathways need to be discussed with respect to both aspects. To provide a complete comprehensive stepwise overview of all the possible reaction pathways with regard to the GC||naf|E|Co(Sep)³⁺|nCYP3A4|Agrs-PEI-PVA electrode in particular, an additional schematic reaction scheme, exhibited in **Figure 5B.23**, which illustrates possible reaction pathways and also explains both the bioelectrocatalytic oxygen reduction current and the bioelectrocatalytic substrate conversion. In addition to this, where relevant, representative equations are given to provide more insight into exact reactions: Let us start with dioxygen, which, as observed in exhibited catalytic studies, showed a distinct increase in reduction peak current (see **Figures 5B.15 I** and **5B.16, 5B.20**), and as such, generally, served as evidence for the electrocatalytic activity of cytochrome P450, based on the rapid binding of dioxygen to the reduced ferrous nCYP3A4, a process with a usual rate in the order of $> 10^6 \text{ M}^{-1} \text{ s}^{-1}$. In this case, without substrate (indinavir) present, the resulting ferrous-dioxygen complex is known to be highly unstable. In this regard, it can simply accept a second electron, but on the contrary, may also release superoxide or alternatively H₂O₂, while it is itself oxidized back to the ferric form. The latter is then reduced again electrochemically, which generates the increase in cathodic (reduction) current. With regard to the exact sequence of the afore-discussed dioxygen reduction process and its associated possible pathways, the following reaction sequence describes the process, and as such, provides a in-depth explanation of the results exhibited for the catalytic studies of the fabricated biosensor.

All enzyme-based reactions are mediated through the Co(Sep)^{3+/2+} species and as such, is preceded by the initial 1e⁻ reduction reaction as shown in **equation 5B-3**.

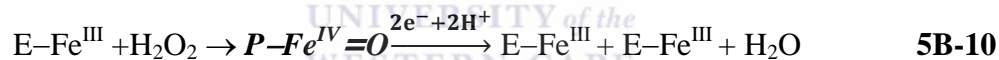
- The $\text{Co}(\text{Sep})^{2+}$ species then in turn reduces the immobilized active enzyme

$$\text{Co}(\text{Sep})^{2+} + n\text{CYP3A4-Fe}^{\text{III}} \rightarrow \text{Co}(\text{Sep})^{3+} + n\text{CYP3A4-Fe}^{\text{II}} \quad \mathbf{5B-6}$$
 - Chemical
- In the presence of oxygen, the reduction of $n\text{CYP3A4-Fe}^{(3+/2+)}$ (**equation 5B-6**) is followed by rapid dioxygen binding (**equation 5B-7**) and introduction of a second electron (**equation 5B-8**), or alternatively, the abstraction of reactive oxygen species (**equation 5B-9**) and regeneration of the ferric state.



- Autooxidation

The electrocatalytic reduction of any generated peroxide will also contribute to catalytic current (**equation 5B-10**).



In the case of the nCYP3A4-based bio-electrocatalytic interaction with the substrate on the other hand, the possible reaction pathways are a bit more complex, as exhibited in the schematic reaction scheme in **Figure 5B.23**. In this regard, after the substrate binding (**reaction 1**), the $\text{Co}(\text{Sep})$ -mediated $1e^-$ reduction of the ferric iron occurs (**reaction 2**). This is followed by binding of dioxygen (**reaction 3**), thus forming the ferrous-dioxygen complex. Following this, through another $1e^-$ transfer interaction, mediated by $\text{Co}(\text{Sep})^{3+/2+}$ (**reaction 4**), the highly reactive peroxy intermediate is formed. Furthermore, the input of protons to the reactive intermediate can result in the cleavage of the O–O bond, so producing a high-valence iron-oxygen complex (i.e. $\text{Fe}(\text{IV})=\text{O}$, also known as Compound I), which at this stage, is then reactive enough to insert an oxygen atom into the substrate (indinavir). On this subject, it must be emphasised that, although electron abstraction from substrates do occur during the

physiological reaction cycle of P450 enzymes, the substrate itself (i.e. indinavir), is unable to reduce the high valence $\text{CYP3A4-Fe}^{\text{V}}=\text{O}$ species directly. Finally, dissociation of the monooxygenated product, ROH, then restores the nCYP3A4 to the starting ferric state (**reaction 5**).

At this stage, the release of reactive oxygen species needs to also be considered, since it is known to be a highly probable envisaged reaction pathway in the P450 reaction cycle, particularly in the case of human microsomal P450 isoenzymes, [67, 73, 77, 87]. In this regard, within the enzyme, the release of superoxide is followed by disproportionation and generation of H_2O_2 , which as explained earlier, in the vocabulary of P450 enzymology, is referred to as the decoupling/uncoupling reaction. Indeed, the uncoupled formation of peroxide has been observed with various mammalian P450 isoenzymes [81]. In the context of the current investigation, as outlined by the scheme in **Figure 5B.23**, the main branching points for uncoupling for the nCYP3A4 may be envisaged at the level of the dioxygen ferrous complex (**reaction 6**) or the ferric-hydroperoxy complex (**reaction 7**) [12, 23, 77]. In the absence of substrate, this catalytic oxygen reduction may effectually regenerate the ferric enzyme, which may again be reduced (**reaction 2**). The concomitant effect will be enhancement of the electrochemical reduction. On the other hand, the peroxide can substitute for oxygen and reducing equivalents in what was earlier described as, the peroxide shunt pathway, in which the formed H_2O_2 directly converts the enzyme to its reactive putative ferryl species, i.e. $\text{nCYP3A4-Fe}(\text{V})=\text{O}$, which is the reactive electrophilic iron oxo intermediate that attacks the substrate for monooxygenative product formation [23]. In fact this reaction pathway has played been identified as minor and major contributory reaction pathways in numerous electrode-based enzyme-substrate electrocatalytic investigations [77, 85, 89, 135]. Still on this subject, this reaction, however, does not occur in association with the consumption of electrons and will thus not lead to catalytic reduction current. A noteworthy aspect to add is that the general process of catalytic oxygen reduction, as well as the catalytic substrate conversion process consume the same number of electrons, and as such,

substrate conversion will not result in a higher electron uptake per cycle, therefore increase of the reduction current should in effect be a result of a increase in rate (hence the further increase in reduction current with indinavir, as shown in **Figures 5B.15 and 5B.16**). In this regard, it is not possible to conclusively elucidate the reaction pathway from net current alone.

With respect to substrate in particular, substrate binds to the six co-ordinate low spin ferric heme (**reaction 1**). In terms of the natural reaction cycle of P450s, binding of the substrate induces the displacement of the axial H₂O molecule from the enzyme active site, and as such, generally triggers the catalytic cycle of the enzyme, resulting in a penta-coordinated high spin substrate-complexed heme [78, 134]. This essentially makes the heme a better electron sink and thus triggers electron transfer from the natural NADPH reducing equivalents; this electron transfer event then initiates the cycle [22]. In the context of the current research investigation, the favourable effect of substrate in tandem with interaction with the reduced Co(Sep) mediator, results in the overall initiation of the catalytic cycle. Dioxygen binds, with a diffusion limited rate constant of $\geq 10^{-6} \text{ M}^{-1} \text{ s}^{-1}$ in the context of P450s in general [22, 77], and in the context of CYP3A4 in particular, the rate constant is estimated to be $5 \times 10^{-5} \text{ M}^{-1} \text{ s}^{-1}$ [67], and as such, the process is not rate limited [77]. A noteworthy cautionary factor to consider at this stage, though is that according to documented research findings, in general, with regard to rate-limiting steps in human CYP3A4 catalysis, uncoupled autooxidation reactions for this enzyme was shown to be 2–3 orders of magnitude faster than in the case of the other P450s [67]. Additionally, product formation in human P450s was generally shown to be slower than the rates of uncoupling reactions, thus, in the absence of substrate the oxy complex in CYP3A4 would usually tend to autoxidise rapidly and return to the ferric heme state [22, 67]. Notwithstanding these factors, it must be said here that catalytic studies in the current research investigation was done by maintaining a 15–20% glycerol content within enzyme region of the reagent layer. The significance of this aspect lies in the fact that according to documented literature, glycerol has been generally shown to confer a

unique stabilizing effect on P450 enzymes [24, 173]. In the context of catalysis in particular, stabilization is thought to occur mainly through slowing down enzyme reaction rates, and reducing non-specific potentially harmful uncoupling interactions, while also providing the necessary lubrication for enzyme catalysis through multiple hydrogen bond capability, conferred by its water mimicking nature [174-175]. Furthermore, in this context, the overall stabilizing effect of glycerol may result in a longer-lived, iron-peroxy species, thus attenuating its premature dissociation before substrate conversion to compound I, which will of course have a favourable effect on enzyme-based substrate hydroxylation [73, 82]. In addition to this, with reference to human microsomal CYP3A4 in particular, prior research has also shown that the bound presence of substrate significantly stabilizes the oxy-ferrous complex against any uncoupling oxygen reduction reactions, while also modulating the escape of any superoxide or hydroperoxyl species from the heme binding pocket [67]. Considering these aspects, and the infinitesimally low detected concentrations of H_2O_2 during enzyme-based catalytic studies, as well as the small relatively small difference between catalytic oxidation current in the absence and in the presence of indinavir (as shown in Figure 5B.15–5B.17) it appears that in the current investigation, “futile” reduction reaction pathways is slower than the substrate conversion, which also consumes electrons. On this note, it must also be said at this stage though, that further studies will be required to completely understand and elucidate the intricate details of the electrocatalytic CYP3A4-reaction.

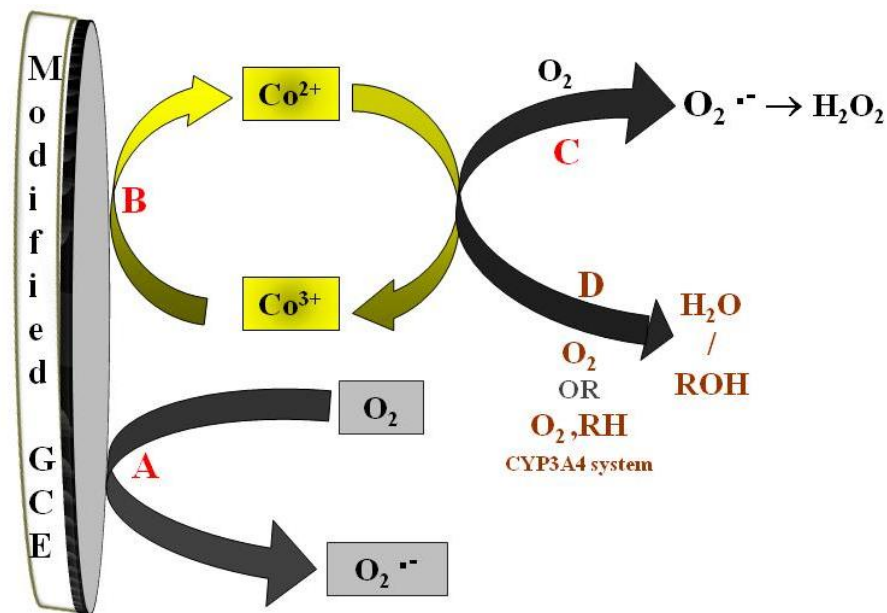


Figure 5B.22 Schematic representation of the reactions occurring at the modified glassy carbon working electrode during electrocatalysis experiments.

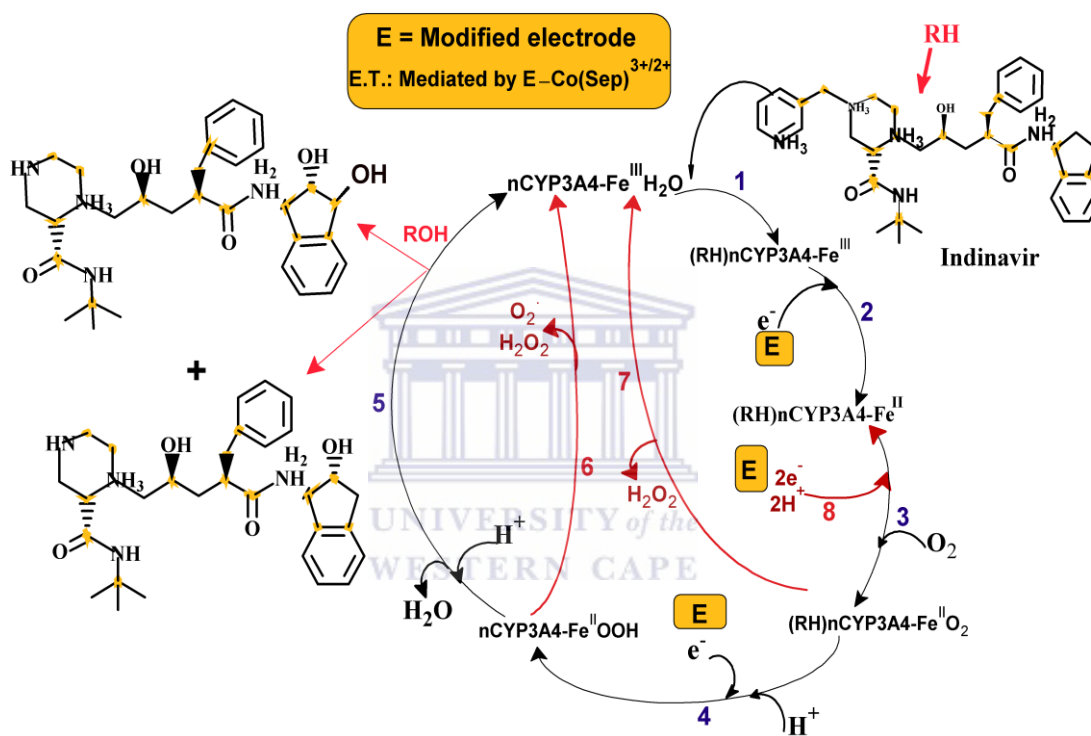


Figure 5B.23 Suggested general scheme of the electrocatalytic reaction of nCYP3A4 [mediated by Co(Sep)] in the presence of oxygen. The presence of bound substrate is marked by (RH). All reaction pathways are included in a catalytic cycle for better indication/illustration of the possible processes.

5B.4 Conclusions

This study demonstrates the successful incorporation of the catalytically active N-terminally modified CYP3A4, consisting only of the heme domain and surrounding apoprotein, synthesized through genetic engineering by over expression in ecoli cells as biorecognition component in a reagentless amperometrically-based

biosensor. Moreover, the nafion-modified GCE, containing the potentiostatically integrated $\text{Co}(\text{Sep})^{3+}$ electroactive mediating species served as pseudo-electron transfer donor species for the nCYP3A4 isoenzyme and as such, enabled the electron transfer for bio-electrocatalytic activity of the enzyme, while the $\text{Co}(\text{Sep})^{3+}$ was in turn continuously regenerated at the modified GCE. In addition to this, the detection and quantification of the PI ARV, indinavir was realized, while the hydrogen peroxide shunt path did not appear to play a role in substrate catalytic interaction. Another important observation is that the working potential, with particular reference to the reduction/activation of dioxygen is was shown to be considerably reduced, as compared to biosensor platform 1 and some other documented studies.

5B.5 Materials and Methods of Investigation

5B.5.1 Preparation of Recombinant N-terminally modified CYP3A4 (nCYP3A4)

5B.5.1.1 Reagents and materials

All categories of materials and reagents (including their specific constituents) used in during this process are comprehensively described and outlined in **table 3B.1**, under the section labelled “The reagents and materials for enzyme expression and purification of N-terminally modified CYP3A4”, in Chapter 3B. An important fact to also emphasize at this stage is that all working solutions used throughout the process of expression and purification of the enzyme was either autoclaved or filtered through specialized filters, or both.

5B.5.1.2 Expression and purification of CYP3A4 construct

This process describes the expression and purification of the human recombinant, heme-thiolate CYP3A4 isoenzyme, in which genetic engineering was used to modify the hydrophobic N-terminal anchor of the CYP450 3A4 isoenzyme, by removal of 25 amino acids from this region, and as such, eventually preparing a N-terminally modified soluble construct tagged with a histidine residue.

From a general perspective, the expression/purification process comprised five consecutive steps, which included (1) inoculation of the preculture; (2) growing the culture and adding specific reactants to induce protein expression in the host cell; (3) disrupting the cell membrane to release proteins (lysis); (4) purification of obtained protein through making use of affinity-based columns; (5) quantification of the obtained product to measure protein concentration. On the other hand, the 'micro-steps' in the actual process was quite an intricate endeavour. Moreover, to ensure successful product formation, it was absolutely necessary that each of these steps were conscientiously and meticulously carried out. Having said that, an outline of the complete protocol is described as follows:

5B.5.1.2.1 Construct expression for CYP3A4/Preculture inoculation

5 mL of the luria broth (LB) medium (see table 3B.1 for constituents of the LB medium) was pipetted into a 50 mL, high density glass vial. To this solution, 10 μ L of the glycerol stock (consisting of the single colony E-coli cells containing the DNA that encodes the N-terminally truncated P450 3A4 isoenzyme), and 5 μ L of a

(previously prepared) 1 M ampicillin (AMP) was added. The so formed mixture (**solution A**), usually referred to as the pre-culture, was then incubated over night (O/N) at 37 °C with shaking at 150 rpm (strict adherence to the temperature was ensured by proper thermostating). With regard to solution A, depending on the amount yield required, usually 2 or 3 samples of solution A was prepared during each expression/purification experiment. On the same day that the pre-culture was prepared, 900 mL terrific broth (TB) medium was also prepared (see table 3B.1), in a 1 L conical flask, which was followed by autoclaving and overnight cooling. The following day, after the 24 hr incubation period, 100 mL (1x) K-phosphate buffer solution was added to the (pre-warmed) TB medium, forming **solution B**. To solution B, the following was added: 1 mL of 1 M AMP, 1 mL of 1 M thiamine and 2.5 mL trace element solution (see table 3B.1 for specific constituents), thus forming **solution C**. Solution C was then divided into two 500 mL samples. The two samples can be referred to as culture C₁ and C₂. To each of the 500 mL cultures, i.e. C₁ and C₂, a 5 mL of the previously incubated solution A (pre-culture) was added, thus forming **solution D₁** and **D₂**. Solution D₁ and D₂ was then incubated at 37 °C with shaking until the the optical density for each culture was between 0.4 – 0.6. It took approximately 3 – 4 h of incubation to attain the required OD. After the desired absorbance readings were attained, δ-aminolevulinic acid (δ - ALA) was added to each of solutions D₁ and solution D₂ to a final concentration of 0.5 mM. Each of the δ - ALA –containing solutions was subsequently incubated at 30 °C, 150 rpm for 30 min. After the 30 min has lapsed, CYP3A4 heme expression was induced in each solution by addition of IPTG to a final concentration of 1 mM. The induced cultures, i.e. solution D₁ and D₂, were then incubated for a total of 18 h at 30 °C, with shaking at 150 rpm.

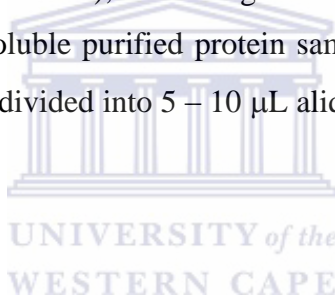
5B.5.1.2.2 Preparation of the crude lysates

Following the 18 h incubation period, the expressed cultures were harvested. For this process, each of the two culture samples were further divided into smaller aliquots in high density centrifuge tubes, followed by centrifugation of each sample at 5 000 rpm for 15 min at 4 °C. During centrifugation, a cell pellet collected at the bottom of each centrifugation tube, which was used in the subsequent steps, while the supernatant was discarded. In this regard, each of the cell pellets was re-suspended in 250 mL 1 x phosphate buffer saline (PBL, pH 7.4). The re-suspension process generally comprised of gentle agitation of the pellets until complete dissolution has taken place, and all solid pellets were suspended in the PBL. After re-suspension, the centrifugation process was repeated at 4 °C, again resulting in cell pelleting. Next, the cell formed pellets were re-suspended in 5 mL lysis buffer (see table 3B.1), following the same 'agitation process' as before. To the re-suspended pellets, lysozyme (to a final concentration of 1 mg mL⁻¹), DNase I (500 U), CaCl₂ (final concentration = 0.5 mM), and MgCl₂ (final concentration 2.5 mM) were all added. It is noteworthy to also add that the lysis suspended cell pellets gave a final volume of approximately 10 mL, therefore the final concentrations of all the latter constituents were with respect to a 10 mL solvent volume. Next, the cell suspensions were incubated on ice for 30 min with very gentle shaking. Following the ice incubation step, the cell suspensions were then subsequently centrifuged at 10 000 *xg* at 4 °C for 30 min and the resulting supernatants, which may be referred to as the crude soluble lysate preparations, were either stored in 100 µL aliquots at -20 °C for later analysis, or were then used for the subsequent protein purification process.

5B.5.1.2.3 Protein purification

The Ni-TED resin (see table 3B.1) was used for the initiation of the protein purification process. The, Ni-TED, with the provided buffers were obtained from the manufacturers. To the Ni-TED HisLink wash buffer obtained was added 75 mM

imidazole. In addition to this, 250 and 500 mM imidazole was also added to the elution buffer which was for use in the sequential elution process involving 2.5 mL of the elution buffer for each elution. The Ni-TED resins were then packed into Pharmacia (PD) – 10 columns. The histidine-tagged crude soluble lysate preparations were then purified with the Ni-TED resins, by affinity. Meanwhile, Centriprep YM – 10 columns were rinsed with 15 mL Milli-Q water by centrifugation at 3000 xg . Next, each resin – purified protein sample was added to a cleaned Centriprep column and centrifuged at 3 000 xg at 4 °C until the protein samples were concentrated to just below 700 μ L. The Centriprep concentration process took approximately 35 min. Following this, each protein concentrate was then added to a Zeba column for buffer exchange into the final P450 storage buffer (see table 3B.1 for constituents), according to the instructions provided by the manufacturer. The final soluble purified protein samples were eluted from the Zeba columns and immediately divided into 5 – 10 μ L aliquots, which was stored at -20 °C until used.



5B.5.1.3 Total protein quantification

The determination of total protein concentrations in the purified protein samples were done with the use of the Bio-Rad protein dye, based on the Bradford micro-assay. In this regard bovine serum albumin (BSA) was used for creation of standard curves. The exact protocol was done according to the manufacturer's instructions. Briefly, 20 mg/mL BSA were prepared in the P450 storage buffer, thus forming solution A. Solution A was then diluted to 100 μ g mL⁻¹, thus forming solution B. Solution B was then used to prepare 5 standard BSA solutions of concentrations, 2-, 4-, 6-, 8- and 10 μ g mL⁻¹. In this regard, three replicates of these standard solutions were prepared. Meanwhile, 1 in 20 dilutions of the purified protein samples were prepared (also in triplicate). Next, 200 μ L concentrated Bardfords

reagent was thoroughly mixed with 800 μL of each standard or purified protein sample working solution. Each of the mixtures were aged for 5 min, after which the absorbance readings were recorded at A595. The results were then used to obtain a calibration curve, from which the purified protein concentrations were estimated. To eventually calculate the molarity, the molecular weights used for the

5B.5.1.3 Spectral analysis of and activity assays the prepared nCYP3A4 construct

5B.5.1.3.1 FTIR spectral analysis

Spectra were recorded by placing a drop of the enzyme-containing solution directly on the gasket of the cell window, as shown in Figure 5B.24. The background spectra of the protein storage solution were also taken and the necessary background subtractions were done with the inherent mathematical software of the system.

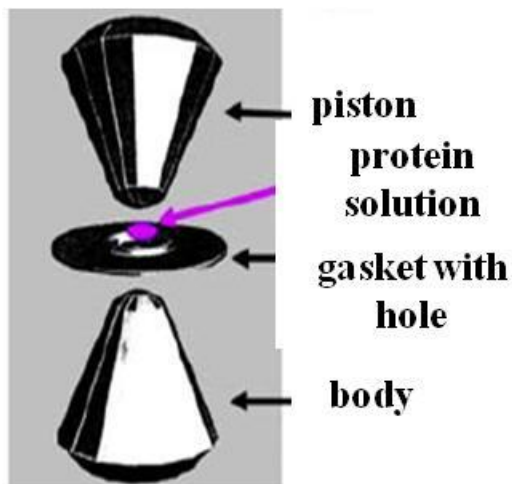


Figure 5B.24 Showing method of FTIR analysis with high-pressure anvil cell for wet nCYP3A4 samples.

5B.5.1.3.2 UV-Vis spectra of resting state nCYP3A4 (nCYP3A4-Fe³⁺) construct

UV-Vis spectra of the resting state nCYP3A4 were taken with 3 M nCYP3A4, in a potassium-phosphate buffer solution, containing 20% glycerol, 1 mM DTT and 0.2 mM EDTA, with a dual-beam spectrometer. The enzyme storage solution was used for background.



5B.5.1.3.3 Activity assay for the nCYP3A4 construct: Carbon monoxide complex

Cytochromes P450 got their name from their atypical spectral properties displaying a characteristic absorption maximum of the reduced carbon-bound complex at 450 nm. Thus the ability of the reduced P450 to produce an absorption peak at 450 nm upon CO binding has been used throughout the years for estimation of the P450 content [21, 23]. In this regard, the method of analysis is still done, according to its discoverers, i.e. according to the method of Omural and Sato [159]:

- A working solution of the synthesized enzyme construct was prepared by dilution of the stock into 50 mM KPBS (pH 7.4), containing glycerol (20% v/v). The glycerol was necessary to stabilize the enzyme against autooxidation

- The solution was argon-degassed and the baselines were recorded with a dual-beam UV-Vis spectrometer (see details of instrument in Chapter 3B).
- Reduction of the protein was then initiated by injection of equimolar concentration of sodium dithionite (made up in a 0.5 mM solution with the buffer). The spectra was then measured at 1.5 – 2 min intervals, until no further reduction was observed. i.e. until no further variation in the 420 nm peak was observed.
- At this point, CO was gently bubbled through the solution for 30 sec intervals followed by intermittent measurement of the spectra until no further increase in the 450 nm peak was observed.
- The difference spectra were then obtained by subtraction of each reduced protein spectrum from the relevant CO – bound reduced spectrum to obtain the final difference spectrum.
- Amount of catalytically active heme – bound protein content was calculated using $\epsilon_{450 - 490} = 91 \text{ mM cm}^{-1}$, whereas inactive (denatured) heme - bound nCYP3A4 content was calculated according to $\epsilon_{420 - 490} = 111 \text{ mM cm}^{-1}$.

5B.5.2 Methods and protocols for biosensor preparation, optimisation studies and voltammetric investigations

Table 5B.2 Materials and reagents used

Reagents and materials for optimized Co(Sep) ³⁺ -mediated nCYP3A4-based biosensor	
Reagents for carrier matrix preparation	1% nafion (pH 7.4); 1mM Co(Sep) ³⁺ (in 100 mM KPBL)

Reagents for outer-film preparation	5% PVA (in 100 mM KPBS), 1% agarose (in milli-Q H ₂ O), PEI in (100 mM KPBS)
nCYP3A4 casting solution	1.5 μM nCYP in 100 mM KPBST, pH 7.4 (See table 3B.1 for exact constituents of buffer)
Reagents for catalytic studies	Molecular dioxygen (O ₂) and indinavir
Reagents and materials for un-mediated nCYP3A4-based biosensor	
Reagents for carrier matrix	1% nafion only (pH 7.4)
Reagents for outer-film preparation	Exactly the same as described in previous section
nCYP3A4 casting solution	Exactly the same as described in previous section
Reagents for catalytic studies	Molecular dioxygen (O ₂) and indinavir
Reagents and materials for Control sensor platform	
Reagents or carrier matrix preparation	1% nafion (pH 7.4); 1mM Co(Sep) ³⁺ (in 100 mM KPBL)
Reagents for outer-film preparation	5% PVA (in 100 mM KPBS), 1% agarose (in milli-Q H ₂ O), PEI in (100 mM KPBS)
Pseudo enzyme casting	BSA in 100 mM KPBST, pH 7.4

Note: For exact constituents of reagents and protocols for preparation of working solutions etc, the reader may consult the relevant subsections in Chapter 3B

5B.5.2.1 Preparation of Co(Sep)³⁺-mediated nCYP3A4-based biosensor (under optimised conditions) for voltammetric characterization and catalytic investigations

The working electrode used in this study was a clean or modified GCE. Before modification, the GCE was activated and pre-treated according to the method outlined in **Section 3B.3.1.1** of Chapter 3. 5 μL 1% nafion (pH 7.4) was subsequently drop coated onto the activated GCE surface. The electrode was then covered with a tight-fitting cover to allow the stable formation of a smooth nafion film. After a dry nafion film has formed the Co(Sep)³⁺ was incorporated into the nafion membrane by potentiostatic electrodeposition. For this process, the a argon-

degassed 100 mM potassium phosphate buffer saline (KPBL, pH 7.4) solution, containing 1 mM cobalt(III) sepulchrate (prepared as described in **Section 3B.2.2.3.2**, Chapter 3) was used as electrolyte medium. The electrodeposition was done at a constant potential of +450 mV for 1 200 sec, after which the modified electrode was rinsed and air dried. The naf-EI-Co(Sep)³⁺ modified GCE (GCE||naf|EI-Co(Sep)³⁺) was then subjected to electrochemical cycling in a 50 mM PBS until a stable background current was obtained. At this point the nCYP3A4-based biosensor was prepared. In this regard, a total of 6 μ L nCYP3A4 (1.5 μ M) was drop-coated onto the GCE||naf|EI-Co(Sep)³⁺ in two 3 μ L aliquots by a sterilized, calibrated glass micro-syringe. In addition to this, each drop-casting step was followed by intermittent setting at 2 °C after each casting step for duration of 5 min each. In addition to this, the enzyme modified electrode was placed in a gentle flow of argon for approximately 5 min, followed by immediate casting of the outer layer solution. In this regard, 7 μ L of the blended ionic polymer-composite solution (prepared as described in **Section 3B.2.2.3.6**, Chapter 3B) was drop-cast onto the GC||naf|EI-Co(Sep)³⁺|nCYP3A4 electrode with a calibrated glass micro-syringe. An important requirement for this step was that both the casting solution and the syringe needed to be pre-warmed in order to prevent pre-mature solidification of the solution. Finally, the prepared biosensor, denoted GCE||naf|EI-Co(Sep)³⁺|nCYP3A4|Agrs-PEI-PVA, was set for eight hours at 2 °C.

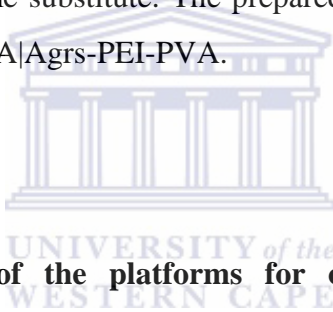
5B.5.2.2 Preparation of un-mediated nCYP3A4-based biosensor for voltammetric characterization and catalytic investigations

The preparation of this biosensor was exactly the same as described in the pre-ceding section, except that in this case, no Co(Sep)³⁺ electrodeposition was done and as such, enzyme casting was done directly after the formation of the base nafion-

film, exactly as described above. This was then followed by casting of the outer-film solution, also done exactly as described above. The prepared biosensor may be denoted, GCE||naf|nCYP3A4|Agrs-PEI-PVA.

5B.5.2.3 Preparation of the Co(Sep)³⁺ based control sensor platform

The sequential steps for preparation of the control sensor platform was exactly the same, as outlined in **Section 5B.5.2.1**. However, in the case of the control platform, instead of the prepared nCYP3A4 construct, bovine serum albumin (BSA) was cast as pseudo enzyme substitute. The prepared control sensor may be denoted GCE||naf|EI-Co(Sep)³⁺|BSA|Agrs-PEI-PVA.



5B.5.2.4 Preparation of the platforms for optimisation of the variables concerning the indinavir amperometric biosensor

5B.5.2.4.1 Preparation of Co(Sep)³⁺-mediated nCYP3A4-based biosensor platform with Eastman-AQ as base layer and crosslinked PVA as outer film

5 μ L of an aqueous 3% EAQ dispersion was drop coated onto a clean, activated GCE with a micro-pipette. The modified GCE was covered with a tightly fitting lid to allow even formation of the EAQ-film. Once dry, the Co(Sep)³⁺ mediating species was incorporated into the pre-formed EAQ using a protocol exactly as described in **Section 5B.5.2.1** above. Since the EAQ-EI-Co(Sep)³⁺ film did not appear very stable, it was not subjected to subsequent electrochemical cycling in a 50 mM PBS before biosensor construction, as in the case of the biosensor with nafion as

base film. The next step involved drop-coating 6 μL of the prepared nCYP3A4 (1.5 μM) with a sterilized calibrated glass microsyringe. Following this, the enzyme-film was set for approximately 5 min at 2 $^{\circ}\text{C}$ followed by further setting under gentle argon flow for 5 min. In the next step, 7 μL of a 5% aqueous PVA solution (prepared as described in **Section 3B.2.2.3.5**, Chapter 3) was cast onto the nCYP3A4-derivitized electrode, as outer film component. PVA is usually labile in aqueous solution and as such, to ensure stable enzyme encapsulation, the cast PVA was subsequently crosslinked. The technique used for crosslinking was customised from standard methods [103, 164]. The method basically comprised acid catalyzed crosslinking with glutaraldehyde (25% v/v). The biosensor, denoted GCE||EAQ|El-Co(Sep)³⁺|nCYP3A4|cIPVA was placed in milli-Q water to remove any unreacted components and stored at 2 $^{\circ}\text{C}$ for further setting .



5B.5.2.4.2 Preparation of Co(Sep)³⁺-mediated nCYP3A4-based biosensor platform with nafion as base layer and crosslinked PVA as outer film

The nafion base layer was formed exactly as described in Section 5B.5.2.1. In addition to this, incorporation of the Co(Sep)³⁺ mediating species into the pre-formed nafion membrane was also done exactly according to the method outlined in Section 5B.5.2.1. The GCE|naf|El-Co(Sep)³⁺ electrode was then subjected to electrochemical cycling in a 50 mM PBS until a stable background current was obtained. Following this, the prepared nCYP3A4 was immobilized in exactly the same manner as outlined in **Section 5B.5.2.4.1**. In addition to this, casting and crosslinking of the PVA outer layer was also done exactly the same as described in **Section 5B.5.2.4.1**. The prepared biosensor is denoted GCE||naf|El-Co(Sep)³⁺|nCYP3A4|cIPVA.

5B.5.2.4.2 Preparation of Co(Sep)³⁺-mediated nCYP3A4-based biosensor platform with nafion as base layer and crosslinked PVA as outer film

In this case the nafion film, Co(Sep)³⁺ incorporation and immobilization of nCYP3A4 was done exactly according to the method outlined in **Section 5B.5.2.1**. In addition to this, the casting of the outer layer solution was also done exactly according to method outlined in the afore-mentioned section. However, the ratio of PEI with respect to the PVA-Agrs was varied by varying the volume of PEI in the casting solution.

5B.5.2.4.3 Preparation of biosensor platforms for nCYP3A4 loading optimisation studies

For investigation of this variable, the amount of nCYP3A4 was varied, while all other variables were kept constant. In this regard, the casting volume of nCYP3A4 was varied, i.e. 4-, 5-, 6-, 7- and 8 μL . In terms of the fabrication of the biosensor platforms, in its entirety, each platform was prepared exactly according to the sequential protocol outlined in **Section 5B.5.2.1**.

5B.5.2.4.4 Preparation of biosensor platforms for Co(Sep)³⁺ potentiostatic loading time optimisation studies

With regard to investigation of this particular variable, the potentiostatic Co(Sep)³⁺ electrodeposition time was varied, while all other parameters were kept absolutely constant. For this purpose, Co(Sep)³⁺ electro-deposit times were varied

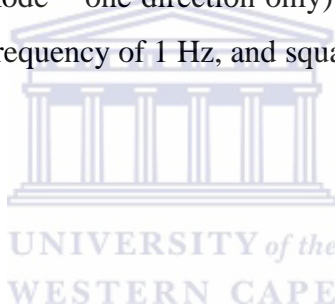
from 300 up to 2 000 sec. Again, as in the previous case, with regard to fabrication of the biosensor platforms, the protocol followed was exactly according to the method outline in **Section 5B.5.2.1**, the only difference, where relevant, being the $\text{Co}(\text{Sep})^{3+}$ electro-deposition times.

5B.5.2.4 Procedures for voltammetric characterization of the prepared platforms

All voltammetric characterization studies were done with a three electrode arrangement as described in **Section 3B.3.1**, Chapter 3B (see also **Figure 3A.8**). The supporting electrolyte used throughout characterization in all cases, were argon-degassed 50 mM phosphate buffer solution (PBS, pH7.4). For cyclic voltammetric investigations, the particular electrode was cathodically scanned from -100 mV to the switch potential, -950 mV (vs Ag/AgCl). Cycling was done until a steady state background current for the Faradaic redox response was observed, and as such, all voltammograms were collected from the 5th cycle onward, when a stable background current was observed. Osteryoung square wave voltammetry (SWV) was done by applying a linear reductive potential scan (cathodic mode – one direction only) between -100 and -950 mV at a step potential of 4 mV, a frequency of 1 Hz, and a square wave amplitude of 25 mV. Differential pulse voltammetry (DPV) for the reduction wave was performed by applying a potential scan from -100 to -950 mV (vs Ag/AgCl), with specific parameters as follows: scan rate = 20 mV s⁻¹, pulse amplitude = 25 mV, sample width = 2 ms, pulse width = 15 ms, pulse period = 200 ms and quiet time = 2 s. For the DPV of the oxidative wave, the electrode was scanned from -950 to -100 mV, while all other parameters were exactly the same of the for the reductive scan.

5B.5.2.5 Procedures for catalytic response investigations

All catalytic response investigations were conducted in un-degassed 50 mM PBS in the presence, or absence of the substrate of interest (i.e. indinavir). Response experiments were done with cyclic voltammetry and square wave voltammetry. In this regard CV and SWV was run in the presence and absence of oxygen and/or indinavir to investigate the $\text{Co}(\text{Sep})^{3+}$ -mediated or un-mediated enzyme-oxygen-substrate interaction. For all cyclic voltammetric investigations, in the presence of oxygen and/or indinavir, the electrode was cathodically scanned from -100 mV to the switch potential, -950 mV (vs Ag/AgCl) at a scan rate of 5 mV s^{-1} . Square wave voltammetric investigations were done by applying a linear reductive potential scan (cathodic mode – one direction only) between -100 and -950 mV at a step potential of 4 mV, a frequency of 1 Hz, and square wave amplitude of 25 mV.



5B.5.2.6 Procedures for investigations of optimisation of the variables

As a sensitivity criterion for the optimisation of the relevant working variables affecting the behaviour of the indinavir biosensor: Firstly, optimisation was done with respect to the working potential for the reduction of oxygen. In this regard, the platforms were evaluated with regard to a lower operating potential which could significantly reduce the overpotential for oxygen reduction as compared to the results obtained for biosensor platform 1, as well as previous investigations involving CYP3A4. Secondly, in terms of response to indinavir, evaluations, where relevant was done with the slope of calibration curves for indinavir for predetermined concentration range as sensitivity criterion. The specific concentration ranges and slopes, etc. are discussed in the relevant results sections in the current chapter.

CHAPTER 6

Summary and Conclusions

6.1 Introduction

In the current chapter the results obtained in association with the two biosensor platforms from the work presented in the dissertation is summarized. In this regard, a summary of each individual results chapter, with particular reference to recapitulating the main and most significant findings and conclusions for that particular chapter is given. In addition to this,

6.2 Summary of individual results chapters

6.2.1 Chapter 4

These results are based on design **path 1**, as shown in the flow diagram exhibited in Chapter 3B.

The detection and quantification of endocrine disruptor compound/priority pollutant, 2,4-DCP have been successfully realized by using the fabricated GCE||naf|CMECo(Sep)³⁺|f|CYP3A4|naf biosensor. The design path for this biosensor platform, was based on sandwich configuration, in which detergent-monomerized, commercially obtained, full-length human recombinant CYP3A4 was entrapped between a cobalt(III) sepulchrates derivatised nafion inner-membrane and a thin nafion outer film. Entrapment of the Co(Sep)³⁺ in the preformed nafion membrane was achieved through simple manual drop-casting and mixing method. In this regard,

FTIR confirmed the existence of the $\text{Co}(\text{Sep})^{3+}$ counter-ion species in the nafion membrane. The variation in the electrochemical characteristics in association with the progression from the nafion-modified GCE, to the reagentless mediator containing fYCYP3A-derivatized biosensor platform confirmed the electron flow from the electrode to the fYCYP3A4 via the (nafion pre-concentrated) $\text{Co}(\text{Sep})^{3+}$ mediator. Moreover, comparative evaluation of the exhibited electrochemically based results for the $\text{GCE}||\text{naf}|\text{CMECo}(\text{Sep})^{3+}|\text{fYCYP3A4}|\text{naf}$ biosensor with that of the $\text{GCE}||\text{naf}|\text{CMECo}(\text{Sep})^{3+}$ carrier matrix, suggested the favourable interaction between the monomerized fYCYP3A4 through possible coulombic and/or hydrophobic interactions of the nafion with the surfactant-type CHAPS detergent.

The voltammetric investigations of the $\text{GCE}||\text{naf}|\text{CMECo}(\text{Sep})^{3+}|\text{fYCYP3A4}|\text{naf}$, revealed a E_m of ≈ -590 mV. Moreover, the surface coverage, Γ , of the electroactive $\text{Co}(\text{Sep})^{3+}$ species was determined as 9.8×10^{-8} mol cm^{-2} . On the other hand, the constant value exhibited for the current function $I_p/v^{1/2}$ suggests that the charge transfer of the biosensor in the absence of oxygen and substrated in the higher scan region is a diffusion-kinetically controlled process. Thus, the D_{ct} , calculated by Randle Sevcik analysis, was determined as 0.5×10^{-8} $\text{cm}^2 \text{ s}^{-1}$. Inter-day electrochemical evaluation of the storage stability of the biosensor revealed a gradual decline in signal in association with progressive leaching of the mediating species from the reagent layer.

With respect to the electrocatalytic investigations, the following findings were made:

- The catalytic increase in $I_{p,c}$ in association with the injection of the substrate, 2,4-DCP, in anaerobic phosphate buffer saline, coupled to the small simultaneous anodic E_p shift, suggested the presence of sufficient residual dioxygen in the substrate containing solution to induce bioelectrocatalytic response from the reduced heme iron, fYCYP3A4- Fe^{2+} for the formation of the active oxy-ferryl species, for effecting hydroxylation of the 2,4-DCP.

- The GCE||naf|CMECo(Sep)³⁺|flCYP3A4|naf biosensor showed an average reduction potential for dioxygen of -600 (± 10) mV, as determined from CV and SWV. With regard to the cyclic voltammetric results in particular, the bio-electrocatalytic response to molecular dioxygen was signified by a considerable increase in $I_{p,c}$ which was simultaneously accompanied by a complete attenuation of the $I_{p,a}$.
- The results exhibiting the catalytic response of the biosensor to the 2,4-DCP, suggested that the presence of the substrate increased the rate of dioxygen binding to the flCYP3A4-Fe²⁺.
- In the presence of increasing 2,4-DCP concentrations, the biosensor exhibited a periodic increase in catalytic peak current in conjunction with each consecutive addition, up to the final concentration.
- The catalytic investigations with the native physiological CYP3A4 substrate, erythromycin, exhibited results that was in complete agreement with the findings as observed for 2,4-DCP. This re-affirmed and corroborated the catalytic response was due to the enzyme-based bio-recognition component, i.e. flCYP3A4.
- Similarly, the inhibition of the bio-electrocatalytic response of the flCYP3A4 in association with the observed decrease in catalytic response signal to 2,4-DCP in the presence of native, physiological CYP3A4 inhibitor, ketoconazole, served as additional re-affirmation of catalytic activity of the bio-recognition component.
- With regard to the calibration curve for 2,4-DCP: The dynamic linear range for this substrate had an upper limit of 45 μA and a sensitivity of 0.038 $\mu\text{A } \mu\text{M}^{-1}$. In addition to this, the LOD was determined as 0.043 $\mu\text{g L}^{-1}$.
- The linear curve for ERM showed a linear range over 4.63 → 26.4 μM , while the dynamic linear range showed an upper limit of 26.4 μA . The sensitivity was determined as 0.323 $\mu\text{A } \mu\text{M}^{-1}$ and the LOD calculated as 1.271 x 10⁻⁵ M.

Overall, the biocatalytic response of the fICYP3A4 to the selected substrates were successfully mediated by the immobilized $\text{Co}(\text{Sep})^{3+}$ species. The manual casting/mixing method thus seemed to be a feasible method of pre-concentrating the mediator within the reagent layer.

6.2.2 Chapter 5A

These results are based on **design path 2**, as shown by the flow diagram exhibited in Chapter 3B.

Here, the incorporation of the electroactive $\text{Co}(\text{Sep})^{3+}$ cationic species into the microstructure of a pre-formed nafion film is successfully achieved through an innovative electrochemically based technique, which involved potentiostatic deposition at a potential of +450 mV for a duration of 1 200 sec. The cyclic voltammetric characterization of the nafion-derivatised GCE, suggested that the nafion film effectively filled approximately 15 – 20% of the active sites of the underlying GCE, but did not substantially impede ET with respect to the underlying electrode, which essentially meant that the pre-formed nafion film could serve as efficient matrix for subsequent incorporation counter-ion species. Moreover, morphological analysis of the nafion film revealed a microstructure with highly evenly formed, smooth consistency and compact nature. The thickness of the nafion membrane was determined as 3.1 μm . With regard to the $\text{Co}(\text{Sep})^{3+}$ modified nafion film, the electrochemical characterization studies indicated fast reversible ET for the metal-centred electroactive species, with an average E_m determined as -615 mV. Moreover, ΔE_p variation for scan rates between 2 \rightarrow 10 mV s^{-1} was negligible, while the average $I_{p,a}/I_{p,c}$ was shown to be ≈ 1 . In addition to this, the GCE||naf|E| $\text{Co}(\text{Sep})^{3+}$ exhibited a stable background current under continuous and/or intermittent cycling, with no indication of variation or reduction in the observed redox signal for scans taken at half hour up to four hour intervals. The total surface

coverage, Γ , of the $\text{Co}(\text{Sep})^{3+}$ electroactive species, determined under conditions of exhaustive electrolysis, was calculated to be $1.537 \times 10^{-5} \text{ mol cm}^{-2}$.

Above and beyond these findings, cumulatively, the electrochemical characterization studies showed the following additional findings:

- The results suggest a strong affinity of nafion for the cationic $\text{Co}(\text{Sep})^{3+}$ species.
- The results also suggest that the novel electrochemical technique allowed the nafion to extract and incorporate the $\text{Co}(\text{Sep})^{3+}$ into the lower density ionic cluster phase in a manner that is inline with its unique inherent structural features. In this regard, uptake of $\text{Co}(\text{Sep})^{3+}$ appeared to be dominated by hydrophobic interactions, rather than normal electrostatic forces.
- The obtained E_m for the naf-El- $\text{Co}(\text{Sep})^{3+}$ was shown to be similar to previously documented results which also involved an electrochemically based method of incorporation, but distinctly different from the results showed for the manual casting/mixing method used for the platform shown in Chapter 4.
- A linear relationship for the current function, $I_p/v^{1/2}$ for both $I_{p,c}$ and $I_{p,a}$ suggested diffusion controlled electrochemistry. In addition to this, the plot of $\log I_p$ vs $\log v$ for both $I_{p,c}$ and $I_{p,a}$, showed slopes of close to the theoretical value of 0.5 for diffusion controlled process. The D_{ct} for the naf-El- $\text{Co}(\text{Sep})^{3+}$ was determined as $2.64 \times 10^{-7} \text{ cm s}^{-1}$.
- The unique method of nafion's cation uptake, which distinctly different and from and more effective than as observed in the case of conventional ion exchange resins and/or electrostatic binding polymers, combine with its inherent phase segregation enabled a three-dimensional charge transport network, providing molecular accessibility and rapid diffusional mass transport of electroactive species.
- The long-term stability evaluation of the GC||naf|El- $\text{Co}(\text{Sep})^{3+}$, revealed a retention of 73% of its original signal following intermittent electrochemical cycling at times and intermittent storage over a five day period.

- FTIR structural investigations confirmed the existence of the $\text{Co}(\text{sep})^{3+}$.

6.2.3 Chapter 5B

The first aspect of importance in this study, was that the human recombinant heme thiolate CYP3A4 was successfully prepared through genetic engineering, as a catalytically active N-terminally modified histidine-tagged, soluble construct, consisting of the heme domain and the surrounding apoprotein. Secondly, the detection and quantification of HAART associated protease inhibitor drug, indinavir, was successfully realized by means of the prepared $\text{GCE}||\text{naf}|\text{EI-Co}(\text{Sep})^{3+}|\text{nCYP3A4}|\text{Agrs-PEI-PVA}$ biosensor. The design path for this particular biosensor was based on a combination of entrapment — encapsulation. In this regard the biological molecule was entrapped behind a modified solid polymer electrolyte nafion membrane, and further encapsulated by a biocompatible ionically crosslinked blended hydrogel outer membrane, consisting of a composite of agarose, poly(vinyl alcohol) and polyethylene imine. Entrapment of the $\text{Co}(\text{Sep})^{3+}$ mediating species within the microstructure of the pre-formed nafion membrane was uniquely done through novel potentiostatic electrodeposition method, for which the major findings were discussed in **Section 6.2.2**.

For the enzyme that was synthesised, the FTIR spectra exhibited major vibrational absorption bands in association with the unique structural characteristics of P450 enzymes, while the catalytically active P450 content was confirmed by the absorption maximum of the reduced CO-bound complex at 450 nm. As for the fabricated $\text{GCE}||\text{naf}|\text{EI-Co}(\text{Sep})^{3+}|\text{nCYP3A4}|\text{Agrs-PEI-PVA}$ biosensor, firstly,

different factors and variables in the construction of biosensor was evaluated, which included:

- 1) the effect of carrier matrix assembly,
 - here optimisation was done with respect to constituents, as well as method of preparation.
- 2) outer layer optimisation,
 - here optimisation was done with respect to film constituents and ratio.
- 3) the optimal enzyme loading amount,
- 4) optimisation of potentiostatic electro-deposition time for cobalt(III) sepulchrate.

Overall, with regard the un-mediated biosensor, GCE||naf|nCYP3A4|Agrs-PEI-PVA, the results suggested weak electronic coupling with the underlying nafion-modified GCE, characterized by ill-formed voltammograms in substrate-free argon-degassed PB electrolyte solution. This translated into high operating potentials, with regard to the biocatalytic reduction of dioxygen, and response to the substrate, indinavir. In particular, the reduction of dioxygen occurred at an average E_p of -664 mV, while average E_p response for indinavir was approximately -700 mV. Nevertheless, overall, the GCE||naf|nCYP3A4|Agrs-PEI-PVA biosensor exhibited the classic additional catalytic current in response to oxygen, as well as indinavir.

With regard to the optimized $\text{Co}(\text{Sep})^{3+}$ mediated biosensor on the other hand, the results were unequivocally different. The bioelectrocatalytic response in the presence of oxygen and indinavir was signified by the emergence of a new peak in the reduction wave, which dominated the cathodic wave. On average, oxygen reduction occurred at -365 mV, while response to indinavir occurred at -369 mV. Moreover, the possible effects of the peroxide shunt pathway appeared to be negligible. The behaviour of the control sensor, for which the active enzyme was replaced by the pseudo carrier enzyme (BSA), an indistinct current increase with

maxima at two peak potentials i.e. ≈ -410 mV and ≈ -645 mV was observed in the presence of oxygen and indinavir. The double peak behaviour was suggested to be ascribed to the effect of reactive H_2O_2 formed in association with the reduction of oxygen in the film of the GCE, as well as the coupling of the $1e^-$ reduction of the mediating species with a fast follow-up chemical reaction with oxygen. Experiments involving investigation with varying indinavir concentration with the GCE||naf|nCYP3A4|Agrs-PEI-PVA biosensor, showed a concentration dependent increase in $I_{p,c}$ in association with consecutive addition of substrate, at the potential of the response of the nCYP3A4- Fe^{2+} . The GCE||naf|BSA|Agrs-PEI-PVA control sensor on the other hand did not exhibit a discernible response to increasing indinavir concentrations.

Above and beyond all these findings, the GCE||naf|nCYP3A4|Agrs-PEI-PVA biosensor exhibited a linear concentration range for the constructed calibration curve in the range of between 2.18×10^{-6} — 3.552×10^{-6} M. The sensitivity was determined as $0.035 \mu\text{A } \mu\text{M}^{-1}$, while the LOD was determined as 59.72 mg L^{-1} . This value for LOD was shown to be of significance in the C_{Max} of ritonavir–boosted indinavir regimen, which is the current proposed method of treatment for administration of indinavir, while also being of significance in patients which are poor metabolisers. The apparent Michaelis Menten constant was determined as $17.54 \mu\text{M}$, which is on the low side, and as such shows affinity of the enzyme for the substrate.

6.3 Critical overview of the studies in this dissertation

In the following segments, some additional findings are highlighted, while comparative evaluations between the design paths are given and a brief overview of achieved aims are given.

Overall, with regard to the pre-formed nafion films and the $\text{Co}(\text{Sep})^{3+}$ modified films, as compared by the techniques used in the two different design paths, i.e. design path 1 and design path 2: The results with reference to the morphological, structural and electrochemical investigation, firstly suggest that a larger amount of nafion yields a better coverage on the underlying GCE. Secondly, still, vacuum conditions, rather than argon drying yields a more evenly formed nafion film. Thirdly, the results suggest that the electrochemically based technique of $\text{Co}(\text{sep})^{3+}$ incorporation into the nafion film is much more superior than the manual casting/mixing method, both with regard to ideal film formation, as well as enabling the incorporation of the $\text{Co}(\text{Sep})^{3+}$ deep within the micro-structure of the nafion membrane. In addition to this, the electrochemically based technique proved to be a more reproducible method of preparation.

All the catalytic studies in the presence of the selected substrate(s), as observed for both biosensor platforms 1 and 2, in effect corroborated documented findings regarding catalytic interactions of CYP3A4 in particular and/or P450 enzymes in general, in which it has been shown that the presence of substrate favourably affects the enzyme-oxygen interaction, by significantly increasing the rate of dioxygen binding to the redox centre. In addition to this, in a critical comparative evaluation, the overpotential for the bioelectrocatalytic reduction of dioxygen was shown to be considerably reduced in the case of biosensor platform 2, as compared to biosensor platform 1.

6.4 Recommendations for future study

1. Although it appears that the major rout of hydroxylation of substrate was formed by the completion of the natural catalytic cycle of the CYP3A4

isoenzyme, further studies will be required to conclusively corroborate all the proposed reaction pathways in the electrochemically driven enzyme catalysis. In particular, the most significant recommended studies would include rotating disk electrochemical studies (to determine exact coupling efficiency), bulk electrolysis, with subsequent analysis of products to determine the exact metabolites formed, and catalysis experiments in the presence of reactive oxygen species scavengers. Additional incubations with H₂O₂ conducted without the use of an electromotive force under the same electrolysis experimental conditions as would be used above, with subsequent analysis of products is also suggested. These experiments are thus recommended for future work.

2. The application of and characterization of GCE||naf|nCYP3A4|Agrs-PEI-PVA with real human plasma was not done, due to time constraints. Thus it is recommended that such studies be conducted in future post-doctoral studies.
3. It is also recommended that additional ex-situ investigations of the complete biosensor platforms be done, both before and after catalytic investigations, which can then be combined with the observed results to have a more comprehensive picture of the changes in the enzyme in association with immobilization, as well as catalytic studies.
4. Probing of the biosensor platforms with

6.5 Overall significance of the study

The results obtained in this dissertation firstly contributes significantly in the overall stride toward decentralized methods of assaying drug concentrations in chronic conditions such as HIV/AIDS, which could eventually serve useful in the quest for alternative analytically based methods for DTM during such chronic conditions. Secondly, with regard to 2,4-DCP, the study is a step forward in research with regard to alternative proposed methods for preparation of small analytical

devices for on-the-spot detection and measurement of environmental samples. Moreover, a fundamental aspect regarding the scope of the dissertation in its entirety is the fact that the natural electron delivery system which is absolutely necessary for the CYP catalytic cycle was replaced by an electromotive force. What is more, is that catalysis was effectuated with just the heme domain of the enzyme, which is a huge milestone, since the application of this kind of human microsomal isoenzymes are by-and-large impeded by the requirement of physiological reducing equivalents, either immobilized within the reagent layer or usually expressed with the enzyme, as a fusion construct. Another milestone is the synthesis and expression of the soluble construct of CYP3A4. In this regard, the full-length native isoenzyme is known to require the obligatory presence of highly expensive additional surfactant-type compounds and/or other monomerisation agents in order to prevent its aggregation.



REFERENCES

1. Lin, J.H., *Role of Pharmacokinetics in the discovery and development of indinavir*. Advanced Drug Delivery Reviews, 1999. **39**: p. 33-49.
2. Barry, M., F. Mulcahy, C. Merry, S. Gibbons, and D. Back, *Pharmacokinetics and potential interactions amongst antiretroviral agents used to treat patients with HIV infection*. Clinical Pharmacokinetics, 1999. **36**(4): p. 289-304.
3. Donato, M.T. and C.J. V., *Strategies and molecular probes to investigate the role of cytochrome P450 in drug metabolism*. Clinical Pharmacokinetics, 2003. **42**(2): p. 153-178.
4. Li, X. and W.K. Chan, *Transport, metabolism and elimination mechanisms of anti-HIV agents*. Advanced Drug Delivery Reviews, 1999. **39**: p. 81-103.
5. Ciccone, C.D., *Pharmacology in rehabilitation*. Contemporary perspectives in rehabilitation (CPR), ed. S.L. Wolf. Vol. 4. 1990, Philadelphia: F.A. Davis. 524.
6. Guengerich, F.P., *Cytochromes P450, drugs and diseases*. Molecular Interventions, 2003. **3**(4): p. 195-204.
7. Gerber, J.H. and E.P. Acosta, *Review: Therapeutic drug monitoring in the treatment of HIV-infection*. Journal of Clinical Virology, 2003. **27**: p. 117-128.
8. Michalets, E.L., *Update: Clinically significant cytochrome P-450 drug interactions*. Pharmacotherapy, 1998. **18**(1): p. 84-112.
9. Zhou, S., E. Chan, L.Y. Lim, U.A. Boelsterli, S.C. Li, J. Wang, Q. Zhang, M. Huang, and A. Xu, *Therapeutic drugs that behave as mechanism-based inhibitors of cytochrome P450 3A4*. Current Drug Metabolism, 2004. **5**(5): p. 415-442.
10. Lin, J.H. and A.Y.H. Lu, *Inhibition and induction of cytochrome P450 and the clinical applications*. Clinical Pharmacokinetics, 1998. **35**(5): p. 361-390.
11. Chiba, M., M. Hensleigh, and J.H. Lin, *Hepatic and intestinal metabolism of indinavir, an HIV protease inhibitor, in rat and human microsomes: Major role of CYP3A*. Biochemical Pharmacology, 1997. **53**: p. 1187-1195.
12. Guengerich, F.P., *Cytochrome P-450 3A4: Regulation and role in drug metabolism*. Annual Review of Pharmacology and Toxicology, 1999. **39**: p. 1-17.
13. Dias, C.L., R.C. Rossi, E.M. Donato, A.M. Bergold, and P.E. Froelich, *LC Determination of ritonavir, a HIV protease inhibitor, in soft gelatin capsules*. Chromatographia, 2005. **62**(11): p. 589-593.
14. Hoffman, C., J. Rockstroh, and F. Mulcahy, eds. *HIV Medicine 2005*. HIV Medicine ed. C. Hoffman, J. Rockstroh, and B.S. Kamps. 2005, Flying Publisher.com: Hamburg Bonn Paris. 189-212.
15. Choi, S.O., N.L. Rezk, and A.D.M. Kashuba, *High-performance liquid chromatography assay for the determination of the HIV-protease inhibitor tipranavir in human plasma in combination with nine other antiretroviral*

- medications*. Journal of Pharmaceutical and Biomedical Analysis, 2007. **43**: p. 1562-1567.
16. Pattarawarapan, M., S. Nangola, T.R. Cressey, and C. Tayapiwatana, *Development of a one-step immunochromatographic strip test for the rapid detection of nevirapine (NVP), a common used antiretroviral drug for the treatment of HIV/AIDS*. Talanta, 2006. **71**: p. 462-470.
 17. Malhotra, B.D. and A. Chaubey, *Biosensors for clinical diagnostics industry*. Sensors and Actuators 2003. **B91**: p. 117-127.
 18. Scott, E.E. and J.R. Halpert, *Structures of cytochrome P450 3A4*. Trends in biochemical sciences, 2005. **30**(1): p. 5-7.
 19. Isin, E.M. and F.P. Guengerich, *Review: Complex reactions catalyzed by cytochrome P450 enzymes*. Biochimica et Biophysica Acta, 2007. **1770**: p. 314-329.
 20. Zhou, S., S.Y. Chan, B.C. Goh, E. Chan, W. Duan, and M. Huang, *Mechanism-based inhibition of cytochrome P450 3A4 by therapeutic drugs*. Clinical Pharmacokinetics, 2005. **44**(3): p. 279-304.
 21. Hannemann, F., A. Bichet, K.M. Ewen, and R. Bernhardt, *Cytochrome P450 systems — biological variations of electron transport chains* Biochimica et Biophysica Acta, 2007. **1770**: p. 330-344.
 22. Meunier, B., S.P. de Visser, and S. Shaik, *Mechanism of oxidation reactions catalyzed by cytochrome P450 enzymes*. Chemical Review, 2004. **104**: p. 3947-3980.
 23. Bernhardt, R., *Cytochrome P450 as versatile biocatalysts*. Journal of Biotechnology, 2006. **124**: p. 128-145.
 24. Omura, T., *Forty years of cytochrome P450*. Biochemical and Biophysical Research Communications, 1999. **266**(3): p. 690-698.
 25. Smith, D., M.J. Ackland, and B.C. Jones, *Properties of cytochrome P450 isoenzymes and their substrates Part2: properties of cytochrome P450 substrates*. DDT, 1997. **2**(11): p. 479-486.
 26. Guengerich, F.P., *Enzymatic oxidation of xenobiotic chemicals*. Critical review of biochemical and molecular biology, 1990. **25**: p. 97-103.
 27. Guenrich, F.P., *Cytochrome P-450 3A4: Regulation and role in drug metabolism*. Annual Review of Pharmacology and Toxicology, 1999. **39**: p. 1-17.
 28. Guenrich, F.P., *Enzymatic oxidation of xenobiotic chemicals*. Critical review of biochemical and molecular biology, 1990. **25**: p. 97-103.
 29. Sakaki, T. and K. Inouye, *Practical application of mammalian cytochrome P450*. Journal of Bioscience and Bioengineering, 2000. **90**(6): p. 583-590.
 30. Coon, M.J., *Cytochrome P450: Nature's most versatile biological catalyst*. Annual Review of Pharmacology and Toxicology, 2005. **45**: p. 1-25.
 31. Isin, E.M. and F.P. Guenrich, *Review: Complex reactions catalyzed by cytochrome P450 enzymes*. Biochimica et Biophysica Acta, 2007. **1770**: p. 314-329.

32. McKinlay, R., J.A. Plant, J.N.B. Bell, and N. Vouvouslis, *Endocrine disrupting pesticides: Implications for risk assesment*. Environment International, 2008. **34**: p. 168-183.
33. Schreinemachers, D.D., *Birth maformations and other adverse perinatal outcomes in four US wheat-producing states*. Environmental Health Perspective, 2003. **111**(9): p. 1259-1264.
34. Mathur, V., P. Bhatnagar, R.G. Sharma, V. Archarya, and R. Sexana, *Breast cancer incidence and exposure to pesticides among women originating from Jaipur*. Environment International, 2002. **28**(5): p. 331-336.
35. Garry, V.V., *Pesticides and children*. Toxicology applications and pharmacology, 2004. **198**(2): p. 152-163.
36. Nicolopoulou, P. and P. Stamanti, *The impact of endocrine disruptors on the female reproductive system*. Human reproductive update, 2001. **7**(3): p. 323-330.
37. Mehmood, Z., D.E. Kelly, and S.L. Kelly, *Cytochrome P450 3A4 mediated metabolism of 2,4-dichlorophenol*. Chemosphere, 1997. **34**(11): p. 2281-2291.
38. Al Momani, F., C. Sans, and S. Esplugas, *A comparative study of the advanced oxidation of 2,4-dichlorophenol*. Journal of Hazardous Materials 2004. **B107**: p. 123-129.
39. Laganà, A., A. Bacaloni, I. De Leva, A. Faberi, G. Fago, and A. Marino, *Occurrence and determination of herbicides and their major transformation products in environmental waters*. Analytica Chimica Acta, 2002. **462**: p. 187-198.
40. Ware, G.W. and D.M. Whitacre, *An introduction to herbicides*, in *The pesticide book*, 6th adition. 2004, MeisterPro Information Resources: Ohio.
41. Mehmood, Z., M.P. Williamson, D.E. Kelly, and S.L. Kelly, *Human cytochrome P450 3A4 is involved in the biotransformation of the herbicide 2,4-dichlorophenoxyacetic acid*. Environmental Toxicology and Pharmacology, 1996. **2**: p. 397-401.
42. World Health Organization, *Chlorophenols in Drinking-water, Background document for preparation of WHO Guidelines for drinking-water quality*, in *Guidelines for drinking water quality*, E.a. Health, Editor. 2003, World Health Organization: Geneva.
43. Jantra, J., H. Zilouei, J. Liu, B. Guieysse, P. Thavarungkul, and P. Kanatharana, *Microbial biosensor for the analysis of 2,4-dichlorophenol*. Analytical Letters, 2005. **38**: p. 1071-1083.
44. D.D., G., *Linking environmental cancer with occupational epidemiology research: the role of the international agency for research on cancer (IARC)*. Journal of Environmental Pathology Toxicology and Oncology, 2000. **19**(1): p. 171-175.
45. EPA method 604, *Phenols in federal register*, in *Part 136,58*, Environmental Protection Agency Part VIII, Editor. 2003, Environmental Protection Agency.
46. Chaubey, A. and B.D. Malhotra, *Review: Mediated biosensors*. Biosensors & Bioelectronics, 2002. **17**: p. 441-456.

47. Guangying, Z., F. Xing, and S. Deng, *A disposable amperometric enzyme immunosensor for rapid detection of vibrio parahaemolyticus in food based on agarose/nano-Au membrane and SPE*. *Electrochemistry Communications*, 2007. **9**: p. 1263-1268.
48. Liu, H.-H., Z.-Q. Tian, Z.-X. Lua, Z.-L. Zhang, M. Zhang, and D.-W. Pang, *Direct electrochemistry and electrocatalysis of heme-proteins entrapped in agarose hydrogel films*. *Biosensors and Bioelectronics*, 2004. **20**: p. 294-304.
49. Hara, M., Y. Yasuda, H. Toyotama, H. Ohkawa, T. Nozawa, and J. Miyake, *A novel ISFET-type biosensor based on P450 monooxygenases*. *Biosensors and Bioelectronics*, 2002. **17**: p. 173-179.
50. Hara, M., S. Iazvovskaia, H. Ohkawa, Y. Asada, and J. Miyake, *immobilization of P450 monooxygenase and chloroplast for use in light-driven bioreactors*. *Journal of Bioscience and Bioengineering*, 1999. **87**(6): p. 793-797.
51. Sanket, T., M. Karve, S. Inamdar, S. Haram, J. Melo, and S. D'Souza, *Development of electrochemical niosensor based on tyrosinase immobilized in composite biopolymeric film*. *Analytical Biochemistry*, 2006. **349**: p. 72-77.
52. Eggins, B.R., *Sensing Elements*, in *ANTS Series: Chemical Sensors and Biosensors*, D.J. Ando, Editor. 2002, John Wiley & Sons, Ltd: Jordanstown Northern Island, UK. p. 77-79.
53. Zhang, S., G. Wright, and Y. Yang, *Materials and techniques for electrochemical biosensor design and construction*. *Biosensors and Bioelectronics*, 2000. **15**: p. 273-282.
54. Sharma, S.K., N. Sehgal, and A. Kumar, *Biomolecules for development of biosensors and their applications*. *Current Applied Physics*, 2003. **3**: p. 307-316.
55. Sharma, A. and K.R. Rogers, *Review article: Biosensors*. *Meas. Sci. Technol.*, 1994. **5**: p. 461-472.
56. Dzyadevych, S.V., V.N. Arkhypova, A.P. Soldatkin, A.V. El'skaya, C. Martelet, and N. Jaffrezic-Renault, *Amperometric enzyme biosensors: Past, present and future*. *ITBM-RBM*, 2008. **29**(171-180).
57. Thévonot, D.R., K. Toth, R.A. Durst, and G.S. Wilson, *Technical report: Electrochemical biosensors: recommended definitions and classification*. *Biosensors & Bioelectronics*, 2001. **16**: p. 121-131.
58. Wang, J., *Amperometric biosensors for clinical and therapeutic drug monitoring: a review*. *Journal of Pharmaceutical and Biomedical Analysis*, 1999. **19**: p. 47-53.
59. Collings, A.F. and F. Caruso, *Biosensors: recent advances*. *Rep. Prog. Phys.*, 1997. **60**(1397-1445).
60. Gerard, M., A. Chaubey, and B.D. Malhotra, *Review: Application of conducting polymers to biosensors*. *Biosensors & Bioelectronics*, 2002. **17**: p. 345-359.
61. Clark, L.C., *Monitor and control of blood and tissue oxygen tensions*. *Trans Am Soc Artif Intern Organs*, 1956. **2**: p. 41-48.
62. Clark, L.C. and C. Lyons, *Electrode systems for continuous monitoring in cardiovascular surgery*. *Ann NY Acad Sci*, 1962. **102**: p. 29-45.

63. Udupke, S.J. and G.P. Hicks, *The enzyme electrode*. Nature, 1967. **214**: p. 986-988.
64. Shumyantseva, V.V., T.V. Bulko, and A.I. Archakov, *Electrochemical reduction of cytochrome P450 as an approach to the construction of biosensors and bioreactors*. Journal of Inorganic Biochemistry, 2005. **99**: p. 1051-1063.
65. Habermüller, K., M. Mosbach, and W. Schuhmann, *Electron-transfer mechanisms in amperometric biosensors*. Fresenius J Anal Chem, 2000. **366**(560-568).
66. Bistolas, N., U. Wollenberger, C. Jung, and F.W. Scheller, *Review: Cytochrome P450 biosensors—a review*. Biosensors and Bioelectronics, 2005. **20**: p. 2408-2423.
67. Denisov, I.G., Y.V. Grinkova, B.J. Baas, and S.G. Sligar, *The ferrous-dioxygen intermediate in human cytochrome P450 3A4: Substrate dependence of formation and decay kinetics*. Journal of Biological Chemistry, 2006. **281**(33): p. 23313-23318.
68. Nazor, J., S. Dannenmann, O.R. Adjei, Y.B. Fordjour, I.T. Ghampson, M. Blanus, D. Roccatano, and U. Schwaneberg, *Laboratory evolution of P450 BM3 for mediated electron transfer yielding an activity improved and reductase independent variant*. Protein Engineering, Design & Selection, 2008. **21**(1): p. 29-35.
69. Kohlmann, C., W. Märkle, and S. Lütz, *Review: Electroenzymatic synthesis*. Journal of Molecular Catalysis B: Enzymatic, 2008. **51**: p. 57-72.
70. Schuhmann, W., *Amperometric enzyme biosensors based on optimised electron-transfer pathways and non-manual immobilisation procedures*. Reviews in Molecular Biotechnology, 2002. **82**: p. 425-441.
71. Udit, A.K., K.D. Hagen, P.J. Goldman, A. Star, J.M. Gillan, H.B. Gray, and M.G. Hill, *Spectroscopy and electrochemistry of cytochrome P450 BM3-surfactant film assemblies*. Journal of the American Chemical Society, 2006. **128**(31): p. 10320-10325.
72. Panico, P., Y. Astuti, A. Fantuzzi, J.R. Durrant, and G. Gilardi, *P450 versus P420: Correlation between cyclic voltammetry and visible absorption spectroscopy of the immobilized heme domain of cytochrome P450 BM3*. Journal of Physical Chemistry B, 2008. **112**: p. 14063-14068.
73. Fleming, B.D., Y. Tian, S.G. Bell, L. Wong, V. Urlacher, and H.A.O. Hill, *Redox properties of cytochrome P450_{BM3} measured by direct methods*. European Journal of Biochemistry, 2003. **270**: p. 4082-4088.
74. Iwuoha, E.I., S. Joseph, Z. Zhang, M.R. Smyth, U. Fuhr, and P.R. Ortiz de Montellano, *Drug metabolism biosensors: electrochemical reactivities of cytochrome P450cam immobilized in synthetic vesicular systems*. Journal of Pharmaceutical and Biomedical Analysis, 1998. **17**: p. 1101-1110.
75. Tian, F., B. Xu, L. Zhu, and G. Zhu, *Hydrogen peroxide biosensor with enzyme entrapped within electrodeposited polypyrrole based on mediated sol-gel derived composite carbon electrode*. Analytica Chimica Acta, 2001. **443**: p. 9-16.

76. Paternolli, C., M. Antonini, P. Ghisellini, and C. Nicolini, *Recombinant cytochrome P450 immobilization for biosensor applications*. *Langmuir*, 2004. **20**: p. 11706-11712.
77. Shumyantseva, V.V., Y.D. Ivanov, N. Bistolos, and F.W. Scheller, *Direct electron transfer of cytochrome P450 2B4 at electrodes modified with nonionic detergent and colloidal clay nanoparticles*. *Analytical Chemistry*, 2004. **76**(20): p. 6064-6052.
78. Shumyantseva, V.V., T.V. Bulko, Y.O. Rudakov, G.P. Kuznetsova, N.F. Samenkova, A.V. Lisitsa, I.I. Karuzina, and A.I. Archakov, *Electrochemical properties of cytochrome P450 using nanostructured electrodes: Direct electron transfer and electro catalysis*. *Journal of Inorganic Biochemistry*, 2007. **101**: p. 859-865.
79. Shumyantseva, V.V., T.V. Bulko, S.A. Usanov, R.D. Schmid, C. Nicolini, and A.I. Archakov, *Construction and characterization of bioelectrocatalytic sensors based on cytochromes P450*. *Journal of Inorganic Biochemistry*, 2001. **87**: p. 185-190.
80. Shumyantseva, V.V., G. Deluca, T.V. Bulko, S. Carrara, C. Nicolini, S.A. Usanov, and A.I. Archakov, *Cholesterol amperometric biosensor based on cytochrome P450scc*. *Biosensors & Bioelectronics*, 2004. **19**: p. 971-976.
81. Dodhia, V.R., C. Sassone, A. Fantuzzi, G.D. Nardo, S.J. Sadeghi, and G. Gilardi, *Modulating the coupling efficiency of human cytochrome P450 CYP3A4 at electrode surfaces through protein engineering*. *Electrochemical Communications*, 2008. **10**: p. 1744-1747.
82. Udit, A.K., N. Hindoyan, M.G. Hill, F.H. Arnold, and H.B. Gray, *Protein-surfactant film voltammetry of wilde-type and mutant cytochrome P450 BM3*. *Inorganic Chemistry*, 2005. **44**(12): p. 4109-4111.
83. Zhang, Z., A.-E.F. Nassar, Z. Lu, J.B. Schenkman, and J.F. Rusling, *Direct electron injection from electrodes to cytochrome P450cam in biomembrane-like films*. *Journal of Chemical Society, Faraday Transactions*, 1997. **93**(9): p. 1769-1774.
84. Lvov, Y.M., Z. Lu, J.B. Schenkman, X. zu, and J.F. Rusling, *Direct electrochemistry of myoglobin and cytochrome P450cam in alternate layer-by-layer films with DNA and other polyions*. *Journal of the American Chemical Society*, 1998. **120**: p. 073-4080.
85. Estavillo, C., Z. Lu, I. Jansson, J.B. Schenkman, and J.F. Rusling, *Epoxidation of styrene by human cyt P450 1A2 by thin film electrolysis and peroxide activation compared to solution reactions*. *Biophysical Chemistry*, 2003. **104**: p. 291-296.
86. Sultana, N., J.B. Schenkman, and J.F. Rusling, *Protein film electrochemistry of microsomes genetically enriched in human cytochrome 450 monooxygenases*. *Journal of the American Chemical Society*, 2005. **127**: p. 13460-13461.
87. Hara, M., *Application of P450s for biosensing: combination of biotechnology and electrochemistry*. *Materials Science and Engineering C*, 2000. **12**: p. 103-109.

88. Schumann, W. and E.M. Bensen, *Biosensors*, in *Instrumentation and Electroanalytical Chemistry*.
89. Udit, A.K. and H.B. Gray, *Review: Electrochemistry of heme-thiolate proteins*. *Biochemical and Biophysical Research Communications*, 2005. **338**: p. 470-476.
90. Schuhmann, W. and E.M. Bensen, *Biosensors*, in *Instrumentation and Electroanalytical Chemistry*.
91. Zanello, P., *Voltammetric Techniques*, in *Inorganic Electrochemistry: Theory, Practice and Application*. 2003, The Royal Society of Chemistry: Cambridge. p. 104-109.
92. Scholz, F., *Cyclic Voltammetry*, in *Electroanalytical Methods: Guide to experiments and applications*, C.M. Rheinau, Editor. 2005, Springer-Verlag: Heidelberg, Germany. p. 57-90.
93. Joseph, W., *Controlled Potential Techniques*, in *Electroanalytical Chemistry*, W. Inc., Editor. 2000, Wiley and Sons Inc.: New York. p. 60-92.
94. Monk, P.M.S., *Analysis by dynamic measurement, B: Systems under convection control*, in *Fundamentals of electroanalytical chemistry*, D.J. Ando, Editor. 2001, John Wiley and Sons Inc.: Chichester, West Sussex, England. p. 194-236.
95. Price, N.C. and L. Stevens, *An introduction to enzyme kinetics*, in *Fundamentals of Enzymology*, D.E. Stevens, Editor. 1986, Oxford University Press: New York. p. 1116-148.
96. Sasaki, T. and K. Inouye, *Review: Practical application of mammalian cytochrome P450*. *Journal of Bioscience and Bioengineering*. **190**: p. 583-590.
97. Miles, C.S., T.W.B. Ost, M.A. Noble, A.W. Munro, and S.K. Chapman, *Review: Protein engineering of cytochromes P-450*. *Biochimica et Biophysica Acta*, 2000. **1543**: p. 383-407.
98. Michaelis, L. and M. Menten, *Die Kinetik der Invertinwirkung*. *Biochemistry* 1913. **Z.49**: p. 333.
99. Robyt, J.F. and B.J. White, *Enzymology*, in *Biochemical Techniques: Theory and Practice*, S.Ewing, L. McClaud, and J. Marsh, Editors. 1987, Brooks/Cole Publishing Company: Monterey, California. p. 291-320.
100. Ugo, P., V. Zangrando, L.M. Moretto, and B. Brunetti, *Ion-exchange voltammetry and electrocatalytic sensing capabilities of cytochrome c at polyethersulphonated ionomer coated glassy carbon electrodes*. *Biosensors and Bioelectronics*, 2002. **17**: p. 479-487.
101. Moretto, L.M., P. Bertoncello, and F.V.P. Ugo, *Electrochemistry of cytochrome c incorporated in Langmuir-Blodgett films of Nafion[®] and Eastman AQ 55[®]*. *Bioelectrochemistry*, 2005. **66**: p. 29-34.
102. Fernández, A.C., C. Mijangos, J.-M. Guenet, and M.T. Cuberes, *New hydrogels based on the interpenetration of physical gels of agarose chemical gels of polyacrylamide*. *European Polymer Journal*, 2009. **45**: p. 932-939.

103. Kim, G.-Y., N.M. Cuong, S.-H. Cho, J. Shim, J.-J. Woo, and S.-H. Moon, *Improvement of an enzyme electrode by poly(vinyl alcohol) coating for amperometric measurement of phenol*. *Talanta*, 2007. **71**: p. 129-135.
104. Shaidarova, L.G., A.V. Gedmina, I.A. Chelnokova, and G.K. Budnikov, *Electrocatalytic oxidation of ethanol on graphite electrodes coated with nafion film with incorporated particles of ruthenium or its complexes*. *Journal of Analytical Chemistry*, 2005. **60**(6): p. 533-539.
105. Zhutaeva, G.V., M.R. Tarasevich, M.V. Radina, and I.S. Chernyshova, *Composites based on phenyl substituted cobalt porphyrins with nafion as catalysts for oxygen electroreduction*. *Russian Journal of Electrochemistry*, 2009. **45**(9): p. 1080-1088.
106. Zhang, W. and G. Li, *Review: Third-Generation biosensors based on the direct electron transfer of proteins*. *Analytical Sciences*, 2004. **20**: p. 603-609.
107. Ruzgas, T., J. Emnéus, L. Gorton, and G. Marko-Varga, *The development of a peroxidase biosensor for monitoring phenol and related aromatic compounds*. *Analytica Chimica Acta*, 1995. **311**: p. 245-253.
108. Li, A.P., D.L. Kaminski, and A. Rasmussen, *Substrates of human hepatic cytochrome P450 3A4*. *Toxicology*, 1995. **104**: p. 1-8.
109. Graham, S.E. and J.A. Peterson, *How similar are P450s and what can their differences teach us*. *Archives of Biochemistry and Biophysics*, 1999. **369**(1): p. 24-29.
110. Fernandes, A.C. and E.A. Ticianelli, *A performance and degradation study of Nafion 212 membrane for proton exchange membrane fuel cells*. *Journal of Power Sources*, 2009. **193**: p. 547-554.
111. Tang, H., S. Peikang, S.P. Jiang, F. Wang, and M. Pan, *A degradation study of Nafion proton exchange membrane of PEM fuel cells*. *Journal of Power Sources*, 2007. **170**: p. 85-92.
112. Shin, S.-J., A.I. Balabanovich, H. Kim, J. Jeong, J. Song, and H.-T. Kim, *Deterioration of Nafion 115 membrane in direct methanol fuel cells*. *Journal of Power Sources*, 191. **191**(312-319).
113. Liang, Z., W. Chen, J. Liu, S. Wang, Z. Zhou, W. Li, G. Sun, and Q. Xin, *FT-IR study of the microstructure of Nafion membrane*. *Journal of Membrane Science*, 2004. **233**: p. 39-44.
114. Barbora, L., S. Acharya, R. Singh, K. Scott, and A. Verma, *A novel composite Nafion membrane for direct alcohol fuel cells*. *Journal of Membrane Science*, 2009. **326**: p. 721-726.
115. Skoog, D.A. and J.J. Leary, *Infrared Absorption Spectroscopy*, in *Principles of Instrumental Analysis, Fourth Edition*, C. Field, Editor. 1992, Harcourt Brace College Publishers: United States of America, New York. p. 253-279.
116. Shao, Z.-G., X. Wang, and I.M. Hsing, *Composite Nafion/polyvinyl alcohol membranes for the direct methanol fuel cell*. *Journal of Membrane Science*, 2002. **210**: p. 147-153.
117. Martin, C.R. and H. Freiser, *Ion-selective electrodes based on an ionic polymer*. *Analytical Chemistry*, 1981. **53**(6): p. 902-904.

118. Heitner-Wirguin, C., *Recent advances in perfluorinated ionomer membranes: structure, properties and applications*. Journal of Membrane Science, 1996. **120**: p. 1-33.
119. Martin, C.R., I. Rubinstein, and A.J. Bard, *Polymer films. 9. Electron and mass transfer in nafion films containing Ru(bpy)₃²⁺*. Journal of the American Chemical Society, 1982. **104**(18): p. 4817-4824.
120. Faulkner, K.M., M.S. Shet, C.W. Fisher, and R.W. Estabrook, *Electrocatalytically driven ω -hydroxylation of fatty acids using cytochrome p450 4A1*. Proc. Natl. Acad. Sci. USA, 1995. **92**: p. 7705-7709.
121. Jezkova, J., E.I. Iwuoha, M.R. Smyth, and K. Vytras, *Stabilization of an Osmium Bis-bipyridyl polymer-modified carbon paste amperometric glucose biosensor using Polyethyleneimine*. Electroanalysis, 1997. **9**(13): p. 978-984.
122. Huang, Q., Z. Lu, and J.F. Rusling, *Composite films of surfactants, nafion, and proteins with electrochemical and enzyme activity*. Langmuir, 1996. **12**: p. 5472-5480.
123. Hong, J., A.A. Moosavi-Movahedi, H. Ghourchian, A.M. Rad, and Rezaei-Zarchi, *Direct electron transfer of horseradish peroxidase on Nafion-cysteine modified gold electrode*. Electro Chimica Acta, 2007. **52**: p. 6261-6267.
124. Dewald, H.D. and J. Chen, *Cyclic voltammetry of [Co(sep)₃]³⁺ incorporated in nafion polymer films on glassy carbon electrodes and ultramicroelectrodes*. Microchemical Journal, 1997. **56**: p. 197-206.
125. Park, T.-M., E.I. Iwuoha, M.R. Smyth, R. Freany, and McShane, *Sol-gel based amperometric biosensor incorporating an osmium redox polymer as mediator for detection of L-lactate*. Talanta, 1997. **44**: p. 973-978.
126. Moore, C.M., S. Kackman, T. Brennan, and S.D. Minter, *Effects of surfactants on the transport properties of redox species through Nafion membranes*. Journal of Membrane Science, 2005. **255**: p. 233-238.
127. Ozoemena, K. and T. Nyokong, *Novel amperometric glucose biosensor based on an ether-linked cobalt(II) phthalocyanine-cobalt(II) tetraphenylporphyrin pentamer as redox mediator*. Electro Chimica Acta, 2006. **51**: p. 5131-5136.
128. Rusling, J.F. and A.-E.F. Nassar, *Enhanced electron transfer for Myoglobin in surfactant films on electrodes*. Journal of the American Chemical Society, 1993. **115**(25): p. 11891-11897.
129. Rusling, J.F. and H. Zhang, *Multilayer films of cationic surfactants on electrodes. Control of charge transport by phase*. Langmuir, 1991. **7**(8): p. 1791-1796.
130. Rusling, J.F. and R.J. Forster, *Electrochemical catalysis with redox polymer and polyion-protein films*. Journal of Colloid and Interface Science, 2003. **262**: p. 1-15.
131. Iwuoha, E.I., D.S. de Villaverde, N.P. Garcia, M.R. Smyth, and J.M. Pingarron, *Reactivities of organic phase biosensors. 2. The amperometric behaviour of horseradish peroxidase immobilised on a platinum electrode modified with an electrosynthetic polyaniline film*. Biosensors & Bioelectronics, 1997. **12**(8): p. 749-761.

132. Nassar, A.-E.F., W.S. Wilis, and J.F. Rusling, *Electron transfer form electrodes to Myoglobin: Facilitated in Surfactant films and blocked by adsorbed biomolecules*. Analytical Chemistry, 1995. **67**(14): p. 2386-2392.
133. Johnson, D.L., B.C. Lewis, D.J. Elliot, J.O. Miners, and L.L. Martin, *Electrochemical characterisation of the human cytochrome P450 CYP2C9*. Biochemical Pharmacology, 2005. **69**: p. 1533-1541.
134. Honeychurch, M.J., H.A.O. Hill, and L. Wong, *The thermodynamics of electron transfer in the cytochrome P450_{cam} enzyme system*. FEBS Letters, 1999. **451**: p. 351-353.
135. Joseph, S., J.F. Rusling, Y.M. Lvov, T. Friedberg, and U. Fuhr, *An amperometric biosensor with human CYP3A4 as novel drug screening tool*. Biochemical Pharmacology, 2003. **65**: p. 1817-1826.
136. Ignaszak, A., N.R. Hendricks, T.T. Waryo, E. Songa, N. Jahed, R. Ngece, A. Al-Ahmed, B. Kgarebe, P.G.L. Baker, and E.I. Iwuoha, *Novel therpauetic biosensor for indinavir—A protease inhibitor antiretroviral drug*. Journal of Pharmaceutical and Biomedical Analysis, 2009. **49**: p. 498-501.
137. Gillam, E.M.J., T. Baba, B.-R. Kim, S. Ohmori, and F.P. Guengerich, *Expression of modified human cytochrome P450 3A4 in Escherichia coli and purification and reconstitution of the enzyme*. Archives of Biochemistry and Biophysics, 1993. **305**(1): p. 123-131.
138. Campuzano, S., R.G.M. Pedrero, F.J.M. de Villena, and J.M. Pingarron, *Preparation, characterization and application of alkanethiol self-assembled monolayers modified with tetrathiafulvalene and glucose oxidase at gold disk electrode*. Journal of Electroanalytical Chemistry, 2002. **526**: p. 92-100.
139. Ayard, A., Y. Naimi, J. Bouet, and J.F. Fauvarque, *Short Communication: Oxygen on platinum electrode coated with Nafion[®]*. Journal of Power Sources, 2004. **130**: p. 50-55.
140. Pillari, K.C., A.S. Kumar, and J. Zen, *Nafion-RuO₂-Ru(bpy)₃²⁺ composite electrodes for efficient electrocatalytic water oxidation*. Journal of Molecular Catalysis A: Chemical, 2000. **160**: p. 277-285.
141. Pillai, K.C., A.S. Kumar, and J. Zeng, *Nafion-RuO₂-Ru(bpy)₃²⁺ composite electrodes for efficient electrocatalytic water oxidation*. Journal of Molecular Catalysis A: Chemical, 2000. **160**: p. 277-285.
142. Hendricks, N.R., T.T. Waryo, O. Arotiba, N. Jahed, P.G.L. Baker, and E.I. Iwuoha, *Microsomal cytochrome P450-3A4 (CYP3A4) nanobiosensor for the determination of 2,4-dichlorophenol - an endocrine disruptor compound*. Electro Chimica Acta, 2009. **54**: p. 1925-1931.
143. Szentirmay, M.S. and C.R. Martin, *Ion-exchange selectivity of nafion films on electrode surfaces*. Analytical Chemistry, 1984. **56**(11): p. 1898-1902.
144. Crespilho, F.N., V. Zucolotto, and C.M.A. Brett, *Enhanced charge transport and incorporation of redox mediators in layer-by-layer films containing PAMAM-encapsulated gold nanoparticles*. Journal of Physical Chemistry B, 2006. **110**(35): p. 17478-17483.

145. Ni, J., H. Ju, H. Chen, and D. Leech, *Amperometric determination of epinephrine with an osmium complex and nafion double-layer membrane modified electrode*. *Analytica Chimica Acta*, 1999. **378**: p. 151-157.
146. Lin, Z., J. Chen, and G. Chen, *An ECL biosensor for glucose based on carbon-nanotube/nafion film modified glass carbon electrode*. *Electrochimica Acta*, 2008. **53**: p. 2396-2401.
147. Ludvigsson, M., J. Lindgren, and J. Tegenfeldt, *FTIR study of water cast in Nafion films*. *Electrochimica Acta*, 2000. **45**: p. 2267-2271.
148. Zen, J.-M., A.S. Kumar, and M.-R. Chang, *Electrocatalytic oxidation and trace detection of amitrole using a nafion/lead-ruthenium oxide pyrochlore chemically modified electrode*. *Electrochimica Acta*, 2000. **45**(1691-1699).
149. Schumann, W. and E.M. Bensen, *Instrumentation and Electroanalytical Methods: Biosensors*, in *Encyclopedia of Electrochemistry*. 2000: Bochum Germany. p. 360-372.
150. Ludvigsson, M., J. Lindgren, and J. Tegenfeldt, *FTIR study of water cast Nafion films*. *Electrochimica Acta*, 2000. **45**: p. 2267-2271.
151. Jung, C., *Fourier transform infrared spectroscopy as a tool to study structural properties of cytochromes P450s (CYPs)*. *Anal Bioanal Chem*, 2008. **392**: p. 1031-1058.
152. Contzen, J. and C. Jung, *Changes in the secondary structure and salt links of Cytochrome P-450_{cam} induced by photoreduction: A fourier transform infrared spectroscopic study*. *Biochemistry*, 1999. **38**(49): p. 16253-16260.
153. Lange, R., J. Pierre, and P. Debey, *Visible and Ultraviolet spectral transitions of camphor-bound cytochrome P-450*. *European Journal of Biochemistry*, 1980. **107**: p. 441-445.
154. Poulos, T.L., *Review: Structural biology of heme monooxygenases*. *Biochemical and Biophysical Research Communications*, 2005. **338**: p. 337-345.
155. Roberts, A.G., A.P. Campbell, and W.M. Atkins, *The thermodynamic landscape of testosterone binding to Cytochrome P450 3A4: Ligand binding and spin state equilibria*. *Biochemistry*, 2005. **44**(4): p. 1353-1366.
156. Mclean, K.J., M.R. Cheesman, S.L. Rivers, A. Richmond, D. Leys, S.K. Chapman, G.A. Reid, N.C. Price, S.M. Kelly, J. Clarkson, W.E. Smith, and A.W. Munro, *Expression, purification and spectroscopic characterization of the cytochrome P450 CYP121 from Mycobacterium tuberculosis*. *Journal of Inorganic Biochemistry*, 2002. **91**: p. 527-541.
157. Pritchard, M.P., R. Ossetian, D.N. Li, C.J. Henderson, B. Burchell, R. Wolf, and T. Friedberg, *A general strategy for the expression of recombinant human cytochrome P450s in Escherichia coli using bacterial signal peptides: Expression of CYP3A4, CYP2D6, and CYP2E1*. *Archives of Biochemistry and Biophysics*, 1997. **345**(2): p. 342-354.
158. Anzenbacher, P. and J. Hudeček, *Focused Review: Difference in flexibility of active sites of cytochrome P450 probed by resonance Raman and UV-Vis absorption spectroscopy*. *Journal of Inorganic Biochemistry*, 2001. **87**: p. 209-213.

159. Omura, T. and R. Sato, *The carbon monoxide-binding pigment of liver microsomes. I. Evidence for its hemoprotein nature* The journal of bioogical chemistry, 1964. **239**(7): p. 2370-2378.
160. Konash, A. and E. Magner, *Electrochemically mediated reduction of Horseradish Peroxidase by 1,1-Ferrocenedimethanol in organic solvents*. Analytical Chemistry, 2005. **77**(6): p. 1647-1654.
161. Hu, N. and J.F. Rusling, *Electrochemistry and catalysis with Myoglobin in hydrated Poly(ester sulphonic acid) ionomer films*. Langmuir, 1997. **13**(15): p. 4119-4125.
162. Yang, J., N. Hu, and J.F. Rusling, *Enhanced electron transfer for hemoglobin in poly(ester sulphonic acid) films on pyrolytic graphite electrodes*. Journal of Electroanalytical Chemistry, 1999. **463**: p. 53-62.
163. Brunetti, B. and P. Ugo, *Factors infuencing the ion-exchange pre-concentration and voltammetric behaviour of redox cations at polyestersulphonated ionomer coated electrodes in acetonitrile solutions*. Journal of Electroanalytical Chemistry, 1999. **1999**(460): p. 38-45.
164. Rao, P.S., B. Smitha, S. Sridhar, and A. Krishnaiah, *Preparation and performance of poly(vinyl alchohol)/polyethyleneimine blend membranes for the dehydration of 1,4-dioxane by pervaporation: Comparison with gluteraldehyde cross-linked membranes*. Separation and Purification Technology, 2006. **48**: p. 244-254.
165. Rao, P.S., S. Sridhar, M.Y. Wey, and A. Krishnaiah, *Pervaporation performance and transport phenomenon of PVA blend membranes for the separation of THF/water azeotropic mixtures*. Polymer Bulletin, 2007. **59**: p. 289-298.
166. Mayuzumi, H., C. Sambongi, K. Hiroya, T. Shimizu, T. Tateishi, and M. Hatano, *Effect of mutations of ionic acids of cytochrome P450 1A2 on catalytic activities toward 7-Ethoxycoumarin and Methanol*. Biochemistry, 1993. **32**(21): p. 5622-5628.
167. Shamsipur, M., M. Najafi, M.M. Hosseini, and H. Shargi, *Electrocatalytic reduction of dioxygen at carbon paste electrode modified with a novel cobalt(III) Schiff's base complex*. Electroanalysis, 2007. **19**(16): p. 1661-1667.
168. Udit, A.K., F.H. Arnold, and H.B. Gray, *Cobaltoceme-mediated catalytic monooxygenation using holo and heme domain cytochrome P450 BM3*. Journal of Inorganic Biochemistry, 2004. **98**: p. 1547-1550.
169. Onuoha, A.C. and J.F. Rusling, *Electroactive Myoglobin-surfactant films in a bicontinuous microemulsion*. Langmuir, 1995. **11**(9): p. 3296-3301.
170. Batsis, J., *Clinical pharmacology of protease inhibitors in HIV infection* TSMJ, 2000. **1**: p. 60-65.
171. Williams, G.C. and P.J. Sinko, *Orla absorption of the HIV protease inhibitors: a current update*. Advanced Drug Delivery Reviews, 1999. **39**: p. 211-238.
172. Mashazi, P.N., K.I. Ozoemena, and T. Nyokong, *Tetracarboxylic acid cobalt phthalocyanine SAM on gold: Potential applications as amperometric sensor for H₂O₂ and fabrication of glucose biosensor*. Electrochimica Acta, 2006. **52**: p. 177-186.

173. Yang, M. and A.I. Cederbaum, *Glycerol increases content and activity of human cytochrome P450 2E1 in a transduced HepG2 cell line by protein stabilisation*. *Alcoholism: Clinical & Experimental Research*, 1997. **21**(2): p. 340-347.
174. Metelitzka, D.I., A.N. Eryomin, and S.A. Usanov, *Quantitative characteristics of the stabilizing effect of glycerol on cytochrome P450 in rabbit liver microsomes*. *Acta Biologica et Medica Germanica*, 1982. **41**(1): p. 17-21.
175. Gosalia, D.N. and S.L. Diamond, *Printing chemical libraries on microarrays for fluid phase nanolitre reactions*. *Proceedings of the National Academy of Science*, 2003. **100**(15): p. 8721-8726.



Appendix



APPENDIX A

Additional results for **Section 5B.2.2: Structural aspects of the genetically engineered his₆-tagged N-terminally modified recombinant CYP3A4 (nCYP3A4)**



Figure A-1 Electronic absorption spectra for the synthesized, N-terminally modified CYP450 3A4 (nCYP3A4). (nCYP3A4-Fe^{II}-carbon monoxide, prepared by reducing nCYP3A4Fe^{III} with excess sodium dithionite and saturating with CO by bubbling for 2 min). Spectra exhibited is the difference spectra taken against references of reduced nCYP3A4 before addition of CO. Working solution of nCYP3A4 was 20 mM potassium phosphate buffer, pH 7.40, 20% glycerol.

APPENDIX B

Additional results for Section 5B.3.1.1:

**Optimisation of the variables concerning the indinavir amperometric biosensor
assembly**



APPENDIX B.1

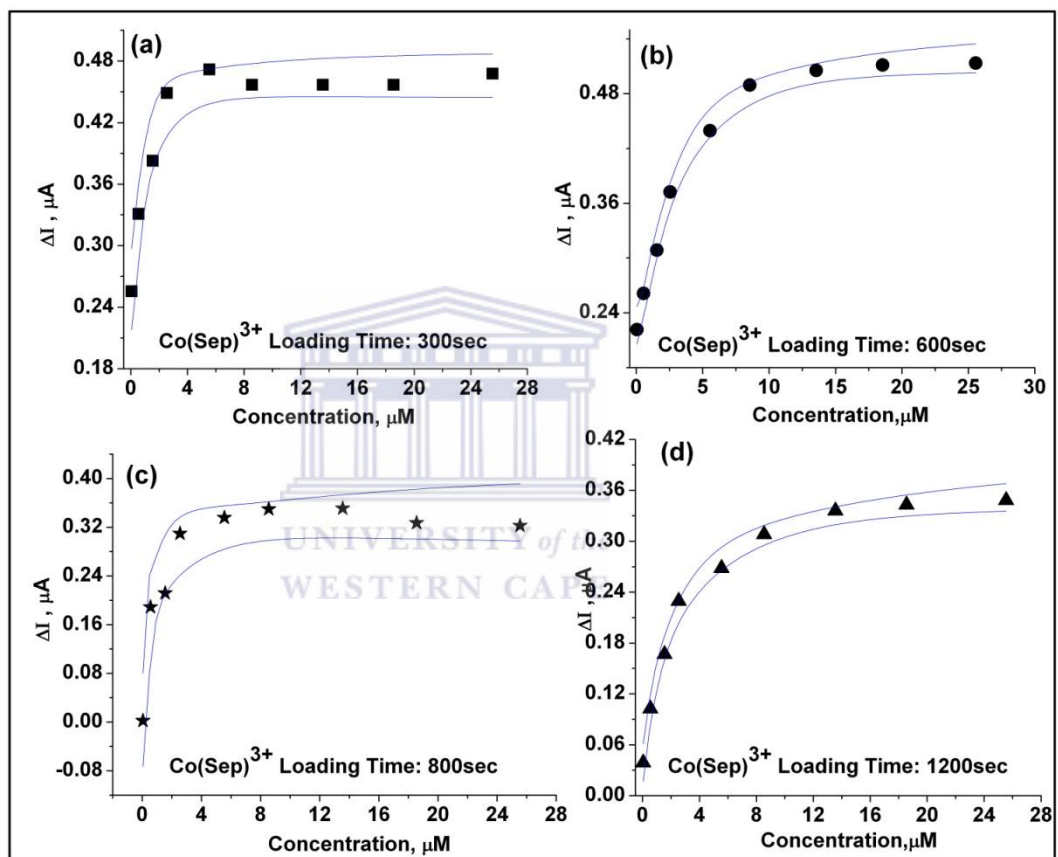
Optimisation of $\text{Co}(\text{Sep})^{3+}$ Loading time:

Figure B.1-1: Typical calibration plots, showing nCYP-based biosensor [GC||naf|El-Co(Sep)³⁺|nCYP3A4] response, to indinavir in the 0.05 – 25.60 μM concentration range for biosensors prepared

APPENDIX B.2

Calibration plots obtained for nCYP3A4 loading optimisation studies:

Table B.2-1: Specific parameters with regard to the calibration plots

Figure	Amount of nCYP3A4 Loaded		Parameters obtained from Regression analysis	
	$\mu\text{g cm}^{-2}$	Units cm^{-2} ($\times 10^{-7}$)	Slope	R^2
a	3.718	3.06	0.029	0.941
b	4.650	3.85	0.038	0.906
c	5.579	4.61	0.043	0.958
d	5.935	4.91	0.043	0.961
e	7.437	6.15	0.021	

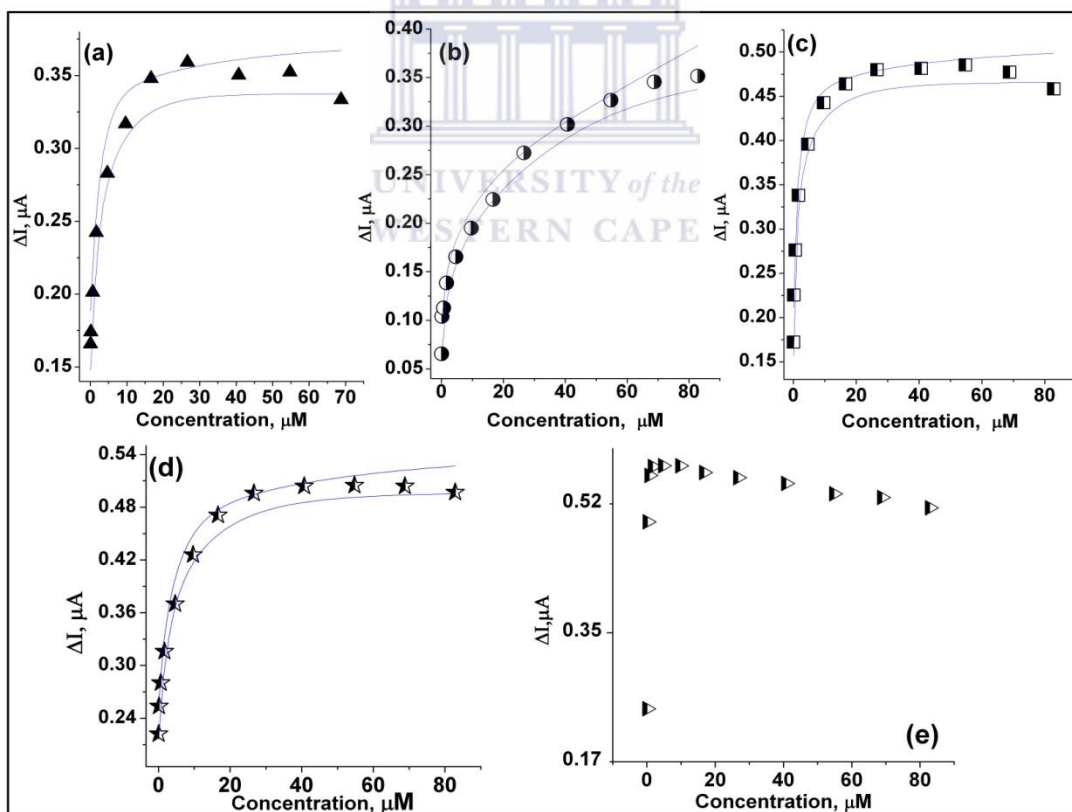
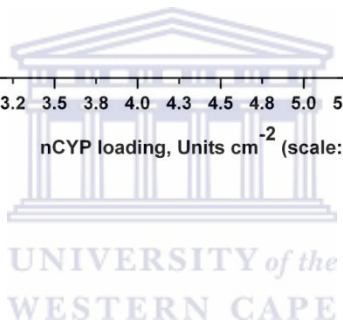
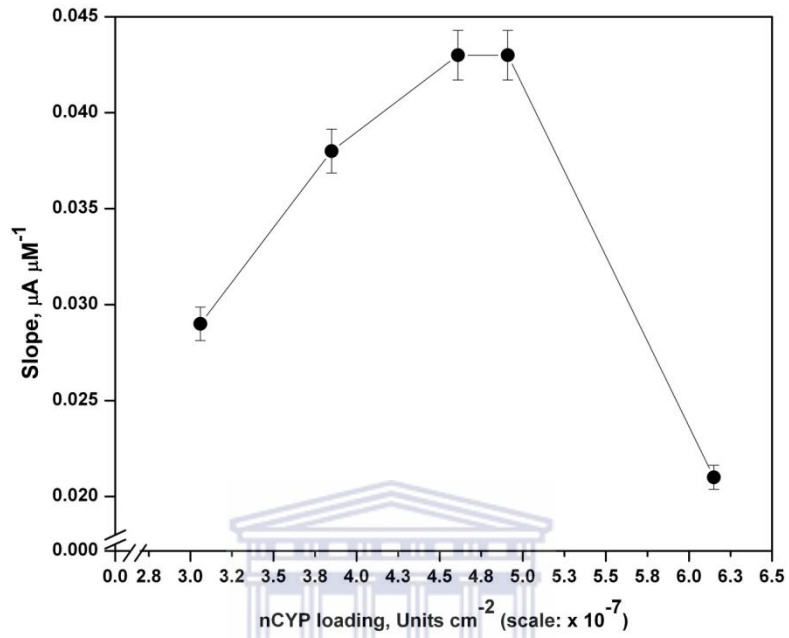


Figure B.2-1:



APPENDIX C

Additional results for section 5B.3.1.2

Voltammetric characterization of the fabricated biosensor (prepared under optimized conditions): General electrochemical behaviour in anaerobic conditions

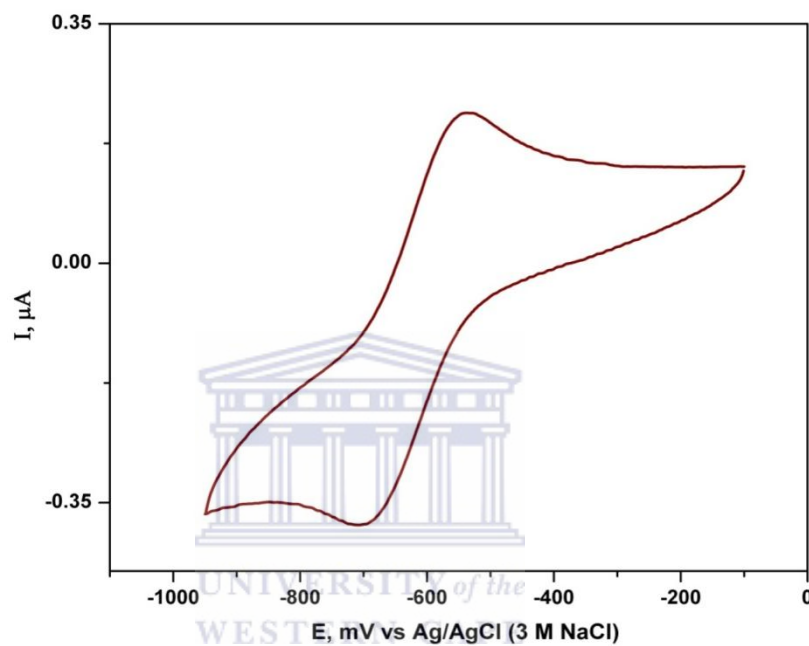


Figure C-1 CV for control sensor (GCE||naf|El-Co(Sep)³⁺|nCYP3A4|Agrs-PEI-PVA. Experimental conditions: Scan taken in argon-degassed PBS (pH 7.45) at 3 mV s⁻¹. Scan direction: cathodically.

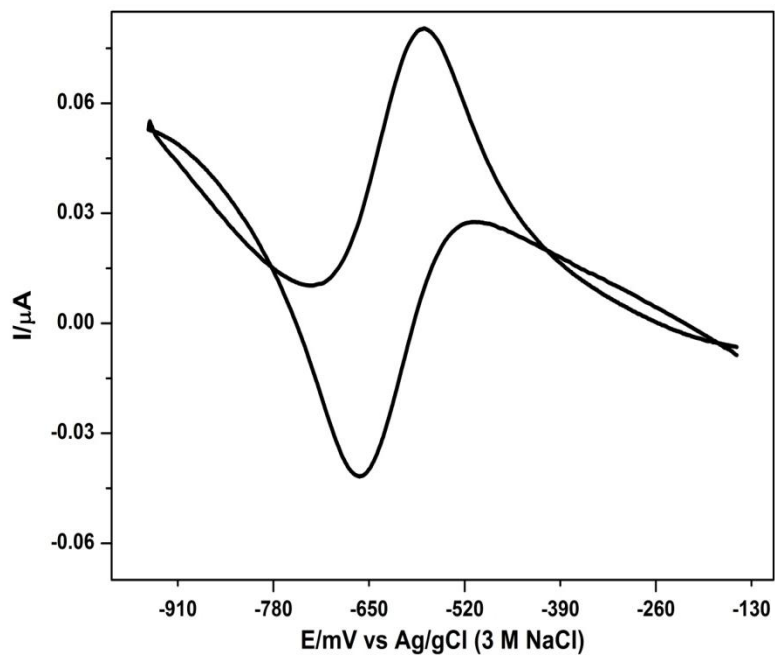


Figure 5B.12 Background-subtracted CV showing GC|naf|Co(Sep)³⁺|nCYP3A4|Agrs-PEI-PVA electrode, showing biosensor response in argon-degassed PB solution. Conditions: $v = 3 \text{ mV s}^{-1}$; scanned cathodically.

